Oxidative Medicine and Cellular Longevity

Effects of Redox Disturbances on Motility, Contractility and Muscle Tissue Pathogenesis

Lead Guest Editor: Christina Karatzaferi
Guest Editors: Marco Sandri, Giorgos Sakkas, and Carine Smith

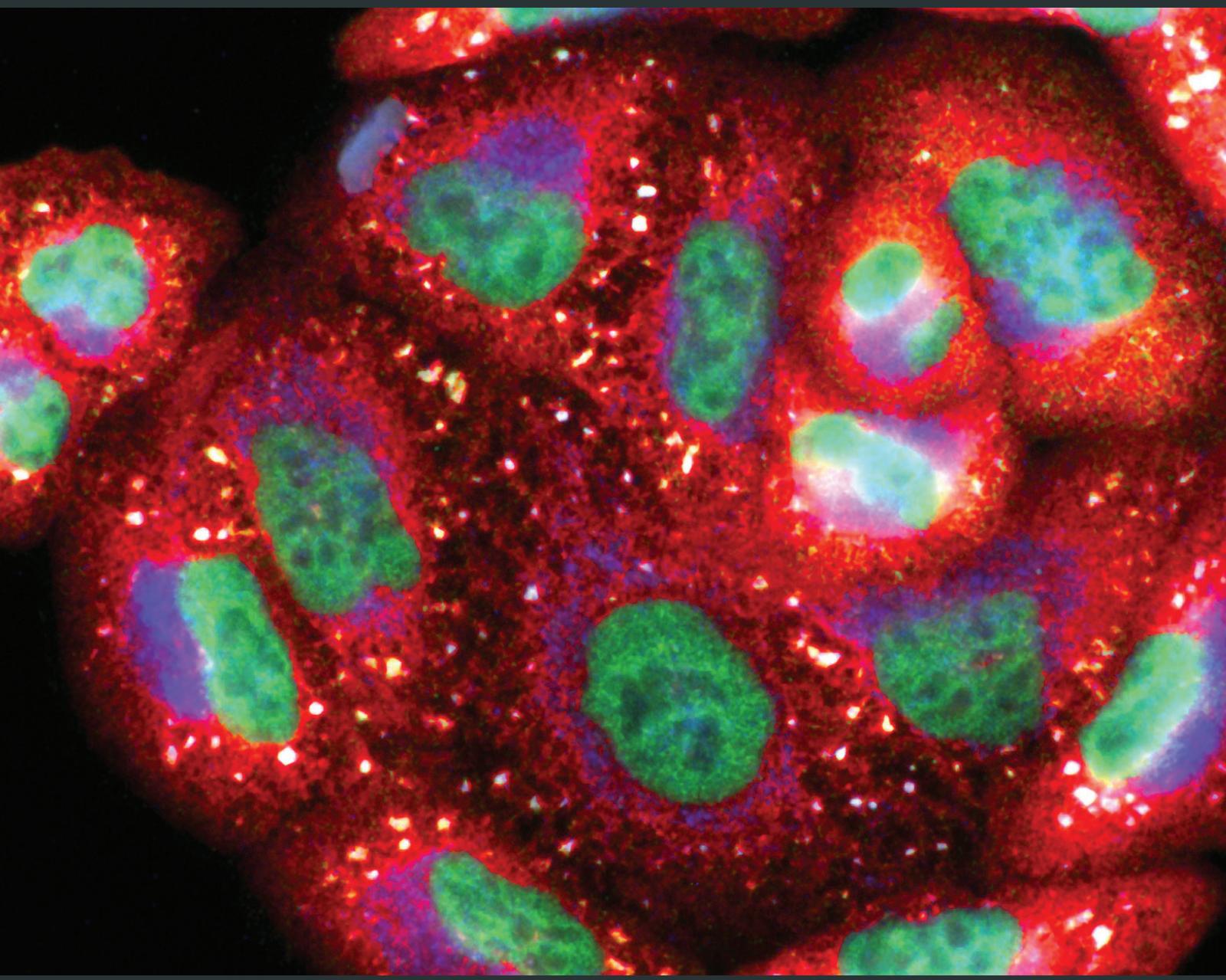

Effects of Redox Disturbances on Motility, Contractility and Muscle Tissue Pathogenesis

Oxidative Medicine and Cellular Longevity

Effects of Redox Disturbances on Motility, Contractility and Muscle Tissue Pathogenesis

Lead Guest Editor: Christina Karatzaferi
Guest Editors: Marco Sandri, Giorgos Sakkas, and Carine Smith

Editorial Board

Contents

Hindawi
Oxidative Medicine and Cellular Longevity
Volume 2019, Article ID 3272035, 2 pages
https://doi.org/10.1155/2019/3272035

Editorial

Effects of Redox Disturbances on Motility, Contractility and Muscle Tissue Pathogenesis

C. Karatzaferi,[1] **M. Sandri**,[2,3] **G. K. Sakkas**,[1] **and C. Smith**[4]

[1]*Experimental Physiology & Therapeutic Exercise Lab, DPESS, University of Thessaly, Greece*
[2]*Venetian Institute of Molecular Medicine (VIMM), Padova, Italy*
[3]*Department of Biomedical Sciences, University of Padova, Padova, Italy*
[4]*Department of Physiological Sciences, Stellenbosch University, Stellenbosch, South Africa*

Correspondence should be addressed to C. Karatzaferi; karatzaferi.c@gmail.com

Received 28 May 2019; Accepted 28 May 2019; Published 16 June 2019

Whether in health or disease, reactive oxygen and nitrogen species (ROS/RNS) affect smooth and striated muscle status and function in ways not always discernible or appreciated. Despite the technological and methodological advancements, some key challenges still exist. On the one hand, one challenge is to appreciate acute effects on contractility and/or bioenergetics within a realistic functional context, effectively linking in vitro observations to in vivo conditions. On the other hand, chronic effects on indices of clinical significance are more difficult to clarify given the interplay of redox status variations with systemic inflammation and autophagy but also with lifestyle factors such as nutrition and physical activity—which impact on systemic health indices, as well as directly on smooth and striated muscles.

Redox disturbances are associated with various hallmarks of health deterioration. Regarding skeletal muscle atrophy, a common denominator of many diseases, it remains quite difficult to discern disuse-induced from disease-induced atrophy and the role of ROS-induced signalling (e.g., Malavaki et al.). That is because prolonged periods of contractile inactivity lead to increased production of intramuscular ROS [1], while both immobilization [2] and unloading [3] have been associated with elevated ROS. Many groups are researching the role of ROS/RNS in disturbing the protein balance from protein synthesis to protein degradation via acceleration of proteolysis and depression of synthesis [4]. Others examine if oxidative stress may help explain chronic disease effects on muscle status [5]. Likewise, there is increasing work on the interplay of autophagy, viewed as an antiaging system, and redox imbalances that may affect the contractile and the neuromuscular junction machineries and may modify the overall progress of neurogenic muscle atrophy (e.g., [6, 7]). Moreover, redox imbalances directly modulate force generation with scientific interest turning towards the interaction between muscle adaptations to chronic redox imbalances and acute responses to ROS accumulation (e.g., [8]). Various international groups and networks have thus undertaken the challenge to characterize the crosstalk between other organ systems and muscles and to decipher the role of redox imbalances in early muscle disease detection, or to monitor longitudinal changes, in order to devise preventive strategies to counteract muscle tissue pathogenesis, whether in striated or smooth muscles.

The aim of the present special issue was to provide updated or novel information regarding the role played by redox disturbances in the development of muscle dysfunction acutely and in the long term, stressing the awareness of these concepts for the monitoring, interpretation, and management of disease effects on muscle.

The themes covered in this issue ranged from molecular insights into the role of abnormalities in processes such as ribosome biogenesis in smooth muscle (Q. Wu et al.) and iron homeostasis in cardiomyocytes (A. Bolotta et al.) in redox status to evidence of strategies which may modulate mitochondrial dysfunction and muscle wasting in sepsis (X. Yu et al., C. Andreani et al.). Two descriptive studies characterized skeletal muscle atrophy in chronic diseases (renal insufficiency and rheumatoid arthritis) and demonstrated

the inadequacy of frequently used circulating redox markers to reflect muscle redox status. Resting plasma redox status, of the indices studied, did not readily correlate with intramuscular levels (K. P. Poulianiti et al.), while different muscles also exhibited distinct differences in predominating antioxidant mechanisms at play (A. B. Oyenihi et al.), highlighting that tissue-specific research approaches are still much needed. In addition, a review provided a holistic picture of oxidative stress-related mechanisms by which ageing muscle loses both mass and strength (P. Szentesi et al.). This review is particularly timely, given not only the increasing average age and life expectancy of the global population but also the increasing evidence for western lifestyle-related accelerated ageing in which skeletal muscle is greatly affected; as are other muscle types. This was demonstrated in rats fed with a hypercaloric diet, where redox disturbances were linked to impaired intestinal contractility (I. L. L. de Souza et al.). Finally, in a model of experimental ischemia/reperfusion injury in rats (Y. Zhang et al.), the integrated crosstalk between nerve stimulation, inflammatory response, redox signalling, and endothelial function was further elucidated.

All of the studies contained in this issue advance our understanding of the effects that redox imbalances may have on muscle properties and pose new exciting questions to be pursued by the scientific community.

Conflicts of Interest

The guest editors declare that there is no conflict of interest regarding the publication of this special issue.

Acknowledgments

The guest editorial team of this special issue acknowledges support from the European Union's Horizon 2020 research and innovation programme MSCAS-RISE "Muscle Stress Relief" under grant agreement no. 645648. The editors wish to thank all authors for submitting their work and the expert reviewers for their valuable contributions in bringing this special issue to completion.

C. Karatzaferi
M. Sandri
G. K. Sakkas
C. Smith

References

[1] S. K. Powers, A. J. Smuder, and A. R. Judge, "Oxidative stress and disuse muscle atrophy: cause or consequence?," *Current Opinion in Clinical Nutrition and Metabolic Care*, vol. 15, no. 3, pp. 240–245, 2012.

[2] H. Kondo, M. Miura, and Y. Itokawa, "Oxidative stress in skeletal muscle atrophied by immobilization," *Acta Physiologica Scandinavica*, vol. 142, no. 4, pp. 527-528, 1991.

[3] J. M. Lawler, W. Song, and S. R. Demaree, "Hindlimb unloading increases oxidative stress and disrupts antioxidant capacity in skeletal muscle," *Free Radical Biology & Medicine*, vol. 35, no. 1, pp. 9–16, 2003.

[4] M. A. Pellegrino, J.-F. Desaphy, L. Brocca, S. Pierno, D. C. Camerino, and R. Bottinelli, "Redox homeostasis, oxidative stress and disuse muscle atrophy," *The Journal of Physiology*, vol. 589, no. 9, pp. 2147–2160, 2011, Pt 9.

[5] A. Kaltsatou, G. K. Sakkas, K. P. Poulianiti et al., "Uremic myopathy: is oxidative stress implicated in muscle dysfunction in uremia?," *Frontiers in Physiology*, vol. 6, p. 102, 2015.

[6] S. Carnio, F. LoVerso, M. A. Baraibar et al., "Autophagy impairment in muscle induces neuromuscular junction degeneration and precocious aging," *Cell Reports*, vol. 8, no. 5, pp. 1509–1521, 2014.

[7] E. Pigna, K. Sanna, D. Coletti et al., "Increasing autophagy does not affect neurogenic muscle atrophy," *European Journal of Translational Myology*, vol. 28, no. 3, p. 7687, 2018.

[8] G. I. Mitrou, K. P. Poulianiti, Y. Koutedakis et al., "Functional responses of uremic single skeletal muscle fibers to redox imbalances," *Hippokratia*, vol. 21, no. 1, p. 3, 2017.

Hindawi
Oxidative Medicine and Cellular Longevity
Volume 2019, Article ID 7064319, 19 pages
https://doi.org/10.1155/2019/7064319

Research Article

Abnormal Ribosome Biogenesis Partly Induced p53-Dependent Aortic Medial Smooth Muscle Cell Apoptosis and Oxidative Stress

Qi Wu,[1] Junmou Hong,[1] Zhiwei Wang,[1] Junxia Hu,[1] Ruoshi Chen,[1] Zhipeng Hu,[1] Bowen Li,[1] Xiaoping Hu,[1] Zhengpei Zhang,[2] and Yongle Ruan[1]

[1]*Department of Cardiothoracic Surgery, Renmin Hospital of Wuhan University, Wuhan, Hubei Province, China*
[2]*Department of Orthopedics, Renmin Hospital of Wuhan University, Wuhan, Hubei Province, China*

Correspondence should be addressed to Zhiwei Wang; wangzhiwei@whu.edu.cn

Received 17 October 2018; Revised 30 March 2019; Accepted 14 April 2019; Published 9 May 2019

Guest Editor: Christina Karatzaferi

Ribosome biogenesis is a crucial biological process related to cell proliferation, redox balance, and muscle contractility. Aortic smooth muscle cells (ASMCs) show inhibition of proliferation and apoptosis, along with high levels of oxidative stress in aortic dissection (AD). Theoretically, ribosome biogenesis should be enhanced in the ASMCs at its proliferative state but suppressed during apoptosis and oxidative stress. However, the exact status and role of ribosome biogenesis in AD are unknown. We therefore analyzed the expression levels of BOP1, a component of the PeBoW complex which is crucial to ribosome biogenesis, in AD patients and a murine AD model and its influence on the ASMCs. BOP1 was downregulated in the aortic tissues of AD patients compared to healthy donors. In addition, overexpression of BOP1 in human aortic smooth muscle cells (HASMCs) inhibited apoptosis and accumulation of p53 under hypoxic conditions, while knockdown of BOP1 decreased the protein synthesis rate and motility of HASMCs. The RNA polymerase I inhibitor cx-5461 induced apoptosis, ROS production, and proliferative inhibition in the HASMCs, which was partly attenuated by p53 knockout. Furthermore, cx-5461 aggravated the severity of AD *in vivo*, but a p53-/- background extended the life-span and lowered AD incidence in the mice. Taken together, decreased ribosome biogenesis in ASMCs resulting in p53-dependent proliferative inhibition, oxidative stress, and apoptosis is one of the underlying mechanisms of AD.

1. Introduction

According to the Global Burden Disease 2010 report, the death rate from aortic aneurysms (AA) and aortic dissection (AD) increased from 2.49 per 100,000 to 2.78 per 100,000 between 1990 and 2010, with higher frequencies among men [1, 2]. The common pathological basis of both is aortic media degeneration (AMD), which is characterized by a decrease in the number of aortic smooth muscle cells (ASMCs) [3] and matrix degeneration [4]. The phenotypic transformation of the ASMCs from the contractile to the proliferative form is involved in the process of AMD. Ribosome biogenesis is an essential process accompanying cell proliferation, and impaired ribosome biogenesis or function in mammalian cells leads to nuclear stress, which can cause cell cycle arrest, senescence, and apoptosis [5]. Studies show that atrophy of the skeletal muscle is partly due to impaired ribosome genesis [6, 7], while hypertrophy is associated with enhanced ribosome biogenesis [8, 9]. In the context of AMD, therefore, one can surmise that ribosome biogenesis is enhanced to aid ASMC proliferation. However, since decreased contractility is another significant change that occurs in the ASMCs during AMD, ribosome biogenesis ought to decrease in these cells. Therefore, the ribosomal status in ASMCs during AMD needs to be clarified.

Ribosome biogenesis is tightly regulated by the PeBoW complex, consisting of BOP1, Pes1, and WDR12, which is involved in 5.8S and 28S ribosomal RNA (rRNA) maturation. A dominant negative mutation in BOP1 has been associated with cell cycle arrest [10], whereas BOP1 overexpression in the liver and colorectal cancer cells increased their migration ability by activating the Wnt pathway [11, 12]. BOP1 has a short half-life due to the PEST motif [13], a common peptide motif in most "short-lived" proteins,

which makes it the core modulator of the PeBoW complex [14]. Mutation in mouse BOP1 reduced the protein synthesis rate by nearly 75% [15]. In addition, blocking PeBoW complex function by Pes1 mutation induced p53 elevation [16], and the accumulation of total and phosphorylated p53 has been observed in the ASMCs during AMD [17].

In this study, we analyzed the potential role of the PeBoW complex in ASMC biology during AMD. We found a marked decrease in BOP1 levels in the aorta of AD patients compared to those of the brain dead donors, which was validated in a mouse model of AD. BOP1 knockdown in human ASMCs (HASMCs) slowed protein renewal, downregulated the contractile proteins α-SMA and MLC, inhibited wound healing ability, induced apoptosis and ROS production, and elevated p53 levels. On the other hand, overexpression of BOP1 slightly impaired the proliferation but inhibited apoptosis and ROS production and p53 accumulation under hypoxic conditions. Furthermore, the specific RNA polymerase I inhibitor cx-5461 reduced protein synthesis and induced apoptosis in the HASMCs. In the murine AD model as well, cx-5461 promoted the occurrence of AD, which was partly rescued in the p53-/- mice. Taken together, BOP1 regulates the redox balance, protein synthesis rate, and contractility and survival of ASMCs, and aberrant BOP1 expression is likely involved in AMD pathogenesis.

2. Materials and Methods

2.1. Clinical Samples. This study protocol was approved by the Clinical Research Ethics Committees of Renmin Hospital of Wuhan University of China. Informed written consent was obtained from all patients. Twenty-eight aortic media specimens were collected from acute type A thoracic AD patients who underwent emergency aortic replacement surgery between April 2017 and August 2017 and displayed no phenotypic characteristics of any of the known genetic cardiac disorders, such as Marfan's syndrome and Loeys-Dietz syndrome. In addition, 14 normal aorta samples were collected from brain dead patients who were registered as heart donors. All samples were carefully removed adventitia and intima. The clinical data of these patients are summarized in Table 1.

Table 1: Clinical characters of the patients enrolled in this study.

	AD group ($n = 28$)	Donor group ($n = 14$)	P value
Male	19/28	13/14	<0.05
Age (mean ± SD)	51.46 ± 11.72	40.71 ± 10.64	<0.05
Hypertension	21/28	6/14	0.403
Type 2 diabetes	1/28	2/14	0.240
Liver complications	10/28	7/14	0.370
Renal complication	11/28	4/14	0.384

2.2. β-Aminopropionitrile Diet-Based Mouse AD Model and p53 Knockout Mouse. The ethical committee of the Renmin Hospital of Wuhan University approved the animal experiments, which were designed in accordance with the Wuhan Directive for Animal Research and the Current Guidelines for the Care and Use of Laboratory Animals published by the National Institutes of Health. A β-aminopropionitrile-(BAPN-) based mouse AD model was established according to a previous report [18]. Three-week-old male C57BL/6 mice were fed a regular diet (control group, $n = 10$) or BAPN diet containing 0.25% (w/w) BAPN (TCI, Japan, Cat# A0796) (BAPN group, $n = 10$). For ribosome biogenesis interference study *in vivo*, mice were injected intraperitoneally (*ip*) with cx-5461 in 50 mM NaH_2PO_4 (pH 4.5) at a dose of 50 mg/kg per day [19] with (cx-5461+BAPN group, $n = 10$) or without a concomitant BAPN diet (cx-5461 group, $n = 10$). The p53 knockout heterozygous (p53+/-) mice were purchased from Jackson Laboratory (Bar Harbor, ME) (stock no. 002101, C57BL/6.129S2-Trp53$^{tm1Tyj/J}$) and crossed to obtain the p53-/- and p53+/+ littermates that were also placed on the BAPN diet to establish AD. All mice were monitored daily, and survival and death reasons were recorded. The aortic samples were collected either when the mice died or at the end of the 8-week study when they were decapitated after anesthetizing with 1% phenobarbital (Sigma, Cat# 57-33-0). The injured aortic tissues were resected and fixed in 4% formaldehyde, while the remaining tissues were stored in liquid nitrogen.

2.3. Histology, Immunohistochemistry/Immunofluorescence, and TUNEL Assay. Resected aortic samples from AD patients, donors, or animal model were fixed in 4% formaldehyde overnight, dehydrated, paraffin-embedded, and cut into 4 μm thick sections. The tissue sections were stained with haematoxylin and eosin (HE), Masson, or elastin Van Giessen (EVG) stains as previously described [20–22]. The severity of broken elastin fibres was graded according to a previous report [23], in terms of the ratio of collagen (blue stained) to muscle fibres (red stained) outside the hematoma which was calculated by the Image J software based on Masson-stained images.

For immunohistochemistry (IHC)/immunofluorescence (IF), the sections were hydrated, heated for antigen retrieval, and treated with hydrogen peroxide to inactivate the endogenous peroxidase as per standard protocols. After blocking with 5% goat serum, the sections were incubated overnight with anti-BOP1 (1 : 200; Bioss Biotechnology, Cat# bs-12877R), anti-Ki67 (1 : 400; Cell Signaling Technology, Cat# 9449), and anti-p53 (1 : 50; Santa Cruz Biotechnology, Cat# sc-126) antibodies, along with the control IgG (1 : 100, Santa Cruz Biotechnology, Cat# sc-2025) at 4°C. The sections were then incubated with horseradish peroxidase- (HRP-) conjugated secondary antibody, washed with PBS, and stained with diaminobenzidine (DAB) (Sangon Biotech, Cat# A600140). The total and positively stained cells in 10 random fields of each aortic media section were counted at ×400 magnification, and the percentage of positive cells was calculated.

8-OHdG is the biomarker that indicated the DNA damage induced by ROS. The sections were processed as above and incubated with primary anti-8-OHdG antibody (1 : 200, Bioss, Cat# bs-1278R) and anti-α-SMA antibody (1 : 200, Servicebio, Cat# GB13044). The slides were then incubated

with a secondary antibody conjugated with a fluorescent label (Cy3-conjugated goat anti-rabbit IgG (H+L) and FITC-conjugated goat anti-mouse IgG (H+L)) (1 : 200, Servicebio, Cat# GB21303 and GB22301) for 1 hour at room temperature and the cell nuclei counterstained with DAPI. Images were captured using a fluorescence microscope (BX63, Olympus, Japan).

The TUNEL assay was performed to detect apoptosis *in situ* using a commercially available kit (In Situ Cell Apoptosis Detection Kit, FITC, Sangon Biotech, Cat# E607178) according to the manufacturer's instructions [24]. Positive TUNEL staining was observed under a fluorescence microscope (TE2000U, Nikon, Tokyo, Japan) using the B-2A filter (450–490 nm excitation filter, 505 nm dichroic mirror, and 520 nm band pass filter) at ×400 magnification. The positively stained cells were counted in 10 random fields and the percentage apoptotic cells were calculated.

2.4. HASMC Culture and Genetic Manipulation. The HASMC line (ATCC® PCS-100-012™) was purchased from the China Centre for Type Culture Collection (CCTCC) and cultured in HASMC complete medium (Procell, Cat# CM-H081) at 37°C under 5% CO_2 and 100% humidity. For serum-free and hypoxic treatment, the cells were cultured at 37°C in serum-free medium under 1% O_2, 5% CO_2, and 99% N_2 in a humidified chamber (Binder, CB-210 hypoxia workstation). BOP1 knockdown in the HASMCs was established by RNA interference using BOP1 (si-BOP1: AUGG CAUGGUGUACAAUGAdTdT) and related scrambled (scr: UUCUCCGAACGUGUCACGUdTdT) siRNAs purchased from RiboBio. Briefly, 8 μl of 20 μM scr or si-BOP1 was diluted in 400 μl Opti-MEM (Gibco, Cat# 31985062) and incubated with 5 μl Lipofectamine 2000 (Invitrogen, Cat# 11668-027) for 25 min in room temperature. The mixture was then added to the HASMCs, and the cells were cultured for 6 h. To overexpress BOP1, HASMCs were transduced with adenovirus carrying BOP1 (Ad-BOP1; Vigene Bioscience Corporation, Cat# VH806931) or GFP (Ad-GFP; Vigene, Cat# CV1001).

2.5. Quantification of Protein Synthesis. The rate of protein synthesis was determined by detecting the amount of puromycin-labeled nascent polypeptides as previously described [25, 26]. The cells are cultured in puromycin-plus medium, which is incorporated into the elongating peptide chains and terminates mRNA translation, resulting in the release of the puromycin-labeled truncated peptides from the ribosome; the amount of which can be determined using antipuromycin antibodies to reflect the rate of protein synthesis. HASMCs transfected with si-BOP1/scr or treated with cx-5461 were incubated with 1 μM puromycin for 40 min, harvested, and lysed. The cell lysates were suitably processed for western blotting, and the nascent proteins were detected using the antipuromycin antibody (1 : 1000; Merck Millipore, Cat# MABE343-AF488). To determine the total protein quantity in each sample, equal amounts of proteins (40 μg) per sample were resolved by SDS-PAGE and the gels were stained with Coomassie blue.

2.6. Cell Viability Assays. HASMCs were seeded in 96-well plates at the density of 3×10^3/190 μl/well and after overnight culture were treated with varying concentrations of cx-5461 (0-20 μM) for 24 hours. For the viability assay, 10 μl tetrazolium salt WST-8 (Cell Counting Kit-8; Keygen, Cat# KGA317) was added to each well (final volume 200 μl), and the optical density at 450 nm was measured. The cell viability was calculated as $OD450_{treated}/OD450_{control} \times 100\%$. To study the effect of p53 on cx-5461-induced cell death, HASMCs were pretreated with 10 μM of the specific p53 inhibitor pifithrin-α (PFTα; Selleck, Cat# S2929) [27] for 12 h before cx-5461 treatment as described above. Similarly, to assess the influence of BOP1 on HASMC survival, the cells were transduced with Ad-BOP1 or Ad-GFP and 24 h later were resuspended and reseeded (0.8×10^3/190 μl/well) in 96-well plates. The cell viability was determined daily for the next 5 days as described.

2.7. Western Blotting. Tissues or cells were washed with cold PBS and lysed in RIPA buffer (Beyotime, Cat# P0013K) supplemented with a protease inhibitor cocktail (Roche, Cat# 04693159001). The cell debris was removed by centrifugation (12000g, 4°C, 10 min) after ultrasonication, and the protein concentration of the cleared lysates was determined by BCA assay (Beyotime, Cat# P0010). Equal amounts of proteins (HASMCs, 20 μg; human aortic tissue, 200 μg; and mouse aortic tissue, 120 μg) were resolved by 8%-12% SDS-PAGE and transferred onto polyvinylidene difluoride (PVDF) membranes (Merck Millipore, Cat# ISEQ00010). After blocking with 5% skimmed milk in PBS buffer, the membranes were incubated overnight with anti-BOP1 (1 : 100; Santa Cruz Biotechnology, Cat# sc-390672), anti-p53 (1:100; Santa Cruz Biotechnology, Cat# sc-126), anti-ACTA2 (smooth muscle cell actin, a-SMA) antibody (1 : 800, Proteintech, Cat# 14395-1-AP), antimyosin light chain-2 (MLC) antibody (1 : 500; Proteintech, Cat# 10906-1-AP), antipuromycin antibody (1 : 400; Merck Millipore, Cat# MABE343-AF488), antiactivated caspase 3 (1 : 1000; Cell Signaling Technology, Cat# 9664), and anti-GAPDH (1 : 5000; Proteintech, Cat# 60004-1-Ig) primary antibodies at 4°C. The membranes were washed and incubated with IRDye-800CW-conjugated goat anti-mouse IgG (1 : 20000; Li-cor, Cat# 926-32210) or goat anti-rabbit IgG (1 : 20000; Li-cor, Cat# 926-32211) secondary antibodies. The membranes were scanned by Odyssey (Li-cor Biosciences), and the grayscale value of each band was qualified by the paired software. At least 3 independent experiments were performed, except for the mouse aortic protein.

2.8. Wound Healing Assays. HASMCs were seeded in six-well plates and cultured till 90% confluence. After starving the cells for 12 h in serum-free medium, the confluent cell monolayer was gently scratched in a straight line with a 100 μl pipette tip. The debris was removed and the edge of the scratch was smoothed with PBS washing. The gap was then monitored by phase contrast microscopy at the indicated time points. A minimum of three independent experiments was performed.

2.9. Cytometric Analysis of Cell Apoptosis. Apoptosis in the HASMCs was detected using the Annexin V-APC/7-AAD apoptosis detection kit (BD Biosciences, Cat# 561012). The cells were harvested and washed twice with PBS containing 5% FBS and resuspended in 500 μl binding buffer provided in the kit. The cells were then incubated with 5 μl Annexin V-APC and 5 μl 7-AAD at room temperature for 15 min in the dark. The percentage of apoptotic cells was detected by flow cytometry using Cell Quest software (BD Biosciences, San Jose, CA, USA).

2.10. Detection of Reactive Oxygen Species (ROS). Production of ROS was detected by 5 μM dihydroethidium (DHE, Yeasen Biotech Co., Cat# 50102ES02). Briefly, HASMCs were pretreated with 10 μM PFTα for 12 h and administrated with varying doses of cx-5461 for 24 h. After that, 5 μM DHE was added in the medium and incubated at 37°C for 20 min. After incubation, HASMCs were washed with PBS, and fluorescence of DHE was detected using a confocal microscope. The ROS accumulation was also detected by DCFH-DA kit (Solarbio, Cat# CA1410). HAS MCs were treated as stated above and stained by DCFH-DA working solution (10 μM). Cellular fluorescence at excitation and emission frequencies of 488 nm and 525 nm, respectively, was measured using flow cytometry (BD FACS Calibur, USA).

2.11. Quantitative Real-Time PCR (qRT-PCR). Total RNA was isolated by RNAiso Plus (Takara, Cat# 9109) according to the manufacturer's instructions. The concentration and purity of RNA were determined using ultraviolet spectrophotometry (Beckman Coulter, USA). The cDNA was synthesized using the RevertAid First Strand cDNA Synthesis Kit (Thermo Scientific, Cat# K1622) according to the manufacturer's instructions. RT-PCR analysis was performed using the SYBR Premix Ex Taq II (Takara, Cat# RR820A) in Biosystems 7500 Real-Time PCR Systems (ABI, USA). The primer sequences were as follows: BOP1 forward: 5′-GTGG GCTTCAACCCCTATGAG-3′, reverse: 5′-CCATGCGAG AGACCTTCTCC-3′; MLC forward: 5′-TTGGGCGAGTG AACGTGAAAA-3′, reverse: 5′-CCGAACGTAATCAGCC TTCAG-3′; α-SMA forward: 5′-AAAAGACAGCTACGTG GGTGA-3′, reverse: 5′-GCCATGTTCTATCGGGTAC TTC-3′; and GAPDH forward: 5′-ACTTTGGTATCGTG GAAGGACTCAT-3′, reverse: 5′-GTTTTTCTAGACGG CAGGTCAGG-3′.

2.12. Statistical Analysis. Statistical analysis was performed using GraphPad Prism 5 software. Measurement data was presented as mean ± SD and compared using Student's *t*-test or *one-way ANOVA* test. Ranking data (elastin broken grading score) were analyzed by *Mann-Whitney test*, and the *chi-squared test* was used to compare incidence of aortic rupture between different groups. A *log-rank (Mantel-Cox) test* was used to compare Kaplan-Meier survival curves. P values < 0.05 were regarded as statistically significant.

3. Results

3.1. BOP1 Expression Is Decreased in ASMCs of AD Patients. The clinical data of 28 AD patients and 14 donors are summarized in Table 1, and significant differences were seen in terms of age and gender. The main features of AMD are loss of ASMCs, collagen accumulation, and fragmentation of elastic fibres. Masson staining showed an increase in the ratio of the collagen to muscle fibres in the aortic media of AD patients compared to that of donors (Figure 1(a), upper panel), while EVG staining indicated fragmented elastic fibres in the AD aortic samples (Figure 1(a), lower panel). BOP1 is the crucial component of PeBoW complex, which regulates rRNA processing, and due to its short half-life on account of the PEST motif, it might be indicative of rRNA maturation. A significant decrease was seen in the BOP1 protein levels in the aortic media of AD patients ($n = 8$) compared to those of the donors ($n = 4$) by western blotting (Figure 1(b)). Furthermore, BOP1 protein expression *in situ* was also downregulated in the ASMCs of AD patients ($n = 28$) compared to donors ($n = 14$) and largely localized to the nucleus (Figures 1(c) and 1(d)). Since ribosome biogenesis is closely related to p53, we further examined the *in situ* p53 expression and found significant elevation and nuclear accumulation (Figure 1(c)) in the aorta of AD patients ($n = 28$) compared to donors ($n = 14$) (Figures 1(c) and 1(d)). We also found accumulative ROS in the ASMCs of AD patient by detecting 8-OHdG (Figure 1(e)).

3.2. Overexpression of BOP1 Attenuated HASMC Apoptosis under Serum-Free and Hypoxic Conditions. HASMCs transduced with Ad-BOP1 showed significant elevation in BOP1 expression levels compared to the Ad-GFP-transduced cells (Figure 2(a)). Since BOP1 is overexpressed in various tumors, we tested its influence on HASMC growth by the CCK-8 assay. Surprisingly, however, overexpression of BOP1 inhibited cell proliferation (Figure 2(b)), although it reversed the time-dependent apoptosis induced in the HASMCs under serum-free and hypoxic conditions (Figures 2(c) and 2(d)). In addition, overexpression of BOP1 significantly alleviated the increased levels of proapoptotic proteins like activated caspase 3 and p53. In the control cells, hypoxia reduced BOP1 expression in a time-dependent manner (Figures 2(e) and 2(f)).

3.3. BOP1 Knockdown Impaired HASMC Protein Synthesis Rate and Motility. To determine the role of BOP1 in HASMC motility, we examined the effect of altering BOP1 expression on the levels of α-SMA and MLC, which are associated with the contractility and motility of HASMCs. BOP1 knockdown decreased the levels of α-SMA and MLC in the HASMCs (Figures 3(a) and 3(b)). In addition, HASMC motility was also assessed by the *in vitro* wound healing assay, which showed significant inhibition of scratch recovery after BOP1 knockdown (Figures 3(d) and 3(e)). To determine the potential effect of BOP1 on the protein synthesis rate in HASMCs, we pretreated cells with puromycin to label the nascent peptides

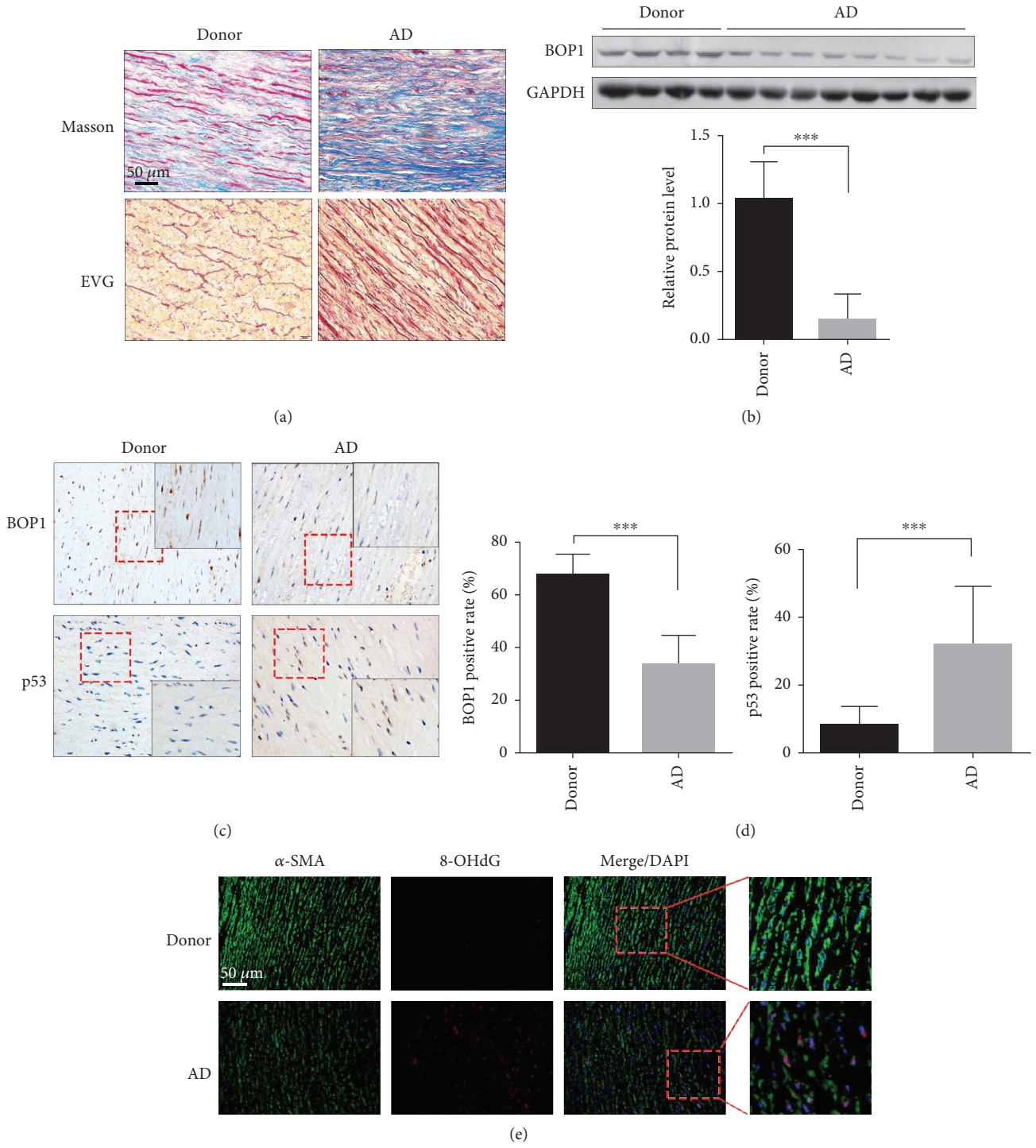

Figure 1: BOP1 expression is decreased in ASMCs of AD patients. (a) Images of Masson staining showed collagen (blue) and muscle fibre (red) in the aortic media derived from AD patients and donors (upper panel). Representative images of EVG staining indicated the broken elastic fibre in aortic samples derived from AD patients and donors (lower panel). (b) BOP1 protein expression in the aortic media of donors ($n = 4$) and AD patients ($n = 8$) was detected by western blotting, and the related expression level was detected by statistical analysis and shown. (c) Representative image of the aortic specimens stained by BOP1 and p53 by performing IHC. (d) The positive rate was detected by statistical analysis and shown. (e) The 8-hydroxy-2′-deoxyguanosine (8-OHdG) level in the aortic media tissues were detected by performing immunofluorescence and the representative images are shown. Scale bar 50 μm. Data are presented as mean ± SD. $^{***}P < 0.001$ determined by Student's t-test.

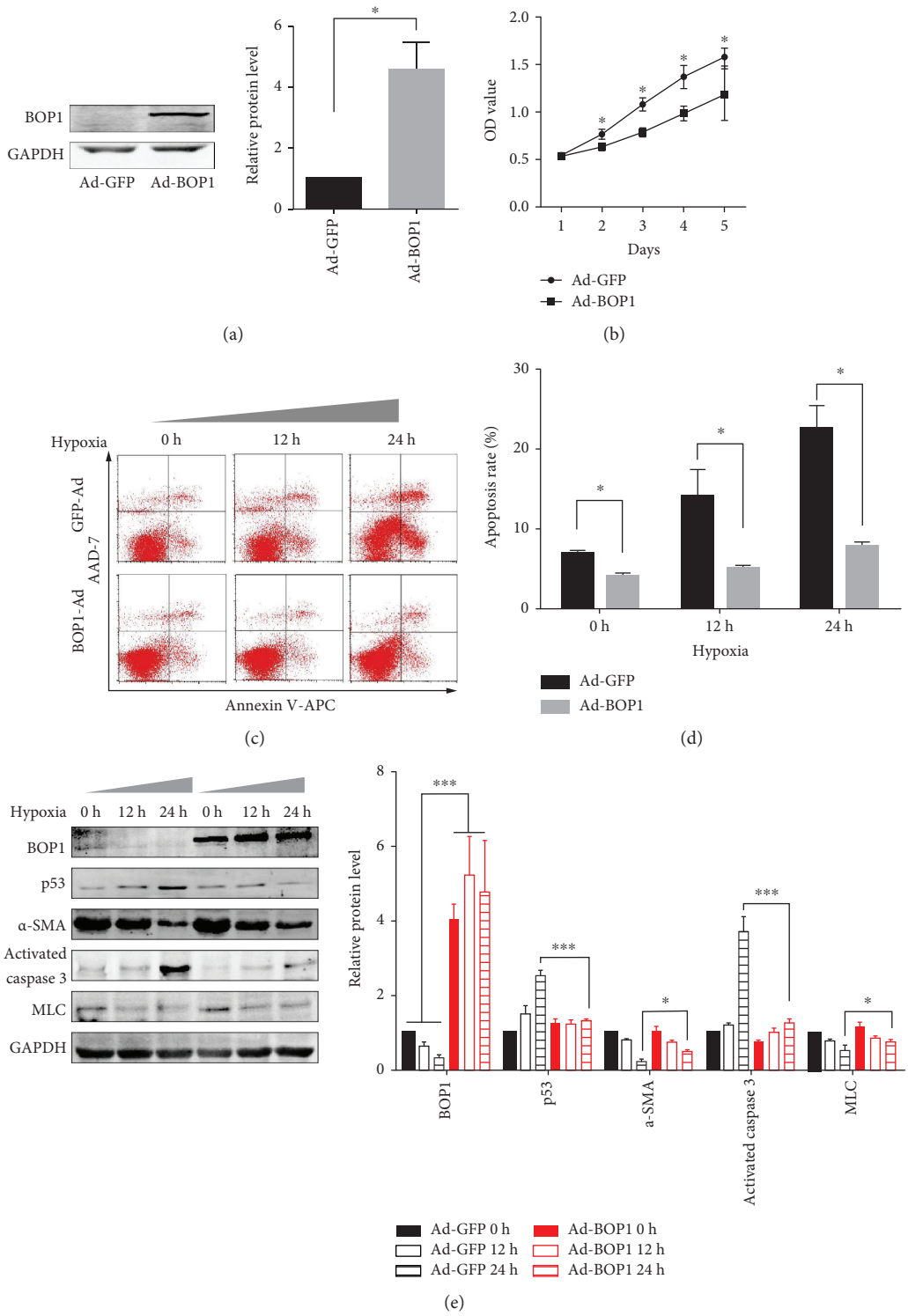

Figure 2: Overexpression of BOP1 attenuated HASMC apoptosis under serum-free and hypoxia condition. (a) The expression of BOP1 in HASMCs was detected after it had been infected with Ad-BOP1 or Ad-GFP for 24 h (left panel). Statistical analysis is shown (right panel). (b) HASMCs were infected with Ad-BOP1 or Ad-GFP for 24 h. The cells were suspended and reseeded in 96-well plates. CCK-8 assays were performed to assess the influence of BOP1 on HASMC proliferative ability. The growth curve is shown. (c) After being infected with Ad-BOP1 or Ad-GFP for 24 h, HASMCs were administrated in serum-free and hypoxia condition for the time shown. Apoptosis was detected by Annexin V-APC/7-AAD staining and flow cytometry followed. The representative images are shown. (d) The statistical analysis of apoptosis rate is shown. (e) Western blotting was performed to detect the BOP1, p53, α-SMA, activated caspase 3, and MLC expression. The representative image is shown (left panel). The statistical analysis is shown (right panel). Data are representative of three independent experiments and presented as mean ± SD. $^{*}P < 0.05$, $^{**}P < 0.01$, and $^{***}P < 0.001$ determined by *one-way ANOVA*.

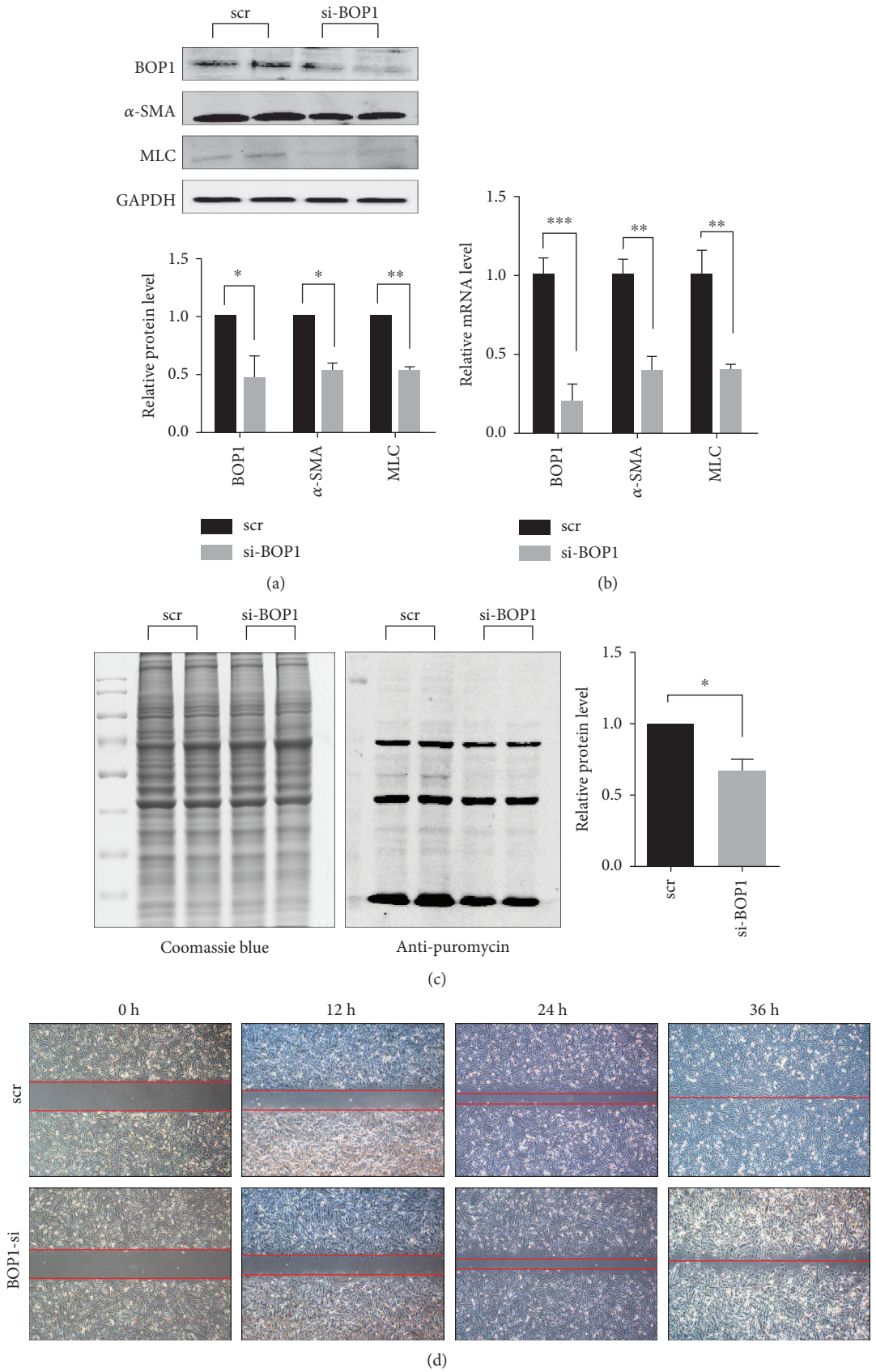

Figure 3: Continued.

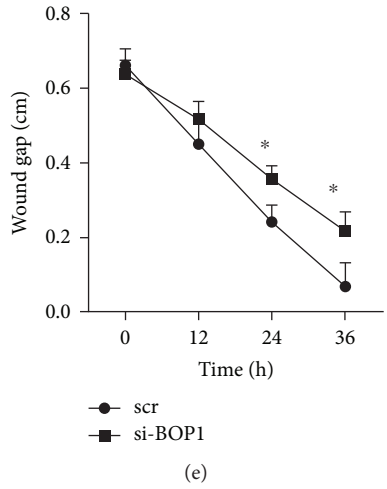

Figure 3: BOP1 knockdown impaired HASMC protein synthesis rate and motility. (a) After being transfected with scramble (scr) or BOP1 siRNA (si-BOP1) for 48 h, the expression of BOP1, α-SMA, and MLC was detected by western blotting. The expression levels were detected by statistical analysis and shown. (b) Real-time PCR was performed to detect the mRNA level of BOP1, α-SMA, and MLC in HASMCs after being transfected with si-BOP1 or scr for 48 h. (c) HASMCs were transfected with si-BOP or scr for 48 h and administrated with puromycin (1 μg/ml) for 40 min to label the nascent protein. The equal amount of protein was electrophoresed and stained with Coomassie blue to indicate the total protein (left panel). Western blotting was performed to detect the nascent protein by using antipuromycin antibody (middle panel). The statistical analysis of nascent protein/total protein is shown (right panel). (d) Wound healing assay detected the mobility of HASMCs after being transfected with si-BOP1 for 48 h and photographed at the indicated time. The red dotted lines indicated the extent of scratches. (e) The extent of scratches was measured and detected by statistical analysis. Data are representative of three independent experiments and presented as mean ± SD. $^{*}P < 0.05$, $^{**}P < 0.01$, determined by Student's t-test.

and detected them using the antipuromycin antibody. As shown in Figure 3(c), BOP1 knockdown significantly decreased protein synthesis rate in HASMCs.

3.4. cx-5461-Mediated Inhibition of RNA Polymerase I Affected Protein Synthesis and p53-Dependent Cell Apoptosis. To elucidate the association between ribosome biogenesis and apoptosis, HASMCs were treated with cx-5461, an inhibitor of RNA polymerase I. CCK-8 assay indicated significant cytotoxicity of cx-5461 in HASMCs ($IC50 = 1 \cdot 27 \pm 0 \cdot 19$ μM), which was however attenuated when the cells were pretreated with the p53 inhibitor PFTα ($IC50 = 9 \cdot 66 \pm 0 \cdot 41$ μM) ($P < 0.001$, Student's t-test; Figure 4(a)). In addition, cx-5461 also resulted in a dose-dependent reduction in nascent protein synthesis (Figure 4(b)), along with increased p53 and activated caspase 3 levels, and a dose-dependent decrease in the levels of BOP1, α-SMA, and MLC (Figure 4(c)). Furthermore, apoptosis and ROS production induced by cx-5461 in HASMCs were attenuated upon PFTα pretreatment (Figures 4(d) and 4(e); Fig. S1). Consistent with this, p53 and activated caspase 3 protein levels also decreased in the PFTα pretreated cells. PFTα also partially reversed the cx-5461-induced decrease in BOP1, α-SMA, and MLC levels (Figure 4(f)).

3.5. Inhibition of RNA Polymerase I by cx-5461 Accelerated AD in Mice. In order to elucidate the effects of ribosome dysfunction on AD, we established a murine AD model based on BAPN diet and treated the animals with cx-5461 (50 mg/kg/day). Mice in the cx-5461+BAPN group ($n = 10$) had an accelerated development and increased severity of AD and shorter life-span compared to the control group ($n = 10$) (Figure 5(b)). EVG staining showed a higher grade of elastin fibre breakdown (Figure 5(a)), while Masson staining revealed a higher collagen-to-muscle fibre ratio in the aortic tissues of the cx-5461+BAPN mice (Figure 5(c)). Mice fed with the BAPN diet also showed decreased BOP1 expression in their ASMCs, which declined further when treated with cx-5461. Furthermore, cx-5461 treatment further increased apoptosis and ROS production in the ASMCs of AD mice and reduced the AD-induced higher proliferative rates (Figure 5(d); Fig. S2). Consistent with this, cx-5461 exacerbated the increase in activated caspase 3 and p53 levels and the decrease in α-SMA and MLC (Figure 5(e)).

3.6. Knocking Out p53 Reduced the Occurrence of AD in Mice. Previous studies have shown that impaired rRNA transcription increases apoptosis in ASMCs, a phenomenon associated with p53 accumulation. Therefore, we established the AD model in p53-/- mice to explore its role in AD. The p53-/- AD mice ($n = 10$) had an extended life-span compared to the p53+/+ AD mice ($n = 13$) (Figure 6(b)). The representative images of the gross aorta are shown in Figure 6(a). All save one (12/13, 92.3%) p53+/+ AD mice died of aortic rupture, hemothorax, and major bleeding, while only 60% (6/10) of the p53-/- AD mice died of aortic rupture and the remaining 30% of aortic aneurysm and 10% of intestinal obstruction (Figure 6(c)). However, no significant differences were observed between the mice in terms of the severity of elastic breakdown and collagen-to-muscle fibre ratio (Figure 6(d)), and only a slight increase was seen in aortic BOP1 expression in the p53-/- AD mice (Figure 6(e)). However, knocking out p53 decreased apoptosis and ROS production and increased the proliferative rate ($Ki67^{+}$ cells) among the ASMCs in the

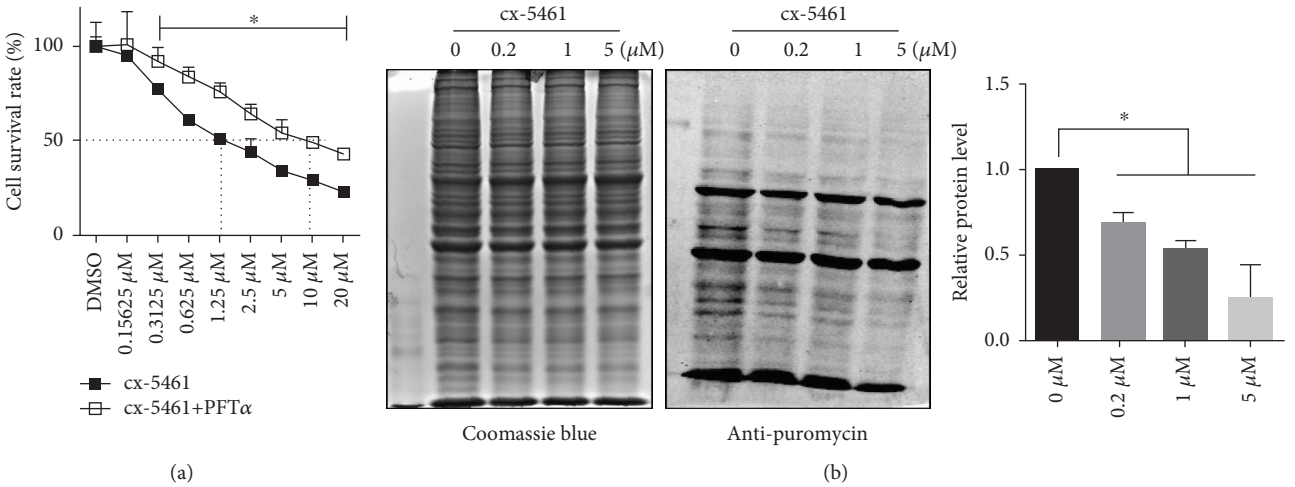

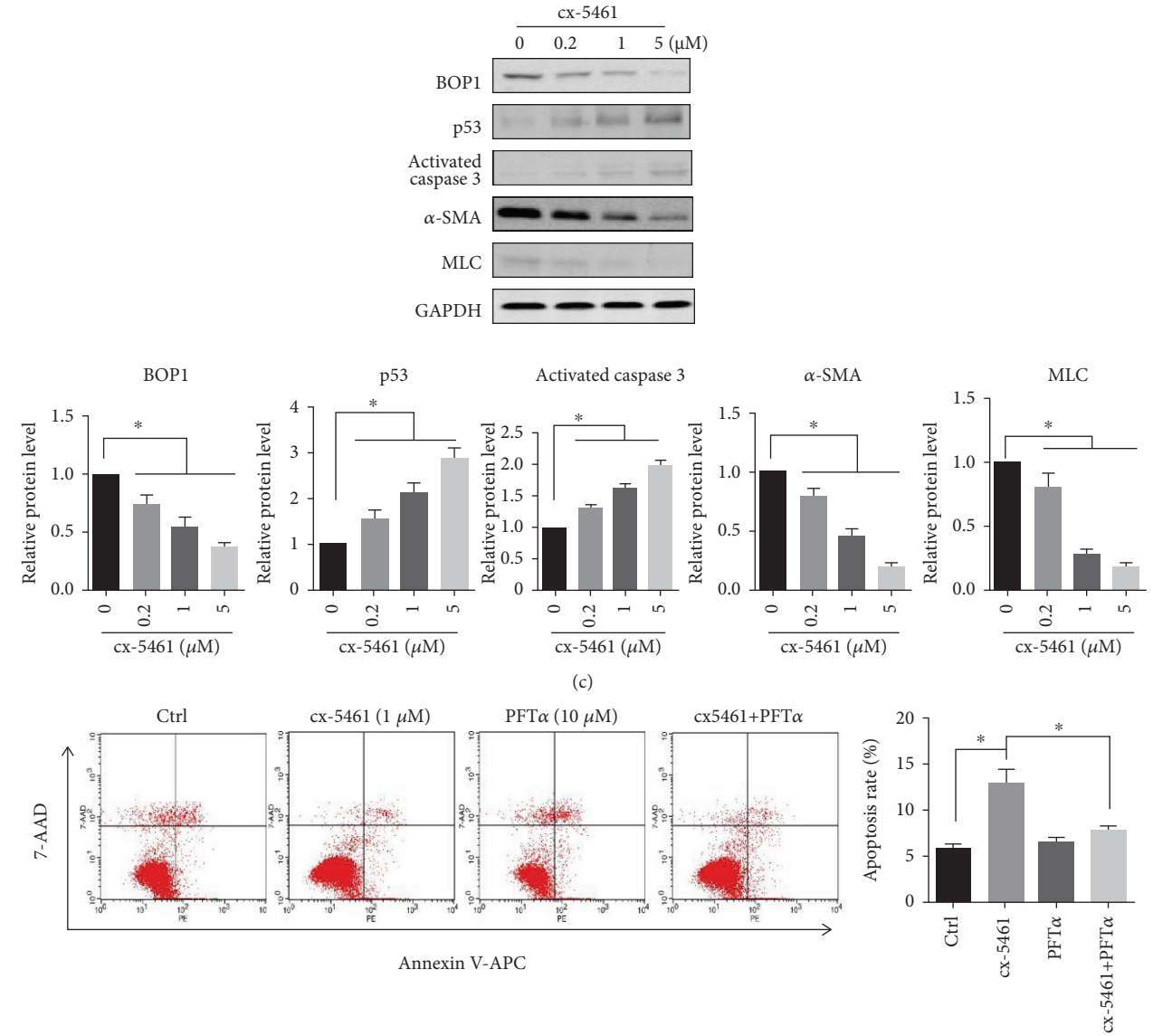

Figure 4: Continued.

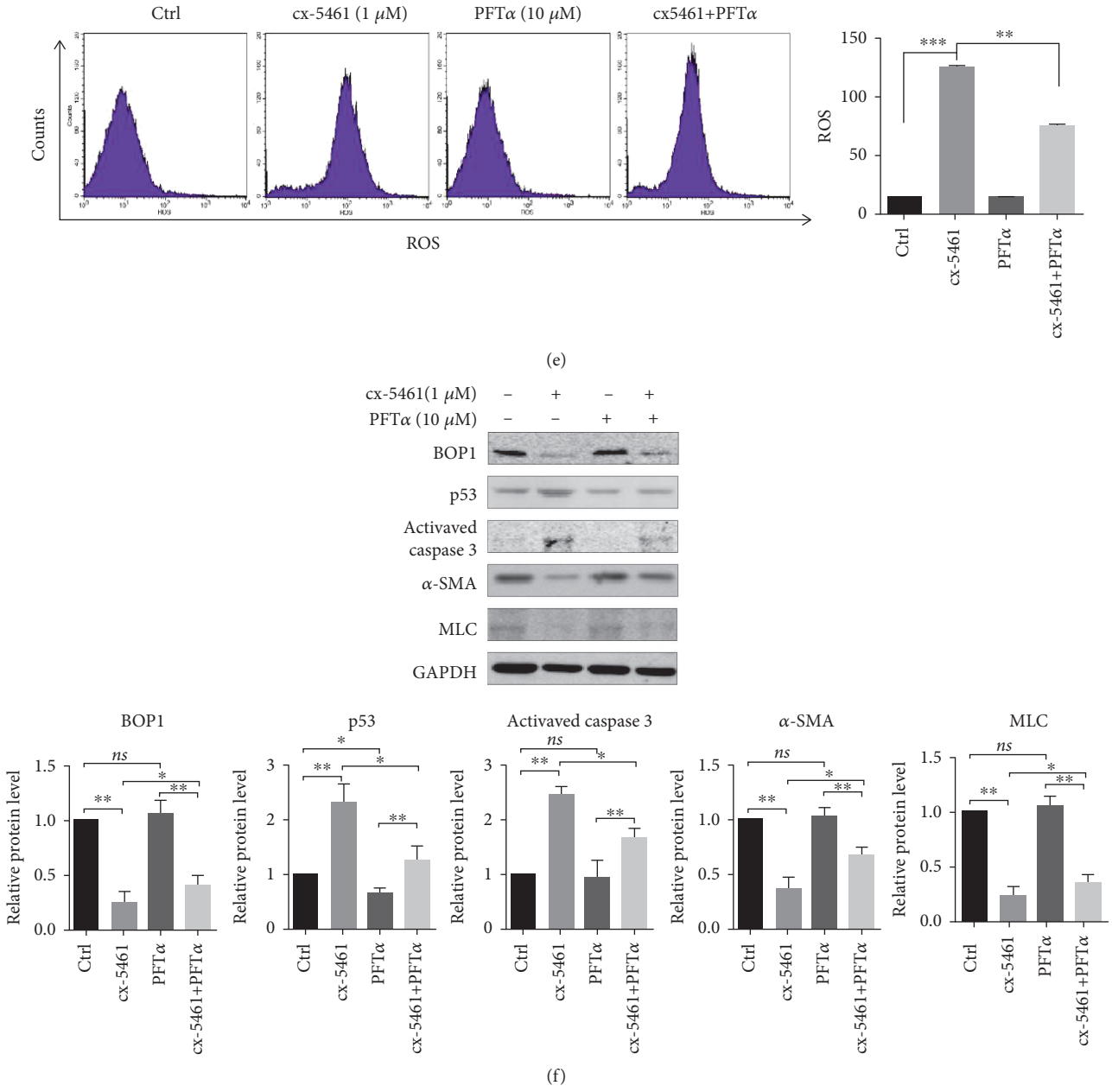

Figure 4: cx-5461 impaired protein synthesis and activated p53-dependent cell apoptosis. (a) HASMCs were pretreated with or without PFTα (10 μM) for 12 h and then administrated with the indicated concentration of cx-5461 for 24 h. The cell survival rate was detected by CCK-8 assays. (b) HASMCs were treated with the indicated concentration of cx-5461 for 24 h and then administrated with puromycin (1 μM) for 40 min. The total protein (Coomassie blue staining, left panel) and the nascent protein (antipuromycin, middle panel) were shown. The statistical analysis of nascent protein/total protein is shown (right panel). (c) HASMCs were administrated with the indicated concentration of cx-5461 for 24 h. Western blotting was performed to detect the BOP1, p53, activated caspase 3, α-SMA, and MLC expression. Representative images are shown (left panel), and the grayscale was measured and detected by statistical analysis (right panel). (d) HASMCs were pretreated with or without PFTα (10 μM) for 12 h, followed by the treatment of cx-5461 (1 μM). Apoptosis was assessed by Annexin V-APC/7-AAD staining and flow cytometry (left panel). The statistical analysis of apoptosis rate is shown (right panel). (e) ROS were detected by DCFH-DA and flow cytometry (left panel). The ROS level is shown (right panel). (f) HASMCs were pretreated with or without PFTα (10 μM) for 12 h, followed by the treatment of cx-5461 (1 μM). Western blotting was performed to detect the BOP1, p53, activated caspase 3, α-SMA, and MLC expression. Representative images are shown (left panel), and the grayscale was measured and detected by statistical analysis (right panel). Data are representative of three independent experiments and presented as mean ± SD; *ns*: no statistical significance; $^{*}P < 0.05$, $^{**}P < 0.01$, determined by *one-way ANOVA*.

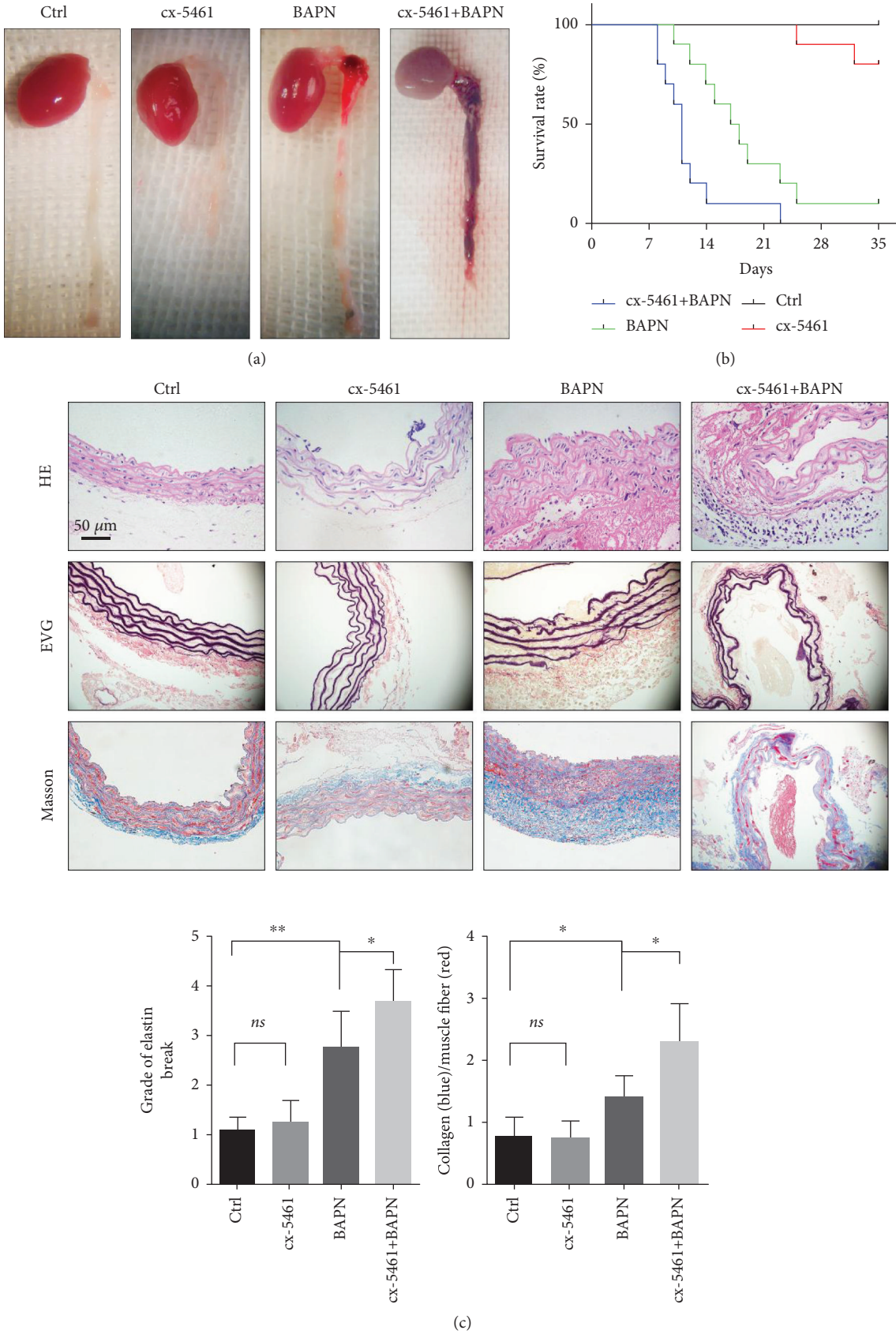

Figure 5: Continued.

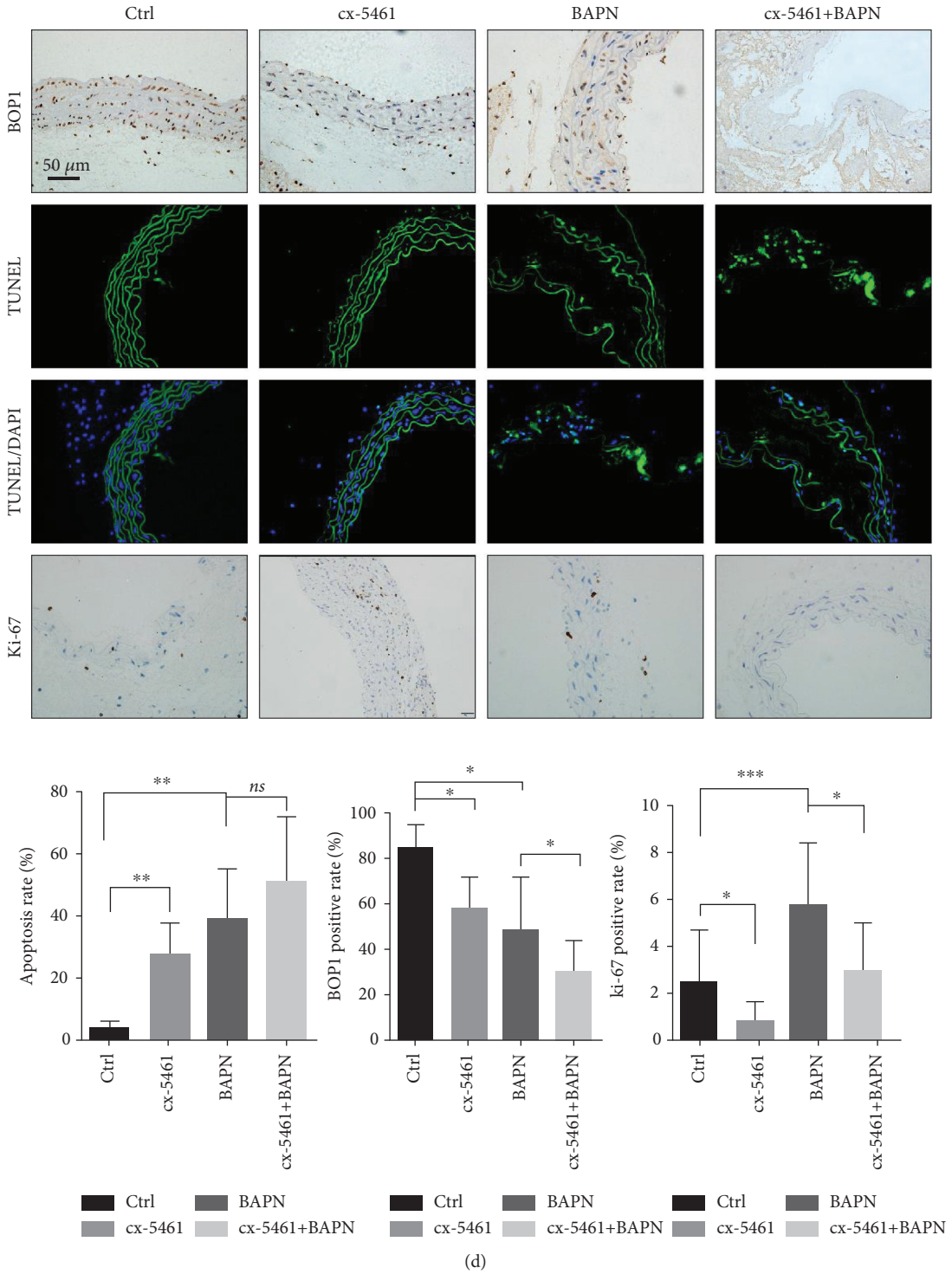

(d)

Figure 5: Continued.

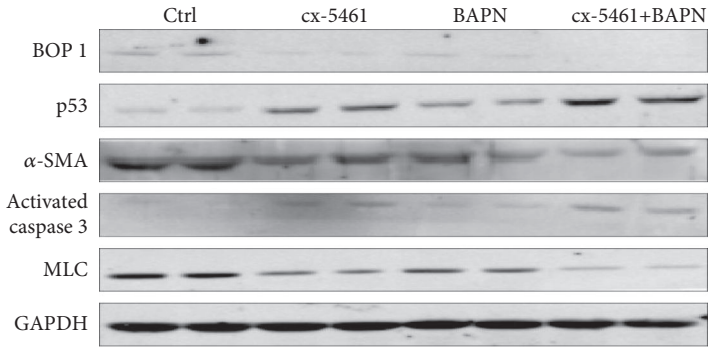

(e)

Figure 5: Inhibition of RNA polymerase I by cx-5461 accelerated AD in mice. (a) Representative images of gross aortic samples are shown. (b) The life-span of each mouse was recorded. Kaplan-Meier survival curve is shown. (c) Representative staining of aorta sections with HE, Masson, and EVG. Graphs show semiquantification of elastic fibre broken grade and collagen/muscle fibre ratio. (d) Representative images of the aortas performed with TUNEL assays, IHC staining with anti-BOP1 antibody and anti-ki-67 antibody. The positive rate is shown (right panels). (e) Western blotting was performed to detect the BOP1, p53, activated caspase 3, α-SMA, and MLC expression of the aortas. Data are presented as mean ± SD. $^{*}P < 0.05$, $^{**}P < 0.01$, and $^{***}P < 0.001$ determined by *one-way ANOVA*.

AD model (Figure 6(e); Fig. S3). Consistent with the results of TUNEL assay, activated caspase 3 levels were decreased in the aortic samples of p53-/- AD mice (Figure 6(f)).

In total, we conceived a possible mechanism that was shown as a diagram (Figure 7). Stress such as hypoxia that probably affects the RNA polymerase I or rRNA processing will result in the decrease of ribosome biosynthesis. In that case, the crucial proteins related to the muscle contraction were decreased. The decrease of "contractile unit" will lead to the impairment of the aortic wall. These abnormal ASMCs cannot fulfill its biological effects of antagonizing blood flow impact. Upon stimulation by the blood pressure, the impaired ASMCs would increase ROS production and trigger p53-dependent apoptosis process. That might be one of the possible mechanisms that underline the AD.

4. Discussion

Under physiological conditions, the ASMCs need to constantly synthesize contractile proteins in order to maintain the stability of the aortic wall and cope with the powerful impact of blood flow [5]. The elastin-contractile unit is a functional and structural unit in the aortic media, which provides a direct connection between the ASMCs and the elastic fibres. The contractile unit in ASMCs is composed of thin filaments and thick filaments. The thick filament is composed of a smooth muscle-specific isoform of myosin heavy chain dimer (SM-MHC; encoded by MYH11) and four light chains (MLC), two regulatory light chains and two essential light chains. The thin filament is aggregated by α-SMA. Any reason that result in a decrease of contractile unit or its function will destroy the stability of the aortic wall [28]. In thoracic AD patients, over 60% of the DNA in ASMCs is hypermethylated indicating lower transcriptional activity and protein translation [29]. The number of ribosomes in a cell is closely related to its protein output, and ribosomal biogenesis and function can be disrupted by deregulated BOP1 expression [30], as well as inhibition of DNA methyltransferase activity [31]. BOP1 was significantly decreased in the aortic tissues of AD patients, and its knockdown in HASMCs impaired cell motility and decreased protein synthesis, as well as the expression of contraction-related proteins like α-SMA and MLC. This result is consistent with the higher susceptibility of individuals harbouring mutations in contraction-associated genes to AD [28, 32].

The phenotypic modulation of ASMCs from stable contractile cells to secretary proliferative cells is the major underlying mechanism of AMD [33, 34]. Microarrays of aortic tissues from AD patients (GEO: GSE52093) indicated increased expression of Ki-67 and PCNA [35, 36]. Contradictory to this observation, however, ASMC numbers generally decrease instead of increasing during AD [37, 38], which could be related to the higher apoptosis rates [39]. In our study, overexpressing BOP1 in HASMCs inhibited proliferation. This is consistent with the findings of Bornkamm et al. who showed that BOP1 expression alone cannot contribute to a fully functional PeBoW complex [40]. Interestingly, serum-free and hypoxic conditions downregulated BOP1 in a time-dependent manner and induced apoptosis, while overexpression of BOP1 inhibited this hypoxia-induced apoptosis and decreased contractile protein levels. Unlike Pes1 and WDR12, the two other proteins of the PeBoW complex, BOP1 has a short half-life on account of its extremely high PEST domain (common peptide motif of rapidly degrading proteins) score of 15.6 [41, 42]. Also, unlike its companion proteins, the expression of BOP1 in colon cancer cells is independent of c-myc activity [14]. Therefore, we hypothesize that the persistently high expression of exogenous BOP1 under hypoxic conditions may compensate for the PeBoW dysfunction caused by the rapid degradation of endogenous BOP1.

In order to impair ribosomal renewal in ASMCs *in vivo*, we treated the AD mice with cx-5461, an inhibitor of rRNA Pol I [43]. cx-5461 accelerated the occurrence of AD, inhibited the proliferation of ASMCs, and induced apoptosis. In a recent study, Ye et al. reported that cx-5461 prevented aortic intima hyperplasia, indicating its clinical potential against atherosclerosis and stenosis [44]. In contrast to our study,

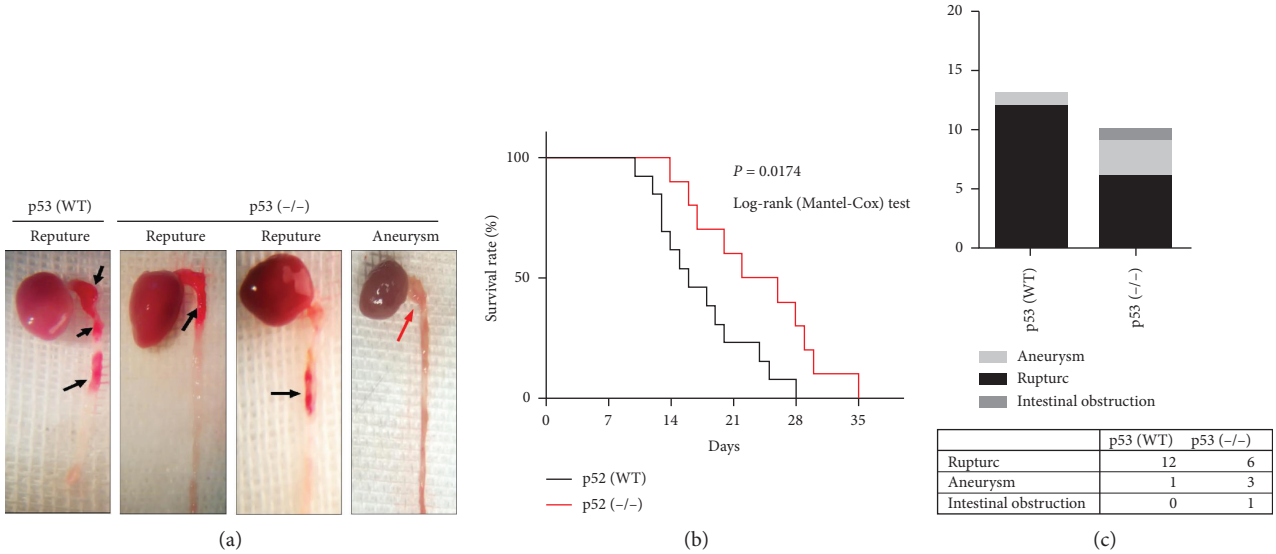

	p53 (WT)	p53 (−/−)
Rupturc	12	6
Aneurysm	1	3
Intestinal obstruction	0	1

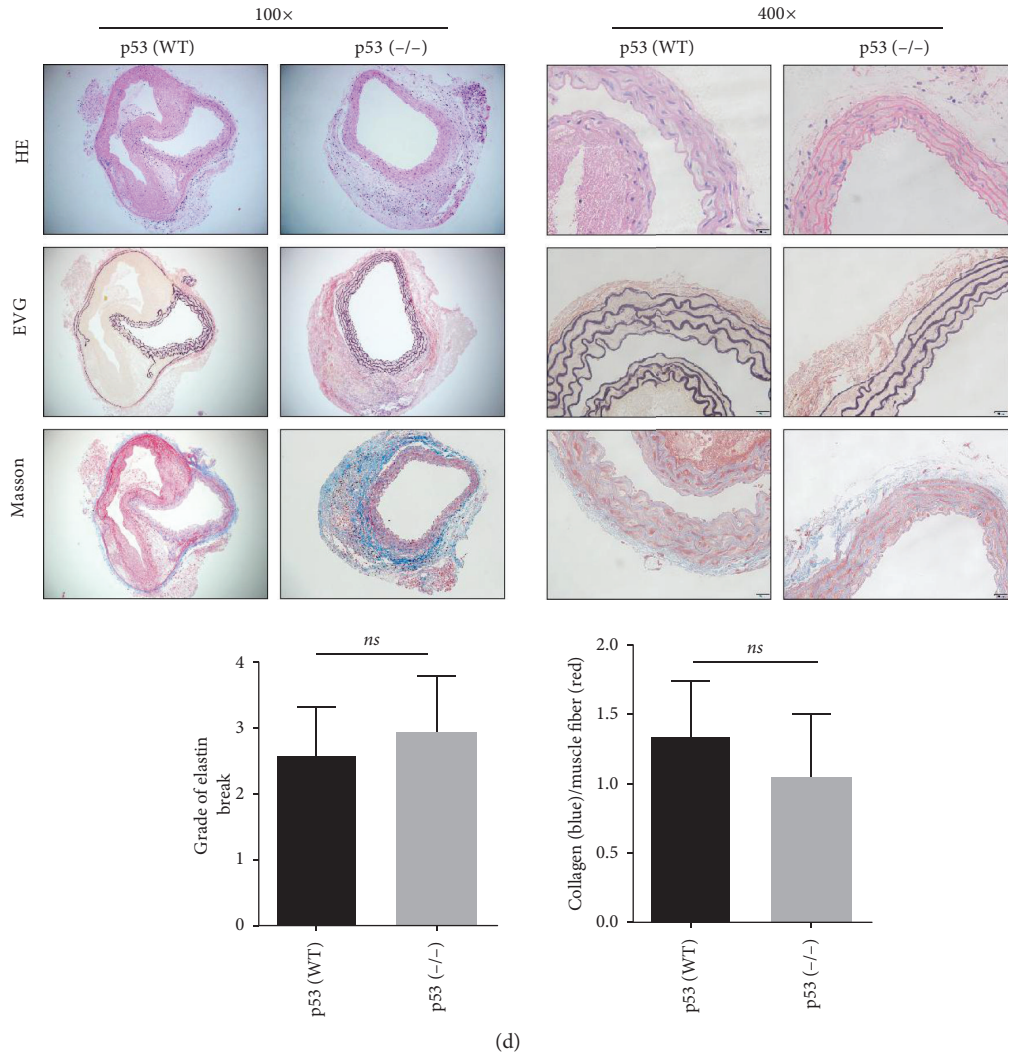

Figure 6: Continued.

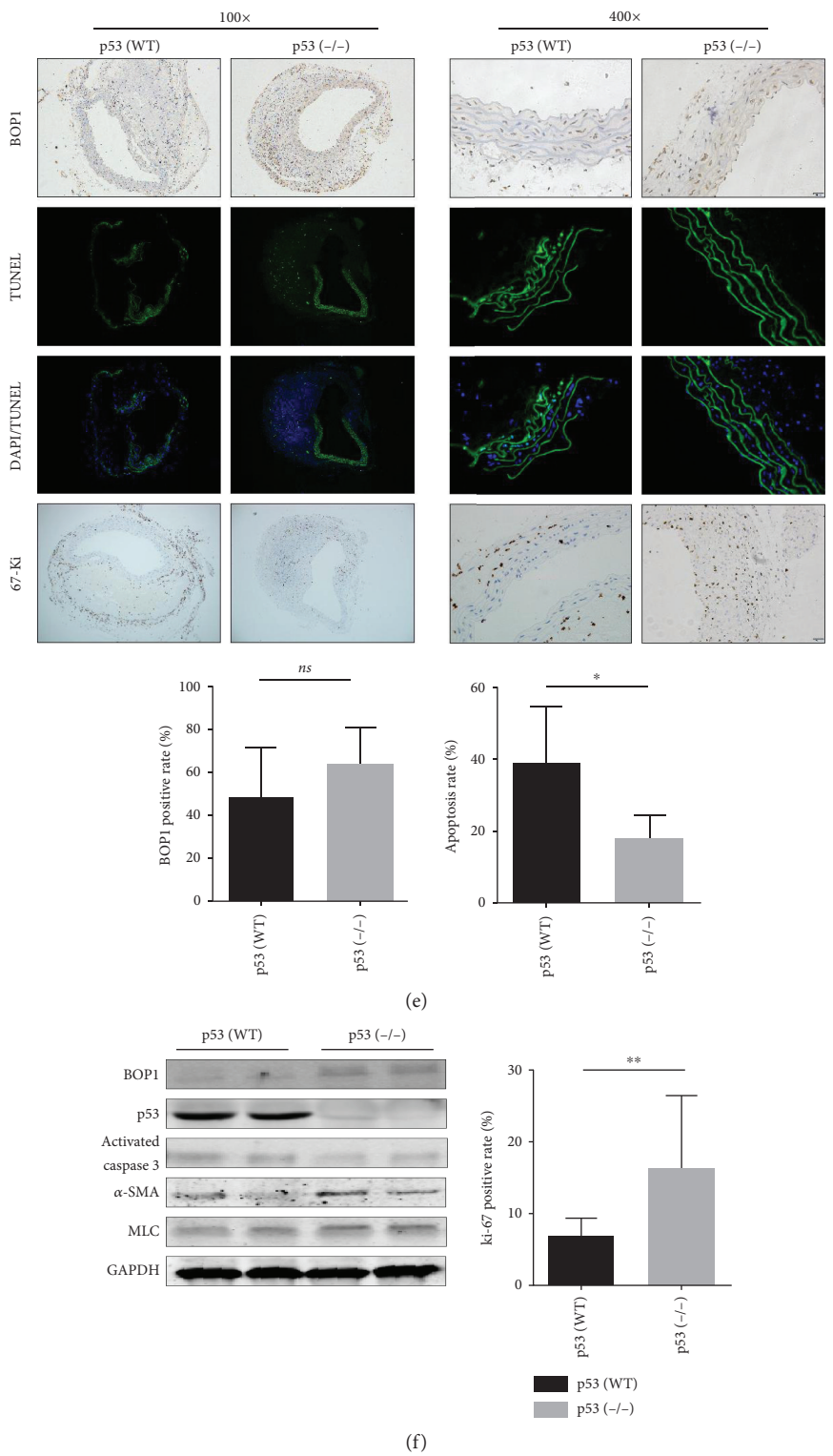

Figure 6: Knockout of p53 reduced the occurrence of AD in mice. (a) Representative images of gross aortic samples are shown. (b) Kaplan-Meier survival curve is shown. (c) The death reason is summarized and shown. (d) Representative staining of aorta sections with HE, Masson, and EVG. Graphs show semiquantification of elastic fibre broken grade and collagen/muscle fibre ratio. (e) Representative images of the aortas performed with TUNEL assays, IHC staining with anti-BOP1 antibody and anti-ki-67 antibody. The positive rate is shown (right panels). (f) Western blotting was performed to detect the BOP1, p53, activated caspase 3, α-SMA, and MLC expression of the aortas. Data are presented as mean ± SD; *ns*: no statistical significance; $^{*}P < 0.05$, $^{**}P < 0.01$, and $^{***}P < 0.001$ determined by *one-way ANOVA*.

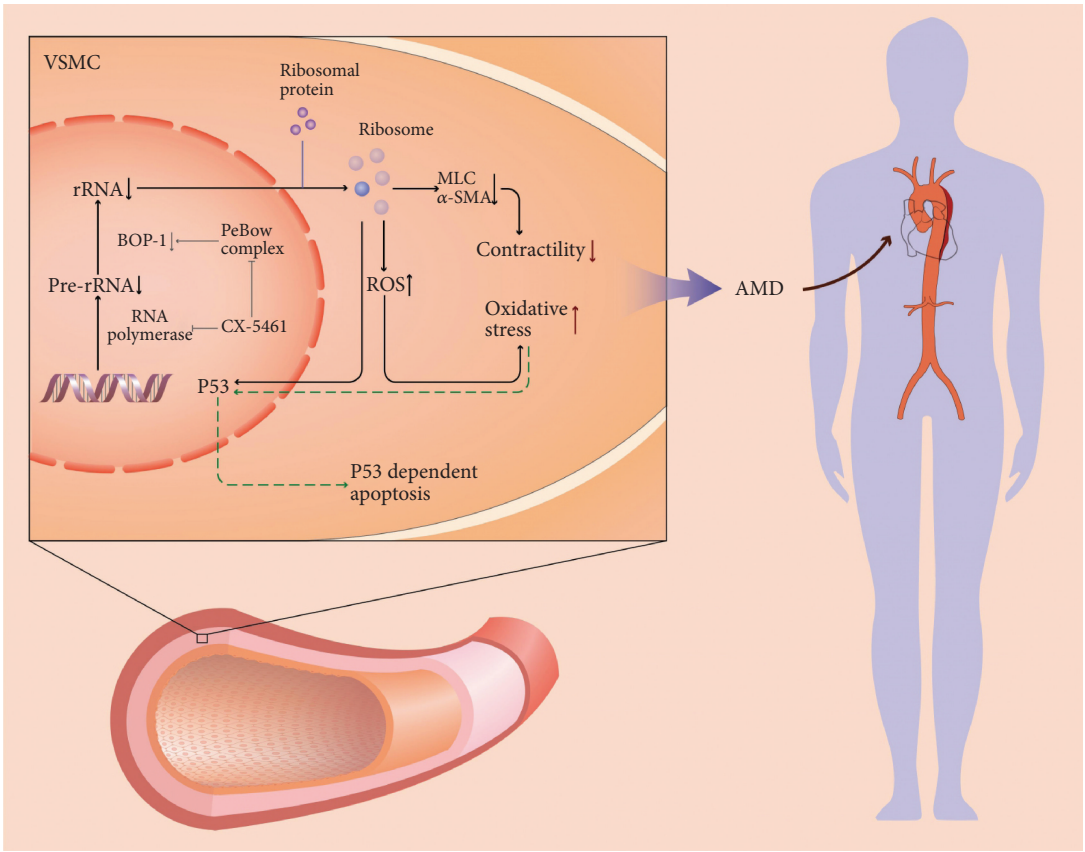

Figure 7: Schematic diagram of the mechanisms of p53-dependent apoptosis and proliferative inhibition in the regulation of abnormal ribosome biogenesis in ASMCs. Stress such as hypoxia that probably affects the RNA polymerase I or rRNA processing will result in the decrease of ribosome biosynthesis. In that case, the crucial proteins related to the muscle contraction were decreased. The decrease of "contractile unit" will lead to the impairment of the aortic wall. These abnormal ASMCs cannot fulfill its biological effects of antagonizing blood flow impact. Upon stimulation by the blood pressure, the impaired ASMCs would increase ROS production and trigger p53-dependent apoptosis process.

however, they showed that cx-5461 only inhibited ASMC proliferation and did not induce apoptosis [43]. Nevertheless, other reports have suggested that cx-5461 is capable of inducing tumor cell apoptosis [45–47]. The different results could be due to the different animal models used in these studies. We induced AD using BAPN, which inhibits the cross-linking of elastic fibres and weakens the structural toughness of the aorta [48]. This in turn results in severe stress on the ASMCs from the blood flow, leading to cellular degeneration and apoptosis.

The cell cycle arrest and apoptosis caused by ribosomal dysregulation are closely related to p53 [46, 47, 49], which is consistent with our results. Depletion of p53 by PFTα partially rescued the cx-5461-induced apoptosis *in vitro*. There are two possible mechanisms that can explain the association between p53 and ribosomal dysfunction. First, the reduction in rRNAs impairs ribosomal assembly, leading to an increase in free ribosomal proteins like ribosomal protein L (RPL) 11, RPL5, and RPL23, which can bind directly to MDM2 [50, 51]. This impedes MDM2-mediated ubiquitination of p53, resulting in apoptosis. The second model considers the mature ribosome as a "truck" that can transport the MDM2-p53 complex out of the nucleus for further degradation [52]. If the number of "trucks" is reduced, p53 accumulates in the nucleus and triggers its downstream proapoptotic signaling. To confirm whether p53-dependent apoptosis is the major cause of ASMC loss in AD, we established the AD model in p53-/- mice. As expected, the p53-/- AD mice survived longer and had lower rates of AD compared to the p53+/+ mice, possibly on account of enhanced proliferation and reduced apoptosis in the ASMCs.

However, knocking out p53 did not alleviate collagen accumulation and elastin breakdown *in vivo*. Almost all the mice that were fed with the BAPN diet eventually died. The AD animal model used in this study was different to the angiotensin II base mouse AD model, which was conducted by the pumping of angiotensin II in ApoE(-/-) mouse. BAPN inhibits cross-linking of elastic fibres and impairs the vascular structure, which increases the susceptibility of the ASMCs to vascular pressure. Furthermore, the structural impairment of elastic fibres decreases the anchoring of the transforming growth factor- (TGF-) β1 and suppresses TGF-β1 signaling in the ASMCs [53]. All these factors ultimately destroy the aorta and cause rapid death.

One limitation of our study was the imbalance in the age and gender distribution between the AD patients and donors,

with significantly younger individuals and more males among the latter. The age bias was due to the fact that brain dead patients over the age of 50 are not considered as organ donors in China, and the gender bias is due to the fact that most organ donors are men. Another shortcoming of this study was that the effect of cx-5461 on p53-/- AD mice could not be evaluated due to the extremely low proportion (2-3%) of the p53-/- offspring produced by crossing p53+/- mice, a phenomenon consistent with Jackson Laboratory's description.

In conclusion, impaired ribosome biogenesis in the ASMCs accelerates cellular loss and leads to AD, a phenomenon that can be attenuated by p53 suppression. Ribosome biogenesis is under investigation as a novel target to treat cancer and intima hyperplasia. In light of our findings, however, the side-effects of targeting ribosome biogenesis and function, especially in patients with high risk of AD, should be strongly considered.

Data Availability

The data used to support the findings of this study are available from the corresponding author upon request.

Conflicts of Interest

There were no potential conflicts of interest to be disclosed.

Authors' Contributions

Qi Wu and Junmou Hong contributed equally to this work.

Acknowledgments

This work was supported by the National Natural Science Foundation of China (Grant No. 81570428 and Grant No. 81600367).

Supplementary Materials

Fig. S1: PFTα inhibited superoxide production induced by cx-5461. HASMCs were pretreated with or without PFTα (10 μM) for 12 h, followed by treatment of cx-5461 (1 μM) for 24 h. The dihydroethidium (DHE) staining was used to detect ROS production (red). Fig. S2: inhibition of RNA polymerase I by cx-5461 promoted the accumulation of ROS in mouse AD model. The 8-OHdG level in mouse aortic medial tissues was detected by performing immunofluorescence and the representative images were shown. Scale bar 200 μm. Fig. S3: knockout of p53 decreased the ROS accumulation in mouse AD model. The 8-OHdG level in mouse aortic medial tissues was detected by performing immunofluorescence and the representative images were shown. Scale bar 200 μm. *(Supplementary Materials)*

References

[1] R. Erbel, V. Aboyans, C. Boileau et al., "2014 ESC guidelines on the diagnosis and treatment of aortic diseases: document covering acute and chronic aortic diseases of the thoracic and abdominal aorta of the adult. The Task Force for the Diagnosis and Treatment of Aortic Diseases of the European Society of Cardiology (ESC)," *European Heart Journal*, vol. 35, no. 41, pp. 2873–2926, 2014.

[2] U. K. A. Sampson, P. E. Norman, F. G. R. Fowkes et al., "Global and regional burden of aortic dissection and aneurysms: mortality trends in 21 world regions, 1990 to 2010," *Global Heart*, vol. 9, no. 1, pp. 171–180.e10, 2014.

[3] S. Durdu, G. C. Deniz, D. Balci et al., "Apoptotic vascular smooth muscle cell depletion via BCL2 family of proteins in human ascending aortic aneurysm and dissection," *Cardiovascular Therapy*, vol. 30, no. 6, pp. 308–316, 2012.

[4] H. Osada, M. Kyogoku, T. Matsuo, and N. Kanemitsu, "Histopathological evaluation of aortic dissection: a comparison of congenital versus acquired aortic wall weakness," *Interactive CardioVascular and Thoracic Surgery*, vol. 27, no. 2, pp. 277–283, 2018.

[5] L. M. Holdt, A. Stahringer, K. Sass et al., "Circular non-coding *RNA ANRIL* modulates ribosomal *RNA* maturation and atherosclerosis in humans," *Nature Communications*, vol. 7, no. 1, article 12429, 2016.

[6] P. Bernabò, T. Tebaldi, E. J. N. Groen et al., "*In vivo* translatome profiling in spinal muscular atrophy reveals a role for SMN protein in ribosome biology," *Cell Reports*, vol. 21, no. 4, pp. 953–965, 2017.

[7] M. Marabita, M. Baraldo, F. Solagna et al., "S6K1 is required for increasing skeletal muscle force during hypertrophy," *Cell Reports*, vol. 17, no. 2, pp. 501–513, 2016.

[8] J. J. Fyfe, D. J. Bishop, J. D. Bartlett et al., "Enhanced skeletal muscle ribosome biogenesis, yet attenuated mTORC1 and ribosome biogenesis-related signalling, following short-term concurrent versus single-mode resistance training," *Scientific Reports*, vol. 8, no. 1, p. 560, 2018.

[9] T. Chaillou, T. J. Kirby, and J. J. McCarthy, "Ribosome biogenesis: emerging evidence for a central role in the regulation of skeletal muscle mass," *Journal of Cellular Physiology*, vol. 229, no. 11, pp. 1584–1594, 2014.

[10] M. Hölzel, M. Rohrmoser, M. Schlee et al., "Mammalian WDR12 is a novel member of the Pes1–Bop1 complex and is required for ribosome biogenesis and cell proliferation," *Journal of Cell Biology*, vol. 170, no. 3, pp. 367–378, 2005.

[11] K. Y. Chung, I. K. C. Cheng, A. K. K. Ching, J. H. Chu, P. B. S. Lai, and N. Wong, "Block of proliferation 1 (BOP1) plays an oncogenic role in hepatocellular carcinoma by promoting epithelial-to-mesenchymal transition," *Hepatology*, vol. 54, no. 1, pp. 307–318, 2011.

[12] J. Qi, Y. Yu, Ö. Akilli Öztürk et al., "New Wnt/β-catenin target genes promote experimental metastasis and migration of colorectal cancer cells through different signals," *Gut*, vol. 65, no. 10, pp. 1690–1701, 2016.

[13] M. Rohrmoser, M. Holzel, T. Grimm et al., "Interdependence of Pes1, Bop1, and WDR12 controls nucleolar localization and assembly of the PeBoW complex required for maturation of the 60S ribosomal subunit," *Molecular and Cell Biology*, vol. 27, no. 10, pp. 3682–3694, 2007.

[14] A. Killian, N. Sarafan-Vasseur, R. Sesboüé et al., "Contribution of the BOP1 gene, located on 8q24, to colorectal tumorigenesis," *Genes Chromosomes Cancer*, vol. 45, no. 9, pp. 874–881, 2006.

[15] R. Liu, V. Iadevaia, J. Averous, P. M. Taylor, Z. Zhang, and C. G. Proud, "Impairing the production of ribosomal RNA

activates mammalian target of rapamycin complex 1 signalling and downstream translation factors," *Nucleic Acids Research*, vol. 42, no. 8, pp. 5083–5096, 2014.

[16] T. Grimm, M. Hölzel, M. Rohrmoser et al., "Dominant-negative Pes1 mutants inhibit ribosomal RNA processing and cell proliferation via incorporation into the PeBoW-complex," *Nucleic Acids Research*, vol. 34, no. 10, pp. 3030–3043, 2006.

[17] B. Gong, Z. Wang, M. Zhang et al., "Disturbed P53-MDM2 feedback loop contributes to thoracic aortic dissection formation and may be a result of TRIM25 overexpression," *Annals of Vascular Surgery*, vol. 40, pp. 243–251, 2017.

[18] T. Kurihara, R. Shimizu-Hirota, M. Shimoda et al., "Neutrophil-derived matrix metalloproteinase 9 triggers acute aortic dissection," *Circulation*, vol. 126, no. 25, pp. 3070–3080, 2012.

[19] R. J. Rebello, E. Kusnadi, D. P. Cameron et al., "The dual inhibition of RNA Pol I transcription and PIM kinase as a new therapeutic approach to treat advanced prostate cancer," *Clinical Cancer Research*, vol. 22, no. 22, pp. 5539–5552, 2016.

[20] Z. Wang, Z. Ren, Z. Hu et al., "Angiotensin-II induces phosphorylation of ERK1/2 and promotes aortic adventitial fibroblasts differentiating into myofibroblasts during aortic dissection formation," *Journal of Molecular Histology*, vol. 45, no. 4, pp. 401–412, 2014.

[21] R. Hu, Z. Wang, Z. Ren, and M. Liu, "Autonomic remodeling may be responsible for decreased incidence of aortic dissection in STZ-induced diabetic rats via down-regulation of matrix metalloprotease 2," *BMC Cardiovascular Disorders*, vol. 16, no. 1, p. 200, 2016.

[22] W. Jiang, Z. Wang, Z. Hu et al., "Highly expressed S100A12 in aortic wall of patients with DeBakey type I aortic dissection could be a promising marker to predict perioperative complications," *Annals of Vascular Surgery*, vol. 28, no. 6, pp. 1556–1562, 2014.

[23] V. Deckert, B. Kretz, A. Habbout et al., "Development of abdominal aortic aneurysm is decreased in mice with plasma phospholipid transfer protein deficiency," *The American Journal of Pathology*, vol. 183, no. 3, pp. 975–986, 2013.

[24] K. Takeda, K. Uchiyama, M. Kinukawa, T. Tagami, M. Kaneda, and S. Watanabe, "Evaluation of sperm DNA damage in bulls by TUNEL assay as a parameter of semen quality," *Journal of Reproduction and Development*, vol. 61, no. 3, pp. 185–190, 2015.

[25] J. Liu, Y. Xu, D. Stoleru, and A. Salic, "Imaging protein synthesis in cells and tissues with an alkyne analog of puromycin," *Proceedings of the National Academy of Sciences of the United States of America*, vol. 109, no. 2, pp. 413–418, 2012.

[26] E. K. Schmidt, G. Clavarino, M. Ceppi, and P. Pierre, "SUnSET, a nonradioactive method to monitor protein synthesis," *Nature Methods*, vol. 6, no. 4, pp. 275–277, 2009.

[27] K.-C. Chan, C.-J. Wang, H.-H. Ho, H.-M. Chen, and C.-N. Huang, "Simvastatin inhibits cell cycle progression in glucose-stimulated proliferation of aortic vascular smooth muscle cells by up-regulating cyclin dependent kinase inhibitors and p53," *Pharmacological Research*, vol. 58, no. 3-4, pp. 247–256, 2008.

[28] D. M. Milewicz, K. M. Trybus, D. C. Guo et al., "Altered smooth muscle cell force generation as a driver of thoracic aortic aneurysms and dissections," *Arteriosclerosis, Thrombosis, and Vascular Biology*, vol. 37, no. 1, pp. 26–34, 2017.

[29] S. Pan, H. Lai, Y. Shen et al., "DNA methylome analysis reveals distinct epigenetic patterns of ascending aortic dissection and bicuspid aortic valve," *Cardiovascular Research*, vol. 113, no. 6, pp. 692–704, 2017.

[30] C. S. Ahn, H. K. Cho, D. H. Lee, H. J. Sim, S. G. Kim, and H. S. Pai, "Functional characterization of the ribosome biogenesis factors PES, BOP1, and WDR12 (PeBoW), and mechanisms of defective cell growth and proliferation caused by PeBoW deficiency in Arabidopsis," *Journal of Experimental Botany*, vol. 67, no. 17, pp. 5217–5232, 2016.

[31] T. Moss, "DNA methyltransferase inhibition may limit cancer cell growth by disrupting ribosome biogenesis," *Epigenetics*, vol. 6, no. 2, pp. 128–133, 2011.

[32] Y. H. Shen and S. A. LeMaire, "Molecular pathogenesis of genetic and sporadic aortic aneurysms and dissections," *Current Problems in Surgery*, vol. 54, no. 3, pp. 95–155, 2017.

[33] J. Huang, T. Wang, A. C. Wright et al., "Myocardin is required for maintenance of vascular and visceral smooth muscle homeostasis during postnatal development," *Proceedings of the National Academy of Sciences of the United States of America*, vol. 112, no. 14, pp. 4447–4452, 2015.

[34] J. Huang, L. Cheng, J. Li et al., "Myocardin regulates expression of contractile genes in smooth muscle cells and is required for closure of the ductus arteriosus in mice," *The Journal of Clinical Investigation*, vol. 118, no. 2, pp. 515–525, 2008.

[35] S. Pan, D. Wu, A. E. Teschendorff et al., "JAK2-centered interactome hotspot identified by an integrative network algorithm in acute Stanford type A aortic dissection," *PLoS One*, vol. 9, no. 2, article e89406, 2014.

[36] D. W. Huang, B. T. Sherman, and R. A. Lempicki, "Systematic and integrative analysis of large gene lists using DAVID bioinformatics resources," *Nature Protocols*, vol. 4, no. 1, pp. 44–57, 2009.

[37] D. Wu, Y. H. Shen, L. Russell, J. S. Coselli, and S. A. LeMaire, "Molecular mechanisms of thoracic aortic dissection," *Journal of Surgical Research*, vol. 184, no. 2, pp. 907–924, 2013.

[38] N. Grewal and A. C. Gittenberger-de Groot, "Pathogenesis of aortic wall complications in Marfan syndrome," *Cardiovascular Pathology*, vol. 33, pp. 62–69, 2018.

[39] L. X. Jia, W. M. Zhang, H. J. Zhang et al., "Mechanical stretch-induced endoplasmic reticulum stress, apoptosis and inflammation contribute to thoracic aortic aneurysm and dissection," *The Journal of Pathology*, vol. 236, no. 3, pp. 373–383, 2015.

[40] G. W. Bornkamm, C. Berens, C. Kuklik-Roos et al., "Stringent doxycycline-dependent control of gene activities using an episomal one-vector system," *Nucleic Acids Research*, vol. 33, no. 16, p. e137, 2005.

[41] S. Rogers, R. Wells, and M. Rechsteiner, "Amino acid sequences common to rapidly degraded proteins: the PEST hypothesis," *Science*, vol. 234, no. 4774, pp. 364–368, 1986.

[42] M. L. Spencer, M. Theodosiou, and D. J. Noonan, "NPDC-1, a novel regulator of neuronal proliferation, is degraded by the ubiquitin/proteasome system through a PEST degradation motif," *Journal of Biological Chemistry*, vol. 279, no. 35, pp. 37069–37078, 2004.

[43] D. Drygin, A. Lin, J. Bliesath et al., "Targeting RNA polymerase I with an oral small molecule CX-5461 inhibits ribosomal RNA synthesis and solid tumor growth," *Cancer Research*, vol. 71, no. 4, pp. 1418–1430, 2011.

[44] Q. Ye, S. Pang, W. Zhang et al., "Therapeutic targeting of RNA polymerase I with the small-molecule CX-5461 for prevention of arterial injury–induced neointimal hyperplasia,"

Arteriosclerosis, Thrombosis, and Vascular Biology, vol. 37, no. 3, pp. 476–484, 2017.

[45] G. Li, J. Shen, J. Cao et al., "Alternative splicing of human telomerase reverse transcriptase in gliomas and its modulation mediated by CX-5461," *Journal of Experimental & Clinical Cancer Research*, vol. 37, no. 1, p. 78, 2018.

[46] H. C. Lee, H. Wang, V. Baladandayuthapani et al., "RNA polymerase I inhibition with CX-5461 as a novel therapeutic strategy to target MYC in multiple myeloma," *British Journal of Haematology*, vol. 177, no. 1, pp. 80–94, 2017.

[47] S. S. Negi and P. Brown, "rRNA synthesis inhibitor, CX-5461, activates ATM/ATR pathway in acute lymphoblastic leukemia, arrests cells in G2 phase and induces apoptosis," *Oncotarget*, vol. 6, no. 20, pp. 18094–18104, 2015.

[48] L. Zhang, Y. F. Pei, L. Wang et al., "Dramatic decrease of aortic longitudinal elastic strength in a rat model of aortic dissection," *Annals of Vascular Surgery*, vol. 26, no. 7, pp. 996–1001, 2012.

[49] J. Quin, K. T. Chan, J. R. Devlin et al., "Inhibition of RNA polymerase I transcription initiation by CX-5461 activates non-canonical ATM/ATR signaling," *Oncotarget*, vol. 7, no. 31, pp. 49800–49818, 2016.

[50] M. S. Dai and H. Lu, "Inhibition of MDM2-mediated p53 ubiquitination and degradation by ribosomal protein L5," *Journal of Biological Chemistry*, vol. 279, no. 43, pp. 44475–44482, 2004.

[51] K. Nishimura, T. Kumazawa, T. Kuroda et al., "Perturbation of ribosome biogenesis drives cells into senescence through 5S RNP-mediated p53 activation," *Cell Reports*, vol. 10, no. 8, pp. 1310–1323, 2015.

[52] C. J. Sherr and J. D. Weber, "The ARF/p53 pathway," *Current Opinion in Genetics & Development*, vol. 10, no. 1, pp. 94–99, 2000.

[53] V. Barry-Hamilton, R. Spangler, D. Marshall et al., "Allosteric inhibition of lysyl oxidase–like-2 impedes the development of a pathologic microenvironment," *Nature Medicine*, vol. 16, no. 9, pp. 1009–1017, 2010.

Hindawi
Oxidative Medicine and Cellular Longevity
Volume 2019, Article ID 8219283, 14 pages
https://doi.org/10.1155/2019/8219283

Research Article

Evidence of Blood and Muscle Redox Status Imbalance in Experimentally Induced Renal Insufficiency in a Rabbit Model

Konstantina P. Poulianiti,[1,2] Aggeliki Karioti,[1] Antonia Kaltsatou,[1] Georgia I. Mitrou,[1,3] Yiannis Koutedakis,[2,4,5] Konstantinos Tepetes,[6] Grigoris Christodoulidis,[6] Giannis Giakas,[2,4] Maria D. Maridaki,[7] Ioannis Stefanidis,[8] Athanasios Z. Jamurtas,[2,4] Giorgos K. Sakkas,[1,3,4] and Christina Karatzaferi[1,3,4]

[1]*Muscle Physiology & Mechanics Group, CREHP, DPESS, University of Thessaly, Trikala 42100, Greece*
[2]*Human Performance Group, CREHP, DPESS, University of Thessaly, Trikala 42100, Greece*
[3]*EMIP/EmPOWER, School of Health Sciences, Plymouth Marjon University, Plymouth PL6 8BH, UK*
[4]*Institute for Research and Technology-CERTH, Thessaly, Trikala 42100, Greece*
[5]*School of Sports, Performing Arts & Leisure, University of Wolverhampton, Wolverhampton WV1 1LY, UK*
[6]*Department of Surgery, School of Medicine, University of Thessaly, Larissa 41110, Greece*
[7]*DPESS, National and Kapodistrian University of Athens, Athens 17237, Daphne, Greece*
[8]*Department of Nephrology, School of Medicine, University of Thessaly, Larissa 41110, Greece*

Correspondence should be addressed to Christina Karatzaferi; karatzaferi.c@gmail.com

Received 19 October 2018; Revised 20 February 2019; Accepted 28 February 2019; Published 4 April 2019

Academic Editor: Fernanda Amicarelli

Chronic kidney disease (CKD) is accompanied by a disturbed redox homeostasis, especially in end-stage patients, which is associated with pathological complications such as anemia, atherosclerosis, and muscle atrophy. However, limited evidence exists about redox disturbances before the end stage of CKD. Moreover, the available redox literature has not yet provided clear associations between circulating and tissue-specific (muscle) oxidative stress levels. The aim of the study was to evaluate commonly used redox status indices in the blood and in two different types of skeletal muscle (psoas, soleus) in the predialysis stages of CKD, using an animal model of renal insufficiency, and to investigate whether blood redox status indices could be reflecting the skeletal muscle redox status. Indices evaluated included reduced glutathione (GSH), oxidized glutathione (GSSG), glutathione reductase (GR), catalase (CAT), total antioxidant capacity (TAC), protein carbonyls (PC), and thiobarbituric acid reactive substances (TBARS). Results showed that blood GSH was higher in the uremic group compared to the control (17.50 ± 1.73 vs. 12.43 ± 1.01, $p = 0.033$). In both muscle types, PC levels were higher in the uremic group compared to the control (psoas: 1.086 ± 0.294 vs. 0.596 ± 0.372, soleus: 2.52 ± 0.29 vs. 0.929 ± 0.41, $p < 0.05$). The soleus had higher levels of TBARS, PC, GSH, CAT, and GR and lower TAC compared to the psoas in both groups. No significant correlations in redox status indices between the blood and skeletal muscles were found. However, in the uremic group, significant correlations between the psoas and soleus muscles in PC, GSSG, and CAT levels emerged, not present in the control. Even in the early stages of CKD, a disturbance in redox homeostasis was observed, which seemed to be muscle type-specific, while blood levels of redox indices did not seem to reflect the intramuscular condition. The above results highlight the need for further research in order to identify the key mechanisms driving the onset and progression of oxidative stress and its detrimental effects on CKD patients.

1. Introduction

Redox homeostasis encompasses the balance between oxidants (or prooxidants) and antioxidants and is maintained by several complex mechanisms. Redox homeostasis can be disrupted due to a dysfunction of any of these mechanisms, resulting in reactive oxygen species (ROS) and/or reactive nitrogen species (RNS) levels and/or a decreased scavenging

capacity, a condition which is described as oxidative stress [1]. ROS, which will form the focus of this work, are highly reactive to proteins, membrane lipids, carbohydrates, and nucleic acids, causing irreversible damage which can affect cell survival and lead to degenerative disorders, disease, and aging [2].

Chronic kidney disease is accompanied by enhanced oxidative stress, which in turn is associated with higher risk of developing cardiovascular disease (CVD), leading to high rates of morbidity and mortality [3, 4]. Moreover, a redox imbalance in CKD is linked to pathological complications such as anemia, inflammation, malnutrition and atherosclerosis, fatigue, muscle wasting, and disuse atrophy [5–7].

Although the harmful effects of oxidative stress have been associated with the progression of CKD, its role during the different stages of the disease has not yet, been fully clarified. The majority of the existing data refer to outcomes from the advanced stages of the disease and mostly to patients undergoing hemodialysis (HD) therapy. In HD patients, four main factors have been proposed to be responsible for the redox imbalance: the uremic milieu, the HD treatment *per se*, the hemoincompatibility of dialysis system, and the concomitant drug treatment [8]. However, possible changes in redox homeostasis during the predialysis stages of CKD have not been investigated extensively probably due to the fact that CKD is "silent" at its early stages. Moreover, patients may progress to renal insufficiency as a secondary outcome of variable primary conditions, from hypertension, diabetes, nephrotic syndrome, etc. [9], conditions where monitoring oxidative stress does not figure as yet as priority of care due to insufficient evidence for clinical relevance [10]. Oxidative stress in predialysis CKD can be attributed to the cytotoxic effects of the progressive loss of renal function as well as insufficient antioxidant defense [11]. Several mechanisms link CKD and oxidative stress, such as uremic toxin-induced endothelial nitric oxide synthase (eNOS) uncoupling [12] and increased nicotinamide adenine dinucleotide phosphate-oxidases (NADPH oxidases (NOX)) activity [13]. Additionally, an emerging antioxidant deficit has been attributed mainly to dietary restrictions, diuretics use, protein energy wasting, and/or decreased intestinal absorption [14, 15].

As renal insufficiency progresses, it is also accompanied by muscular weakness and wasting, exercise intolerance, and premature fatigue, characteristics which are collectively termed as uremic myopathy [16]. Several studies have indicated that CKD is also characterized by modifications of muscle bioenergetics which also contribute to a reduction in muscle performance [17–20]. Hemodialysis treatment and/or uremia *per se* contributes to an increase in molecular oxidative damage which in turn can contribute in the deterioration of skeletal muscle functionality. This is because animal studies have shown that experimentally induced oxidative stress causes myofibrillar protein modification that promotes degradation free radical oxidation [21–23]. Moreover, the susceptibility of skeletal muscle to ROS may be differentiated depending on muscle type (fast vs. slow) [24], nutrition [25], and lifestyle habits [26]. This and other evidence collectively suggest that skeletal muscle can become extremely susceptible to degradation due to the combined effects of uremia and redox disturbances.

The aim of the current study was to evaluate possible redox disturbances in the predialysis stages of CKD, using an animal model of renal insufficiency. More specifically, we evaluated redox status indices not only in the blood but also in two different types of skeletal muscle, the fast-twitch/glycolytic psoas and the slow-twitch/oxidative soleus from the same animal donor. We also examined whether blood redox status indices could be reflecting the skeletal muscle redox status.

2. Material and Methods

2.1. Animal Model. The uremic model was based on surgical protocol modified from Gotloib et al., [22] using sham operation for the control group. All animal procedures, including surgery and euthanasia, were approved by the ethics committee of the University of Thessaly (decision 2-2/10-10-2012 and 914/10-11-2014) and the scientific committee of the University Hospital of Larisa, Greece (decision 1/4-1-2012). Animals were under veterinary care, in accordance with the National and European guidelines for the care and use of laboratory animals (EU Directive 2010/63/EU for animal experiments).

New Zealand white rabbits (female, $N = 15$) were first acclimatized to the laboratory animal unit of Medical School (University of Thessaly, Greece) for 48 hours. All animals were 5-6 months old and weighted approximately 2600 g. The animals were housed in a controlled environment with stable conditions of room temperature (RT) (22–24°C) and lighting (12 : 12 h light-dark cycle). All rabbits were fed with the same special rabbit chow containing low levels of protein (78.8 g casein "protein" per kg diet), potassium, calcium, phosphorus, and sodium (prepared by Research Diets Inc., USA; formulation code: D07122101). This was decided because key biomarkers (e.g., GSH levels) can be affected by diet [10]. Water was provided ad libitum.

After acclimatization, surgical procedures were performed (sham operation for control animals, control group, and partial nephrectomy for experimental animals, uremic group). Animals were anaesthetized by intravenous administration of a solution mixture of ketamine hydrochloride 100 mg/ml (Imalgene® 1000; Merial, Duluth, Georgia, USA) and xylazine 20 mg/ml (Rompun®; Bayer, Leverkusen, Germany), 87% and 13%, respectively (proportion 6.69 : 1 approximately). The initial dosage for the induction of anesthesia was 0.3 ml/kg body weight of the above solution mixture, i.e., Imalgene® (87%) and Rompun® (13%), intravenously (i.v.). The maintenance of anesthesia was achieved by a dose of propofol (10 mg/kg BW). Three hours before the intervention, each animal had only access to water and not to food and its weight was measured on a precision scale. Animal temperature was maintained via a heating pad.

For the uremic group, nine animals ($N = 9$) underwent removal of the left kidney after careful ligation of the left renal artery and vein and partial nephrectomy (3/4) of the right kidney. For the control group, six age-matched animals ($N = 6$) underwent sham operation. Twelve weeks after the

surgery, the animals were weighed and then sacrificed by injection of sodium pentobarbital solution (50 mg/ml) which was applied in a dosage of 100 mg/kg BW followed by bilateral thoracotomy. Immediately after cardiac arrest, sample collections were done. All sample collection as well as subsequent handling and analyses were done in a blind design. It should be noted that special care was taken not to induce oxidation of glutathione, as mentioned below.

2.2. Blood Sampling and Treatment. Blood samples (5 ml) were collected by a heparinized syringe from rabbits' heart and aorta and were placed into ethylene diamine tetraacetic acid- (K_2EDTA-) containing tubes (Vacutainer Plus Plastic K_2EDTA; Becton Dickinson). For plasma collection, blood samples were centrifuged immediately at 1370 × g for 10 min at 4°C and the supernatant was carefully collected. The remaining packed erythrocytes were lysed with 1 : 1 (*v*:*v*) distilled water, inverted vigorously, and centrifuged at 4000 × g for 15 min at 4°C. The supernatant red blood cell (RBC) lysate designated was collected. Finally, in order to obtain serum, another portion of blood sample (5 ml) was collected and placed into separate tubes containing clot activator, left for 20 min to clot at RT, centrifuged at 1370 × g, at 4°C for 10 min, and the supernatant was collected. All supernatant samples were aliquoted in Eppendorf tubes, stored at -80°C, and thawed only once before analysis.

2.3. Skeletal Muscle Sampling and Homogenization. Psoas and soleus muscle samples were harvested from the control (sham-operated) and uremic groups. These muscles were selected as two representative muscles, one a typical fast-twitch muscle (psoas, composed primarily of type IIX fast-twitch muscle fibers [23, 27]) and the other a typical slow-twitch muscle (soleus, composed primarily of type I slow-twitch muscle fibers). Muscle samples were frozen immediately in liquid nitrogen and stored at -80°C. For analysis, each tissue sample was thawed, excised, and kept chilled throughout homogenization. A weighted portion of each muscle was washed several times with ice-cold normal saline and was placed into prechilled tubes containing cold homogenization buffer (138 mM NaCl, 2.7 mM KCl, 1 mM EDTA, pH 7.4) and a mix of protease inhibitors (1 μM aprotinin, 1 μg/ml leupeptin, and 1 mM PMSF). Initial homogenization was achieved with an electrical homogenizer (MICCRA D-9) for 10 min with intermediate pauses of 10 s/20 s. Then an ultrasound homogenizer (UP50H) was used for 1-2 min, with intermediate pauses as before. Homogenates were filtered through four layers of medical gauze to remove connective tissue debris, incubated for 10 min at 4°C, and centrifuged at 10,000 × g for 10 min at 4°C. The supernatant homogenate was aliquoted in multiple portions and stored at -80°C for subsequent analyses.

2.4. Biochemical and Hematological Analyses

2.4.1. Urea, Creatinine. Circulating levels of urea and creatinine were assessed, the two hallmark biomarkers that evidence renal insufficiency [28]; their concentrations in serum were determined with the colorimetric method using commercially available kits (ab83362, Abcam, United Kingdom, and ab65340, Abcam, United Kingdom), respectively, with a 96-well microtiter plate and a programmable microplate reader (Biochrom, Asys Expert 96, United Kingdom). Urea and creatinine concentrations in unknown samples were determined by comparison with the standard curves.

2.4.2. Total Protein. Total protein concentration in plasma and skeletal muscle (psoas, soleus) homogenates was determined spectrophotometrically using the bicinchoninic acid (BCA) protein assay kit (Pierce, Thermo Fisher Scientific, USA). In plasma, total protein concentration was determined in order to estimate the final concentration of protein carbonyls. In muscle homogenates, total protein concentrations were determined in order to estimate the final concentrations of reduced and oxidized glutathione and protein carbonyls as well as the activities of catalase and glutathione reductase.

2.4.3. Hemoglobin, Hematocrit, and Red Blood Cell (RBC) Count Analysis. CKD is associated with anemia [29]. Thus, hemoglobin, hematocrit, and red blood cell count were determined using a commercially available kit and procedures (Dutch Diagnostics BV, Zutphen, Netherlands) to examine if the model promoted the development of anemia.

2.5. Evaluation of Redox Status. All materials for redox marker assays were purchased from Sigma (St. Louis, MO, USA). We examined markers for antioxidant capacity, such as TAC, GSH, GR, and CAT, and markers of protein and lipid oxidation such as protein carbonyls and TBARS, respectively.

2.5.1. GSH Determination. The tripeptide GSH is the most abundant nonprotein thiol and one of the main components of antioxidant capacity [30]. GSH concentration was determined in RBC lysate and skeletal muscle homogenate samples according to Rahman et al. [31], using a 96-well microtiter plate and a programmable microplate reader (Biochrom, Asys Expert 96). Briefly, samples were deproteinized with 5% trichloroacetic acid (TCA) (1 : 1 *v*/*v*) centrifuged at 16,000 × g for 10 min, and the supernatant was collected. The following reagents were added in order (all reagents in 0.1 M potassium phosphate buffer, pH 7.5, with 5 mM EDTA) to 96-well flat-bottom plate (CytoOne) in duplicate: 20 μl of glutathione standard (0.103 to 26.4 μM) or the sample to be assayed, 120 μl of freshly prepared (5,5′-dithiobis 2-nitrobenzoic acid) DTNB (2 mg/3 ml), glutathione reductase (10 units), and 60 μl of dihydronicotinamide-adenine dinucleotide phosphate NADPH (2 mg/3 ml) mix solution (1*v* : 1*v*). The absorbance at 415 nm was measured every 30 s, for 3 min, at RT. The rate of increase in absorbance per minute was calculated by linear regression. GSH concentration in unknown samples was determined by comparison with the standard curve.

2.5.2. GSSG Determination. GSSG concentration was determined in RBC lysate and skeletal muscle homogenate samples according to Giustarini et al. [32], modified for using a 96-well microtiter plate and a programmable microplate reader. Samples were deproteinized with 5% TCA (1 : 1 *v*/*v*) centrifuged at 16,000 × g for 10 min, and the supernatant

was collected. To avoid the rapid oxidation of GSH to GSSG, through the deproteination procedure, and the consequent overestimation of GSSG, the alkylating reagent N-ethylmaleimide (NEM) 310 mM was added upon collection of blood sample or the tissue homogenization. This was extracted before the actual measurement with three volumes of dichloromethane DCM, carefully collecting the upper volume of the ensuing bilayer (typically 750 μl of DCM for 250 μl of deproteinized supernatant), vortexed 5 min at 800 rpm at room temperature (RT), and centrifuged at 14,000 × g for 30 s at 4°C. To measure GSSG, the following reagents were added in order (all reagents in 0.1 M potassium phosphate buffer, pH 7.5, with 5 mM EDTA) to 96-well flat-bottom plate (CytoOne) in duplicate: 20 μl of glutathione disulfide standard (0.103 to 26.4 μM) or the sample to be assayed, 120 μl of freshly prepared DTNB (2 mg/3 ml) and glutathione reductase (10 units) mix solution (1v : 1v), and 60 μl of NADPH (2 mg/3 ml). The absorbance at 415 nm was measured every 30 s, for 3 min, at RT. The rate of increase in absorbance per minute was calculated by linear regression. GSSG concentration in unknown samples was determined by comparison with the standard curve.

2.5.3. Determination of GR Activity. Glutathione reductase (GR) activity is important in the evaluation of tissue redox state but also has an antiapoptotic role [33]. GR activity was determined in RBC lysate and skeletal muscle homogenate samples according to Cribb et al. [34], using a 96-well microtiter plate and a programmable microplate reader. To measure GR activity, the following reagents were added in order (all reagents in 0.1 M sodium phosphate buffer, pH 7.5, with 1 mM EDTA) to 96-well flat-bottom plate (CytoOne) in duplicate: 150 μl of 0.1 mM DTNB, 10 μl of NADPH (10 mg/ml; 12 mM), and 20 μl of reductase standard (0.015 to 0.50 U/ml) or the sample to be assayed. The reaction was initiated by the addition of 10 μl of GSSG (1 mg/ml; 3.25 mM). For blank wells, no GSSG was added. The absorbance at 415 nm was measured every 30 s, for 3 min, at RT. The rate of increase in absorbance per minute was calculated by linear regression. GR activity in unknown samples was determined by comparison with the standard curve.

2.5.4. TAC Determination. Total antioxidant capacity (TAC) is a method which is frequently used to assess the antioxidant status of biological samples and can evaluate the antioxidant response against the free radicals produced in a given condition [35]. TAC was determined in plasma and skeletal muscle homogenate samples according to Janaszewska and Bartosz [36], based on the scavenging of 2,2-diphenyl-1-picrylhydrazyl (DPPH) free radical. DPPH stock solution (10 mM) was prepared by dissolving 0.02 g DPPH in 5 ml of methanol and mix in the stirrer. The working solution was obtained by diluting the stock solution 100 times with methanol. In 20 μl of plasma or homogenate, 480 μl of 10 mM sodium potassium phosphate (pH 7.4) and 500 μl of 0.1 mM DPPH were added and incubated in the dark for 30 min at RT. The samples were centrifuged for 3 min at 20,000 × g and 900 μl of the supernatant was transferred into a clean plastic cuvette. The absorbance was read at 530 nm using a spectrophotometer. TAC values were presented as mM of DPPH reduced to 2,2-diphenyl-1picrylhydrazine (DPPH : H).

2.5.5. Determination of CAT Activity. Catalase is a common enzyme found in nearly all living organisms exposed to oxygen and catalyzes the decomposition of hydrogen peroxide to water and oxygen playing a key role in protecting the cell from oxidative damage by ROS [37]. CAT activity was determined in RBC lysate and skeletal muscle homogenate samples according to Aebi [37]. 20 μl of RBC lysate or homogenate was added to 2975 μl of sodium potassium phosphate buffer 67 mM, pH 7.4, and the samples were incubated at 37°C for 10 min. 5 μl of hydrogen peroxide 30% was added and the change in absorbance was immediately read at 240 nm for 2 min. One unit of catalase is equal to 1 μmol of hydrogen peroxide H_2O_2 decomposed/minute. Results were normalized to hemoglobin content in the blood sample and to total protein content in muscle homogenate samples.

2.5.6. PC Determination. Protein carbonylation is a type of protein oxidation that can be promoted by ROS. It usually refers to a process that forms reactive ketones or aldehydes that can be reacted by 2,4-dinitrophenylhydrazine (DNPH) to form hydrazones [38]. PC concentration was determined in plasma and skeletal muscle homogenate samples according to Fields and Dixon [39]. In 50 μl of plasma or homogenate, 50 μl of 20% TCA was added, incubated in the ice bath for 15 min, and centrifuged at 15,000 × g for 5 min at 4°C and the supernatant was discarded. Afterwards, 500 μl of 14 mM DNPH, in 2.5 N hydrochloric acid HCl, for the sample or 500 μl of 2.5 N HCl for the blank was added to the pellet. Both samples were incubated in the dark at RT for 1 h, with intermittent vortexing every 15 min. Samples were centrifuged at 15,000 × g for 5 min at 4°C. The supernatant was discarded and 1 ml of 10% TCA was added, vortexed, and centrifuged at 15,000 × g for 5 min at 4°C. The supernatant was discarded, and 1 ml of ethanol-ethyl acetate (1 : 1 v/v) was added, vortexed, and centrifuged at 15,000 × g for 5 min at 4°C. The washing step was repeated two more times. Finally, the supernatant was discarded, and 1 ml of 5 M urea (pH 2.3) was added, vortexed, and incubated at 37°C for 15 min. The samples were centrifuged at 15,000 × g for 3 min at 4°C, and the absorbance was read at 375 nm. Protein carbonyl values were obtained by using the molar extinction coefficient of DNPH (22 mM·cm^{-1}).

2.5.7. TBARS Determination. Lipid peroxides are oxidative degradation products of lipids with malondialdehyde (MDA) to be considered as the main marker in lipid peroxidation [40]. The TBARS assay is the simplest and most popular method for quantifying lipid peroxidation in biological samples [41]. In 100 μl of plasma or homogenate, 500 μl of 35% TCA and 500 μl of 200 mM Tris-HCl (pH 7.4) were added and incubated at RT for 10 min. Afterwards, 1 ml of 2 M sodium sulfate Na_2SO_4 and 55 mM thiobarbituric acid (TBA) solution was added and incubated at 95°C for

Table 1: Biochemical and hematological indices in the control and uremic groups.

	Control group ($n = 6$)	95% confidence interval		Uremic group ($n = 9$)	95% confidence interval		p
		Lower bound	Upper bound		Lower bound	Upper bound	
Total protein (mg/ml)	68.59 ± 2.12	64.44	72.75	67.89 ± 2.28	63.41	72.37	0.825
Creatinine (mg/dl)	1.28 ± 0.15	1.11	1.45	2.45 ± 0.37	1.72	3.19	0.018*
Urea (mg/dl)	38 ± 4.3	33.43	43.24	60 ± 11.52	37.42	82.58	0.114
Hemoglobin (mg/dl)	11.08 ± 0.92	10.33	11.81	9.80 ± 0.30	8.22	11.77	0.368
Hematocrit (%)	35.24 ± 0.79	34.54	35.93	26.06 ± 1.85	22.43	29.69	0.001*
RBC ($\times 10^6/\mu$l)	5.10 ± 0.17	4.95	5.25	3.92 ± 0.29	3.36	4.48	0.005*

Data are presented as mean ± SEM. The exact statistical significance value p and the 95% confidence intervals are reported.

45 min. The samples were cooled on ice for 5 min and were vortexed. 1 ml of 70% TCA was added, vortexed, and centrifuged at 15,000 × g for 3 min at 25°C. The absorbance of the supernatant was read at 530 nm. A baseline absorbance was taken into account by running a blank along with all samples during the measurement. The calculation of TBARS concentration was obtained using the molar extinction coefficient of MDA (15,600 mol/l).

2.5.8. Uric Acid Determination. Uric acid is not only a by-product of purine metabolism, but it can also maintain protection against oxidative damage acting as an electron donor and scavenging peroxyl radicals, hydroxyl radicals, and singlet oxygen [42, 43]. Uric acid concentration in the serum was measured on a Clinical Chemistry Analyzer Z 1145 (Zafiropoulos Diagnostica, Athens, Greece) using commercially available kits (Zafiropoulos Diagnostica). 6 μl of serum was added to 600 μl of working reagent; samples were incubated for 1 min at 37°C and the absorbance was read at 340 nm.

2.6. Statistical Analysis. Data were analyzed using the commercially available statistical software package SPSS 22. Results were expressed as mean ± SEM and 95% confidence intervals.

Initially duplicate values were averaged before further statistical treatment. The Shapiro-Wilk test was performed to initially test whether the data were normally distributed, as it was the case.

An independent t-test was conducted to examine whether there were any differences in blood redox status indices between the control group and the uremic group. Similarly, an independent t-test was conducted to examine whether there were any differences in biochemical and hematological indices between the control group and the uremic group.

Two-way MANOVA (two groups × two muscles) was conducted to examine the effects of uremia and muscle type on muscle redox status indices. Significant interactions and main effects were further investigated using LSD post hoc analysis for multiple group comparisons.

Possible relationships between indices were examined using Pearson correlation coefficient analysis in pool and per group (control, uremic) data.

The significance level was set at $p \leq 0.05$.

3. Results

Both surgery procedures (3/4 partial nephrectomy and sham operation) were well tolerated by animals as they presented with a normal after-surgery recovery. At the end of the twelve-week period postsurgery, animals' average body weight was 3728 ± 336.47 g for control and 2935 ± 288.70 g for the uremic group ($p > 0.05$).

3.1. Biochemical and Hematological Analyses. Renal insufficiency in the uremic group, compared to control, was reflected in the significantly raised ($p < 0.05$) blood creatinine levels (Table 1). However, urea levels were not significantly different between the groups ($p > 0.05$). Significant differences were found in the hematological profile of the uremic group compared to the control group. More specifically, hematocrit levels and RBC count were significantly lower in the uremic group compared to the control ($p = 0.005$) and ($p = 0.001$), respectively. All biochemical and hematological indices are represented in Table 1.

3.2. Blood Redox Status Analysis. All blood redox status indices are presented in Table 2. GSH concentration was significantly higher in the RBC of the uremic group compared to the control ($t(9) = -2.071$, $p = 0.033$). TBARS concentration tended to be higher in the plasma of the uremic group compared to the control ($p = 0.060$). No significant differences ($p > 0.05$) were found in the rest of redox status indices evaluated in the blood between the two groups. Furthermore, we found no relationship between TAC levels with hematological parameters.

3.3. Muscle Redox Status Analysis. No significant group main effects were found for antioxidant capacity indices ($p > 0.05$) for the two groups. Significant group main effects were found for PC concentration ($F_{(1,21)} = 8.902$, $p = 0.007$) in both muscle types. The LSD post hoc test revealed that PC concentration was significantly higher in the uremic group compared to the control group. No group main effects were found for TBARS.

Muscle type appeared to affect the level of some indices for both the uremic and control groups. Significant muscle type main effects were found for total protein concentration ($F_{(1,21)} = 23.166$, $p = 0.001$) with protein content of the psoas being higher than the soleus for both groups. Regarding

Table 2: Blood redox status indices in the control and uremic groups.

Blood	Control group ($n = 6$)	95% confidence interval		Uremic group ($n = 9$)	95% confidence interval		p
		Lower bound	Upper bound		Lower bound	Upper bound	
Uric acid (mg/dl)	1.39 ± 0.25	0.907	1.886	1.93 ± 0.38	1.18	2.67	0.263
GSH (μmol/g protein)	12.43 ± 1.01	10.448	14.412	17.50 ± 1.73	14.12	20.88	0.033*
GSSG (μmol/g protein)	0.027 ± 0.006	0.016	0.039	0.048 ± 0.010	0.028	0.067	0.110
Ratio (GSH/GSSG)	481 ± 53	376.357	585.642	425.28 ± 61.19	305.36	545.21	0.511
GR (U/g protein)	176.40 ± 25	127.393	225.423	153.1 ± 15.84	122.04	184.15	0.425
TAC (μmol DPPH/ml)	0.786 ± 0.033	0.719	0.852	0.759 ± 0.041	0.679	0.838	0.611
CAT (U/mg protein)	342.02 ± 17.69	307.35	376.68	303.63 ± 15.63	273.01	334.26	0.131
PC (nmol/mg protein)	0.603 ± 0.09	0.427	0.780	0.620 ± 0.066	0.491	0.748	0.888
TBARS (nmol/ml)	5.12 ± 0.42	4.292	5.948	7.03 ± 0.81	5.44	8.62	0.060

Data are presented as mean ± SEM. The exact statistical significance value p and the 95% confidence intervals are reported. GSH: reduced glutathione; GSSG: oxidized glutathione; TAC: total antioxidant capacity; CAT: catalase; PC: protein carbonyls; TBARS: thiobarbituric acid reactive substances, * statistical significance between the control and uremic groups, $p < 0.05$.

antioxidant capacity, GSH concentration ($F_{(1,21)} = 6.175$, $p = 0.021$) was higher in the soleus, TAC levels ($F_{(1,21)} = 18.316$, $p = 0.001$) were higher in the psoas, and catalase activity ($F_{(1,21)} = 20.597$, $p = 0.001$) and GR activity ($F_{(1,21)} = 7.498$, $p = 0.012$) were higher in the soleus in both the control and uremic groups.

The LSD post hoc test revealed that total protein and TAC levels were significantly lower in the soleus compared to the psoas muscle in both the control and uremic groups. Additionally, the soleus demonstrated higher levels of TBARS and PC levels as well as higher GSH levels, catalase, and GR activities compared to the psoas muscle in both groups.

Levels of PC concentration were higher in the soleus muscle in both groups ($F_{(1,21)} = 6.410$, $p = 0.019$) (Figure 1). TBARS concentration was also higher in the soleus ($F_{(1,21)} = 14.703$, $p = 0.001$) in both the control and uremic groups, respectively.

Finally, no interactions were found between the examined muscle types (psoas, soleus) and groups (control, uremic) for all the redox status indices ($p > 0.05$). All the results are summarized in Table 3.

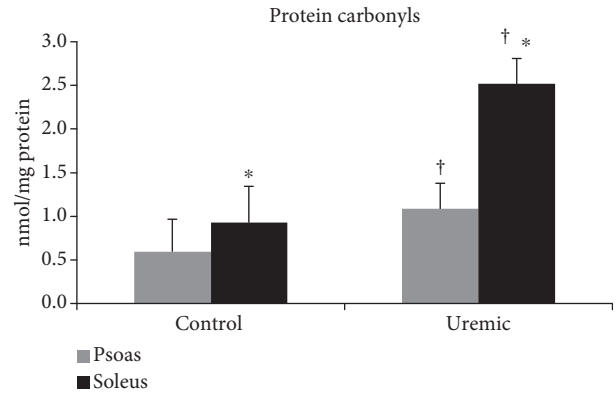

Figure 1: Protein carbonyl concentrations for the psoas (control: 0.596 ± 0.372 nmol/mg protein, 95% CI: lower-upper bound: 0.179-1.370; uremic: 1.086 ± 0.294 nmol/mg protein 95% CI: lower-upper bound: 0.474-1.699) and the soleus (control: 0.929 ± 0.41 nmol/mg protein, 95% CI: lower-upper bound: 0.063-1.795; uremic: 2.52 ± 0.29 nmol/mg protein, 95% CI: lower-upper bound: 1.905-3.129) in the control and uremic groups. * depicts significant differences between the control and uremic groups; † depicts significant differences between the psoas and soleus muscles, $p < 0.05$.

3.4. Associations between Blood and Muscle Levels of Redox Indices. No statistically significant correlation between blood levels and muscle levels emerged for any of the antioxidant capacity and the oxidative stress indices examined in this study. This was the case either in when analysis was performed for the pool of samples or for each group separately ($p > 0.05$). Moreover, no correlations between blood levels and specific muscle type levels were observed ($p > 0.05$). Finally, no correlations were found between hematological indices and antioxidants or oxidative stress indices in the blood and skeletal muscle ($p > 0.05$).

Statistically significant correlations emerged from selective redox status indices, between the two types of skeletal muscle which however were differentiated by the group. Thus, in the uremic group, we observed strong and significant correlations in PC levels ($r = 0.913$, $p = 0.002$), in GSSG levels ($r = 0.766$, $p = 0.027$), and in CAT levels ($r = 0.743$, $p = 0.035$) between the soleus and psoas muscle samples. However, such correlations were not strong or statistically significant for the control group (Figure 2).

4. Discussion

We examined redox status indices in the blood and in two different types of skeletal muscle in an animal model mimicking the predialysis stage of CKD. Our main findings were that PC levels were higher in the uremic group in both muscle types and that the soleus had higher levels of TBARS, PC, GSH, CAT, and GR and lower TAC compared to the psoas in both groups. Additionally, the GSH concentration was

Table 3: Psoas and soleus muscle biochemical and redox status indices in the control and uremic groups.

	Psoas muscle						Soleus muscle					
	Control group ($n = 5$)$^{\neq}$	95% confidence interval		Uremic group ($n = 8$)$^{\neq}$	95% confidence interval		Control group ($n = 5$)$^{\neq}$	95% confidence interval		Uremic group ($n = 8$)$^{\neq}$	95% confidence interval	
		Lower bound	Upper bound		Lower bound	Upper bound		Lower bound	Upper bound		Lower bound	Upper bound
Total protein (mg/ml)	5.753 ± 0.43	4.865	6.642	4.537 ± 0.34	3.836	5.240	3.155 ± 0.478†	2.161	4.148	3.29 ± 0.33$^{\#}$	2.588	3.992
GSH (μmol/g protein)	5.539 ± 1.69	2.014	9.065	6.087 ± 1.34	3.300	8.875	8.09 ± 1.89†	4.155	12.039	11.41 ± 1.34$^{\#}$	8.625	14.20
GSSG (μmol/g protein)	0.265 ± 0.09	0.060	0.470	0.322 ± 0.07	0.160	0.484	0.331 ± 0.11	0.102	0.560	0.472 ± 0.78	0.310	0.634
Ratio (GSH/GSSG)	18.66 ± 11.11	-4.455	41.775	25.60 ± 8.787	7.326	43.874	46.62 ± 12.43	20.782	72.468	33.61 ± 8.79	15.34	51.89
GR (U/g protein)	10.59 ± 2.25	5.912	15.273	12.72 ± 1.78	9.018	16.419	18.41 ± 2.52†	13.184	23.651	16.42 ± 1.78$^{\#}$	12.724	20.125
TAC (μmol DPPH/ml)	0.595 ± 0.06	0.458	0.732	0.519 ± 0.05	0.411	0.627	0.322 ± 0.07†	0.169	0.476	0.264 ± 0.05$^{\#}$	0.155	0.372
CAT (U/mg protein)	6.992 ± 4.71	-2.799	16.785	5.721 ± 3.72	-2.020	13.463	29.09 ± 5.26†	18.140	40.063	23.60 ± 3.72$^{\#}$	15.863	31.346
TBARS (nmol/ml)	3.179 ± 1.06	0.983	5.376	2.297 ± 0.835	0.561	4.034	6.81 ± 1.18†	4.350	9.262	6.25 ± 0.83$^{\#}$	4.511	7.984

Data are presented as mean ± SEM. Confidence intervals are reported. TBARS: thiobarbituric acid reactive substances; GSH: reduced glutathione; GSSG: glutathione oxidized; TAC: total antioxidant capacity; CAT: catalase. †Statistical significance between control psoas and control soleus, $^{\#}$statistical significance between uremic psoas and uremic soleus, $p < 0.05$. $^{\neq}$It should be noted that muscle analysis refers to $n = 5$ for the control and $n = 8$ for the uremic group as a batch of samples became inappropriate for analysis.

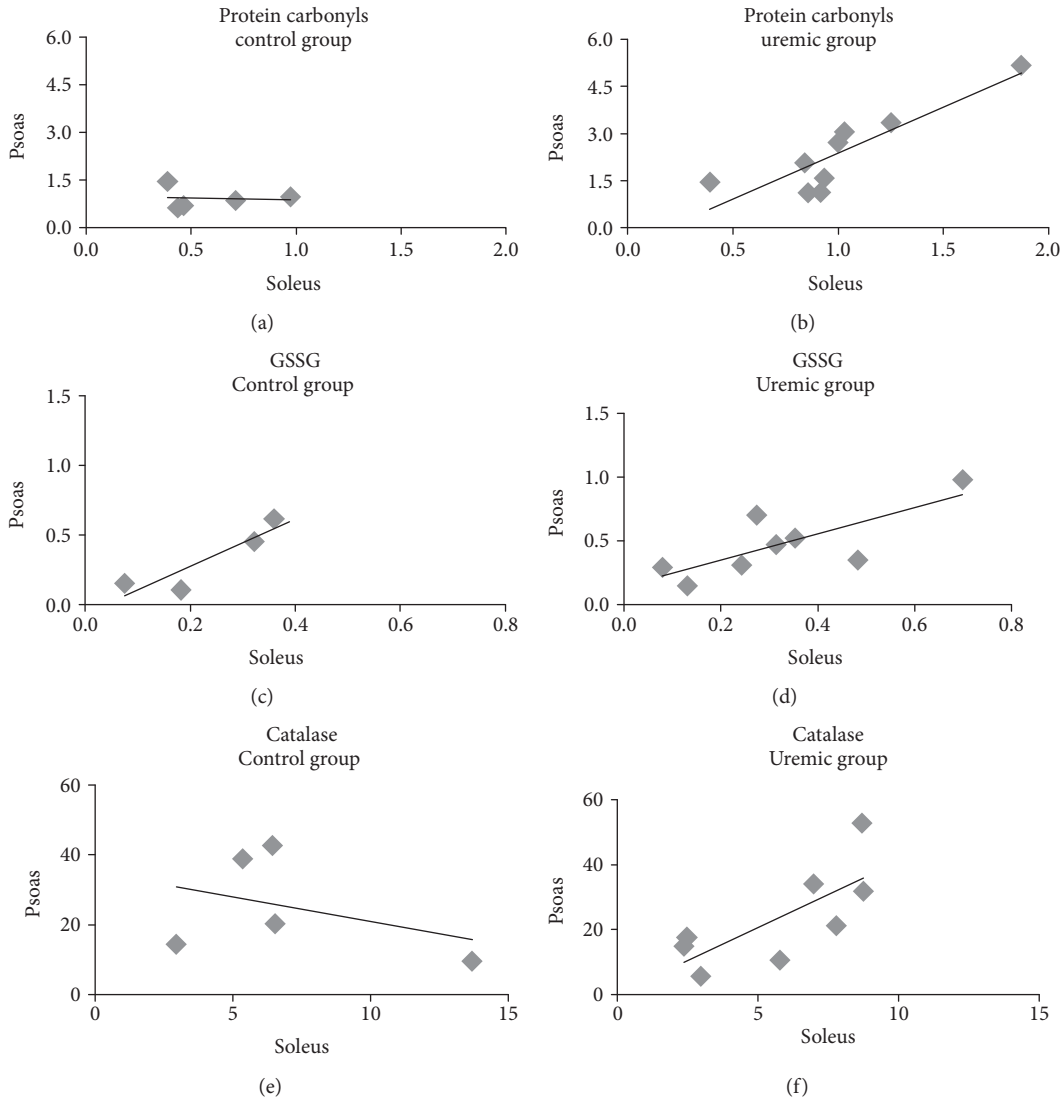

Figure 2: Correlation of protein carbonyl (PC) concentration (a, b), oxidized glutathione (GSSG) concentration (c, d), and catalase (CAT) activity (e, f) between the psoas and soleus muscles in the control and uremic groups, respectively. Only in the uremic group correlations were statistically significant for (b) PC levels ($r = 0.913$, $p = 0.002$), (d) GSSG levels ($r = 0.766$, $p = 0.027$), and (f) CAT activity ($r = 0.743$, $p = 0.035$).

significantly higher in the RBC of the uremic group compared to the control group. Moreover, we found no significant correlations in redox status indices between the blood and skeletal muscle.

The results demonstrated that early during the development of CKD there is an alteration in muscle redox homeostasis; importantly, both oxidative damage and antioxidant capacity seemed to be muscle type-specific. Very importantly, as it will be discussed below, we observed no association between the blood and muscle levels of the biomarkers examined, which bears significance for their prospective use in monitoring muscle pathology development.

The animal model was successfully established as it is reflected by the increases in creatinine and urea in the uremic group as compared to the control group, in agreement with observations by others using a similar model (e.g., Taes et al. [44]). Urea levels in the uremic group were almost double than those in the control group that difference was not statistically significant. This could be due to the small number of animals and animal variability. However, as a clinical observation, the doubling of urea is indicative of a considerably compromised renal function [44, 45]. Moreover, the hematological disturbances in the uremic group (significantly lower hematocrit and RBC compared to control) indicated the development of anemia, which is similar to the human condition [29].

Considering the antioxidant capacity, we observed a 40% higher GSH concentration in uremic blood samples compared to control. GSH is a primary antioxidant molecule which belongs to the endogenous defense against ROS and its role is critical for the cellular redox environment [46], since it is the most abundant nonprotein thiol that counteracts oxidative stress [47]. There are conflicting results regarding GSH concentration in CKD patients, which sometimes

appear to depend on the severity of the disease and sometimes not. Thus, in moderately uremic predialysis patients, Bober et al. found higher levels of GSH compared to age-matched healthy individuals [48], in agreement to our observations. However, in other studies, lower GSH levels in the whole blood of CKD predialysis patients have been observed compared to controls [49–51] interpreted as a depletion in the antioxidant reserve. Alhamdani [52] evaluated the glutathione biosynthetic pathway in advanced uremia and hemodialysis measuring GSH levels and γ-glutamyl cysteine synthetase (γ-GCS) and glutathione synthetase (GSH-S) activities in nondialysis, hemodialysis, and continuous ambulatory peritoneal dialysis patients. Significant decreases in GSH levels and γ-GCS activity but not in GSH-S activity were observed in all groups of patients compared to healthy individuals. Thus, low activity of γ-GCS, the rate-limiting enzyme of GSH biosynthesis, may negatively affect *de novo* synthesis of GSH in those patients with low levels of GSH.

The observed increased levels of GSH concentration in uremic blood samples in our study could be attributed to an upregulation of its synthesis in response to a greater demand, especially, given the almost doubling of blood GSSG in the uremic group (levels being 1.77-fold of those of the control group). This observation, despite not reaching statistical significance, indicates a tendency for increased levels of hydrogen peroxide or lipid peroxides, similar to human studies [50]. Nonetheless, CAT also reduces hydrogen peroxide to water, but there was no statistical difference in the activity of the specific antioxidant enzyme between the two groups in our study (still, CAT activity tended to be lower in erythrocytes of the uremic group). CAT is located in peroxisomes while GSH and GPx are found mainly in the cytosol [53]. This subcellular compartmentalization is undoubtedly important for hydrogen peroxide detoxification. Based on the above, it appeared that hydrogen peroxide scavenging in circulation was undertaken to a greater degree by the glutathione redox cycling mechanism than CAT in our CKD model.

In patient studies, while general clinical guidelines are followed, dietary approaches can greatly influence GSH levels, contributing to literature's conflicting reports. GSH concentration is decreased by fasting, low-protein diets, or diets limiting in sulfur amino acids such as cysteine [54]. However, administration of α-lipoic acid, a naturally occurring thiol compound, increases GSH levels in several cell types and tissues [54–56] and also restores intracellular GSH in several pathological conditions [54]. Moreover, selenium (Se) as an integral part of the enzyme GPx plays a key role in GSH levels [57]. In our study, both control and uremic animals followed the same diet, carefully designed not to tax the remaining kidney function, similarly to diet guidelines followed by patients, while providing balanced nutrients and minerals, to minimize any diet-induced effect on GSH levels.

Muscle analysis per group and per muscle type indicated redox disturbances in the skeletal muscle of the uremic group. The significant increase in PC levels by approximately 1.82-fold for the psoas and 2.71-fold for the soleus in uremic compared to control psoas and soleus, respectively, points to increased levels of sarcomeric protein carbonylation. It is well established that oxidized proteins undergo diverse structure and functional changes including change in their hydrophobicity which makes them more susceptible to proteolysis [58]. Carbonylation, which is an irreversible and irreparable protein modification, tags proteins to be led through proteolysis or to form high-molecular weight aggregates through direct oxidation of side chains of lysine, arginine, proline, and threonine residues, among other amino acids. Such carbonylated aggregates can become cytotoxic and have been associated with a large number of age-related disorders [59].

Moreover, our findings are in agreement with those reported by Lim et al. [60] in the skeletal muscle of HD patients. Our results of increased PC levels in the skeletal muscle of the animal model, and the available patient evidence by Lim et al., fit with the projection of the development of muscle atrophy, which is a well-established component of uremic myopathy in end-stage hemodialysis patients [61]. Such interpretation is also corroborated by the recent finding of moderate atrophy in the psoas muscle fibers of chronically uremic animals [62]. Moreover, Lim et al. also found increased TBARS levels, for which, in agreement to the overall disease profile, we reported a tendency for increased levels in the muscle. We cannot exclude the formation of protein aggregates, but considering other evidence on progressive atrophy and the young age of the animals studied, we consider that increased PC levels are a plausible indication of atrophy mechanisms under way in predialysis stages of renal insufficiency. Taking into account the role of carbonyl stress in vascular damage [63] and the generally impaired functionality of the muscle in CKD [61, 62], early measures protecting muscle protein and vasculature from oxidation could prove of great importance for patients before progressing into the end stage where HD aggravates the redox imbalance [11] and further negative effects on muscle status accumulate.

The observed tendency for an increase in blood TBARS levels of the uremic group compared to the control group possibly revealed a predisposition towards lipid peroxidation [64], a pathogenetic factor in atherosclerosis [65]. Furthermore, lipid peroxidation negatively affects erythrocyte membrane integrity, playing a major role to their half-life shortening and thus to the development of anemia [56]. This agrees with our observation of lower RBC and Hct in our predialysis model. Papavasiliou et al. [66] found statistically significant increased TBARS levels in the plasma of predialysis patients with stages 3-5 CKD compared to healthy individuals. In the same study, patients on stages 1-2 CKD exhibited a tendency for higher TBARS levels compared to healthy individuals. In addition, stages 1-2 CKD patients exhibited significantly lower MDA levels compared to the stages 3-5 CKD patients [66]. Regarding HD patients, the large majority of studies reported increased TBARS levels in the plasma compared to healthy individuals [48, 63, 67–70], reflecting extensive lipid peroxidation, while erythropoietin treatment can help mitigate redox disturbances and inflammation, especially in the long term [70].

Taking all the above into consideration together with our findings, it could be concluded that blood lipid peroxidation in CKD emerges from the early stages of renal insufficiency.

Skeletal muscle wasting is a characteristic of several chronic diseases [71] including kidney disease. In previous work, some of us have demonstrated a fiber-type specificity of atrophy in HD patients [61, 72]. Here, we examined the redox status of the slow-twitch soleus (expressing mainly myosin heavy chain type I) and the fast-twitch psoas (expressing mainly the fast myosin heavy chain IIX) [23, 27]. Overall, the soleus muscle presented with higher levels of TBARS and PC levels but also with higher GSH levels and catalase and GR activities compared to the psoas muscle in both groups. Thus, while due to its mitochondrial content, the soleus may be expected to experience a higher oxidative stress load at the same time it appeared better equipped to withstand it, in agreement with the limited literature existing in patients [4].

One of the suggested mechanisms to explain muscle catabolism involves the tumor necrosis factor-α (TNF-α) [73, 74], via the regulation of hormones and catabolic cytokines [75–77] and can also promote muscle loss by stimulating the ubiquitin gene expression [78] and activating the nuclear factor NF-κB [79]. In HD patients, Li et al. [80] observed that TNF-α can directly trigger protein loss and decrease in myosin heavy chain fast (MHCf) levels in the skeletal muscle. It is also known that TNF-α/NF-κB signaling pathway is widely affected from endogenous ROS. TNF-α widely excites mitochondria ROS production, promoting TNF-α/NF-κB activation [81, 82], a process which seems to be tissue-specific [80]. In line with these reports, human studies [4] indicate greater atrophy in fast-twitch muscles, perhaps via mitochondrial dysfunction in the uremic environment. Taking into consideration that fast muscle is the type mostly affected in patients [61], perhaps the redox disturbances in the psoas muscle eventually contributes to the literature observations of atrophy. On the other hand, despite the expected increased levels of mitochondrial function, the presence of higher concentrations of GSH, CAT, and GR in our study indicated that healthy soleus may have a higher antioxidant capacity than healthy psoas. In response to an augmented oxidative load due to renal insufficiency, uremic soleus appears to have further upregulated its defenses in the predialysis CKD stage, resisting the detrimental effects of ROS.

The present study evaluated the possible relationships between redox status indices in the blood and skeletal muscle under chronic renal insufficiency. Notably, we observed no correlation between the redox indices evaluated in the blood and their levels in the two different types of skeletal muscle (psoas, soleus). Correlation analysis was further expanded to explore the differences obtained in the redox markers at the blood and muscle levels in relation to parameters related to the development of anemia. However, we observed no correlation between these indices.

Although the accessibility to all tissues is feasible in animal models providing the opportunity to evaluate redox status in the tissue of interest, in humans, several difficulties and ethical limitations in such invasive processes exist, especially in patients. Thus, in the majority of human studies, redox status indices have been evaluated in the blood and results are extrapolated in tissues. However, due to limited studies [83, 84], it remains uncertain if and in which cases evaluating redox status indices in the blood adequately reflects the redox status in tissues. Rodriguez et al. [83] found that protein carbonyl concentrations were moderately ($r = 0.51$) correlated between the blood and skeletal muscle (vastus lateralis) in patients with chronic obstructive pulmonary disease. Veskoukis et al. [84] reported that four redox status indices (PC, GSH, GSSG, and catalase) in the blood adequately reflected the oxidative stress changes that happened in healthy skeletal muscle (rat gastrocnemius) after exercise and/or xanthine oxidase inhibition. This discrepancy could be explained by the differences in methodology adopted such as the type of animal model, muscle used (e.g., in Veskoukis et al. gastrocnemius, which has a different myosin composition than rabbit psoas), lab protocols, and the renal dysfunction per se having possibly an overarching systemic effect that could mask muscle's contribution to blood levels of redox indices.

If a disease state is implicated then not only the primarily suffering organic system could be contributing to a redox imbalance (as e.g., the kidney [85]) but also secondarily affected systems (e.g., muscle), as well as systemic inflammation [60, 86] and vascular stress [87] could be implicated. Measuring redox status in the blood in such a complex state may not thus allow clear conclusions with regard to tissue levels because high levels of generalized oxidative stress or increased blood antioxidant capacity could be masking the contribution of oxidative damage originating in the skeletal muscle. We cannot exclude the possibility that if uremic or control animals were exercised blood ROS levels might have reflected skeletal muscle levels. Based however on our data, in a small number of animals, with tissue samples on the resting state, we cannot presently recommend that any blood marker, among those studied, could reliably reflect intramuscular redox status.

The findings of this study should be considered in the light of some limitations. We observed statistically significant correlations in the levels of critical redox indices between the soleus and the psoas in the uremic group and not in the control, which could partly reflect the disease-induced modification of muscle properties without excluding an effect of small sample size. A bigger number of animals could better clarify the tendencies for some indices examined, perhaps also including a nonoperated control group. However, due to the high cost of the model and ethical considerations, this was not possible in the present work. While we implemented an extensive panel of redox homeostasis, based on the established laboratory expertise, future work could extend this assessment to additional redox indices and enzymes (e.g., those upstream of catalase such as superoxide dismutase (SOD)) or also consider the emerging ratio between SOD and CAT [88], the role of peroxiredoxin proteins [89]. Moreover, future work should examine the interplay between molecular mechanisms of atrophy and renal insufficiency as well as the association between a set of inflammatory biomarkers and the progression of CKD. Finally, it could be of interest to obtain data from a group of uremic rabbits also treated with antioxidant compound to evaluate the responsiveness of redox balance in the blood and in the muscle tissues.

5. Conclusion

In conclusion, the results of this work demonstrate that even in the predialysis stages of CKD there is an emergence of oxidative stress in the blood and a possibly adaptive response by the upregulation of the blood antioxidant defense. Moreover, carbonyl formation in both fast and slow skeletal muscle types, an indication of protein oxidation that can lead to protein degradation and proteolysis, emerges as a plausible early stimulus towards muscle atrophy observed later in advanced CKD. Last but not the least, it was found that blood levels of the redox status indices studied here did not reflect muscle concentrations. More work is needed in the direction of succeeding in less invasive monitoring of early muscle-related redox imbalances taking into consideration specific disease effects, age, and available techniques.

Our results showed redox disturbances both in the blood and muscle in an early stage of renal insufficiency, highlighting the need for further research in redox challenges imposed by chronic renal insufficiency on the skeletal muscle with a view of preserving muscle status before progression to the end stage of disease.

Abbreviations

BCA: Bicinchoninic acid
BW: Body weight
CKD: Chronic kidney disease
CVD: Cardiovascular disease
DCM: Dichloromethane
DNPH: 2,4-Dinitrophenylhydrazine
DPPH: 2,2-Diphenyl-1-picrylhydrazyl
DTNB: 5,5′-Dithiobis 2-nitrobenzoic acid
EDTA: Ethylenediaminetetraacetic acid
γ-GCS: γ-Glutamyl cysteine synthetase
GPx: Glutathione peroxidase
GSH: Reduced glutathione
GSH-S: Glutathione synthetase
GSSG: Oxidized glutathione
GR: Glutathione reductase
HCl: Hydrochloric acid
HD: Hemodialysis
H_2O_2: Hydrogen peroxide
KCl: Potassium chloride
K_2EDTA: Ethylene diamine tetra-acetic acid
MDA: Malondialdehyde
MHCf: Myosin heavy chain fast
NaCl: Sodium chloride
NADPH: Dihydronicotinamide-adenine dinucleotide phosphate
Na_2SO_4: Sodium sulfate
NEM: N-Ethylmaleimide
NF-κB: Nuclear factor κB
ox-LDL: Oxidatively modified low-density lipoprotein
PC: Protein carbonyls
PMSF: Phenylmethylsulfonyl fluoride
RBC: Red blood cell
ROS: Reactive oxygen species
RT: Room temperature
SEM: Standard error of the mean
SOD: Superoxide dismutase
TAC: Total antioxidant capacity
TBA: Thiobarbituric acid
TBARS: Thiobarbituric acid reactive substances
TCA: Trichloroacetic acid
t-GSH: Total glutathione
TNF-a: Tumor necrosis factor-α.

Data Availability

The data used to support the findings of this study are available from the corresponding author upon request.

Conflicts of Interest

The authors declare that there is no conflict of interest regarding the publication of this paper.

Acknowledgments

This work was supported by the European Union (European Social Fund, ESF) and Greek national funds through the Operational Program "Educational and Lifelong Learning" of the National Strategic Reference Framework (NSRF), Research Funding Program: Thales (MuscleFun Project-MIS 377260) Investing in Knowledge Society through the European Social Fund, and the European Union Horizon 2020 Research and Innovation Programme "H2020 MSCAS-RISE-Muscle Stress Relief" under grant agreement no. 645648.

References

[1] B. Halliwell, "Free radicals and antioxidants: a personal view," *Nutrition Reviews*, vol. 52, no. 8, pp. 253–265, 1994.

[2] D. Trachootham, W. Lu, M. A. Ogasawara, N. R. D. Valle, and P. Huang, "Redox regulation of cell survival," *Antioxidants & Redox Signaling*, vol. 10, no. 8, pp. 1343–1374, 2008.

[3] B. Bayés, M. C. Pastor, J. Bonal, A. Foraster, and R. Romero, "Oxidative stress, inflammation and cardiovascular mortality in haemodialysis—role of seniority and intravenous ferrotherapy: analysis at 4 years of follow-up," *Nephrology, Dialysis, Transplantation*, vol. 21, no. 4, pp. 984–990, 2006.

[4] A. Kaltsatou, G. K. Sakkas, K. P. Poulianiti et al., "Uremic myopathy: is oxidative stress implicated in muscle dysfunction in uremia?," *Frontiers in Physiology*, vol. 6, p. 102, 2015.

[5] J. Himmelfarb and R. M. Hakim, "Oxidative stress in uremia," *Current Opinion in Nephrology and Hypertension*, vol. 12, no. 6, pp. 593–598, 2003.

[6] T. Grune, O. Sommerburg, and W. G. Siems, "Oxidative stress in anemia," *Clinical Nephrology*, vol. 53, Supplement 1, pp. S18–S22, 2000.

[7] P. Stenvinkel and P. Barany, "Anaemia, rHuEPO resistance, and cardiovascular disease in end-stage renal failure; links to inflammation and oxidative stress," *Nephrology, Dialysis, Transplantation*, vol. 17, no. 90005, pp. 32–37, 2002.

[8] B. Canaud, J. P. Cristol, M. Morena, H. Leray-Moragues, J. Y. Bosc, and F. Vaussenat, "Imbalance of oxidants and antioxidants in haemodialysis patients," *Blood Purification*, vol. 17, no. 2-3, pp. 99–106, 1999.

[9] K. Yamagata, K. Ishida, T. Sairenchi et al., "Risk factors for chronic kidney disease in a community-based population: a 10-year follow-up study," *Kidney International*, vol. 71, no. 2, pp. 159–166, 2007.

[10] J. Frijhoff, P. G. Winyard, N. Zarkovic et al., "Clinical relevance of biomarkers of oxidative stress," *Antioxidants & Redox Signaling*, vol. 23, no. 14, pp. 1144–1170, 2015.

[11] K. P. Poulianiti, A. Kaltsatou, G. I. Mitrou et al., "Systemic redox imbalance in chronic kidney disease: a systematic review," *Oxidative Medicine and Cellular Longevity*, vol. 2016, Article ID 8598253, 19 pages, 2016.

[12] L. Sibal, S. C Agarwal, P. D Home, and R. H Boger, "The role of asymmetric dimethylarginine (ADMA) in endothelial dysfunction and cardiovascular disease," *Current Cardiology Reviews*, vol. 6, no. 2, pp. 82–90, 2010.

[13] M. Yu, Y. J. Kim, and D. H. Kang, "Indoxyl sulfate-induced endothelial dysfunction in patients with chronic kidney disease via an induction of oxidative stress," *Clinical Journal of the American Society of Nephrology*, vol. 6, no. 1, pp. 30–39, 2011.

[14] H. F. Tbahriti, A. Kaddous, M. Bouchenak, and K. Mekki, "Effect of different stages of chronic kidney disease and renal replacement therapies on oxidant-antioxidant balance in uremic patients," *Biochemistry Research International*, vol. 2013, Article ID 358985, 6 pages, 2013.

[15] M. Jankowska, B. Rutkowski, and A. Debska-Slizien, "Vitamins and microelement bioavailability in different stages of chronic kidney disease," *Nutrients*, vol. 9, no. 3, 2017.

[16] J. M. Campistol, "Uremic myopathy," *Kidney International*, vol. 62, no. 5, pp. 1901–1913, 2002.

[17] N. Brautbar, "Skeletal myopathy in uremia: abnormal energy metabolism," *Kidney International Supplement*, vol. 16, pp. S81–S86, 1983.

[18] J. Metcoff, S. Dutta, G. Burns, J. Pederson, B. Matter, and O. Rennert, "Effects of amino acid infusions on cell metabolism in hemodialyzed patients with uremia," *Kidney International Supplement*, vol. 16, pp. S87–S92, 1983.

[19] S. Del Canale, E. Fiaccadori, N. Ronda, K. Söderlund, C. Antonucci, and A. Guariglia, "Muscle energy metabolism in uremia," *Metabolism*, vol. 35, no. 11, pp. 981–983, 1986.

[20] K. G. Avin, N. X. Chen, J. M. Organ et al., "Skeletal muscle regeneration and oxidative stress are altered in chronic kidney disease," *PLoS One*, vol. 11, no. 8, article e0159411, 2016.

[21] T. Nagasawa, T. Hatayama, Y. Watanabe, M. Tanaka, Y. Niisato, and D. D. Kitts, "Free radical-mediated effects on skeletal muscle protein in rats treated with Fe-nitrilotriacetate," *Biochemical and Biophysical Research Communications*, vol. 231, no. 1, pp. 37–41, 1997.

[22] L. Gotloib, P. Crassweller, H. Rodella et al., "Experimental model for studies of continuous peritoneal'dialysis in uremic rabbits," *Nephron*, vol. 31, no. 3, pp. 254–259, 1982.

[23] N. Hamalainen and D. Pette, "The histochemical profiles of fast fiber types IIB, IID, and IIA in skeletal muscles of mouse, rat, and rabbit," *The Journal of Histochemistry and Cytochemistry*, vol. 41, no. 5, pp. 733–743, 1993.

[24] A. McArdle, D. Pattwell, A. Vasilaki, R. D. Griffiths, and M. J. Jackson, "Contractile activity-induced oxidative stress: cellular origin and adaptive responses," *American Journal of Physiology-Cell Physiology*, vol. 280, no. 3, pp. C621–C627, 2001.

[25] B. Franzke, B. Halper, M. Hofmann et al., "The impact of six months strength training, nutritional supplementation or cognitive training on DNA damage in institutionalised elderly," *Mutagenesis*, vol. 30, no. 1, pp. 147–153, 2015.

[26] P. Bonaldo and M. Sandri, "Cellular and molecular mechanisms of muscle atrophy," *Disease Models & Mechanisms*, vol. 6, no. 1, pp. 25–39, 2013.

[27] S. Aigner, B. Gohlsch, N. Hamalainen et al., "Fast myosin heavy chain diversity in skeletal muscles of the rabbit: heavy chain IId, not IIb predominates," *European Journal of Biochemistry*, vol. 211, no. 1-2, pp. 367–372, 1993.

[28] M. H. Rouhani, M. Mortazavi Najafabadi, F. Moeinzadeh, A. Esmaillzadeh, A. Feizi, and L. Azadbakht, "Comparison of three diet quality indices for patients with chronic kidney disease," *Archives of Iranian Medicine*, vol. 20, no. 8, pp. 474–480, 2017.

[29] J. L. Babitt and H. Y. Lin, "Mechanisms of anemia in CKD," *Journal of the American Society of Nephrology*, vol. 23, no. 10, pp. 1631–1634, 2012.

[30] B. P. Yu, "Cellular defenses against damage from reactive oxygen species," *Physiological Reviews*, vol. 74, no. 1, pp. 139–162, 1994.

[31] I. Rahman, A. Kode, and S. K. Biswas, "Assay for quantitative determination of glutathione and glutathione disulfide levels using enzymatic recycling method," *Nature Protocols*, vol. 1, no. 6, pp. 3159–3165, 2006.

[32] D. Giustarini, I. Dalle-Donne, A. Milzani, P. Fanti, and R. Rossi, "Analysis of GSH and GSSG after derivatization with N-ethylmaleimide," *Nature Protocols*, vol. 8, no. 9, pp. 1660–1669, 2013.

[33] S. J. Kim, H. J. Jung, D. H. Hyun, E. H. Park, Y. M. Kim, and C. J. Lim, "Glutathione reductase plays an anti-apoptotic role against oxidative stress in human hepatoma cells," *Biochimie*, vol. 92, no. 8, pp. 927–932, 2010.

[34] A. E. Cribb, J. S. Leeder, and S. P. Spielberg, "Use of a microplate reader in an assay of glutathione reductase using 5,5′-dithiobis(2-nitrobenzoic acid)," *Analytical Biochemistry*, vol. 183, no. 1, pp. 195-196, 1989.

[35] J. Xie and K. M. Schaich, "Re-evaluation of the 2,2-diphenyl-1-picrylhydrazyl free radical (DPPH) assay for antioxidant activity," *Journal of Agricultural and Food Chemistry*, vol. 62, no. 19, pp. 4251–4260, 2014.

[36] A. Janaszewska and G. Bartosz, "Assay of total antioxidant capacity: comparison of four methods as applied to human blood plasma," *Scandinavian Journal of Clinical and Laboratory Investigation*, vol. 62, no. 3, pp. 231–236, 2002.

[37] H. Aebi, "[13] Catalase in vitro," *Methods in Enzymology*, vol. 105, pp. 121–126, 1984.

[38] Y. J. Suzuki, M. Carini, and D. A. Butterfield, "Protein carbonylation," *Antioxidants & Redox Signaling*, vol. 12, no. 3, pp. 323–325, 2010.

[39] R. Fields and H. B. F. Dixon, "Micro method for determination of reactive carbonyl groups in proteins and peptides, using 2,4-dinitrophenylhydrazine," *The Biochemical Journal*, vol. 121, no. 4, pp. 587–589, 1971.

[40] K. Yagi, "Simple assay for the level of total lipid peroxides in serum or plasma," *Methods in Molecular Biology*, vol. 108, pp. 101–106, 1998.

[41] J. A. Buege and S. D. Aust, "[30] Microsomal lipid peroxidation," *Methods in Enzymology*, vol. 52, pp. 302–310, 1978.

[42] R. R. Howell and J. B. Wyngaarden, "On the mechanism of peroxidation of uric acids by hemoproteins," *The Journal of Biological Chemistry*, vol. 235, pp. 3544–3550, 1960.

[43] A. Sevanian, K. J. A. Davies, and P. Hochstein, "Conservation of vitamin C by uric acid in blood," *Journal of Free Radicals in Biology & Medicine*, vol. 1, no. 2, pp. 117–124, 1985.

[44] Y. E. C. Taes, J. R. Delanghe, A. S. de Vriese, R. Rombaut, J. van Camp, and N. H. Lameire, "Creatine supplementation decreases homocysteine in an animal model of uremia," *Kidney International*, vol. 64, no. 4, pp. 1331–1337, 2003.

[45] M. J. Murray, *Proceedings of the North American Veterinary Conference: January 7-11, 2006, Orlando, Florida*, North American Veterinary Conference, 2006.

[46] D. M. Small, J. S. Coombes, N. Bennett, D. W. Johnson, and G. C. Gobe, "Oxidative stress, anti-oxidant therapies and chronic kidney disease," *Nephrology*, vol. 17, no. 4, pp. 311–321, 2012.

[47] S. C. Lu, "Glutathione synthesis," *Biochimica et Biophysica Acta (BBA) - General Subjects*, vol. 1830, no. 5, pp. 3143–3153, 2013.

[48] J. Bober, K. Kedzierska, E. Kwiatkowska et al., "Does oxidative stress affect the activity of the sodium-proton exchanger?," *Annales Academiae Medicae Stetinensis*, vol. 56, no. 3, pp. 5–12, 2010.

[49] N. Sahni, K. L. Gupta, S. V. Rana, R. Prasad, and A. K. Bhalla, "Intake of antioxidants and their status in chronic kidney disease patients," *Journal of Renal Nutrition*, vol. 22, no. 4, pp. 389–399, 2012.

[50] M. Annuk, M. Zilmer, L. Lind, T. Linde, and B. Fellström, "Oxidative stress and endothelial function in chronic renal failure," *Journal of the American Society of Nephrology*, vol. 12, no. 12, pp. 2747–2752, 2001.

[51] I. Ceballos-Picot, V. Witko-Sarsat, M. Merad-Boudia et al., "Glutathione antioxidant system as a marker of oxidative stress in chronic renal failure," *Free Radical Biology & Medicine*, vol. 21, no. 6, pp. 845–853, 1996.

[52] M.-S. S. Alhamdani, "Impairment of glutathione biosynthetic pathway in uraemia and dialysis," *Nephrology, Dialysis, Transplantation*, vol. 20, no. 1, pp. 124–128, 2005.

[53] O. Baud, A. E. Greene, J. Li, H. Wang, J. J. Volpe, and P. A. Rosenberg, "Glutathione peroxidase-catalase cooperativity is required for resistance to hydrogen peroxide by mature rat oligodendrocytes," *The Journal of Neuroscience*, vol. 24, no. 7, pp. 1531–1540, 2004.

[54] P. G. Paterson and B. H. J. Juurlink, "Nutritional regulation of glutathione in stroke," *Neurotoxicity Research*, vol. 1, no. 2, pp. 99–112, 1999.

[55] G. P. Biewenga, G. R. M. M. Haenen, and A. Bast, "The pharmacology of the antioxidant lipoic acid," *General Pharmacology*, vol. 29, no. 3, pp. 315–331, 1997.

[56] E. Peuchant, M. C. Delmas-Beauvieux, L. Dubourg et al., "Antioxidant effects of a supplemented very low protein diet in chronic renal failure," *Free Radical Biology & Medicine*, vol. 22, no. 1-2, pp. 313–320, 1997.

[57] R. A. Sunde and W. G. Hoekstra, "Structure, synthesis and function of glutathione peroxidase," *Nutrition Reviews*, vol. 38, no. 8, pp. 265–273, 1980.

[58] R. E. Pacifici and K. J. A. Davies, "[51] Protein degradation as an index of oxidative stress," *Methods in Enzymology*, vol. 186, pp. 485–502, 1990.

[59] T. Nyström, "Role of oxidative carbonylation in protein quality control and senescence," *The EMBO Journal*, vol. 24, no. 7, pp. 1311–1317, 2005.

[60] P. S. Lim, Y. M. Cheng, and Y. H. Wei, "Increase in oxidative damage to lipids and proteins in skeletal muscle of uremic patients," *Free Radical Research*, vol. 36, no. 3, pp. 295–302, 2002.

[61] G. K. Sakkas, D. Ball, T. H. Mercer, A. J. Sargeant, K. Tolfrey, and P. F. Naish, "Atrophy of non-locomotor muscle in patients with end-stage renal failure," *Nephrology, Dialysis, Transplantation*, vol. 18, no. 10, pp. 2074–2081, 2003.

[62] G. I. Mitrou, K. P. Poulianiti, Y. Koutedakis et al., "Functional responses of uremic single skeletal muscle fibers to redox imbalances," *Hippokratia*, vol. 21, no. 1, pp. 3–3, 2017.

[63] X. Chen, T. Mori, Q. Guo et al., "Carbonyl stress induces hypertension and cardio-renal vascular injury in Dahl salt-sensitive rats," *Hypertension Research*, vol. 36, no. 4, pp. 361–367, 2013.

[64] A. Ayala, M. F. Munoz, and S. Arguelles, "Lipid peroxidation: production, metabolism, and signaling mechanisms of malondialdehyde and 4-hydroxy-2-nonenal," *Oxidative Medicine and Cellular Longevity*, vol. 2014, Article ID 360438, 31 pages, 2014.

[65] D. Steinberg, "Low density lipoprotein oxidation and its pathobiological significance," *The Journal of Biological Chemistry*, vol. 272, no. 34, pp. 20963–20966, 1997.

[66] E. C. Papavasiliou, C. Gouva, K. C. Siamopoulos, and A. D. Tselepis, "Erythrocyte PAF-acetylhydrolase activity in various stages of chronic kidney disease: effect of long-term therapy with erythropoietin," *Kidney International*, vol. 68, no. 1, pp. 246–255, 2005.

[67] G. Haklar, I. Yeğenağa, and A. Süha Yalçin, "Evaluation of oxidant stress in chronic hemodialysis patients: use of different parameters," *Clinica Chimica Acta*, vol. 234, no. 1-2, pp. 109–114, 1995.

[68] O. Sommerburg, T. Grune, H. Hampl et al., "Does long-term treatment of renal anaemia with recombinant erythropoietin influence oxidative stress in haemodialysed patients?," *Nephrology, Dialysis, Transplantation*, vol. 13, no. 10, pp. 2583–2587, 1998.

[69] T. Sakata, R. Furuya, T. Shimazu, M. Odamaki, S. Ohkawa, and H. Kumagai, "Coenzyme Q10 administration suppresses both oxidative and antioxidative markers in hemodialysis patients," *Blood Purification*, vol. 26, no. 4, pp. 371–378, 2008.

[70] Z. M. Dimitrijevic, T. P. Cvetkovic, V. M. Djordjevic et al., "How the duration period of erythropoietin treatment influences the oxidative status of hemodialysis patients," *International Journal of Medical Sciences*, vol. 9, no. 9, pp. 808–815, 2012.

[71] N. J. Espat, E. M. Copeland, and L. L. Moldawer, "Tumor necrosis factor and cachexia: a current perspective," *Surgical Oncology*, vol. 3, no. 5, pp. 255–262, 1994.

[72] G. K. Sakkas, A. J. Sargeant, T. H. Mercer et al., "Changes in muscle morphology in dialysis patients after 6 months of aerobic exercise training," *Nephrology, Dialysis, Transplantation*, vol. 18, no. 9, pp. 1854–1861, 2003.

[73] M. Buck and M. Chojkier, "Muscle wasting and dedifferentiation induced by oxidative stress in a murine model of cachexia is prevented by inhibitors of nitric oxide synthesis and antioxidants," *The EMBO Journal*, vol. 15, no. 8, pp. 1753–1765, 1996.

[74] S. Ahmad, M. D. Karlstad, M. A. Choudhry, and M. M. Sayeed, "Sepsis-induced myofibrillar protein catabolism in rat skeletal muscle," *Life Sciences*, vol. 55, no. 18, pp. 1383–1391, 1994.

[75] L. Tessitore, P. Costelli, and F. M. Baccino, "Humoral mediation for cachexia in tumour-bearing rats," *British Journal of Cancer*, vol. 67, no. 1, pp. 15–23, 1993.

[76] J. M. Dayer, B. Beutler, and A. Cerami, "Cachectin/tumor necrosis factor stimulates collagenase and prostaglandin E_2 production by human synovial cells and dermal fibroblasts," *The Journal of Experimental Medicine*, vol. 162, no. 6, pp. 2163–2168, 1985.

[77] J. Gelin, L. L. Moldawer, C. Lönnroth, B. Sherry, R. Chizzonite, and K. Lundholm, "Role of endogenous tumor necrosis factor α and interleukin 1 for experimental tumor growth and the development of cancer cachexia," *Cancer Research*, vol. 51, no. 1, pp. 415–421, 1991.

[78] M. Llovera, C. García-Martínez, N. Agell, F. J. López-Soriano, and J. M. Argilés, "TNF can directly induce the expression of ubiquitin-dependent proteolytic system in rat soleus muscles," *Biochemical and Biophysical Research Communications*, vol. 230, no. 2, pp. 238–241, 1997.

[79] A. A. Beg, T. S. Finco, P. V. Nantermet, and A. S. Baldwin Jr, "Tumor necrosis factor and interleukin-1 lead to phosphorylation and loss of IκBα: a mechanism for NF-κB activation," *Molecular and Cellular Biology*, vol. 13, no. 6, pp. 3301–3310, 1993.

[80] Y. P. Li, R. J. Schwartz, I. D. Waddell, B. R. Holloway, and M. B. Reid, "Skeletal muscle myocytes undergo protein loss and reactive oxygen-mediated NF-κB activation in response to tumor necrosis factor α," *The FASEB Journal*, vol. 12, no. 10, pp. 871–880, 1998.

[81] K. Schulze-Osthoff, A. C. Bakker, B. Vanhaesebroeck, R. Beyaert, W. A. Jacob, and W. Fiers, "Cytotoxic activity of tumor necrosis factor is mediated by early damage of mitochondrial functions. Evidence for the involvement of mitochondrial radical generation," *The Journal of Biological Chemistry*, vol. 267, no. 8, pp. 5317–5323, 1992.

[82] T. Hennet, C. Richter, and E. Peterhans, "Tumour necrosis factor-α induces superoxide anion generation in mitochondria of L929 cells," *The Biochemical Journal*, vol. 289, no. 2, pp. 587–592, 1993.

[83] D. A. Rodriguez, S. Kalko, E. Puig-Vilanova et al., "Muscle and blood redox status after exercise training in severe COPD patients," *Free Radical Biology & Medicine*, vol. 52, no. 1, pp. 88–94, 2012.

[84] A. S. Veskoukis, M. G. Nikolaidis, A. Kyparos, and D. Kouretas, "Blood reflects tissue oxidative stress depending on biomarker and tissue studied," *Free Radical Biology & Medicine*, vol. 47, no. 10, pp. 1371–1374, 2009.

[85] S. V. Shah, R. Baliga, M. Rajapurkar, and V. A. Fonseca, "Oxidants in chronic kidney disease," *Journal of the American Society of Nephrology*, vol. 18, no. 1, pp. 16–28, 2007.

[86] D. M. Silverstein, "Inflammation in chronic kidney disease: role in the progression of renal and cardiovascular disease," *Pediatric Nephrology*, vol. 24, no. 8, pp. 1445–1452, 2009.

[87] S. Arguelles, S. Garcia, M. Maldonado, A. Machado, and A. Ayala, "Do the serum oxidative stress biomarkers provide a reasonable index of the general oxidative stress status?," *Biochimica et Biophysica Acta-General Subjects*, vol. 1674, no. 3, pp. 251–259, 2004.

[88] A. Crawford, R. G. Fassett, J. S. Coombes et al., "Glutathione peroxidase, superoxide dismutase and catalase genotypes and activities and the progression of chronic kidney disease," *Nephrology, Dialysis, Transplantation*, vol. 26, no. 9, pp. 2806–2813, 2011.

[89] E. El Eter and A. A. Al-Masri, "Peroxiredoxin isoforms are associated with cardiovascular risk factors in type 2 diabetes mellitus," *Brazilian Journal of Medical and Biological Research*, vol. 48, no. 5, pp. 465–469, 2015.

Hindawi
Oxidative Medicine and Cellular Longevity
Volume 2019, Article ID 7623023, 11 pages
https://doi.org/10.1155/2019/7623023

Research Article

New Insights into the Hepcidin-Ferroportin Axis and Iron Homeostasis in iPSC-Derived Cardiomyocytes from Friedreich's Ataxia Patient

Alessandra Bolotta,[1,2] **Provvidenza Maria Abruzzo**,[1,2] **Vito Antonio Baldassarro**,[3] **Alessandro Ghezzo**,[1] **Katia Scotlandi**,[4] **Marina Marini**,[1,2] **and Cinzia Zucchini**[1]

[1]*Department of Experimental, Diagnostic and Specialty Medicine, Bologna University, 40126 Bologna, Italy*
[2]*IRCCS Fondazione Don Carlo Gnocchi, 20148 Milan, Italy*
[3]*Interdepartmental Centre for Industrial Research in Health Sciences and Technologies (ICIR-HST), University of Bologna, 40064 Ozzano, Bologna, Italy*
[4]*CRS Development of Biomolecular Therapies, Experimental Oncology Laboratory, Orthopedic Rizzoli Institute, 40136 Bologna, Italy*

Correspondence should be addressed to Provvidenza Maria Abruzzo; provvidenza.abruzzo2@unibo.it

Received 11 September 2018; Accepted 4 December 2018; Published 27 March 2019

Guest Editor: Giorgos Sakkas

Iron homeostasis in the cardiac tissue as well as the involvement of the hepcidin-ferroportin (HAMP-FPN) axis in this process and in cardiac functionality are not fully understood. Imbalance of iron homeostasis occurs in several cardiac diseases, including iron-overload cardiomyopathies such as Friedreich's ataxia (FRDA, OMIM no. 229300), a hereditary neurodegenerative disorder. Exploiting the induced pluripotent stem cells (iPSCs) technology and the iPSC capacity to differentiate into specific cell types, we derived cardiomyocytes of a FRDA patient and of a healthy control subject in order to study the cardiac iron homeostasis and the HAMP-FPN axis. Both CTR and FRDA iPSCs-derived cardiomyocytes express cardiac differentiation markers; in addition, FRDA cardiomyocytes maintain the FRDA-like phenotype. We found that FRDA cardiomyocytes show an increase in the protein expression of HAMP and FPN. Moreover, immunofluorescence analysis revealed for the first time an unexpected nuclear localization of FPN in both CTR and FRDA cardiomyocytes. However, the amount of the nuclear FPN was less in FRDA cardiomyocytes than in controls. These and other data suggest that iron handling and the HAMP-FPN axis regulation in FRDA cardiac cells are hampered and that FPN may have new, still not fully understood, functions. These findings underline the complexity of the cardiac iron homeostasis.

1. Introduction

Iron is a trace metal essential for numerous biological processes. Its homeostasis is finely regulated, since both iron excess and deficiency are potential detrimental. In fact, iron excess favors the formation of oxygen radicals, while iron deficiency impairs enzyme functionality affecting oxygen metabolism. It has been demonstrated that the dysregulation of iron homeostasis is involved in different pathological conditions, including cancer, anemia, neurodegenerative disorders, and cardiac diseases [1]. Iron deficiency was found to occur in heart failure patients, independently of normal systemic iron concentration, causing morphological and functional mitochondrial alterations and consequently ATP depletion [2]. These dysfunctions, in turn, impair cardiac contractility and relaxation. Ironically, cardiomyopathy can be induced also by systemic iron overload, as in hereditary hemochromatosis (HH) and β-thalassemia, and by iron misdistribution in the cellular organelles, as in Friedreich's ataxia (FRDA) [3]. Iron excess causes an alteration of systolic and diastolic functions through the decrease of L-type channel activity, essential for the heart contraction. In addition, at

the cellular level, iron misdistribution in cellular organelles, such as the mitochondria, can damage the cells through oxygen radical production. Cardiomyocytes, being endowed of poor antioxidant defenses, are more susceptible to reactive species of oxygen (ROS) damage via Fenton and Heiber-Weiss-typereactions [3, 4]. Iron homeostasis is regulated by several proteins involved in the iron uptake, transport, storage, and export. These proteins cooperate with ferrireductases, ferroxidases, and chaperones to regulate the cellular iron trafficking and to limit the unbound labile iron pool (LIP), potential source of ROS. Iron exists within heme molecules such as hemoglobin and cytochromes or in iron-sulfur cluster- (ISC-) containing proteins such as succinate dehydrogenase; moreover, nonheme/non-ISC iron-containing proteins are present in the cells [5]. Nonheme iron is transported into the cells by iron-binding proteins, such as transferrin. Cellular uptake of iron from transferrin is initiated by the binding of transferrin to transferrin receptor 1 (TFRC). TFRC is a transmembrane protein that assists iron uptake through receptor-mediated endocytosis of iron-loaded transferrin [5]. In addition, iron chaperones such as frataxin, a nuclear-encoded protein localized into the mitochondrial matrix, act as iron sensor and storage proteins as well as iron chaperons during cellular Fe-S cluster biosynthesis [6].

In iron homeostasis, a central regulatory mechanism is the binding of the hormone hepcidin (HAMP) to the iron exporter ferroportin (FPN). FPN is the only iron-exporting protein localized in the cell membrane; it was independently discovered by three different groups [7–9]. The FPN structure has not been completely defined; it is characterized by 9-12 transmembrane domains (TMs), organized into two six-helix halves, which are connected by a large cytoplasmic loop between the 6^{th} and the 7^{th} domain [10, 11]. Furthermore, whether the functional form of FPN is monomeric or dimeric remains an open question. Genetic and biochemical evidences support the dimeric form [12]. However, different groups reported that FPN is a monomer, and that, in this form, it is able to bind HAMP [13, 14]. Regulation of FPN occurs at multiple levels, transcriptional, posttranscriptional, and posttranslational. FPN expression is regulated at the transcriptional level by hypoxia inducible factor-2alpha (HIF2α) in response to hypoxia and inflammation; moreover, it is induced by iron heme and other metals. Posttranscriptionally, FPN synthesis is regulated by iron regulatory proteins (IRPs), which bind to an iron responsive element (IRE) located in its $5'$UTR. In addition, posttranslational regulation of FPN is mediated by HAMP. HAMP binds FPN and triggers its internalization, ubiquitination, and subsequent lysosomal degradation [10, 11].

At systemic level, circulating HAMP is synthesized by the liver, where it is induced in iron overloading conditions and is inhibited by iron deficiency due to anemia, hypoxia, ineffective erythropoiesis, and inflammation [10, 11]. HAMP is also expressed in the heart, brain, kidney, and placenta [15]; in these tissues, its role is less defined, but it is likely involved in iron handling. HAMP expression is regulated by different members of the TGF-β superfamily, including BMP (bone morphogenetic protein) receptors, associated BMP ligands, and the cytoplasmic SMAD transcription factor [16]. Moreover, it is been shown that Atoh8 (atonal bHLH transcription factor 8) contributes to hepcidin regulation in response to iron levels by interacting with Id1 proteins [17]. Cardiac expression of HAMP is induced in response to hypoxia and inflammation [18]. Upregulation of HAMP occurs in heart ischemia [19], while its downregulation was described in a mouse model of dilated cardiomyopathy [20]. Moreover, Hsieh et al. [21] showed that apoptosis was induced by the knockdown of HAMP by siRNA in human cardiomyocytes treated with ferrous iron. Anomalies of HAMP-FPN axis affect the heart functionality. Mouse cardiac FPN knockouts show dilated cardiomyopathy and iron deposits in cardiomyocytes [22]. In addition, it has been shown that HAMP knockout at the cardiac level leads to an increase in cardiac FPN; moreover, HAMP loss or HAMP unresponsiveness is associated to cardiac hypertrophy and apoptosis [23]. In addition, heart autoptic tissue of FRDA patients revealed macrophagic inflammatory infiltrate with high levels of HAMP and iron deposits [24]. To the mechanisms of iron uptake, transport, storage, and export mentioned above, one should add those that regulate the utilization of iron and its correct subcellular distribution. Noteworthy, a still underestimated subcellular compartment involved in iron trafficking is the nucleus, where iron-sulfur clusters associated with DNA repair enzymes [25] and transcription factors have been described [26]. Iron transporters and storage proteins, such as the divalent metal transporter 1 (DMT1), lactoferrin, and ferritin, are associated to the nucleus [27].

The deregulation of iron compartmentalization is very often associated with neurodegenerative pathologies such as Friedrich's ataxia, a progressive neurodegenerative disorder characterized by degeneration of central and peripheral nervous systems and associated with hypertrophic cardiomyopathy and iron deposits [28]. Cardiomyopathy and subsequent cardiac failure is the most common cause of death in FRDA patients [29], where expanded GAA repeats in intron 1 of the frataxin gene (FXN) cause its partial deficit [30]. Physiological functions of frataxin involve iron binding and storage, biogenesis of heme and iron-sulfur clusters, and iron sensing; data suggest that further—still undetermined—functions are present. Frataxin depletion results in mitochondrial dysfunction, mitochondrial iron accumulation, and ROS production [5, 31]. In this context, the complex relationship between the mitochondrial aberrations, iron imbalance and frataxin dysfunction, has contributed to the difficulty of deciphering the molecular mechanisms underlying the iron homeostasis imbalance and consequently of identifying effective therapeutic molecules to mitigate the cardiac hypertrophy. Moreover, the lack of a model that can recapitulate the phenotypic and genotypic characteristics of FRDA contributes to the poor knowledge of the underlying mechanisms of this disease.

Aim of the present study is to generate and characterize iPSC-derived cardiomyocytes as a cellular model to explore the HAMP-FPN axis and investigate the iron homeostasis in FRDA cardiac phenotype. Differentiation of iPSC-derived cardiomyocytes was monitored by cardiac gene analysis with real-time PCR and evaluation of cardiac proteins by cytofluorimetric and immunofluorescence methods.

2. Material and Methods

2.1. Human-Induced Pluripotent Stem Cells (hiPSCs). Human iPSCs derived from a healthy subject and from a FRDA patient were obtained from the NIGMS Human Genetic Cell Repository at the Coriell Institute for Medical Research: (GM 23280∗A and GM23404∗B, respectively) and generated through fibroblast reprogramming according to the Yamanaka method [32]. Table S1 reports genotypic and phenotypic features of the subjects.

2.2. Cardiomyocyte Derivation from hiPSCs. Differentiation of hiPSCs in cardiomyocytes was performed according to the GiWi method by Lian et al. [33]. The detailed protocol and the timeline of cardiac differentiation are reported in Figure S1.

2.3. Flow Cytometric Analysis. For cytometric analysis, wells were washed with PBS 1x and cardiomyocytes were dissociated with trypsin-EDTA 0.25% and then fixed in 1% paraformaldehyde for 20 min at room temperature and 90% cold methanol for 15 min. Cells (0.5×10^6) were centrifuged and the pellet incubated with primary anti-troponin T (TNNT2) antibody (Thermo Fisher Scientific, Waltham, MD) overnight at 4°C in a buffer containing 5% BSA and 1% Triton X-100 in PBS. Secondary antibody (Alexa Fluor 488 Goat anti-mouse IgG1) was added, and the samples were incubated for 30 min at room temperature, after which the nuclei were stained with DAPI. Samples were acquired using a FACSCalibur instrument and analyzed with the CellQuest software (Becton Dickinson, Italy). The primary and secondary antibody and the dilutions used are listed in Table S2.

2.4. Immunostaining Analysis. Cardiomyocytes were washed with PBS 1x and were dissociated with trypsin-EDTA 0.25% and then seeded on 0.1% gelatin-coated coversplis at 1×10^5cells/mL. After two days, the cells were fixed in 4% paraformaldehyde for 15 min at room temperature. The primary and secondary antibody and the dilutions used are listed in Table S2. Cardiomyocytes were incubated overnight at 4°C with the primary antibody in a buffer containing 5% nonfat dry milk and 0.4% Triton X-100 in PBS. Cells were washed three times for 5 min in PBS 1x. Subsequently, the cardiomyocytes were incubated with the secondary antibody for 20 min at room temperature, followed by nuclear staining with mounting medium containing DAPI (Santa Cruz Biotechnology, DBA, Italy). Images of cardiomyocytes were obtained using a fluorescence microscope (Leica DMLB Fluo MS15062).

2.5. RNA Isolation and cDNA Synthesis. Total RNA was extracted with TRIzol™ reagent (Invitrogen, Milan, Italy) following the manufacturer's instructions. RNA quality was measured by evaluation of 28S and 18S rRNA band sharpness after denaturing electrophoresis. RNA purity and concentration were assessed by spectrophotometer evaluation (Ultrospec 3000, Pharmacia Biotech, Cambridge, UK) at 230, 260, and 280 nm. Reverse transcription (800 ng of RNA template) was performed in a final volume of 20 μL using the iScript cDNA Synthesis Kit (Bio-Rad, Hercules, CA) following the manufacturer's instructions. The cDNA thus obtained was stored at -20°C and used for qRT-PCR analysis.

2.6. Quantitative RT-PCR Analysis. Quantitative RT-PCR was performed according to Abruzzo et al. [34] in a Bio-Rad CFX96 real-time thermal cycler using the SsoAdvanced™ SYBR® Green Supermix (Bio-Rad Laboratories, Hercules, CA). The primer sequences for target and housekeeping genes (β-actin, GAPDH) are listed in Table S3. Primers were designed with *PRIMER3* and *AMPLIFY* software and, whenever possible, were designed as to span an exon-exon junction. All primers were purchased from Sigma-Aldrich (St. Louis, MO). Data were analyzed with the software CFX Manager software (Bio-Rad Laboratories, Hercules, CA), by using the $2^{-\Delta\Delta CT}$ method [35]; data were normalized with the housekeeping genes β-actin and GAPDH; primer efficiency in the real-time PCR reaction was between 95% and 105% [36].

2.7. Bioinformatic Analysis of Ferroportin Protein Sequence. In order to evaluate whether a nuclear localization signal (NLS) is present in FPN, its protein sequence was analyzed by cNLS Mapper, a freely available software (http://nls-mapper.iab.keio.ac.jp/cgi-bin/NLS_Mapper_form.cgi). cNLS is a bioinformatic tool useful to predict the NLS specific for the $\alpha\beta$ importin pathway; it yields the NLS scores (levels of NLS activities). Four NLS profiles are calculated: class 1/2, class 3, class 4, and bipartite NLSs. cNLS Mapper extracts putative NLS sequences with a score equal to or more than the selected cutoff score. Each amino acid residue at each position within an NLS class yields a score that sums up in order to characterize the entire NLS activity. Higher scores (8, 9, or 10) indicate the exclusive localization in the nucleus; scores 7 or 8 indicate a partial localization in the nucleus; scores 3, 4, or 5 suggest that the protein is localized both in the nucleus and in the cytoplasm. Scores 1 or 2 define the exclusive localization in the cytoplasm [37].

2.8. Confocal Analysis of Ferroportin. Confocal microscopy was used to study the presence of the FPN in the nuclei of iPSC-derived cardiomyocytes. Sections were scanned with a Nikon Ti-E fluorescence microscope coupled to an A1R confocal system and the NIS-Elements AR 3.2 software. A diode laser system with 405 wavelength output, air-cooled argon-ion laser system with 488 wavelength output, and yellow diode-pumped solid-state laser system with 561 wavelength output were used. Images were acquired with oil immersion 60x with an optical resolution of 0.18 micron, 2x scanner zoom, and 1024×1024 pixel resolution. All the z stacks were collected in compliance with optical section separation (z interval) values suggested by the NIS-Elements AR 3.2 software. Three random fields per sample were acquired, containing at least 10 cells per sample. Stacks were 0.850 μm for a total of 14 images. 3D images were analyzed by the Imaris software (Bitplane, Concord, MA). The algorithm of the software is able to detect the nuclei, marked by DAPI, and create an isosurface on the blue fluorescence. Then, the green fluorescence, corresponding to the total FPN signal,

was quantified only inside the nuclei isosurfaces. In addition, the volume of each nucleus was measured and analyzed.

2.9. Western Blot Analysis. Cardiomyocytes were lysed in 50 mM Tris-HCl (pH 8.0), 150 mM NaCl, NP-40 1%, and protease inhibitor mix (Roche, Sigma-Aldrich, Saint Louis, MO). Protein concentration was determined using Bradford protein assay (Bio-Rad Laboratories, Hercules, CA). 45 μg of protein samples was solubilized in Laemmli buffer 4x (200 mM Tris-HCl, pH 6.8, 5% SDS, 25% glycerol, 0.04% bromophenol blue, and 5% beta-mercaptoethanol) for 1 h in ice bath. Precast gradient gels (Mini-PROTEAN TGX stain-free protein gel, 4-15% polyacrylamide) (Bio-Rad Laboratories, Hercules, CA) were used. Mini-PROTEAN TGX gels contain trihalo compounds, which, in the presence of UV light, react with tryptophan residues producing fluorescence, proportional to the total protein amount of the sample. Gels were electroblotted onto nitrocellulose membranes (pore sizes: 0.45 μm). Membranes were exposed to UV light in order to visualize the protein band integrity and the efficiency of transfer. After blocking in Tris-buffered saline (TBS 1x) containing 0.1% Tween-20 (TBS-T), nonfat milk 5%, and 1% BSA for 1 h at room temperature, membranes were probed overnight at 4°C with the primary antibodies and then washed three times with TBS-T and incubated with rabbit-IgG HRP-conjugated secondary antibody, dissolved in blocking buffer for 1 hour at room temperature. Details about primary and secondary antibodies used are listed in Table S2. Finally, membranes were incubated with ECL chemiluminescent reagent (Western Bright ECL HRP substrate, Advansta, CA, USA) and exposed to an X-ray film (Aurogene s.r.l., Rome, Italy). Densitometric analysis was performed by means of Bio-Rad Gel Doc 2000. Density of specific protein bands was normalized to the β-actin band.

2.10. Statistical Analysis. For quantitative RT-PCR, statistical analysis was performed by the CFX Manager software (Bio-Rad Laboratories, Hercules, CA) and qbase plus (http://www.biogazelle.com/). For Western blot, the statistical analysis was performed by Student's t-test. A value of $p < 0.05$ was considered statistically significant.

3. Results

3.1. Cardiomyocyte Differentiation from hiPSCs. The differentiation of cardiomyocytes (CMs) from iPSCs was successfully repeated four times. Movies SM1 and SM2, reported in the Supplementary Materials, show beating CMs from both control and FRDA cultures. Notably, some of the beating areas found in cardiomyocyte cultures derived from FRDA iPSCs were unsynchronized, in contrast with the remarkable synchronization of control cardiomyocyte cultures.

3.2. Cardiomyocyte Characterization. The characterization of cardiomyocyte differentiation was obtained by evaluating the synthesis of four heart-specific genes: GATA4, a transcription factor specific for the cardiac lineage; SIRPA, a nonreceptorial tyrosine protein-phosphatase, exclusively expressed on the surface of hiPSC-derived cardiomyocytes [38]; and TNNT2 and actinin 2, two cardiac structural proteins. Messenger RNAs from control and FRDA CMs and iPSCs were compared by qRT-PCR and results are shown in Figure 1(a) as the average of four independent differentiation procedures. Cardiac-specific genes were significantly upregulated in CMs with respect to iPSCs in both control and FRDA samples.

Moreover, TNNT2 protein was evaluated by FACS analysis in CMs (Figure 1(b)). FACS analysis showed that the efficiency of CM differentiation from iPSCs was 80-90%.

Finally, the immunofluorescence analysis demonstrated that TNNT2 costained with the heavy myosin chain (MF20) proteins (Figure 1(c)) in both control and FRDA CMs. TNNT2 fluorescence suggests that both control and FRDA CMs display the typical sarcomeric organization.

3.3. Maintenance of the FRDA-Like Phenotype in iPSCs and CMs. To determine whether FRDA iPSCs and CMs maintained the FRDA-like phenotype, the gene expression of FXN was analyzed. As expected, the expression of FXN gene in FRDA iPSCs was about 30% of control iPSCs (Figure 2). Moreover, cardiac differentiation did not alter the pathological phenotype; the expression of FXN in FRDA CMs was about 55% with respect to control. An average of four independent experiments is shown.

3.4. TFRC Gene Expression Is Upregulated in FRDA CMs. The mRNA abundance of the key iron homeostasis-related genes was assessed in control and FRDA CMs by qRT-PCR. Data are shown in Figure 3 as the average of four independent differentiation procedures. The expression of transferrin receptor (TFRC) was significantly increased in iPSC-CMs FRDA. Moreover, also the mRNA levels of HAMP, FPN, and ATOH8, a transcription factor involved in HAMP regulation, showed a trend to increase. No relevant difference was evidenced in the expression of FTH1 gene.

3.5. Protein Expression of HAMP and FPN Is Increased in FRDA CMs. To validate gene expression data, the protein amount of HAMP and FPN by Western blot was evaluated in whole lysates of both CTR and FRDA CMs. A representative image and the densitometric analysis of the bands are shown in Figures 4(a) and 4(b); the average of three independent differentiation experiments is reported. A significant increase of HAMP and FPN (about 2.5 and 2.0 times, respectively) was found in FRDA CMs compared to controls. It should be noted that FPN antibody detects two bands, at about 72 kDa and 62 kDa, respectively, both of which were more intense in FRDA CMs with respect to controls. Ross et al. [39] described two FPN bands, at ~65 and ≈55 kDa, respectively, in T-REx™/FPN-V5 cells and demonstrated that the heavier isoform was glycosylated.

3.6. FPN Nuclear Localization in iPSC-Derived CMs. FPN protein localization and expression was assessed by immunostaining using confocal microscopy. Figure 5(a) clearly demonstrates a nuclear localization of FPN in both CTR and FRDA CMs. Moreover, the analysis of FITC fluorescence intensity (Figure 5(b)) showed that (i) the amount of FPN was significantly lower in the nuclei from FRDA CMs compared to controls and (ii) decrease was stronger when

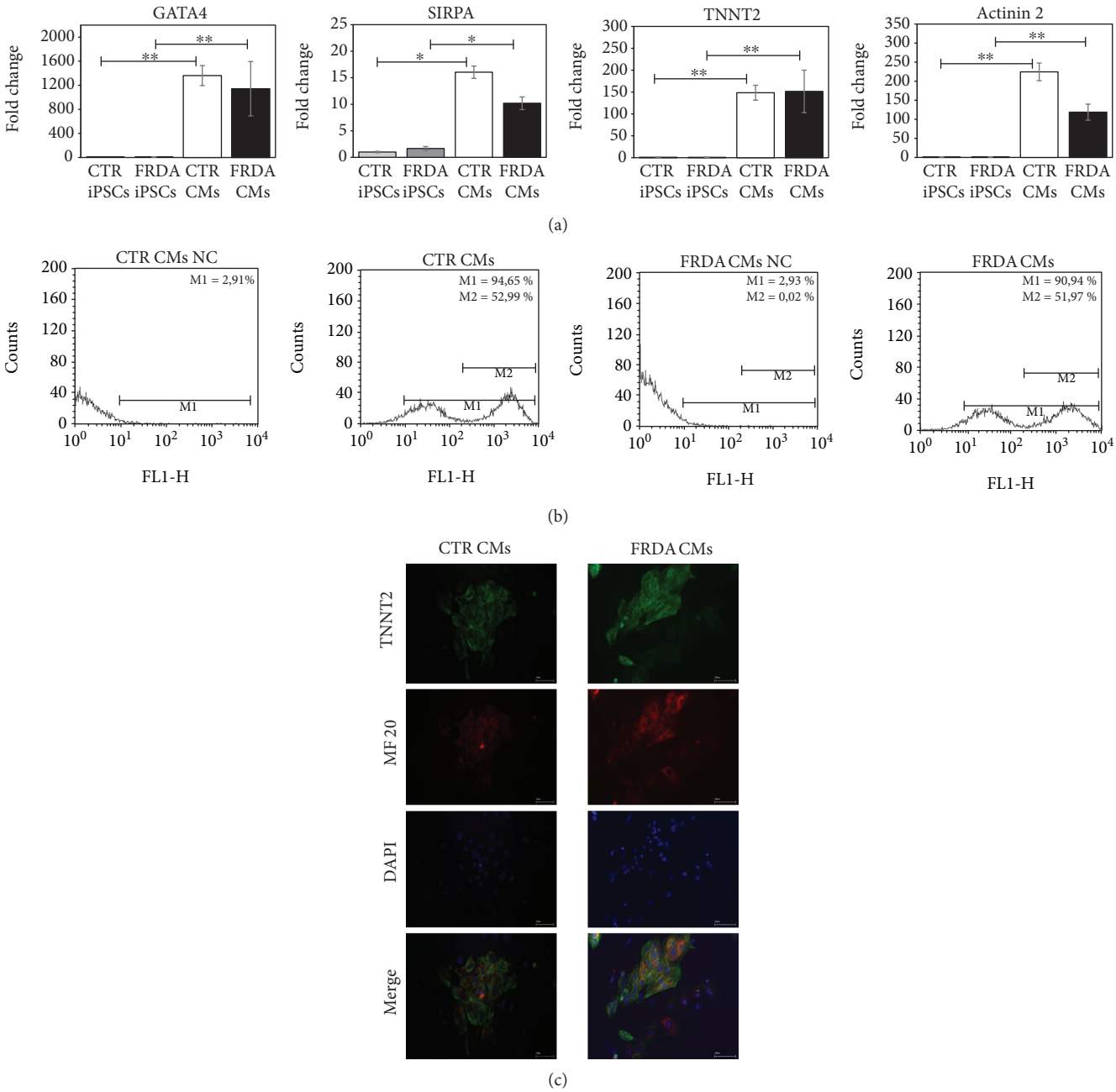

Figure 1: Characterization of CTR and FRDA iPSCs and iPSC-derived CMs. (a) Gene expression of four specific cardiac genes, GATA4, SIRPA, TNNT2, and actinin 2 characterized by qRT-PCR. Data were normalized with two housekeeping genes, β-actin and GAPDH; for each gene, the normalized expression value of CTR iPSCs was set to 1, and all other gene expression data were reported to that sample. PCR was run in triplicate; data are from four independent differentiation experiments and are expressed as mean ± SEM. $^{*}p < 0.05$; $^{**}p < 0.01$. (b) A representative flow cytometer analysis of CTR and FRDA CMs stained with TNNT2. NC negative control was stained with secondary antibody only; M1: percentage of TNNT2-positive CMs; M2: percentage of CMs highly positive to TNNT2. (c) A representative immunofluorescence image of CTR and FRDA CMs. TNNT2 is stained in green; heavy myosin chain (MF 20) is stained in red; the nuclei are stained with DAPI (blue). Scale bar 50 μm.

normalized to the volume of the nucleus, which (iii) is greater in FRDA CMs than in control. Since the nuclear localization of FPN had not been previously described, we used the cNLS Mapper software to identify, if present, nuclear localization signals (NLS) in the FPN protein sequence (NP_055400). This analysis revealed three predicted bipartite nuclear localization sequences: a sequence of 29 aa in 223 position (LWKVYQKTPALAVKAGLKEEETELKQLNL) with 3.3 score, a sequence of 32 aa (WLRRKCGLVRTGLISGLAQL-SCLILCVISVF) in 362 position with 3.1 score, and finally a sequence of 29 aa (KAGLKEEETELKQLNLHKDTEPK-PLEGTH) in 236 position with 3.8 score (Figure 5(c)). The NLS score analysis suggests that FPN can be localized in both the nucleus and cytoplasm.

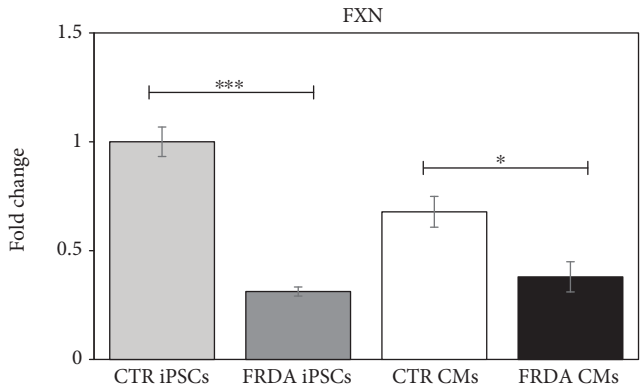

Figure 2: Evaluation of the FRDA-like phenotype in iPSCs and CMs. qRT-PCR of FXN gene expression in both CTR and FRDA iPSCs and CMs. Data were normalized with two housekeeping genes, β-actin and GAPDH; the normalized FXN expression value of CTR iPSCs was set to 1, and all other gene expression data were reported to that sample. Data are from four independent differentiation experiments and are expressed as mean ± SEM. $^{*}p < 0.05$; $^{***}p < 0.001$.

4. Discussion

In the present study, we describe some relevant features of iron homeostasis in iPSC-derived cardiomyocytes from one healthy control and one FRDA-affected patient. Cardiomyocytes were shown to fully express cardiac differentiation markers. Both FRDA iPSCs and CMs maintained the pathological phenotype, characterized by low levels of frataxin mRNA; however, frataxin expression in FRDA CMs was not as reduced as in iPSCs relative to control CMs. A similar result was reported by Hick et al. [40], who ascribed such difference to the reduced number of GAA repeats in the CM beating areas with respect to iPSCs of the same subject. Spontaneously beating areas were observed at 9-12 days from the start of the induction procedure, but FRDA beating areas were desynchronized, in agreement with similar results reported by Hick et al. [40].

Several studies pointed out the importance of iron homeostasis in the cardiac tissue; however, to date, the local regulation of iron in cardiomyocytes has not been fully characterized. In particular, the HAMP-FPN axis seems to be crucial for heart function [15, 22, 23]. Cardiac iron dysregulation was described in several disorders including FRDA, which is characterized by iron maldistribution within subcellular compartments, leading to mitochondrial iron accumulation and cytosolic iron depletion [5, 28, 41]. In the present study, cardiomyocytes were derived from CTR and FRDA human iPSCs in order to study some features of iron homeostasis, focusing the attention to the HAMP-FPN axis. This cellular model was already exploited by Lee et al. [42] to study the gene and protein expression of a group of iron-handling proteins in FRDA. To our knowledge, iron distribution within the cell compartments has not yet been evaluated in the iPSC-derived CM cellular model. The lack of such evaluation is a limitation of the present study, but this issue will be addressed in future research.

In the present study, a number of iron homeostasis-related genes and proteins were found to be dysregulated in FRDA CMs. Elevated HAMP expression has been already described in FRDA autoptic heart tissues [24], but the authors attributed HAMP overexpression to macrophagic inflammatory infiltrate. On the contrary, our results suggest that the increase in HAMP content is due to its overexpression in FRDA CMs.

In turn, HAMP downregulates the cellular amount of FPN, causing its lysosomal degradation [10, 11]. At variance with the expected decrease of FPN levels, HAMP upregulation in FRDA CMs was not accompanied by a decrease in FPN, rather a significant increase of FPN (protein) was observed.

In a different context, both FPN and HAMP were found to be significantly decreased in brain tissue of Alzheimer's disease patients, where oxidative stress is known to occur [43].

Our data show that the upregulation of HAMP and FPN in FRDA CMs is accompanied by the upregulation of TFRC. Huang et al. [44] found a decrease of FPN and an increase of TFRC in the heart of a conditional frataxin knockout (mutant) mice. It is difficult to compare our in vitro data with this study, which makes use of an animal model, where a complex interplay between local and systemic iron homeostasis takes place, and where frataxin expression is almost completely abolished. It is our opinion that our observations may reflect a dysregulation of these iron-handling proteins in FRDA CMs. Since it is known that oxidative stress affects FRDA neuronal and cardiac cells [45], it is possible that FPN loses its responsiveness to HAMP downregulation owing to the oxidation of key cysteine residues located in the HAMP- and FPN-interacting sites [46–48]. It can be envisioned that these cysteine residues are not oxidized in a "normal" low iron context, where oxidative stress is not present and HAMP downregulates FPN in order to avoid a further iron depletion. However, in the cytoplasm of FRDA cardiomyocytes, an unusual concurrence of low iron concentration AND oxidative stress is present, which would favor the inability of HAMP to downregulate FPN and to avoid iron leakage. Obviously, this is only one out of several other hypotheses, and further investigations need to be carried out for its validation or disproval.

The presence of FPN in the nuclei of CTR and FRDA CMs was demonstrated in this study for the first time. This finding suggests that FPN, traditionally considered as a transmembrane protein, could play a role in the maintenance of nuclear iron homeostasis. Henle et al. [49] described specific iron-binding sites on DNA. Moreover, other proteins involved in iron cellular trafficking, such as the divalent metal transporter 1 (DMT1), lactoferrin, and ferritin [27], have been found in the nuclear compartment. It is possible that the nuclear localization of FPN underscores a protective role from excess free iron in the nuclear compartment. Surprisingly, we found a lesser amount of nuclear FPN in FRDA cardiomyocytes with respect to controls, a result that seems to support the finding of DNA oxidative stress markers (8-OXO-dg) in FRDA patients [50]. On the other hand, the fact that FPN is less abundant in the nuclei of FRDA CMs than in controls is not necessarily in contradiction with the increase in both mRNA and protein FPN in FRDA

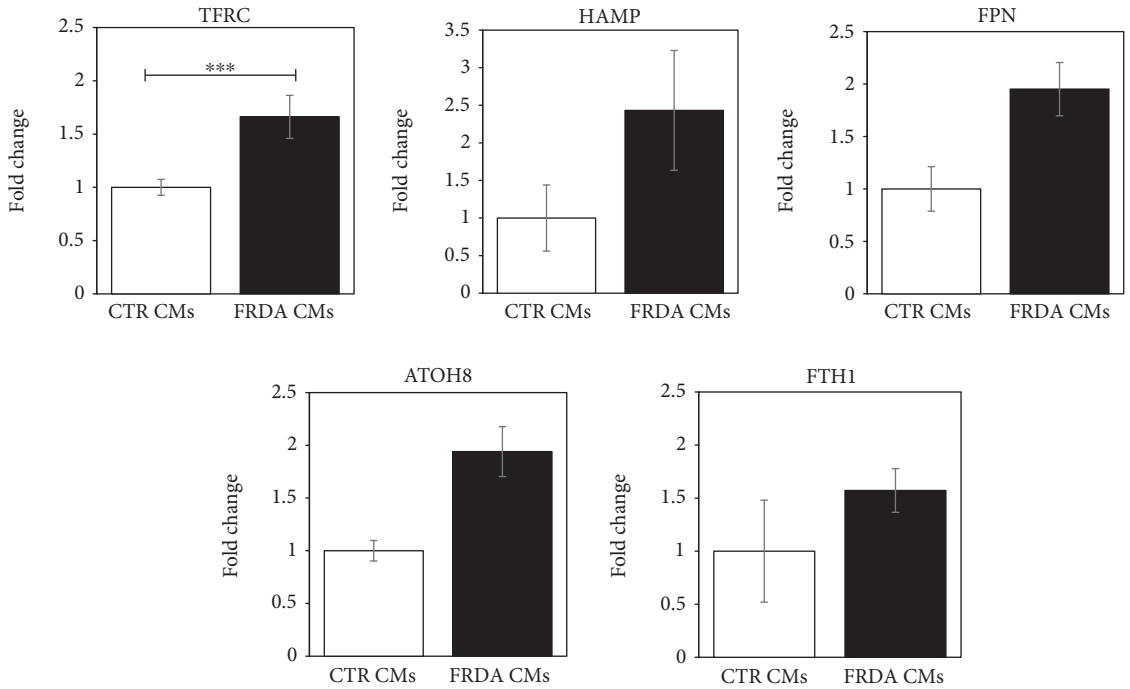

Figure 3: Gene expression of proteins involved in iron homeostasis in CTR and FRDA CMs. Expression levels of TFRC, HAMP, FPN, ATOH8, and FTH1 genes in CTR and FRDA CMs evaluated by qRT-PCR. Data were normalized with two housekeeping genes, β-actin and GAPDH; for each gene, the normalized expression value of CTR CMs was set to 1, and all other gene expression data were reported to that sample. Data are from four independent differentiation experiments and are expressed as mean ± SEM. $^{***}p < 0.001$.

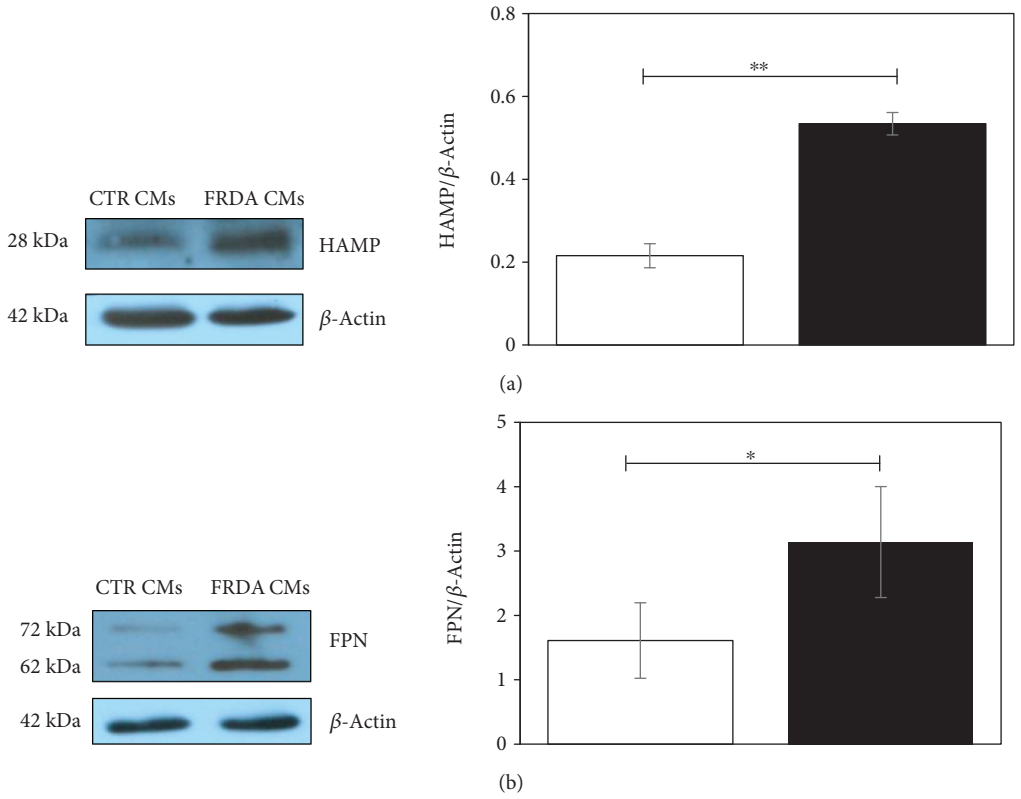

Figure 4: Protein expression of HAMP and FPN. (a) A representative Western blot image of HAMP expression. The band densities were analyzed by densitometry and normalized to β-actin. Histogram showing means ± Std Dev of HAMP/β-actin. (b) A representative Western blot image of FPN expression. The band densities were analyzed by densitometry and normalized to β-actin. Histogram showing means ± Std Dev of FPN/β-actin. Data are from three independent differentiation experiments. $^{*}p < 0.05$; $^{**}p < 0.01$.

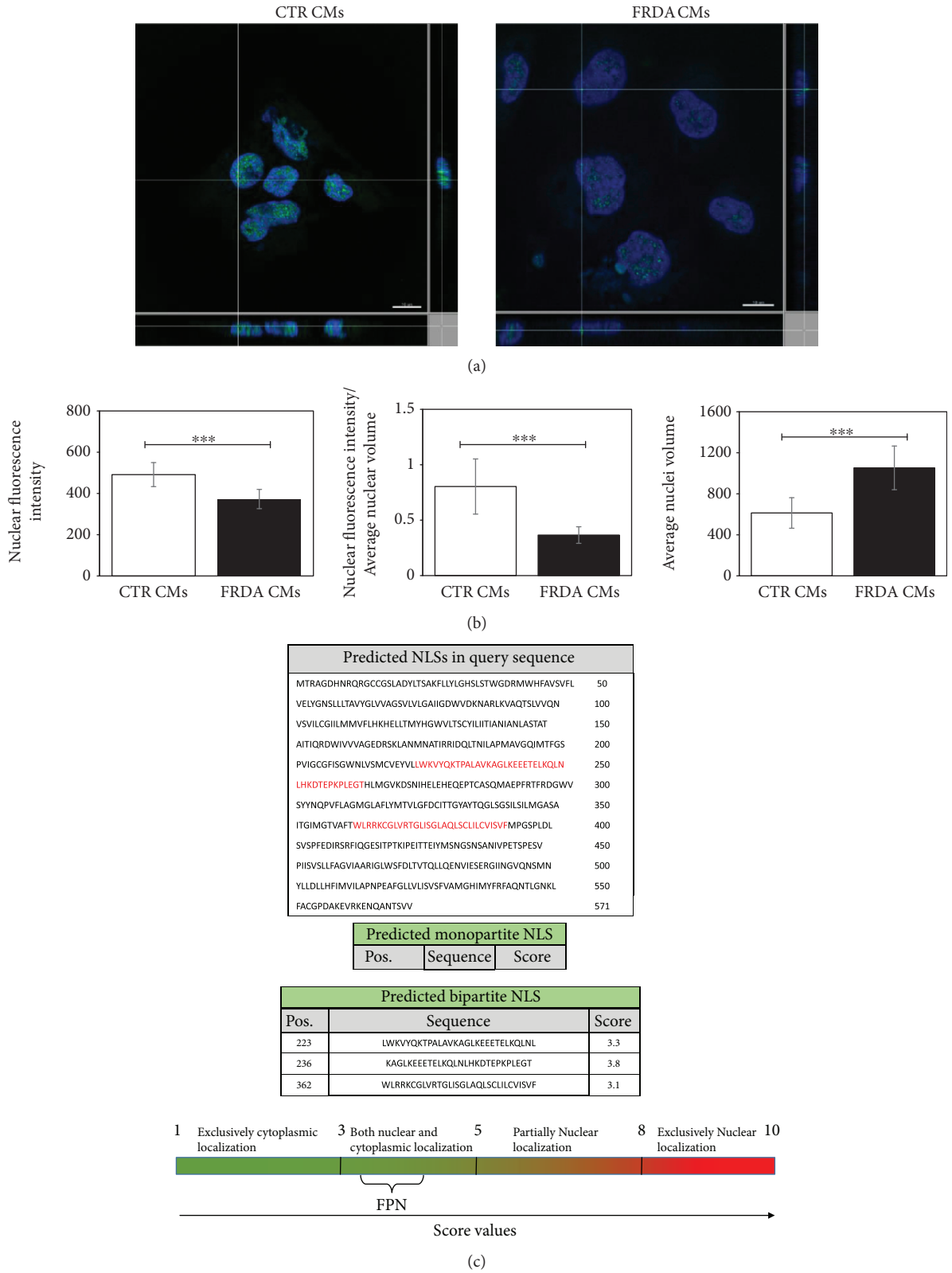

Figure 5: FPN nuclear localization in iPSC-derived CMs. (a) A representative confocal microscopy 3D image projection of FITC-stained FPN (green) protein expression in both CTR and FRDA CMs; the nuclei are counterstained with DAPI (blue). Scale bar equal 10 μm. (b) (i) Quantitative analysis of nuclear FITC fluorescence intensity in both CTR and FRDA CMs, (ii) quantitative analysis of nuclear FITC fluorescence intensity normalized to the average nuclear volume in both CTR and FRDA CMs, and (iii) average nuclear volume in both CTR and FRDA CMs; $^{***}p < 0.001$. (c) Bioinformatic analysis of FPN (NP_055400), using cNLS Mapper, predicted three bipartite NLS with a score value >3 indicating that the protein localizes both in the nucleus and in the cytoplasm.

cardiomyocytes, since Western blots were carried out in whole cell lysates, which include cytoplasmic FPN. A limitation of the present study is the lack of quantification of cytoplasmic FPN, either by confocal microscopy (which would require the delimitation of cell boundary by a specific staining) or by subcellular fractioning. This will be addressed by future studies.

The regulation of FPN distribution among the different subcellular compartments is a relevant issue, not yet afforded by researchers; in fact, the presence of 9-12 transmembrane domains supports its localization in the plasma membrane and its role of iron exporter and makes less likely a cytoplasmic and a nuclear localization. Thus, the nuclear localization of FPN we document here needs to be discussed not only in terms of novel FPN function(s), but also within the context of membrane and organelle trafficking and of final destination of proteins characterized by hydrophobic domains calling for a plasma membrane localization.

Finally, the presence of the enlarged nuclei, which was described here to occur in FRDA cardiomyocytes, has been reported in other cardiac pathologies, such as in hypertrophic and in dilated cardiomyopathy [51]. These morphological data need to be further investigated.

5. Conclusions

Cardiomyocytes derived from iPSCs retained the FRDA-like phenotype. Important alterations in the expression of HAMP and FPN, two proteins that play pivotal roles in cardiac iron homeostasis, are described here. Moreover, a novel nuclear localization of FPN in cardiomyocytes is reported, which suggests a potential new physiological function of this protein. These findings may have important implications in the understanding of cardiac iron homeostasis in both physiological and pathological conditions, such as FRDA. In particular, FRDA cardiomyocytes appear to be unable to exploit HAMP-operated regulation of FPN, which might be one of the reasons why iron distribution within the cell is impaired, thus leading to increase in the free iron pool. This, together with the defective assembly of mitochondrial proteins, would lead to chronic oxidative stress in FRDA cardiac cells. As pointed out by many authors [52–54], oxidative stress does not only lead to cell damage and apoptosis but also plays a role in adverse remodeling and contractile dysfunctions, as seen in FRDA patients.

Abbreviations

ATOH8: Atonal BHLH transcription factor 8
BMPs: Bone morphogenetic proteins
CMs: Cardiomyocytes
DMT1: Divalent metal transporter 1
FACS: Flow cytometry
FPN: Ferroportin
FRDA: Friedreich's ataxia
FTH1: Ferritin heavy chain 1
FXN: Frataxin gene
GAPDH: Glyceraldehyde-3-phosphate dehydrogenase
HAMP: Hepcidin
HH: Hereditary hemochromatosis
hiPSCs: Human-induced pluripotent stem cells
IF: Immunofluorescence
IREs: Iron regulatory elements
IRPs: Iron regulatory proteins
ISC: Iron-sulfur cluster
LIP: Labile iron pool
MF 20: Myosin heavy chain
NLS: Nuclear localization signal
ROS: Reactive oxygen species
TFRC: Transferrin receptor 1
TNNT2: Cardiac troponin T
TMs: Transmembrane domains.

Data Availability

The data used to support the findings of this study are available from the corresponding author upon request.

Disclosure

The funding organizations had no role in the study design, data collection and analysis, decision to publish, or preparation of the manuscript.

Conflicts of Interest

Authors declare the absence of conflicts of interest. The authors hereby declare that they have no financial relationships to disclose in relation to this article.

Authors' Contributions

Marina Marini and Cinzia Zucchini share coseniorship.

Acknowledgments

This work has been supported by a grant from the AISA (Italian Association of Patients with Ataxic Syndrome) and by a grant from the "Fondazione Luisa Fanti Melloni," University of Bologna, Italy. The authors would like to thank Dr. Filippo Fortuna for believing in this research and for supporting it in any possible way and Dr. Martina Rossi for her help.

Supplementary Materials

Supplementary 1. Table S1: phenotypic data of control subject and FRDA patient from which iPSCs were generated by Coriell Institute Repositories. Table S2: list of primary and secondary antibodies used in cytofluorimetry (FACS), immunofluorescence (IF), and Western blot (WB) analysis. Table S3: primer sequences and amplicon length of the genes analyzed by real-time PCR in iPSC-derived cardiomyocytes. β-Actin and GADPH were used as housekeeping genes.

Supplementary 2. Figure S1: timeline of iPSC-derived cardiomyocyte differentiation protocol.

Supplementary 3. SM1: CTR cardiomyocytes.

Supplementary 4. SM2: FRDA cardiomyocytes.

References

[1] R. Gozzelino and P. Arosio, "Iron homeostasis in health and disease," *International Journal of Molecular Sciences*, vol. 17, no. 1, 2016.

[2] M. F. Hoes, N. Grote Beverborg, J. D. Kijlstra et al., "Iron deficiency impairs contractility of human cardiomyocytes through decreased mitochondrial function," *European Journal of Heart Failure*, vol. 20, no. 5, pp. 910–919, 2018.

[3] S. Dev and J. L. Babitt, "Overview of iron metabolism in health and disease," *Hemodialysis International*, vol. 21, Supplement 1, pp. S6–S20, 2017.

[4] E. Gammella, S. Recalcati, I. Rybinska, P. Buratti, and G. Cairo, "Iron-induced damage in cardiomyopathy: oxidative-dependent and independent mechanisms," *Oxidative Medicine and Cellular Longevity*, vol. 2015, Article ID 230182, 10 pages, 2015.

[5] D. J. R. Lane, A. M. Merlot, M. L.-H. Huang et al., "Cellular iron uptake, trafficking and metabolism: key molecules and mechanisms and their roles in disease," *Biochimica et Biophysica Acta (BBA) - Molecular Cell Research*, vol. 1853, no. 5, pp. 1130–1144, 2015.

[6] K. C. Kondapalli, N. M. Kok, A. Dancis, and T. L. Stemmler, "Drosophila frataxin: an iron chaperone during cellular Fe-S cluster bioassembly," *Biochemistry*, vol. 47, no. 26, pp. 6917–6927, 2008.

[7] S. Abboud and D. J. Haile, "A novel mammalian iron-regulated protein involved in intracellular iron metabolism," *Journal of Biological Chemistry*, vol. 275, no. 26, pp. 19906–19912, 2000.

[8] A. Donovan, A. Brownlie, Y. Zhou et al., "Positional cloning of zebrafish ferroportin1 identifies a conserved vertebrate iron exporter," *Nature*, vol. 403, no. 6771, pp. 776–781, 2000.

[9] A. T. McKie, P. Marciani, A. Rolfs et al., "A novel duodenal iron-regulated transporter, IREG1, implicated in the basolateral transfer of iron to the circulation," *Molecular Cell*, vol. 5, no. 2, pp. 299–309, 2000.

[10] H. Drakesmith, E. Nemeth, and T. Ganz, "Ironing out ferroportin," *Cell Metabolism*, vol. 22, no. 5, pp. 777–787, 2015.

[11] D. M. Ward and J. Kaplan, "Ferroportin-mediated iron transport: expression and regulation," *Biochimica et Biophysica Acta*, vol. 1823, no. 9, pp. 1426–1433, 2012.

[12] I. De Domenico, D. M. Ward, G. Musci, and J. Kaplan, "Evidence for the multimeric structure of ferroportin," *Blood*, vol. 109, no. 5, pp. 2205–2209, 2007.

[13] E. Pignatti, L. Mascheroni, M. Sabelli, S. Barelli, S. Biffo, and A. Pietrangelo, "Ferroportin is a monomer in vivo in mice," *Blood Cells, Molecules, and Diseases*, vol. 36, no. 1, pp. 26–32, 2006.

[14] A. E. Rice, M. J. Mendez, C. A. Hokanson, D. C. Rees, and P. J. Bjorkman, "Investigation of the biophysical and cell biological properties of ferroportin, a multipass integral membrane protein iron exporter," *Journal of Molecular Biology*, vol. 386, no. 3, pp. 717–732, 2009.

[15] D. Vela, "Balance of cardiac and systemic hepcidin and its role in heart physiology and pathology," *Laboratory Investigation*, vol. 98, no. 3, pp. 315–326, 2018.

[16] P. J. Schmidt, "Regulation of iron metabolism by hepcidin under conditions of inflammation," *Journal of Biological Chemistry*, vol. 290, no. 31, pp. 18975–18983, 2015.

[17] L. Kautz, D. Meynard, A. Monnier et al., "Iron regulates phosphorylation of Smad1/5/8 and gene expression of Bmp6, Smad7, Id1, and Atoh8 in the mouse liver," *Blood*, vol. 112, no. 4, pp. 1503–1509, 2008.

[18] U. Merle, E. Fein, S. G. Gehrke, W. Stremmel, and H. Kulaksiz, "The iron regulatory peptide hepcidin is expressed in the heart and regulated by hypoxia and inflammation," *Endocrinology*, vol. 148, no. 6, pp. 2663–2668, 2007.

[19] G. Simonis, K. Mueller, P. Schwarz et al., "The iron-regulatory peptide hepcidin is upregulated in the ischemic and in the remote myocardium after myocardial infarction," *Peptides*, vol. 31, no. 9, pp. 1786–1790, 2010.

[20] L. Zhang, D. Lu, W. Zhang et al., "Cardioprotection by Hepc1 in cTnTR141W transgenic mice," *Transgenic Research*, vol. 21, no. 4, pp. 867–878, 2012.

[21] Y. P. Hsieh, C. H. Huang, C. Y. Lee, C. Y. Lin, and C. C. Chang, "Silencing of hepcidin enforces the apoptosis in iron-induced human cardiomyocytes," *Journal of Occupational Medicine and Toxicology*, vol. 9, no. 1, p. 11, 2014.

[22] S. Lakhal-Littleton, M. Wolna, C. A. Carr et al., "Cardiac ferroportin regulates cellular iron homeostasis and is important for cardiac function," *Proceedings of the National Academy of Sciences*, vol. 112, no. 10, pp. 3164–3169, 2015.

[23] S. Lakhal-Littleton, M. Wolna, Y. J. Chung et al., "An essential cell-autonomous role for hepcidin in cardiac iron homeostasis," *Elife*, vol. 5, 2016.

[24] A. H. Koeppen, R. L. Ramirez, A. B. Becker et al., "The pathogenesis of cardiomyopathy in Friedreich ataxia," *PLoS One*, vol. 10, no. 3, article e0116396, 2015.

[25] Y. Wu and R. M. Brosh, "DNA helicase and helicase-nuclease enzymes with a conserved iron-sulfur cluster," *Nucleic Acids Research*, vol. 40, no. 10, pp. 4247–4260, 2012.

[26] A. S. Fleischhacker and P. J. Kiley, "Iron-containing transcription factors and their roles as sensors," *Current Opinion in Chemical Biology*, vol. 15, no. 2, pp. 335–341, 2011.

[27] K. J. Thompson, M. G. Fried, Z. Ye, P. Boyer, and J. R. Connor, "Regulation, mechanisms and proposed function of ferritin translocation to cell nuclei," *Journal of Cell Science*, vol. 115, Part 10, pp. 2165–2177, 2002.

[28] S. Michael, S. V. Petrocine, J. Qian et al., "Iron and iron-responsive proteins in the cardiomyopathy of Friedreich's ataxia," *Cerebellum*, vol. 5, no. 4, pp. 257–267, 2006.

[29] A. Y. Tsou, E. K. Paulsen, S. J. Lagedrost et al., "Mortality in Friedreich ataxia," *Journal of the Neurological Sciences*, vol. 307, no. 1-2, pp. 46–49, 2011.

[30] V. Campuzano, L. Montermini, M. D. Molto et al., "Friedreich's ataxia: autosomal recessive disease caused by an intronic GAA triplet repeat expansion," *Science*, vol. 271, no. 5254, pp. 1423–1427, 1996.

[31] M. Pandolfo, "Iron metabolism and mitochondrial abnormalities in Friedreich ataxia," *Blood Cells, Molecules and Diseases*, vol. 29, no. 3, pp. 536–547, 2002.

[32] K. Takahashi and S. Yamanaka, "Induction of pluripotent stem cells from mouse embryonic and adult fibroblast cultures by defined factors," *Cell*, vol. 126, no. 4, pp. 663–676, 2006.

[33] X. Lian, J. Zhang, S. M. Azarin et al., "Directed cardiomyocyte differentiation from human pluripotent stem cells by modulating Wnt/β-catenin signaling under fully defined conditions," *Nature Protocols*, vol. 8, no. 1, pp. 162–175, 2012.

[34] P. M. Abruzzo, M. Marini, A. Bolotta et al., "Frataxin mRNA isoforms in FRDA patients and normal subjects: effect of

tocotrienol supplementation," *BioMed Research International*, vol. 2013, Article ID 276808, 9 pages, 2013.

[35] K. J. Livak and T. D. Schmittgen, "Analysis of relative gene expression data using real-time quantitative PCR and the 2(-delta delta C(T)) method," *Methods*, vol. 25, no. 4, pp. 402–408, 2001.

[36] M. W. Pfaffl, "A new mathematical model for relative quantification in real-time RT-PCR," *Nucleic Acids Research*, vol. 29, no. 9, pp. 45e–445, 2001.

[37] S. Kosugi, M. Hasebe, N. Matsumura et al., "Six classes of nuclear localization signals specific to different binding grooves of importin α," *Journal of Biological Chemistry*, vol. 284, no. 1, pp. 478–485, 2008.

[38] N. C. Dubois, A. M. Craft, P. Sharma et al., "SIRPA is a specific cell-surface marker for isolating cardiomyocytes derived from human pluripotent stem cells," *Nature Biotechnology*, vol. 29, no. 11, pp. 1011–1018, 2011.

[39] S. L. Ross, K. Biswas, J. Rottman et al., "Identification of antibody and small molecule antagonists of ferroportin-hepcidin interaction," *Frontiers in Pharmacology*, vol. 8, p. 838, 2017.

[40] A. Hick, M. Wattenhofer-Donze, S. Chintawar et al., "Neurons and cardiomyocytes derived from induced pluripotent stem cells as a model for mitochondrial defects in Friedreich's ataxia," *Disease Models & Mechanisms*, vol. 6, no. 3, pp. 608–621, 2013.

[41] H. Puccio, D. Simon, M. Cossée et al., "Mouse models for Friedreich ataxia exhibit cardiomyopathy, sensory nerve defect and Fe-S enzyme deficiency followed by intramitochondrial iron deposits," *Nature Genetics*, vol. 27, no. 2, pp. 181–186, 2001.

[42] Y.-K. Lee, P. W.-L. Ho, R. Schick et al., "Modeling of Friedreich ataxia-related iron overloading cardiomyopathy using patient-specific-induced pluripotent stem cells," *Pflügers Archiv - European Journal of Physiology*, vol. 466, no. 9, pp. 1831–1844, 2014.

[43] A. Raha, R. Vaishnav, R. Friedland, A. Bomford, and R. Raha-Chowdhury, "The systemic iron-regulatory proteins hepcidin and ferroportin are reduced in the brain in Alzheimer's disease," *Acta Neuropathologica Communications*, vol. 1, no. 1, p. 55, 2013.

[44] M. L.-H. Huang, E. M. Becker, M. Whitnall, Y. S. Rahmanto, P. Ponka, and D. R. Richardson, "Elucidation of the mechanism of mitochondrial iron loading in Friedreich's ataxia by analysis of a mouse mutant," *Proceedings of the National Academy of Sciences*, vol. 106, no. 38, pp. 16381–16386, 2009.

[45] M. Perdomini, A. Hick, H. Puccio, and M. A. Pook, "Animal and cellular models of Friedreich ataxia," *Journal of Neurochemistry*, vol. 126, Supplement 1, pp. 65–79, 2013.

[46] X. B. Liu, F. Yang, and D. J. Haile, "Functional consequences of ferroportin 1 mutations," *Blood Cells, Molecules, and Diseases*, vol. 35, no. 1, pp. 33–46, 2005.

[47] A. Fernandes, G. C. Preza, Y. Phung et al., "The molecular basis of hepcidin-resistant hereditary hemochromatosis," *Blood*, vol. 114, no. 2, pp. 437–443, 2009.

[48] J. B. Jordan, L. Poppe, M. Haniu et al., "Hepcidin revisited, disulfide connectivity, dynamics, and structure," *Journal of Biological Chemistry*, vol. 284, no. 36, pp. 24155–24167, 2009.

[49] E. S. Henle, Z. Han, N. Tang, P. Rai, Y. Luo, and S. Linn, "Sequence-specific DNA cleavage by Fe2+-mediated Fenton reactions has possible biological implications," *Journal of Biological Chemistry*, vol. 274, no. 2, pp. 962–971, 1999.

[50] J. B. Schulz, T. Dehmer, L. Schols et al., "Oxidative stress in patients with Friedreich ataxia," *Neurology*, vol. 55, no. 11, pp. 1719–1721, 2000.

[51] P. A. Harvey and L. A. Leinwand, "The cell biology of disease: cellular mechanisms of cardiomyopathy," *The Journal of Cell Biology*, vol. 194, no. 3, pp. 355–365, 2011.

[52] M. Seddon, Y. H. Looi, and A. M. Shah, "Oxidative stress and redox signalling in cardiac hypertrophy and heart failure," *Heart*, vol. 93, no. 8, pp. 903–907, 2007.

[53] D. B. Sawyer, "Oxidative stress in heart failure: what are we missing?," *The American Journal of the Medical Sciences*, vol. 342, no. 2, pp. 120–124, 2011.

[54] H. Tsutsui, S. Kinugawa, and S. Matsushima, "Oxidative stress and heart failure," *American Journal of Physiology-Heart and Circulatory Physiology*, vol. 301, no. 6, pp. H2181–H2190, 2011.

Hindawi
Oxidative Medicine and Cellular Longevity
Volume 2019, Article ID 2484678, 11 pages
https://doi.org/10.1155/2019/2484678

Research Article

Redox Status and Muscle Pathology in Rheumatoid Arthritis: Insights from Various Rat Hindlimb Muscles

A. B. Oyenihi, T. Ollewagen, K. H. Myburgh, Y. S. L. Powrie, and C. Smith

Department of Physiological Sciences, Stellenbosch University, South Africa

Correspondence should be addressed to C. Smith; csmith@sun.ac.za

Received 19 October 2018; Revised 21 December 2018; Accepted 29 January 2019; Published 26 March 2019

Academic Editor: Ilaria Peluso

Due to atrophy, muscle weakness is a common occurrence in rheumatoid arthritis (RA). The majority of human studies are conducted on the *vastus lateralis* muscle—a muscle with mixed fiber type—but little comparative data between multiple muscles in either rodent or human models are available. The current study therefore assessed both muscle ultrastructure and selected redox indicators across various muscles in a model of collagen-induced rheumatoid arthritis in female Sprague-Dawley rats. Only three muscles, the *gastrocnemius*, *extensor digitorum longus* (*EDL*), and *soleus*, had lower muscle mass (38%, 27%, and 25% loss of muscle mass, respectively; all at least $P < 0.01$), while the *vastus lateralis* muscle mass was increased by 35% ($P < 0.01$) in RA animals when compared to non-RA controls. However, all four muscles exhibited signs of deterioration indicative of rheumatoid cachexia. Cross-sectional area was similarly reduced in *gastrocnemius*, *EDL*, and *soleus* (60%, 58%, and 64%, respectively; all $P < 0.001$), but *vastus lateralis* (22% smaller, $P < 0.05$) was less affected, while collagen deposition was significantly increased in muscles. This pathology was associated with significant increases in tissue levels of reactive oxygen species (ROS) in all muscles except the *vastus lateralis*, while only the *gastrocnemius* had significantly increased levels of lipid peroxidation (TBARS) and antioxidant activity (FRAP). Current data illustrates the differential responses of different skeletal muscles of the hindlimb to a chronic inflammatory challenge both in terms of redox changes and resistance to cachexia.

1. Introduction

There can be no doubt that individuals suffering from rheumatoid arthritis (RA) have significantly decreased quality of life. In addition to the chronic pain and other primary symptoms arising from the inflammatory processes in joints, the majority of patients also report skeletal muscle weakness [1]. However, there is a disconnection between the degree of rheumatoid cachexia (defined as arthritis-associated loss of muscle mass with little or no loss of fat mass [2]) and the relatively more severe degree of muscle weakness experienced. Initially, the more severe loss of strength was ascribed to joint deformation and pain [3], but more recently, contractile dysfunction, mediated by tumor necrosis factor (TNF), was implicated, with TNF reported to decrease ?specific force by increasing cytosolic oxidant activity in the muscle [4].

The pathology of skeletal muscle in patients with RA is clearly complex and much research has already been conducted in this context, so that at least a partial picture of role players is available. For example, while neuromuscular fatigue (assessed by electromyography) was reported to weakly correlate with subjective perception of fatigue and physical activity level, it did not correlate to either clinical profile or treatment features [5]. This suggests that while advancement of emotional well-being should form part of treatment strategy, neuromuscular pathology is probably not a major role player in RA. In contrast, increased muscle inflammatory cytokine levels, altered expression of genes involved in muscle repair and glycolytic metabolism, as well as increased levels of fibrosis-associated amino acids, correlated with disease progression, physical inactivity, and pain in a large cohort of RA patients [6]. These data, generated from the *vastus lateralis* muscle, and specifically the finding related to altered glycolytic metabolism, raised the question of whether different muscles or muscles with different fiber type distributions may be differentially sensitive to RA-associated pathology.

Given both the significant implication of inflammation in RA and the interlinked nature of inflammation and oxidative stress, attention should also be extended to redox status, in order to form a more holistic picture of pathological maladaptations that could potentially be targeted by intervention. In an elegant study on the slow-twitch *soleus* muscle from rats subjected to collagen-induced arthritis (CIA), peroxynitrite-induced oxidative damage to myofibrillar proteins was implicated in measured deficits of muscle force production, such as shorter maximal contraction velocity and slower twitch contraction and relaxation [7]. The same group subsequently illustrated similar deficits in force production—also ascribed to reactive nitrogen species—in the fast-twitch *extensor digitorum longus* (*EDL*) muscle [8]. These studies sketch a fairly fiber-type independent picture of muscle pathology in this model. However, these observations were made at a relatively advanced time point (≈day 45, with last booster shot on day 28) and do not allow for direct interpretations on specific mechanisms at play during the earlier, disease development phase. Furthermore, the degree to which different muscle types are compromised in CIA has not been comprehensively and comparatively assessed.

The aim of the current study was therefore to assess muscle morphology and selected aspects of muscle pathology and redox changes in four different hindlimb muscles in rats with collagen-induced arthritis. A somewhat milder model (day 35, with last booster shot on day 8) was employed in order to elucidate the extent to which free radical involvement and endogenous antioxidant mechanisms may contribute to early pathology in different muscles.

2. Materials and Methods

2.1. Ethics Statement and Animal Handling. The Stellenbosch University Animal Research Ethics Committee ethically cleared this study (Protocol number: SU-ACUD17-00034). Twenty (20) female Sprague-Dawley rats weighing 180–200 g were procured from the Stellenbosch University small laboratory animal breeding facility. They were housed in groups of 5 rats per cage in a temperature- and humidity-controlled room (23 ± 1°C, 40–60% humidity) with a set 12 h light-dark cycle and fed standard commercially available rat chow and tap water *ad libitum*. After acclimatization to the new environment for about 7 days, rats were randomly divided into two groups of 10 rats each—normal control (NC) and collagen-induced rheumatoid arthritis (RA). All experimental animals received humane care according to the principles outlined in the National Research Foundation *Guide for the Care and Use of Laboratory Animals*.

2.2. Collagen-Induced Rheumatoid Arthritis Model

2.2.1. Chemicals. Bovine collagen type II, incomplete Freund's adjuvant, and rat anti-collagen IgG ELISA kit were purchased from Chondrex Inc., WA, USA. Isoflurane (Isofor) was purchased from Safeline Pharmaceuticals, Johannesburg, South Africa. All other chemicals and reagents used in this study were of analytical grade and purchased from Sigma-Aldrich (MO, USA) or Merck (Darmstadt, Germany) unless otherwise stated.

2.2.2. Experimental Design. The well-established rat collagen-induced arthritis (CIA) method [9, 10] was used to induce arthritis in the RA group. Briefly, bovine heterologous type II collagen was first dissolved in 0.01 N glacial acetic acid (2 mg/ml) before an emulsion was prepared using an equal volume of incomplete Freund's adjuvant. This emulsion was slowly injected intradermally twice just above the tail region of each rat under isoflurane anesthesia, 7 days apart. The time of onset of swelling in rat paws was recorded. The progression of clinical symptoms was monitored daily and scored as follows: 0 =no swelling; 1 =erythema and digits swollen; 2 =erythema, digits, and pad swollen; and 3 =erythema, also digits, pad,joints and entire leg swollen. The total score for each rat was given as the addition of all affected paws, so the highest attainable score was 10 for each rat, as previously described [11].

After the 5-week experimental period, all rats were killed by guillotine decapitation and the trunk blood was immediately collected into tubes via a heparinized funnel. The plasma was subsequently separated after centrifugation at 2,000g for 10 minutes using a Spectrafuge 24D centrifuge (Labnet International Inc., NJ, USA). The *EDL*, *gastrocnemius*, and *soleus* and *vastus lateralis* muscles from the hindquarters of each rat were removed carefully, weighed, snap-frozen in liquid nitrogen, and then stored at -80°C until subsequent analysis.

2.2.3. Validation of Model via Plasma Anti-Collagen IgG Titer. The successful induction of arthritis in rats was confirmed by the production of antibodies to type II collagen using the rat anti-collagen IgG ELISA kit (Chondrex Inc., WA, USA) and following the manufacturer's protocol.

2.3. Muscle Histology. Frozen tissues (*EDL*, *gastrocnemius*, and *vastus lateralis*) were sectioned in 10 μm cross sections with a cryostat (Leica CM1860 UV, Leica Biosystems Nussloch GmbH, Germany) at -25°C and stored at -20°C. To ensure consistency between samples, a predetermined section was cut off the proximal end of each sample (differed between muscle types) before sectioning occurred. This is particularly important in the *vastus lateralis* as different fiber type proportions exist in the different areas (superficial vs. deep and proximal vs. distal) [12]. Sections were allowed to thaw at room temperature for 20 minutes before staining.

2.3.1. Hematoxylin and Eosin Staining. H&E staining was used to view the overall muscle structure. Hematoxylin binds to and stains all DNA/RNA structures blue. Eosin counterstains all proteins of the tissue pink. Slides were submerged in the following order for one minute each, excluding eosin which was stained for 30 seconds: dH_2O, two changes of Mayer's hematoxylin, warm tap water, Scott's tap water, dH_2O, eosin, H_2O, 95% ethanol, 100% ethanol, and finally clearance in xylene. Once stained, the slides were mounted with mounting media (DPX, 06522, Sigma-Aldrich, USA) and covered with a cover slip for viewing.

2.3.2. Picrosirius Red Staining. Sirius red is a polyazo dye which is specifically used for staining collagen. The stain dyes collagen bright red, leaving muscle fibers, cytoplasm, and red blood cells a lighter yellow/red color. Picrosirius red differs from sirius red staining with the addition of picric acid which prevents the indiscriminate staining of noncollagenous structures by sirius red.

Sections were fixed in neutral buffered formalin for 30 minutes. Slides were rinsed in dH_2O and stained with Weigert's hematoxylin for 8 minutes. Sections were washed in 3 changes of water followed by staining with picrosirius solution for one hour. Picrosirius solution was made up of 0.5 g sirius red F3B (CI35780, Sigma-Aldrich, USA) in 500 ml saturated aqueous picric acid (197378, Sigma-Aldrich, USA). Sections were washed in 0.5% acetic acid (A6283, Sigma-Aldrich, USA) in dH_2O twice for 5 minutes each. Sections were then dehydrated in changes of ethanol (70%, 95%, and 100%) and then cleared in xylene (296325, Sigma-Aldrich, USA), and cover slips were mounted with mounting media (DPX, 06522, Sigma-Aldrich, USA).

2.3.3. Image Acquisition. All histological slides were viewed using bright-field microscopy (Nikon Eclipse E400), mounted with a camera (Nikon DS-Fi2), and processed through a digital sight processor (DS-U3, Nikon, Japan). Image processing was done on Nikon Instruments Software (NIS-Elements v4.10) on a desktop computer (Dell, USA) running Windows 7 (Microsoft, USA). Images were taken at 100x and 200x magnifications (magnification was calculated from ocular lens (10x) multiplied by objective lens (10x/20x)).

2.3.4. Image Analysis. The cross-sectional area of the fibers was measured using H&E sections and ImageJ software (version 1.49, Wayne Rasband). 50 fibers per sample were measured. In order to assess fibrosis, picrosirius red images were analyzed using ImageJ software (version 1.49, Wayne Rasband) with the color deconvolution plug-in as developed by Landini (version 1.5). The picrosirius stains were processed using the ImageJ RGB option. Briefly, the plug-in unmixes the RGB image into three 8-bit images with a color lookup table that corresponds to the respective vector colors. The analysis measurements were set to measure "area," "area fraction," "limit to threshold," and "display label." The threshold of each of the three images was adjusted allowing the measurement of (1) the background, (2) the connective tissue, and (3) total tissue. Percentage of fibrosis in the tissue (×100 magnification) was calculated as follows: (1) background was subtracted from both the connective tissue and total tissue and (2) the following formula was used: percentage of fibrosis = (connective tissue/(connective tissue + total tissue)) ∗ 100.

2.4. Sample Analysis for Redox Status

2.4.1. Oxidative Stress. Frozen *vastus lateralis*, *soleus*, *EDL*, and *gastrocnemius* tissues were thawed on ice and homogenized 100 mg/ml in 10 mM phosphate-buffered saline (PBS, pH 7.2) and centrifuged at 10,000g for 15 min at 4°C to obtain the supernatants used for the analyses. The presence of reactive oxygen species (ROS) in tissue homogenates was evaluated by the ROS-dependent oxidation of the nonfluorescent 2′,7′-dichlorofluorescein- (DCF-) DiOxyQ probe to the highly fluorescent DCF using the OxiSelect™ ROS assay kit (Cell Biolabs Inc., CA, USA) and following the manufacturer procedure. The ferric ion reducing antioxidant power (FRAP) value in all muscle homogenates was determined by measuring the reduction of ferric tripyridyltriazine (Fe^{3+}-TPTZ) complex to the ferrous (Fe^{2+}) form by antioxidants as detailed earlier by Benzie and Strain [13]. This is monitored by the change in absorption at 593 nm in a SPECTROstar Nano® absorbance plate reader (BMG Labtech, Ortenberg, Germany). Lipid peroxidation in muscle homogenates was evaluated by the formation of the stable product—malondialdehyde (MDA)—in a reaction medium containing thiobarbituric acid (TBA). We used the method described by Varshney and Kale [14] but with slight modifications: briefly, the MDA formed in tissues highly reacts with TBA under acidic conditions to form a complex that is better purified by the addition of butanol and saturated sodium chloride and absorbs maximally at 532 nm using a SPECTROstar Nano® absorbance plate reader (BMG Labtech, Ortenberg, Germany).

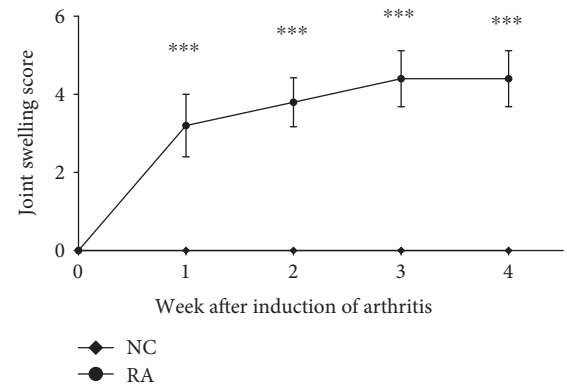

Figure 1: Weekly scores indicative of clinical symptoms of arthritis development in a collagen-induced rheumatoid arthritis model in female Sprague-Dawley rats ($n = 10$ per group). Statistical analysis: one-way ANOVA with repeated measures and Bonferroni post hoc test. ***, $p < 0.0001$ significantly different from controls.

2.5. Statistical Analysis. Effects were compared for statistical significance using Student's *t*-tests or one- or two-way analysis of variance (ANOVA) as appropriate, with Bonferroni post hoc tests where applicable. Data are presented as means and standard deviations, unless otherwise indicated. Statistical significance was set at $P < 0.05$.

3. Results

Successful induction of relatively mild rheumatoid arthritis was confirmed by clinical observations (Figure 1). Onset of joint swelling was typically within 11-18 days after the initial exposure to collagen. In addition, significantly elevated levels of anti-collagen antibody titer were measured in RA animals (0.02 ± 0.007 g/ml plasma; $P < 0.0001$) when

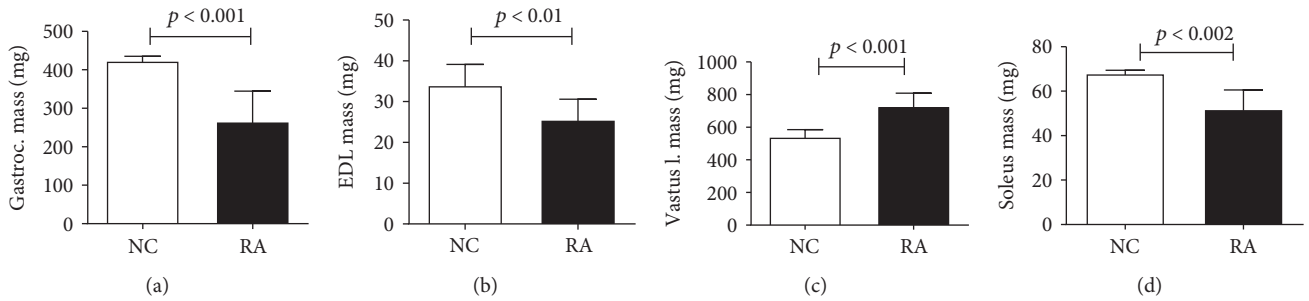

Figure 2: Muscle mass of different rat hindlimb skeletal muscles on day 35 of CIA ($n = 10$ per group). Bars indicate mean mass of muscle (left and right muscle weights were averaged for each animal) and error bars are standard deviations. Statistical analysis: Student's t-test.

compared to non-RA controls, in which antibody levels were not detectable.

RA animals exhibited significant decreases in skeletal muscle mass in the *EDL*, *gastrocnemius*, and *soleus* muscles, but that of *vastus lateralis* significantly increased (Figure 2).

RA animals exhibited clear signs of myofiber atrophy (Figures 3 and 4), inflammation (Figure 5), and fibrosis (Figure 6) when compared to control animals. In line with the significantly decreased muscle mass, the *gastrocnemius*, *soleus*, and *EDL* muscles exhibited generalized cachexia which was characterized by a ≈60% reduction in myofiber cross-sectional area across all cells (Figures 3(a)–3(f), 3(j)–3(l)). In these muscles, a significant number of fibers undergoing degradation were visible, as well as edema and inflammatory cell infiltrate. In contrast, as suggested by the lack of muscle mass loss, *vastus lateralis* myofibers seemed least affected by RA, with cross-sectional area of fibers decreasing by only ≈20% (Figures 3(g)–3(i)). In this muscle group, the pattern of cachexia was also more varied: while some fibers of smaller cross-sectional area are visible, normal-sized fibers are still abundant. No evidence of myofiber degradation was visible in *vastus lateralis* sections analyzed.

An analysis of fiber size distribution (Figure 4) confirms these observational data. The *gastrocnemius*, *soleus*, and *EDL* muscles exhibited a shift to the left for fiber size, with very high frequency of small fiber size. The *vastus lateralis* muscle did not show a clear shift to the left, although frequency of smaller fibers did appear somewhat higher. Although inflammation was not a specific focus of this paper and specific inflammatory markers were not assessed, the RA animals clearly exhibited moderately severe levels of inflammation in the *soleus*, *gastrocnemius*, and *EDL* muscles, where inflammation was visible in the perivascular areas as well as in between individual myofibers (Figures 5(a) and 5(b)). In addition, intrafiber necrosis was visible in several cells (Figure 5(c)). These features were not clearly visible in the *vastus* muscle.

In terms of fibrosis (collagen accumulation), the *vastus lateralis* and *EDL* muscles exhibited a significant 50% increase when compared to their respective controls. A similar result was obtained in the *soleus* but did not reach statistical significance. In contrast, the *gastrocnemius* muscle was most severely compromised, exhibiting a striking 200% increase in collagen accumulation (Figure 6).

In terms of redox status, total reactive oxygen species (ROS) levels seemed to correspond to muscle pathology in RA, as ROS was significantly increased in the *gastrocnemius*, *EDL*, and *soleus*, but not *vastus*, muscles of RA animals when compared to controls (Figure 7(a)). TBARS was assessed as a measure of oxidative stress-associated membrane damage through lipid peroxidation (Figure 7(b)). When considering controls only, the lowest ROS production seen in the *gastrocnemius* muscle corresponded to lowest levels of TBARS in this muscle, with highest TBARS levels measured in the *EDL* and *soleus* muscles. This relatively poorer picture in terms of oxidative damage in the control *EDL* and *soleus* muscles was not matched by a relative increase in antioxidant capacity (FRAP) (Figure 7(c)), suggesting that under normal conditions, these muscles are relatively more compromised than the *gastrocnemius* muscle in this context. In RA animals, lipid peroxidation (TBARS) levels were only significantly elevated from control levels in the *gastrocnemius* muscle (Figure 7(b)). Similarly, antioxidant capacity (FRAP) was similar and unchanged by RA in most muscles, with the exception of the *gastrocnemius* muscle, in which it was significantly increased in response to RA (Figure 7(c)).

4. Discussion

The current study expands on available literature by presenting a comparative assessment of different hindlimb skeletal muscles affected by CIA in a rat model. A specific novel component is the comparison of four different muscles with different fiber type distributions, including the *vastus lateralis*, in which human studies are typically conducted. Importantly, a recent study conducted in humans reported that intramuscular (*vastus lateralis*) levels of inflammatory parameters, such as the inflammatory cytokines, did not correspond to the profile in circulation [6], which highlights the importance of tissue-specific investigation and the relevance of the study reported here.

Data presented here clearly illustrates the debilitating nature of CIA and validates this model as an accurate simulation of muscle pathology in rheumatoid arthritis. Current data for the first time provides a comparative histological assessment of four muscles, three of which (the *gastrocnemius*, *soleus*, and *EDL* muscles) are directly associated with the primarily affected joint (ankle), while the other (*vastus lateralis*) is more proximal. The fact that all four muscle groups exhibited signs of cachexia, albeit it much less severe in the *vastus lateralis*, suggests that inactivity-based atrophy is not the only contributor to the pathology observed and that

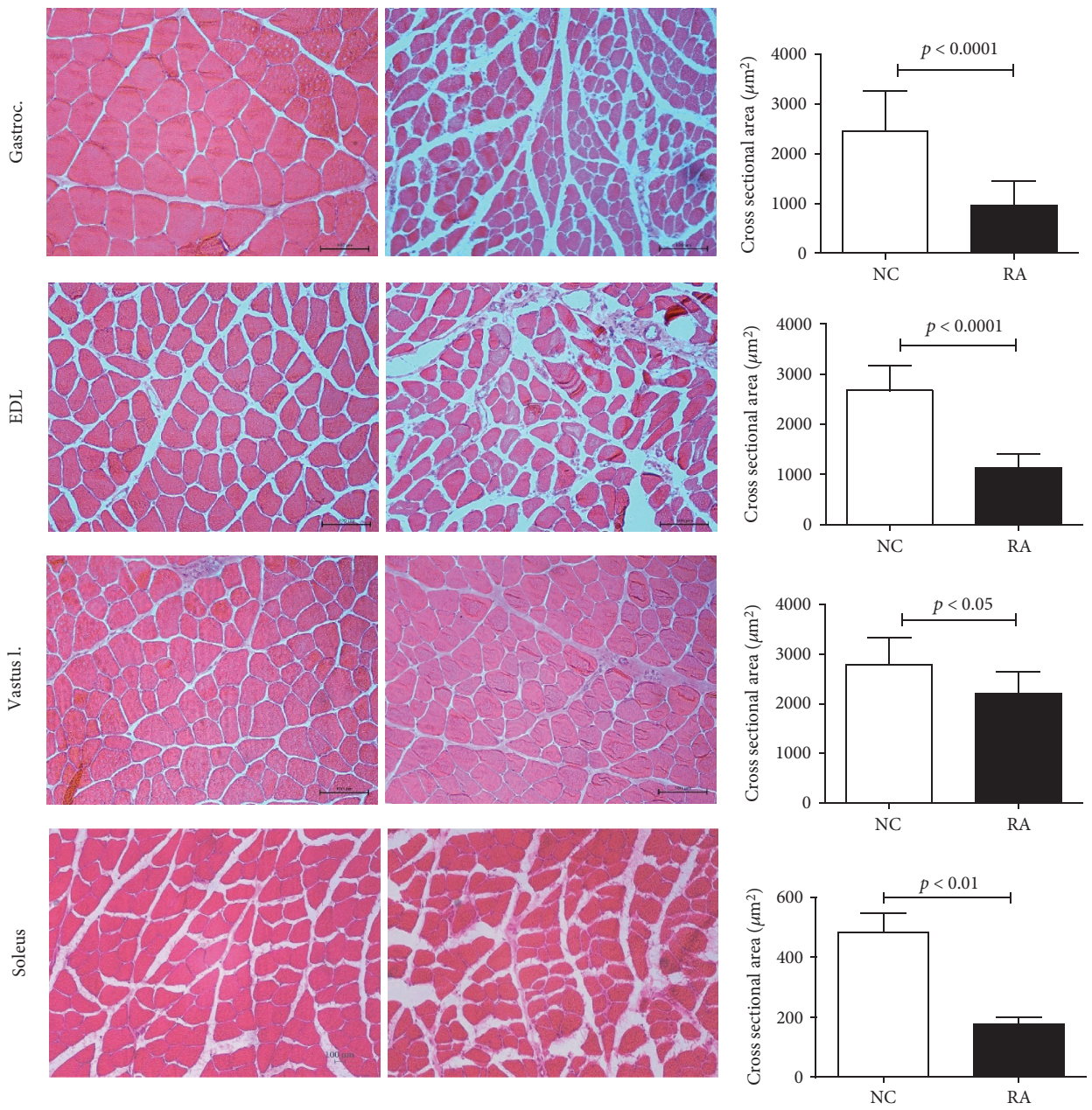

Figure 3: Representative H&E images and cross-sectional area of the *gastrocnemius* (a–c), *EDL* (d–f), and *vastus lateralis* (g–i) muscles depicting ultrastructural changes in female rats subjected to CIA ($n = 10$ per group) (normal control left; CIA right). 200x magnification. Scale bar represents 100 μm. Statistical analysis: Student's t-test.

circulating mediators likely impact significantly on all muscle groups, irrespective of their anatomical position. This generalized muscle deterioration is in line with the human clinical profile of RA [15] and further validates our model.

The smaller fiber size observed in all muscle groups assessed in the current study could theoretically be the result of a shift in fiber type favoring type I oxidative fiber phenotype, which is generally smaller than glycolytic myofibers. This is however unlikely, since skeletal muscle wasting in COPD and other chronic diseases characterized by chronic inflammation has been reported to be associated with a shift in phenotype towards type II glycolytic fibers [16, 17]—which are incidentally also most susceptible to cachexia in general [18, 19] and specifically also to arthritis-associated cachexia [20]. This led to the hypothesis that a loss of muscle oxidative phenotype may result in increased susceptibility to inflammation [16] and oxidative stress-induced cachexia.

The inclusion of more muscle groups in the current study provided the opportunity to gain novel insights and indeed suggested that fiber type and metabolic preference alone are not major determinants of the sensitivity of myofibers to rheumatoid cachexia. In the current study, the extent of muscle fiber atrophy was similar for the *soleus*, *gastrocnemius*, and *EDL* muscles—muscles which share an anatomical site in the lower hindlimb but differ in terms of fiber type distribution and metabolic preference. The lack of more extended

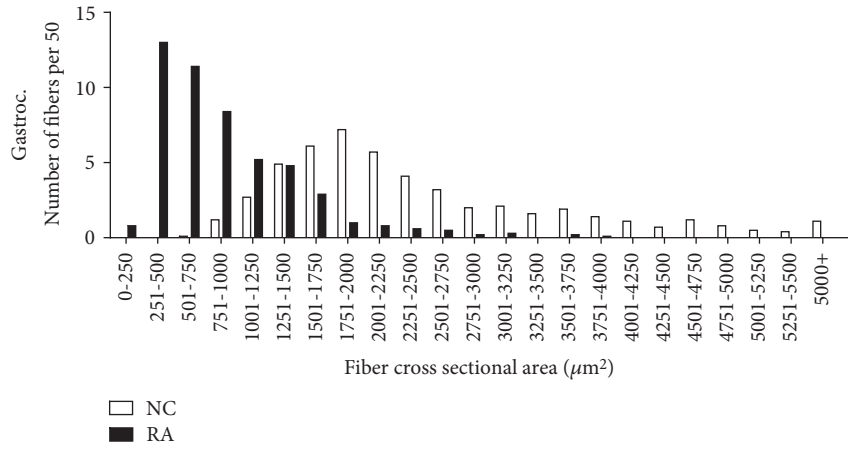

(a)

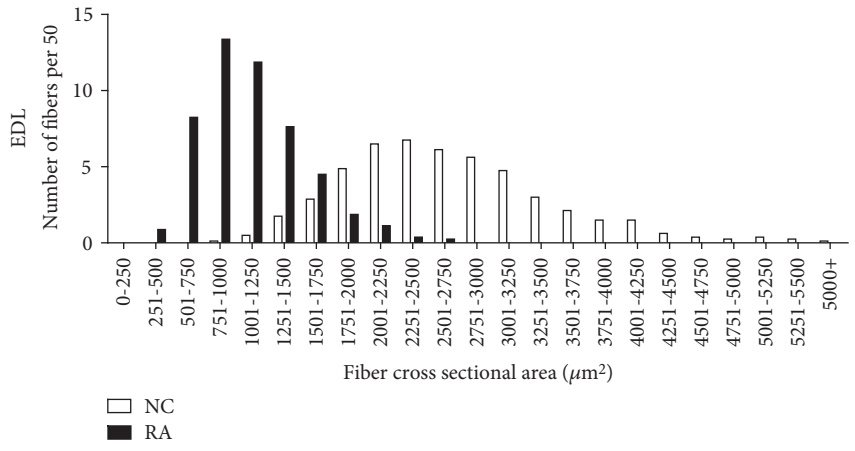

(b)

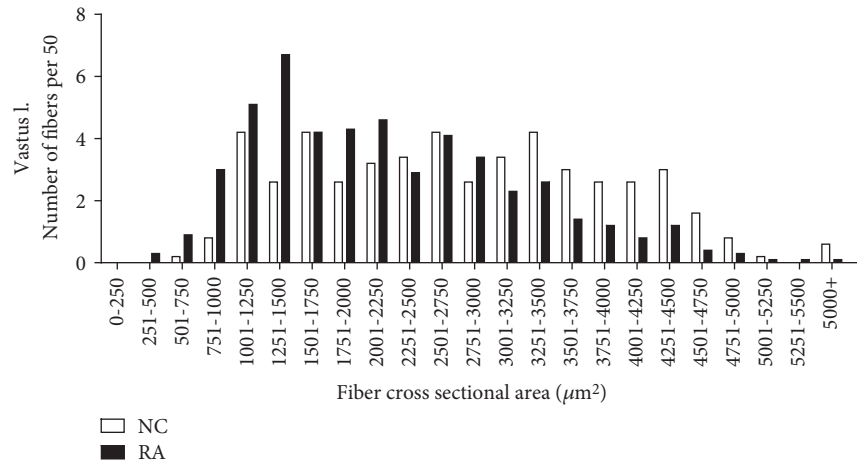

(c)

Figure 4: Continued.

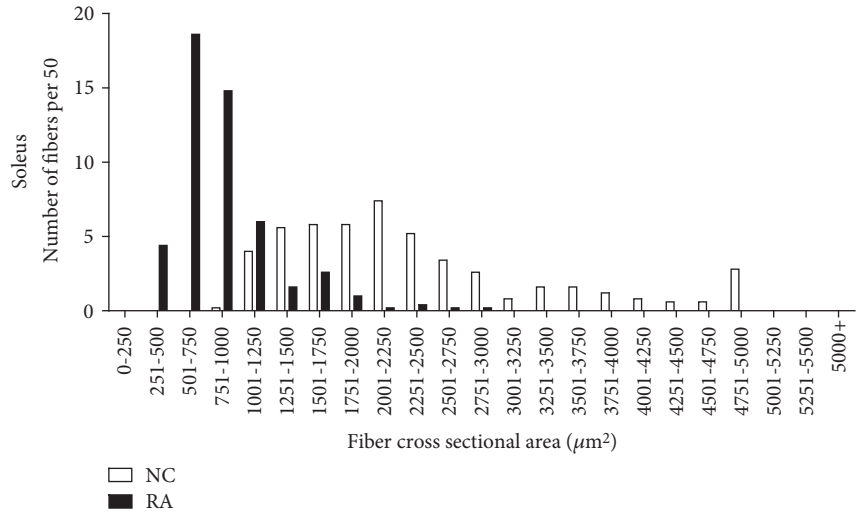

(d)

FIGURE 4: Distribution of fiber cross-sectional area across different muscle groups ($n = 10$ per group). Frequency data is expressed as number of fibers out of a total of 50 fibers counted per sample.

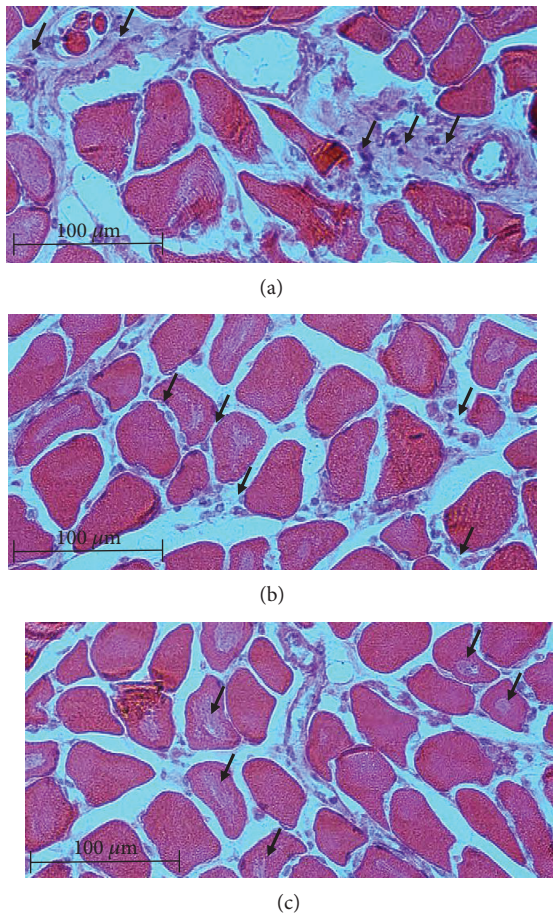

(a)

(b)

(c)

FIGURE 5: Representative high-resolution H&E stained images illustrating inflammatory cell infiltration in (a) perivascular and (b) interfiber areas, as well as (c) intrafiber necrosis. 200x magnification. Scale bar represents 100 μm.

time points in the cross-sectional design of the current study however did not allow for assessment of change within the same muscle over time, to determine if muscles with different fiber types or metabolic preferences may respond differently over time or with disease progression. Thus, causal mechanisms potentially at play should be investigated in a study with longitudinal design including early, medium, and long-term disease progression time frames. The extent of inflammation and its effect on muscle deterioration should also be considered in such a study of longitudinal design.

In the current study, diffusely spread inflammation was clearly visible in muscle assessed, but a comprehensive assessment of inflammation was beyond the current scope. Nevertheless, skeletal muscle fibrosis has previously been linked to inflammatory processes and was quantitatively assessed. Fibrosis resulting from inflammation and associated oxidative damage in various models specifically links ROS production to modulation of transforming growth factor beta (TGF-β) signaling in the context of mitochondrial dysfunction [21–24]. This prompted an investigation into potential differences in redox status between the different muscles. Indeed, in the current study, even in the absence of CIA, the *vastus lateralis*, *EDL*, and *soleus* muscles exhibited higher levels of TBARS than the *gastrocnemius* muscle, which also exhibited lower ROS levels than all other muscles assessed. This is in line with previous reports of differential inherent superoxide dismutase activity, glutathione peroxidase activity, and malondialdehyde levels in different muscles (diaphragm, *soleus*, and *gastrocnemius*) [25]. When subjected to CIA, even though ROS increased in the *gastrocnemius*, *EDL*, and *soleus*, FRAP remained unchanged in the *EDL* and *soleus*, while in contrast, in the *gastrocnemius* muscle, FRAP increased significantly in response to the increased ROS of RA. Together, these data suggest that the *EDL* and *soleus* muscles may have relatively less inherent antioxidant capacity to react to oxidative stressors when compared to the *gastrocnemius* muscle, which was able to mount a

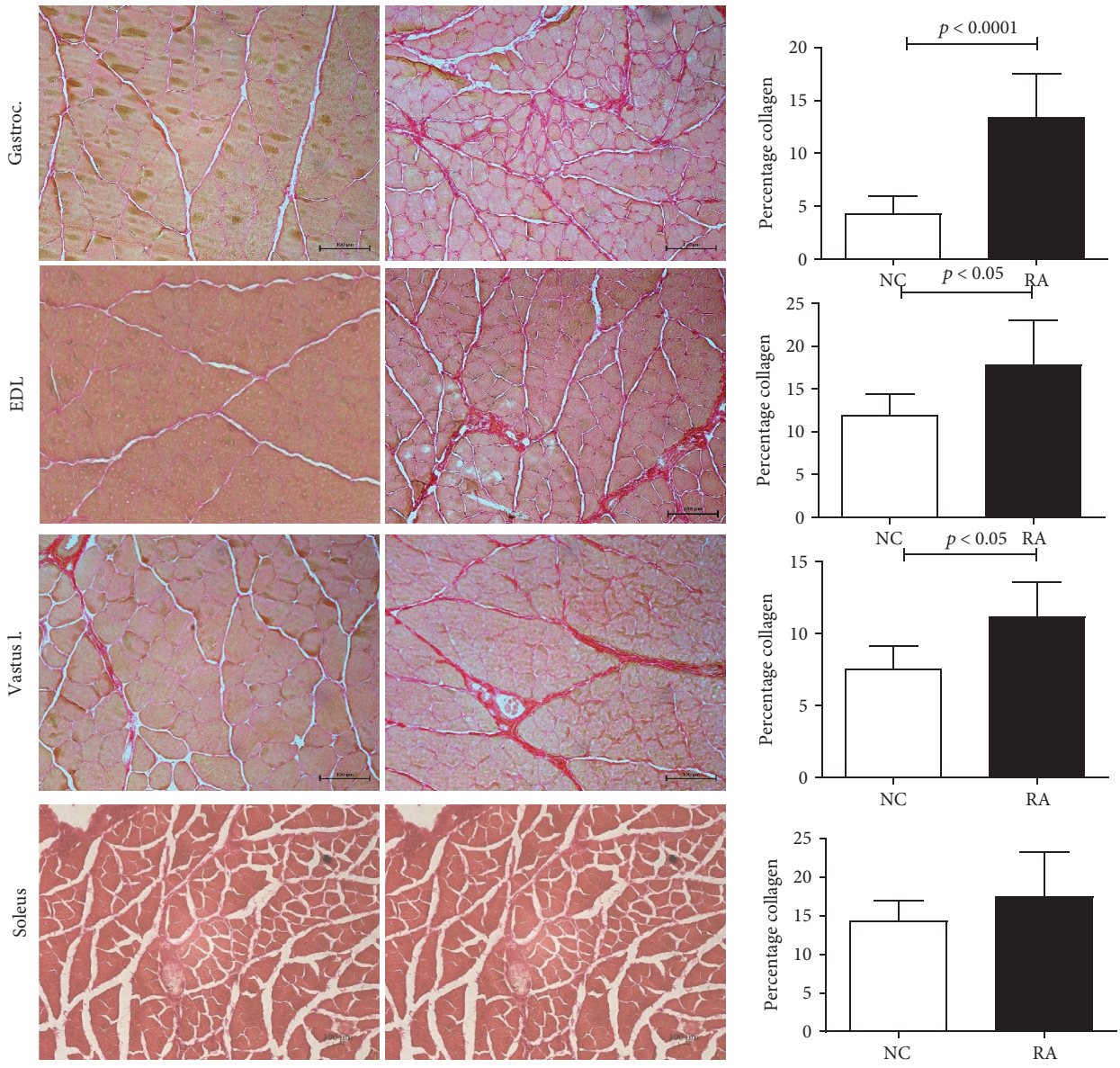

Figure 6: Representative images and percentage fibrosis of *gastrocnemius* (a–c), *EDL* (d–f), and *vastus lateralis* (g–i) in female rats subjected to CIA ($n = 10$ per group) using picrosirius red staining (normal control left; CIA right). 200x magnification. Scale bar represents 100 μm. Statistical analysis: Student's t-test.

significant antioxidant response. Despite this, the *gastrocnemius* muscle exhibited a worse profile in terms of malondialdehyde (MDA) production. We propose that the *EDL* and *soleus* muscles may possess antioxidant mechanisms other than those assessed by the FRAP assay, which could have upregulated activity in response to CIA and by which membrane integrity may be maintained. These mechanisms would be independent of ferric iron reduction specifically, which is assessed by the FRAP assay reported here. This interpretation is in line with the report in a model of high-fat diet-induced oxidative stress in rats, which reported that increased ROS production (reduced mitochondrial H_2O_2 emission, increased palmitate oxidation, and increased mRNA expression of NADPH complex) in muscle was paralleled by an increased ROS buffering capacity (increased mRNA expression of the antioxidant proteins, manganese superoxide dismutase (MnSOD), glutathione reductase, and mitochondrial thioredoxin-dependent peroxide reductase 3 and 5) [26]. Another mechanism by which this may potentially be achieved in the current context is that the *EDL* and *soleus* muscles may contain relatively higher concentrations of vitamin E, which is known to contribute to cell membrane repair after oxidative damage. In line with this, although the majority of data was generated in preclinical models and no comparison between muscles with different fiber types could be found, several beneficial effects of vitamin E were recently reported in the context of age-related sarcopenia. These included myoblast proliferation and differentiation, survival, membrane repair, mitochondrial efficiency, and maintenance of muscle mass and contractile capacity [27]. Of

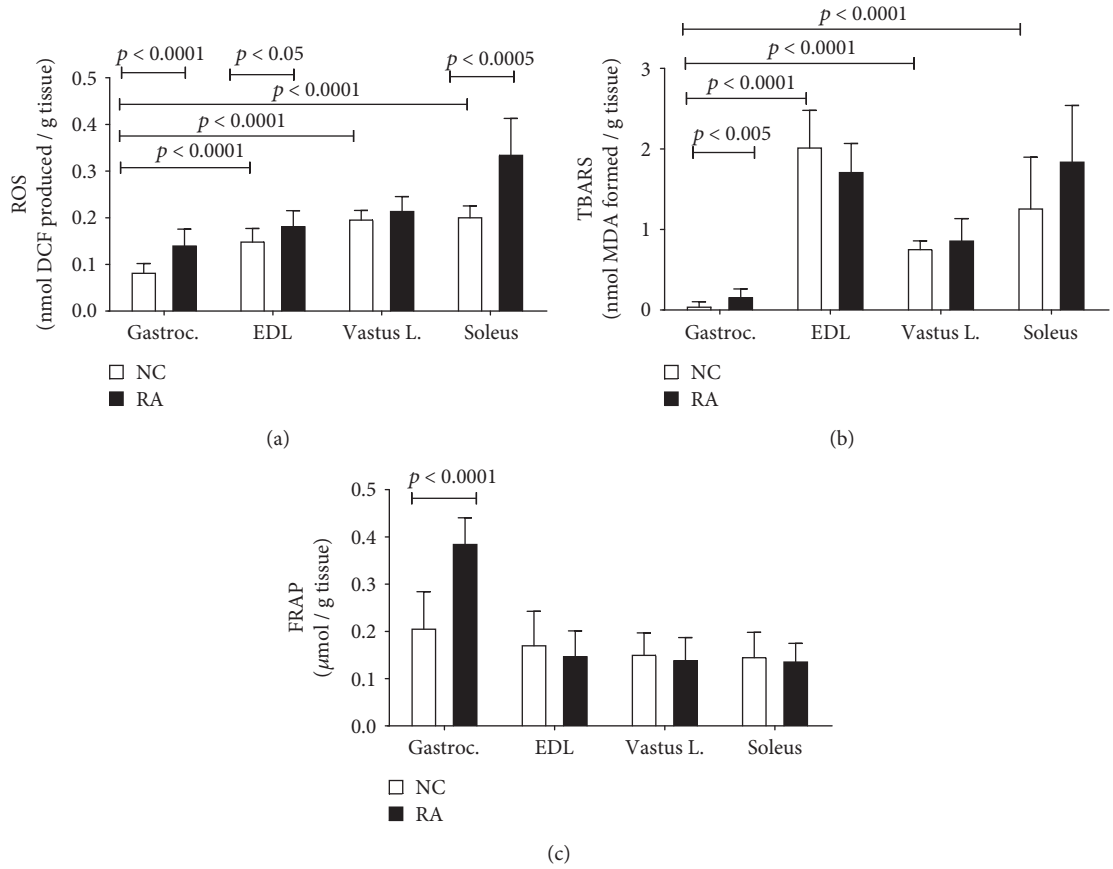

Figure 7: Redox status of rat muscles in female rats subjected to CIA, as measured by total ROS (a), TBARS (b), and FRAP (c) assays, respectively ($n = 10$ per group). Bars indicate means and error bars are standard deviations. Statistical analysis: 2-way ANOVA with Bonferroni post hoc tests.

particular relevance to the current discussion, vitamin E supplementation was shown to prevent upregulation of muscle ring finger 1 (MuRF1) and caspase-9 and caspase-12 mRNA in unloaded rat muscle and to decrease upregulation of muscle calpain, caspase-3, and atrogin-1 (MAFbx) mRNA [28]. This would suggest that in addition to its antioxidant effect, vitamin E may also modulate atrophy via more direct inhibitory action on proteolytic pathways. The review by Chung and colleagues [27] highlighted the lack of clinically relevant information currently available on vitamin E content or protective properties in skeletal muscle, which up to now has been limited by methodological constraints. This warrants further investigations in order to elucidate how endogenous protective mechanisms may be exploited by exogenous means for therapeutic benefit.

Redox status is a major determinant of muscle pathology—and specifically chronic disease-related cachexia. The current study focused on oxidative stress resulting from reactive oxygen species. However, both oxidative and nitrosative stresses may also come into play here, as both have been implicated in cancer cachexia [29]. In addition, in rodents injected with lipopolysaccharide (LPS) to induce oxidative stress, inducible nitric oxide synthase (iNOS) was implicated as a role player in relatively greater resistance to atrophy and ubiquitin-associated protein degradation in oxidative, but not glycolytic fibers [17]. This suggests that future studies should also determine the interaction between these species but also that antioxidant treatments should be investigated as preventative modality or adjuvant treatment in RA. Indeed, astaxanthin—a powerful antioxidant—was reported to attenuate immobilization-induced increased collagen deposition via modulation of oxidative stress, most notably via altered SOD-1 and TGF-β signaling in rats [24]. Similarly, the antioxidant flavone mixture isoflavin-β was reported to attenuate toxin-induced loss of *gastrocnemius* muscle mass by preventing the oxidative modification of proteins [30].

Another observation that has remained unnoticed up to now is the fact that in the rodent model of CIA, the response in the *vastus lateralis* muscle was different from other muscles assessed here and also different from results previously reported for the *EDL* and *soleus* in rodent models of arthritis [7, 8]. Current data suggest that although the *vastus lateralis* myofibers exhibited some signs of deterioration, total muscle mass actually increased significantly. The fiber size variation in this muscle did not display the characteristic left shift associated with cachectic atrophy, although the mean cross-sectional area was somewhat reduced. This suggests that the *vastus* may have been recruited as usual for gait despite the presence of RA-related symptoms. In contrast, the severe pathology evident in the *gastrocnemius* and *EDL* muscle groups may have resulted not only from systemic effects

but also due to lesser recruitment for gait and posture. This result stresses the importance of data interpretation in conjunction with clinical observations.

In terms of limitations, although not directly assessed, in our opinion, muscle mass is unlikely to have been influenced by energy intake, as animals did not exhibit clear loss of appetite. In terms of disuse as a confounding factor, although RA animals walked with a limp due to affected joints, they still moved around readily in their cages. Furthermore, a comparative study between immobilization and CIA-associated muscle atrophy has reported both proteolytic and regenerative pathways to be upregulated in RA (but not in experimentally immobilized) animals [31]. Thus, disuse is unlikely to have been a major confounding factor in the current study. Finally, edema was not quantified in the current study, but may aid in the interpretation of, e.g., the increased *vastus lateralis* muscle mass despite the presence of other signs of atrophy. Inclusion of this measure in studies investigating inflammatory mechanisms in the context of RA-associated muscle deterioration could further elucidate differences in the responses of different muscles to the challenges of RA.

5. Conclusion

Data presented here highlight the relevance of muscle-specific (and not just fiber-type-specific) assessment of redox profile to determine its role in muscles' atrophy response to experimentally induced rheumatoid arthritis. Furthermore, current data indicating differential responses by different muscles suggest that in human studies, it would be prudent to investigate muscle response to RA in more than one muscle. This would provide more insight into whether loadbearing and non-loadbearing muscles, or muscles at different anatomical proximities from clinically affected joints, are also differentially affected in humans in terms of disease-related cachexia. Similarly, given the inherently different redox profiles and seemingly different predominating endogenous antioxidant mechanisms at play in the different muscles as demonstrated in rats here, interventions aimed at improving redox status should take into consideration conditions in (and responses of) more muscles than just the human *vastus lateralis*, as different muscles may have different therapeutic requirements in this context.

Data Availability

Data will be made available by authors on request.

Conflicts of Interest

No conflict of interest.

Acknowledgments

The authors would like to thank Jed Pheneger from Bolder Biopath (Boulder, CO, USA) for invaluable advice on the practical execution of the rheumatoid arthritis induction protocol. The South African National Research Foundation is acknowledged for the financial support and contribution to the salary of ABO.

References

[1] T. Yamada, M. M. Steinz, E. Kenne, and J. T. Lanner, "Muscle weakness in rheumatoid arthritis: the role of Ca^{2+} and free radical signaling," *eBioMedicine*, vol. 23, pp. 12–19, 2017.

[2] J. Walsmith and R. Roubenoff, "Cachexia in rheumatoid arthritis," *International Journal of Cardiology*, vol. 85, no. 1, pp. 89–99, 2002.

[3] P. S. Helliwell and S. Jackson, "Relationship between weakness and muscle wasting in rheumatoid arthritis," *Annals of the Rheumatic Diseases*, vol. 53, no. 11, pp. 726–728, 1994.

[4] M. B. Reid and J. S. Moylan, "Beyond atrophy: redox mechanisms of muscle dysfunction in chronic inflammatory disease," *The Journal of Physiology*, vol. 589, no. 9, pp. 2171–2179, 2011.

[5] R. C. Do Espirito Santo, M. G. Pompermayer, R. R. Bini et al., "Neuromuscular fatigue is weakly associated with perception of fatigue and function in patients with rheumatoid arthritis," *Rheumatology International*, vol. 38, no. 3, pp. 415–423, 2018.

[6] K. M. Huffman, R. Jessee, B. Andonian et al., "Molecular alterations in skeletal muscle in rheumatoid arthritis are related to disease activity, physical inactivity, and disability," *Arthritis Research & Therapy*, vol. 19, no. 1, p. 12, 2017.

[7] T. Yamada, N. Place, N. Kosterina et al., "Impaired myofibrillar function in the soleus muscle of mice with collagen-induced arthritis," *Arthritis and Rheumatism*, vol. 60, no. 11, pp. 3280–3289, 2009.

[8] T. Yamada, O. Fedotovskaya, A. J. Cheng et al., "Nitrosative modifications of the Ca2+ release complex and actin underlie arthritis-induced muscle weakness," *Annals of the Rheumatic Diseases*, vol. 74, no. 10, pp. 1907–1914, 2015.

[9] D. L. Asquith, A. M. Miller, I. B. Mcinnes, and F. Y. Liew, "Animal models of rheumatoid arthritis," *European Journal of Immunology*, vol. 39, no. 8, pp. 2040–2044, 2009.

[10] K. Kannan, R. A. Ortmann, and D. Kimpel, "Animal models of rheumatoid arthritis and their relevance to human disease," *Pathophysiology*, vol. 12, no. 3, pp. 167–181, 2005.

[11] P. Hawkins, R. Armstrong, T. Boden et al., "Applying refinement to the use of mice and rats in rheumatoid arthritis research," *Inflammopharmacology*, vol. 23, no. 4, pp. 131–150, 2015.

[12] T. A. Kohn and K. H. Myburgh, "Regional specialization of rat quadriceps myosin heavy chain isoforms occurring in distal to proximal parts of middle and deep regions is not mirrored by citrate synthase activity," *Journal of Anatomy*, vol. 210, no. 1, pp. 8–18, 2007.

[13] I. F. F. Benzie and J. J. Strain, "The ferric reducing ability of plasma (FRAP) as a measure of "antioxidant power": the FRAP assay," *Analytical Biochemistry*, vol. 239, no. 1, pp. 70–76, 1996.

[14] R. Varshney and R. K. Kale, "Effects of calmodulin antagonists on radiation-induced lipid peroxidation in microsomes," *International Journal of Radiation Biology*, vol. 58, no. 5, pp. 733–743, 1990.

[15] T. Sokka, A. Häkkinen, H. Kautiainen et al., "Physical inactivity in patients with rheumatoid arthritis: data from twenty-one countries in a cross-sectional, international study," *Arthritis and Rheumatism*, vol. 59, no. 1, pp. 42–50, 2008.

[16] A. H. V. Remels, H. R. Gosker, R. C. J. Langen, and A. M. W. J. Schols, "The mechanisms of cachexia underlying muscle dysfunction in COPD," *Journal of Applied Physiology*, vol. 114, no. 9, pp. 1253–1262, 2013.

[17] Z. Yu, P. Li, M. Zhang, M. Hannink, J. S. Stamler, and Z. Yan, "Fiber type-specific nitric oxide protects oxidative myofibers against cachectic stimuli," *PLoS One*, vol. 3, no. 5, article e2086, 2008.

[18] P. Li, R. E. Waters, S. I. Redfern et al., "Oxidative phenotype protects myofibers from pathological insults induced by chronic heart failure in mice," *The American Journal of Pathology*, vol. 170, no. 2, pp. 599–608, 2007.

[19] R. Minnaard, M. R. Drost, A. J. M. Wagenmakers, G. P. van Kranenburg, H. Kuipers, and M. K. C. Hesselink, "Skeletal muscle wasting and contractile performance in septic rats," *Muscle & Nerve*, vol. 31, no. 3, pp. 339–348, 2005.

[20] M. López-Menduiña, A. I. Martín, E. Castillero, M. A. Villanúa, and A. López-Calderón, "Systemic IGF-I administration attenuates the inhibitory effect of chronic arthritis on gastrocnemius mass and decreases atrogin-1 and IGFBP-3," *American Journal of Physiology. Regulatory, Integrative and Comparative Physiology*, vol. 299, no. 2, pp. R541–R551, 2010.

[21] F. J. Gonzalez-Gonzalez, N. S. Chandel, M. Jain, and G. R. S. Budinger, "Reactive oxygen species as signaling molecules in the development of lung fibrosis," *Translational Research*, vol. 190, pp. 61–68, 2017.

[22] M. Kozakowska, K. Pietraszek-Gremplewicz, A. Jozkowicz, and J. Dulak, "The role of oxidative stress in skeletal muscle injury and regeneration: focus on antioxidant enzymes," *Journal of Muscle Research and Cell Motility*, vol. 36, no. 6, pp. 377–393, 2015.

[23] R. M. Liu and L. P. Desai, "Reciprocal regulation of TGF-β and reactive oxygen species: a perverse cycle for fibrosis," *Redox Biology*, vol. 6, pp. 565–577, 2015.

[24] T. Maezawa, M. Tanaka, M. Kanazashi et al., "Astaxanthin supplementation attenuates immobilization-induced skeletal muscle fibrosis via suppression of oxidative stress," *The Journal of Physiological Sciences*, vol. 67, no. 5, pp. 603–611, 2017.

[25] C. Caillaud, G. Py, N. Eydoux, P. Legros, C. Prefaut, and J. Mercier, "Antioxidants and mitochondrial respiration in lung, diaphragm, and locomotor muscles: effect of exercise," *Free Radical Biology & Medicine*, vol. 26, no. 9-10, pp. 1292–1299, 1999.

[26] R. A. Pinho, D. M. Sepa-Kishi, G. Bikopoulos et al., "High-fat diet induces skeletal muscle oxidative stress in a fiber type-dependent manner in rats," *Free Radical Biology & Medicine*, vol. 110, pp. 381–389, 2017.

[27] E. Chung, H. Mo, S. Wang et al., "Potential roles of vitamin E in age-related changes in skeletal muscle health," *Nutrition Research*, vol. 49, pp. 23–36, 2018.

[28] S. Servais, D. Letexier, R. Favier, C. Duchamp, and D. Desplanches, "Prevention of unloading-induced atrophy by vitamin E supplementation: links between oxidative stress and soleus muscle proteolysis?," *Free Radical Biology & Medicine*, vol. 42, no. 5, pp. 627–635, 2007.

[29] E. Barreiro, B. de la Puente, S. Busquets, F. J. López-Soriano, J. Gea, and J. M. Argilés, "Both oxidative and nitrosative stress are associated with muscle wasting in tumour-bearing rats," *FEBS Letters*, vol. 579, no. 7, pp. 1646–1652, 2005.

[30] P. C. Marinello, S. S. Bernardes, F. A. Guarnier et al., "Isoflavin-β modifies muscle oxidative stress and prevents a thyrotoxicosis-induced loss of muscle mass in rats," *Muscle & Nerve*, vol. 56, no. 5, pp. 975–981, 2017.

[31] V. de Oliveira Nunes Teixeira, L. I. Filippin, P. R. Viacava, P. G. de Oliveira, and R. M. Xavier, "Muscle wasting in collagen-induced arthritis and disuse atrophy," *Experimental Biology and Medicine*, vol. 238, no. 12, pp. 1421–1430, 2013.

Hindawi
Oxidative Medicine and Cellular Longevity
Volume 2019, Article ID 9208949, 10 pages
https://doi.org/10.1155/2019/9208949

Research Article

Vagus Nerve Stimulation Attenuates Acute Skeletal Muscle Injury Induced by Ischemia-Reperfusion in Rats

Yifeng Zhang,[1,2,3] Hewei Li,[4] Menglong Wang,[1,2,3] Guannan Meng,[1,2,3] Zhenya Wang,[1,2,3] Jielin Deng,[1,2,3] Meng Wang,[1,2,3] Qianqian Zhang,[1,2,3] Shengli Yang,[5] and Hong Jiang[1,2,3]

[1]*Department of Cardiology, Renmin Hospital of Wuhan University, Wuhan 430060, China*
[2]*Cardiovascular Research Institute, Wuhan University, Wuhan 430060, China*
[3]*Hubei Key Laboratory of Cardiology, Wuhan 430060, China*
[4]*Department of Orthopedics, Liyuan Hospital, Tongji Medical College, Huazhong University of Science and Technology, Wuhan 430077, China*
[5]*Cancer Center, Union Hospital, Tongji Medical College, Huazhong University of Science and Technology, Wuhan 430022, China*

Correspondence should be addressed to Shengli Yang; yangshengli2014@yahoo.com and Hong Jiang; whujianghong@163.com

Received 17 September 2018; Revised 3 December 2018; Accepted 18 December 2018; Published 28 February 2019

Guest Editor: Carine Smith

Vagus nerve stimulation (VNS) has been shown to attenuate ischemia-reperfusion (I/R) injury in multiple organs. The present study aimed at investigating whether VNS could exert protective effects against I/R injury in the skeletal muscle. Male Sprague-Dawley rats were randomly divided into 3 groups: the control, I/R, and I/R+VNS groups. The skeletal muscle I/R (SMI/R) model was induced by occlusion of the left femoral artery for 2.5 hours followed by reperfusion for 2 hours. The vagal nerve trunk was separated, and VNS was performed during the whole I/R process. The intensity of VNS was optimized in each rat to obtain a 10% reduction in the heart rate relative to the value before stimulation. After the experiment, the blood sample and left gastrocnemius muscle tissues were collected for histological examination, biochemical analysis, and molecular biological detection. During the I/R process, VNS significantly reduced cellular apoptosis, necrosis, and inflammatory cell infiltration compared to sham VNS. The VNS treatment also decreased the inflammatory response, alleviated oxidative stress, and improved vascular endothelial function ($p < 0.05$ for each). In contrast, the I/R group showed an opposite effect compared to the control group. The present study indicated that VNS could protect against SMI/R injury by suppressing excessive inflammation, alleviating oxidative stress, and preserving vascular endothelial function.

1. Introduction

Skeletal muscle ischemia-reperfusion (SMI/R) injury is a common disease in clinical practice. It often influences the function of the skeletal muscle and can even be life-threatening [1]. However, there are few effective treatments for SMI/R [2]. Thus, novel effective therapies are needed to prevent SMI/R injury. Numerous studies have demonstrated that the pathogenesis of SMI/R injury is associated with inflammation responses and oxidative stress [3]. Vagus nerve stimulation (VNS) has been shown to exert anti-inflammatory and antioxidative effects [4–6]. Most recently, VNS has been demonstrated to improve I/R injury in multiple organs, including the heart, brain, and kidney [7–9]. VNS applied during the I/R process could reduce the infarct area and improve the prognosis. More importantly, our clinical study has shown that transcutaneous VNS can markedly attenuate myocardial I/R injury in acute myocardial infarction patients undergoing primary percutaneous coronary intervention [10]. However, the protective effects of VNS against SMI/R injury remain unknown. In the present study, using an acute SMI/R model in rats, we aimed to demonstrate the protective effects of VNS against SMI/R injury and further explore the potential mechanisms.

2. Materials and Methods

2.1. Animals and Experimental Groups. Healthy male Sprague-Dawley rats (250-300 g) were included in this study,

and all animals were supplied by the Experimental Animal Center of Renmin Hospital of Wuhan University. The study conformed to the Guidelines for the Care and Use of Laboratory Animals published by the US National Institutes of Health (NIH Publication, revised 1996). All animal studies were reviewed and approved by the Renmin Hospital of Wuhan University Animal Care and Use Committee (ethics clearance number was WDRM. 20180308).

Rats were randomized into 3 groups and received the following treatments: sham operation (control group, $n = 6$), SMI/R with sham VNS (I/R group, $n = 6$), and SMI/R with VNS (I/R+VNS group, $n = 6$). Detailed study protocol is summarized in Figure 1(a).

2.2. Acute SMI/R Model. Rats were anesthetized with 2% pentobarbital sodium (40 mg/kg body weight) by intraperitoneal injection. Surface electrocardiography was performed with a PowerLab data acquisition system (8/35, ADInstruments, Bella Vista, Australia). The left femoral artery was exposed by blunt dissection and a pair of atraumatic microvascular clamps were placed (in the control group, only femoral artery exposure was performed). The presence of pulsation under the clamp was checked. After 2.5 h of ischemia, the microvascular clamps were removed and the left hind limb received 2 h of reperfusion as previously described [11].

2.3. VNS. The left cervical vagal trunk was isolated as a stimulating target (see Figure 1(b)). Continuous stimulation (20 Hz, 0.1 ms in duration, square waves) was delivered by a stimulator (S20, Jinjiang, Chengdu City, China) through a pair of Teflon-coated silver hooks (0.1 mm in diameter) on the cervical vagal trunk. The stimulation level was defined as the voltage level sufficient to slow the sinus rate or atrioventricular (AV) conduction at 10%, as previously described [12]. The VNS threshold was determined once again prior to each hour of stimulation.

2.4. Blood and Tissue Sample Collection. After the entire experimental progress, blood samples were collected from the inferior vena cava. Serum was collected by centrifugation at 3,000 rpm, for 15 min. Tissue specimens were collected from the first half of the left gastrocnemius muscle venter. Each tissue specimen was separated into three parts. The major part (about $5 \times 5 \times 10\,mm^3$) was used for histological analysis. The two minor parts (about $2 \times 2 \times 2\,mm^3$) were used for biochemical and molecular biological analysis. All blood and tissue samples for biochemical and molecular biological analysis were stored at -80°C until use.

2.5. Histological Examination. The skeletal muscle tissue samples were submerged in 10% paraformaldehyde solution for 48 h, dehydrated sequentially in an ascending gradient of ethanol, and rinsed in xylene. Then, the tissues were embedded in paraffin. Sections of 5 μm thick were stained with hematoxylin and eosin (H&E) and then examined under a light microscope.

The muscle injury area was estimated in each gastrocnemius muscle section under a microscope according to Yin et al. [13].

Terminal deoxynucleotidyl transferase dUTP nick end labeling (TUNEL) staining was performed with a commercially available kit (Roche Biochemicals, Mannheim, Germany) according to the manufacturer's protocol. Tissue sections were deparaffinized and then hydrated with ethanol. After hydration, the sections were treated with protease K, rinsed with phosphate-buffered saline (PBS), and then incubated with TUNEL reaction reagents. After washing with PBS, the sections were treated with 4′,6-diamidino-2-phenylindole (DAPI) and incubated in a dark environment at room temperature. Stained sections were analyzed using a fluorescence microscope (Nikon DS-U3, Japan). Cells with nuclei containing irregular green particles were defined as TUNEL-positive cells. Cell death was viewed and detected in three random fields of each muscle section and averaged. The TUNEL-positive cell ratio was recorded.

2.6. Analysis of Serum Creatine Kinase (CK) and Lactate Dehydrogenase (LDH) in Serum Levels. Serum CK and LDH levels, which reflect skeletal muscle injury severity, were assessed using commercial kits (Changchun Huili Biotech Co. Ltd. China) according to the manufacturer's protocol.

2.7. Measurement of Malondialdehyde (MDA), Myeloperoxidase (MPO), and Superoxide Dismutase (SOD) Content Levels in Serum and Tissues. Tissue and serum samples from the control, I/R, and I/R+VNS groups were homogenized. The tissue MPO activity level, the tissue and serum MDA concentration, and SOD activity levels were assayed using commercially available kits (Nanjing Jiancheng Bioengineering Institute, Nanjing City, China) according to the manufacturer's protocol. The samples after reaction were detected by a spectrophotometer. The maximum absorbance values determined for MDA, MPO, and SOD were 532 nm, 460 nm, and 550 nm, respectively.

2.8. Western Blot Analysis. Frozen skeletal muscle tissues were lysed with a RIPA lysis buffer (Aspen Biotechnology, Wuhan, China), supplemented with phenylmethanesulfonyl fluoride (Aspen). After homogenization, the supernatant was collected for protein concentration determination using a BCA protein assay kit (Aspen). Equal amounts of protein solution from the homogenates were subjected to SDS-PAGE and then transferred onto a nitrocellulose membrane. After the membrane was blocked with 5% fat-free milk, it was incubated with rabbit anti-endothelial nitric oxide synthase antibody (eNOS, 1 : 1000 dilution, Abcam, Cambridge, UK), rabbit anti-intercellular adhesion molecule 1-antibody (ICAM-1, 1 : 500 dilution, Biorbyt, UK), rabbit anti-vascular cell adhesion molecule-1 antibody (VCAM-1, 1 : 1000 dilution, Abcam, Cambridge, UK), rabbit anti-interleukin 1 beta antibody (IL-1β, 1 : 1000 dilution, Abcam, Cambridge, UK), rabbit anti-IL-6 antibody (1 : 1000 dilution, Affinity, San Francisco, USA), and rabbit anti-tumor necrosis factor alpha antibody (TNF-α, 1 : 1000 dilution, Proteintech Group, Inc. Wuhan, China). After washing three times with Tris-buffered saline containing Tween (TBST), the membranes were incubated with HRP-goat anti-rabbit antibody (Aspen) at room temperature for 30 min and then washed four times with TBST. The protein bands were visualized by the

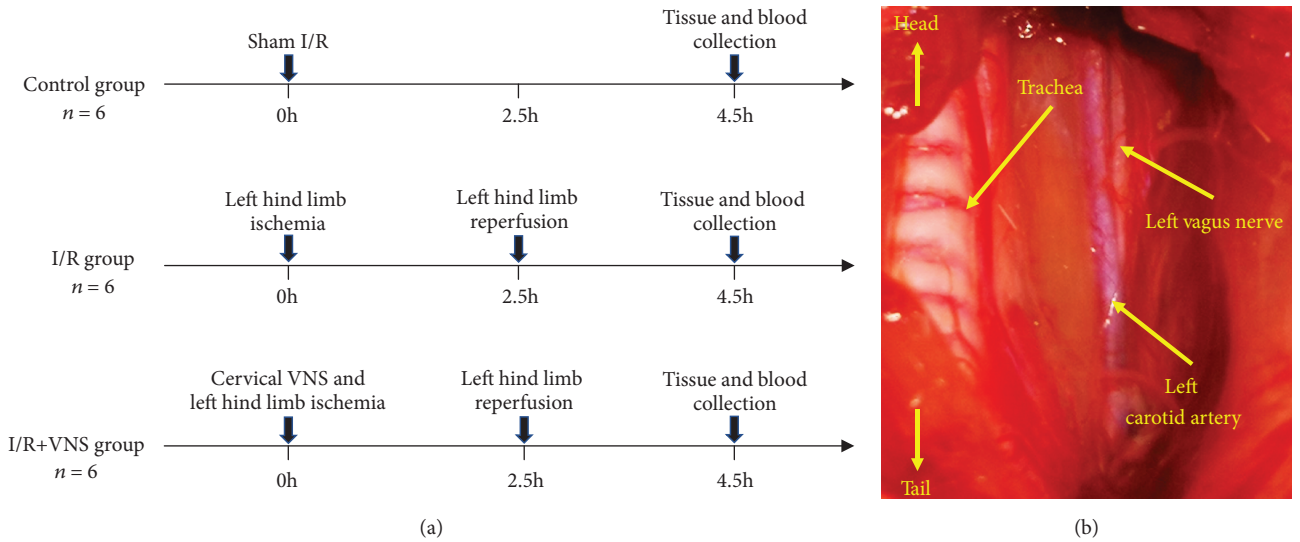

Figure 1: Experimental protocol (a) and location of the vagus nerve (b). I/R: ischemia-reperfusion; VNS: vagus nerve stimulation.

chemiluminescence method and quantified using analytical software (AlphaEase FC, USA). The relative expression of target proteins was normalized to β-actin from the same sample, and the data was normalized by the mean value of the control group.

2.9. qRT-PCR. Total RNA was extracted from the frozen skeletal muscle tissues using a Trizol reagent (Invitrogen Life Technologies) according to the manufacturer's protocol. First strand cDNA was synthesized using PrimeScript™ RT Reagent Kit with gDNA Eraser (TaKaRa Bio Inc.). Candidate gene expression levels were measured using an RT-PCR thermocycler (StepOne™ Life Technologies) with the following specific primers: IL-1β, forward: 5′-GTGG CAGCTACCTATGTCTTGC-3′, reverse: 5′-CCACTTGTT GGCTTATGTTCTGT-3′; IL-6, forward: 5′-TGGAGTTCC GTTTCTACCTGG-3′, reverse: 5′-GGTCCTTAGCCACT CCTTCTGT-3′; and TNF-α, forward: 5′-CACCACGCTCT TCTGTCTACTG-3′, reverse: 5′-GCTACGGGCTTGTCAC TCG-3′. The mRNA level for each target gene was calculated using the Delta-Delta-CT method and normalized to the β-actin mRNA level from the same sample. The primers for β-actin were as follows: forward: 5′-CGTTGACATCC GTAAAGACCTC-3′, reverse: 5′-TAGGAGCCAGGGCA GTAATCT-3′.

2.10. Statistical Analysis. Continuous variables are expressed as the mean ± SD and were analyzed by one-way ANOVA. All data were analyzed using GraphPad Prism version 7.0 software (GraphPad Software, Inc. San Diego, CA), and two-tailed $p \leq 0.05$ was considered significant.

3. Results

3.1. VNS Significantly Alleviated SMI/R Injury. As shown in Figure 2(a), skeletal muscle tissues in the I/R group showed muscle cell degeneration, necrosis, sarcoplasmic dissolution, and neutrophil infiltration. The extent of these changes was alleviated in the I/R+VNS group. Figure 2(b) shows that the gastrocnemius muscle injury area in the high-power field (HPF) was highest in the I/R group, significantly lower in the I/R+VNS group, and lowest in the control group.

Figure 2(c) shows that the CK and LDH levels were significantly higher in the I/R group than in the control group (CK, 5060.31 ± 847.02 vs. 233.13 ± 98.01 U/L, $p < 0.05$; LDH, 847.96 ± 120.20 vs. 298.50 ± 73.10 U/L, $p < 0.05$). The CK and LDH levels were significantly attenuated by the VNS treatment (CK, 1849.44 ± 456.94 vs. 5060.31 ± 847.02 U/L, $p < 0.05$; LDH, 625.65 ± 81.51 vs. 847.96 ± 120.20 U/L, $p < 0.05$).

TUNEL staining was used to detect skeletal muscle cell apoptosis among the three groups. The percentage of TUNEL-positive cells was significantly increased in the I/R group compared with the control group (32.83 ± 4.62% vs. 1.67 ± 1.21%, $p < 0.05$). In the I/R+VNS group, the percentage of TUNEL-positive cells was significantly decreased compared with that in the I/R group (13.83 ± 2.59% vs. 32.83 ± 4.62%, $p < 0.05$) (see Figure 3).

3.2. VNS Significantly Mitigated the Inflammatory Response in the Skeletal Muscle after I/R. As shown in Figure 4, the mRNA and protein expression levels of proinflammatory factors IL-1β, IL-6, and TNF-α were markedly increased in the I/R group compared with the control group (mRNA expression: IL-1β, 2.92 ± 0.44 vs. 1.00 ± 0.08; IL-6, 2.80 ± 0.20 vs. 1.00 ± 0.13; and TNF-α, 3.88 ± 0.31 vs. 1.00 ± 0.17, $p < 0.05$ for each. Protein expression: IL-1β, 4.03 ± 0.58 vs. 1.00 ± 0.42; IL-6, 3.20 ± 0.32 vs. 1.00 ± 0.31; and TNF-α, 4.40 ± 0.62 vs. 1.00 ± 0.6, $p < 0.05$ for each). VNS significantly mitigated the increased expression of levels of inflammatory markers (mRNA expression: IL-1β, 1.71 ± 0.11 vs. 2.92 ± 0.44; IL-6, 1.76 ± 0.09 vs. 2.80 ± 0.20; and TNF-α, 2.42 ± 0.15 vs. 3.88 ± 0.31, $p < 0.05$ for each. Protein expression: IL-1β, 2.29 ± 0.51 vs. 4.03 ± 0.58; IL-6,

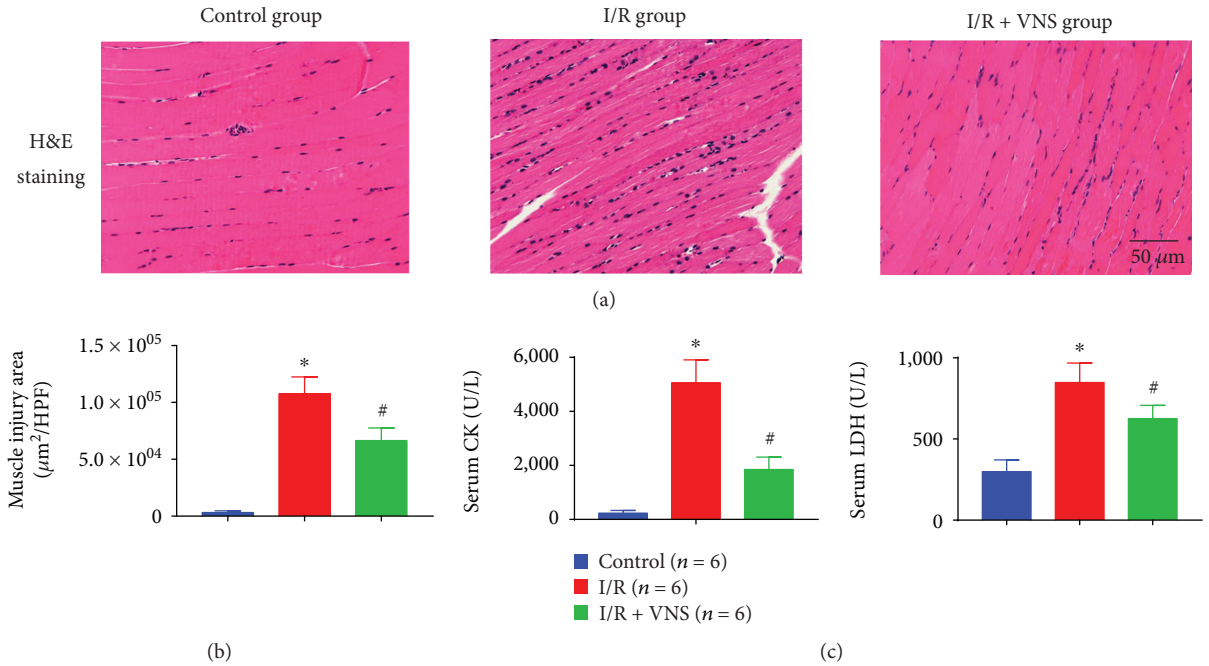

FIGURE 2: VNS alleviates skeletal muscle injury. (a) Control group: normal skeletal muscle cell shape and arrangement; I/R group: skeletal muscle cell degeneration and necrosis, wide range of inflammatory cell accumulation; I/R+VNS group: mixed normal and pathological skeletal muscle cells, little inflammatory cell infiltration. (b) The muscle injury area in the three groups. (c) The serum concentration of CK and LDH. $^{*}p < 0.05$ vs. control group; $^{\#}p < 0.05$ vs. I/R group; HPF: high-power field; CK: creatine kinase; LDH: lactic dehydrogenase.

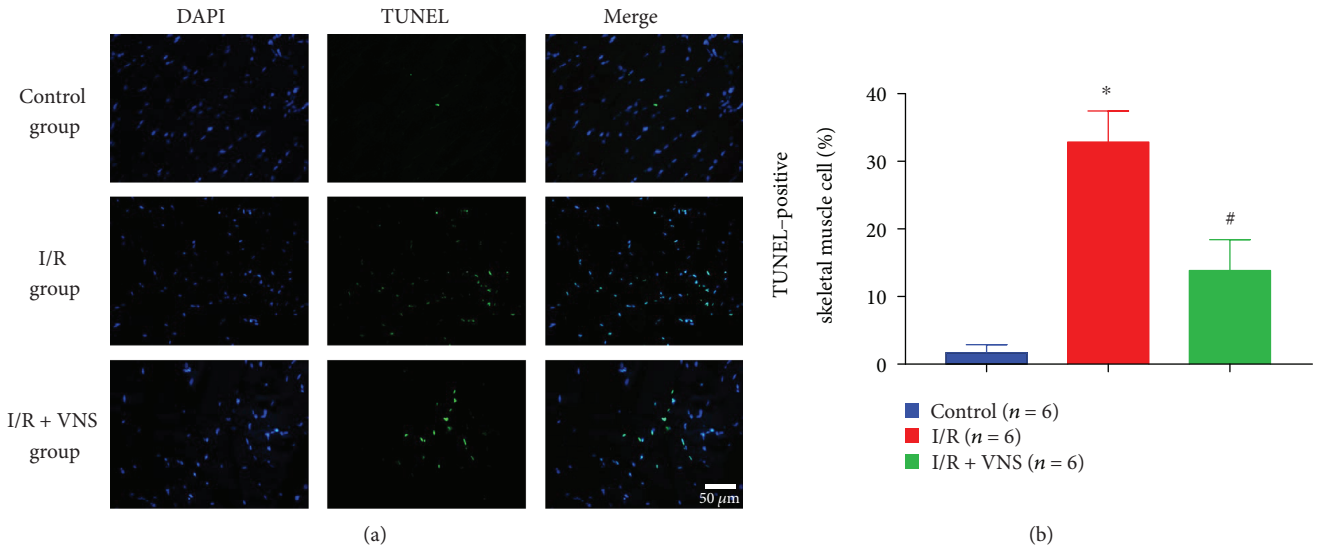

FIGURE 3: Effect of VNS on skeletal muscle cell apoptosis. (a) Representative images showing immunofluorescence staining for DAPI (blue) and TUNEL (green) in skeletal muscle cell nuclei from the control, I/R, and I/R+VNS groups. (b) Quantification of skeletal muscle cell apoptosis. $^{*}p < 0.05$ vs. control group; $^{\#}p < 0.05$ vs. I/R group.

1.83 ± 0.43 vs. 3.20 ± 0.32; and TNF-α, $2.70 \pm 0.0.74$ vs. 4.40 ± 0.62, $p < 0.05$ for each).

3.3. VNS Significantly Attenuated Oxidative Stress in Skeletal Muscle after I/R. The MPO activity in skeletal muscle tissues was used to indicate the neutrophilic infiltration severity. I/R injury significantly increased the MPO activity compared with the sham operation (0.40 ± 0.06 vs. 0.13 ± 0.02 U/g, $p < 0.05$). In contrast, VNS significantly alleviated the increase in MPO activity after I/R (0.25 ± 0.04 vs. 0.40 ± 0.06 U/g, $p < 0.05$) (see Figure 5(c)). The changes in the MDA and SOD concentrations in skeletal muscle tissues are shown in Figures 5(a)-5(b). As a biomarker of oxidative stress, the MDA level was significantly increased in tissues after I/R (1.29 ± 0.14 vs. 0.54 ± 0.08 nmol/mg protein, $p < 0.05$). In contrast, as a biomarker of antioxidant activity, the SOD was

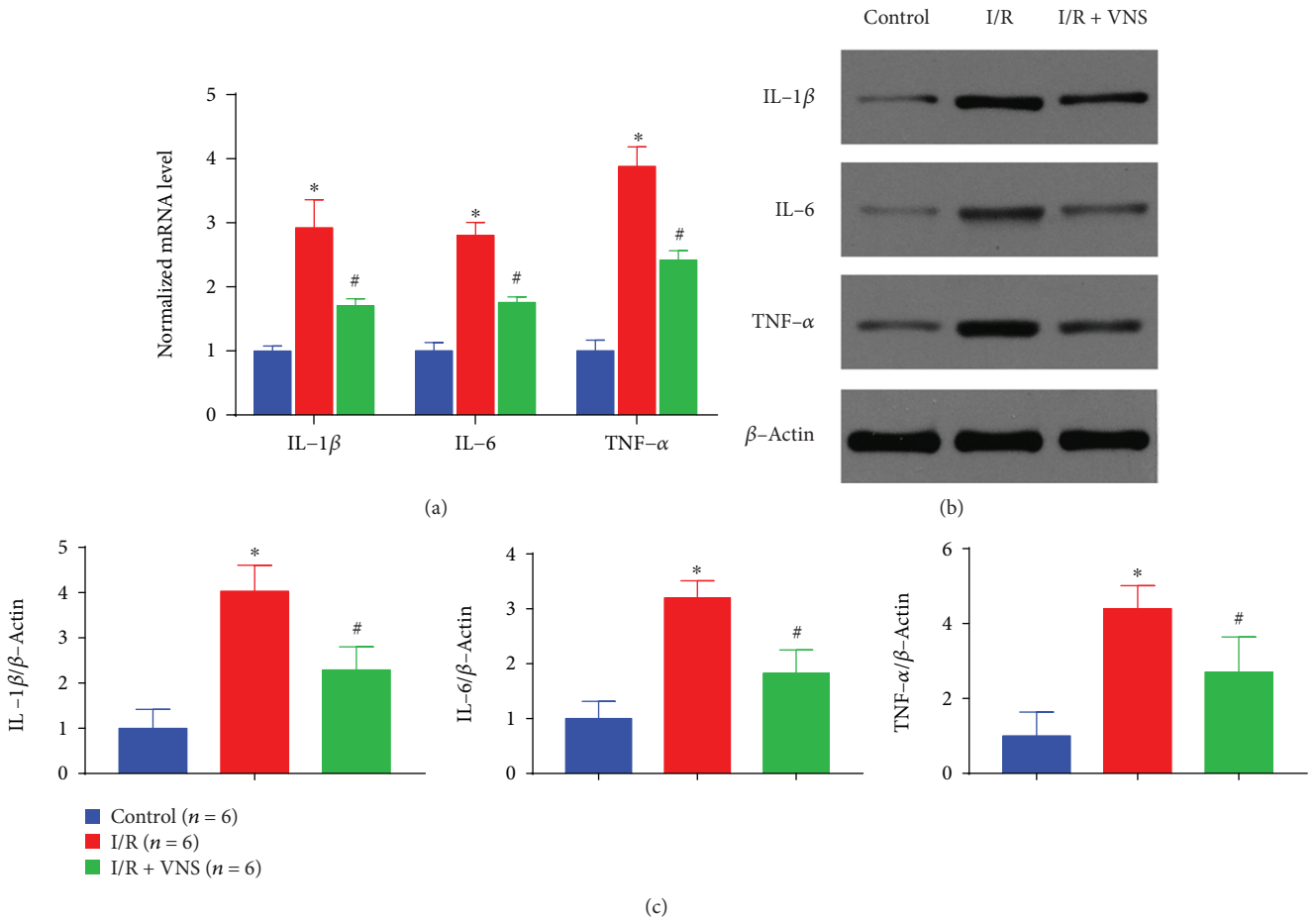

FIGURE 4: VNS mitigates inflammation in SMI/R injury. (a) Relative mRNA levels of IL-1β, IL-6, and TNF-α in the control, I/R, and I/R+VNS groups. (b, c) Representative blots and relative protein expression of IL-1β, IL-6, and TNF-α among different groups. $^{*}p < 0.05$ vs. control group; $^{\#}p < 0.05$ vs. I/R group. IL-1β: interleukin-1β; IL-6: interleukin-6; TNF-α: tumor necrosis factor-α.

significantly decreased in tissues after I/R (39.26 ± 7.85 vs. 118.85 ± 23.00 U/mg protein, $p < 0.05$). However, VNS during I/R markedly mitigated these changes (MDA, 0.92 ± 0.07 vs. 1.29 ± 0.14 nmol/mg protein; SOD, 68.31 ± 14.46 vs. 39.26 ± 7.85 U/mg protein, $p < 0.05$). Similar variation trends were observed for the serum MDA and SOD levels (see Figures 5(d)-5(e)). Compared to the control group, the I/R group showed significantly different serum MDA and SOD levels (MDA, 8.58 ± 0.88 vs. 4.32 ± 0.62 nmol/mL; SOD, 175.14 ± 13.10 vs. 383.93 ± 26.28 U/mL, $p < 0.05$ for both), while VNS markedly attenuated these changes (MDA, 6.19 ± 0.80 vs. 8.58 ± 0.88 nmol/mL; SOD, 305.37 ± 14.76 vs. 175.14 ± 13.10 U/mL, $p < 0.05$ for both).

3.4. VNS Significantly Protected Vascular Endothelial Function in the Skeletal Muscle after I/R. Endothelial function was evaluated by the expression of eNOS, ICAM-1, and VCAM-1. Figure 6(b) shows that I/R significantly decreased the expression level of eNOS and increased the expression levels of ICAM-1 and VCAM-1, while VNS exerted a protective effect on endothelial function and relieved the above changes. The relative expression of eNOS, ICAM-1, and VCAM-1 in the control and I/R groups were 1.00 ± 0.09 vs. 0.25 ± 0.10, 1.00 ± 0.28 vs. 5.15 ± 0.77, and 1.00 ± 0.20 vs. 3.82 ± 0.59, respectively, with $p < 0.05$ for all. VNS significantly relieved the changes described above (0.59 ± 0.16 vs. 0.25 ± 0.10, 3.40 ± 0.83 vs. 5.15 ± 0.77, and 2.14 ± 0.61 vs. 3.82 ± 0.59 for eNOS, ICAM-1, and VCAM-1, respectively, $p < 0.05$ for all).

4. Discussion

In the present study, we provide novel evidence that VNS during SMI/R injury could ameliorate skeletal muscle injury, as shown by alleviated cellular apoptosis, degeneration and inflammatory cell infiltration, and reduced serum CK and LDH levels compared to sham VNS. The underlying mechanisms of this protective effect involve inhibiting excessive inflammation and oxidative stress and protecting endothelial function. To the best of our knowledge, this is the first study to apply VNS to treat SMI/R injury.

It is well known that the innervation of the autonomic nervous system plays a vital role during organic I/R injury, including SMI/R injury. Sympathetic nerves are distributed in the adventitia of arteries in the skeletal muscle [14]. Increasing the sympathetic tone will lead to enhanced noradrenaline release, which results in vasoconstriction via direct activation of the α-receptors and inhibition of

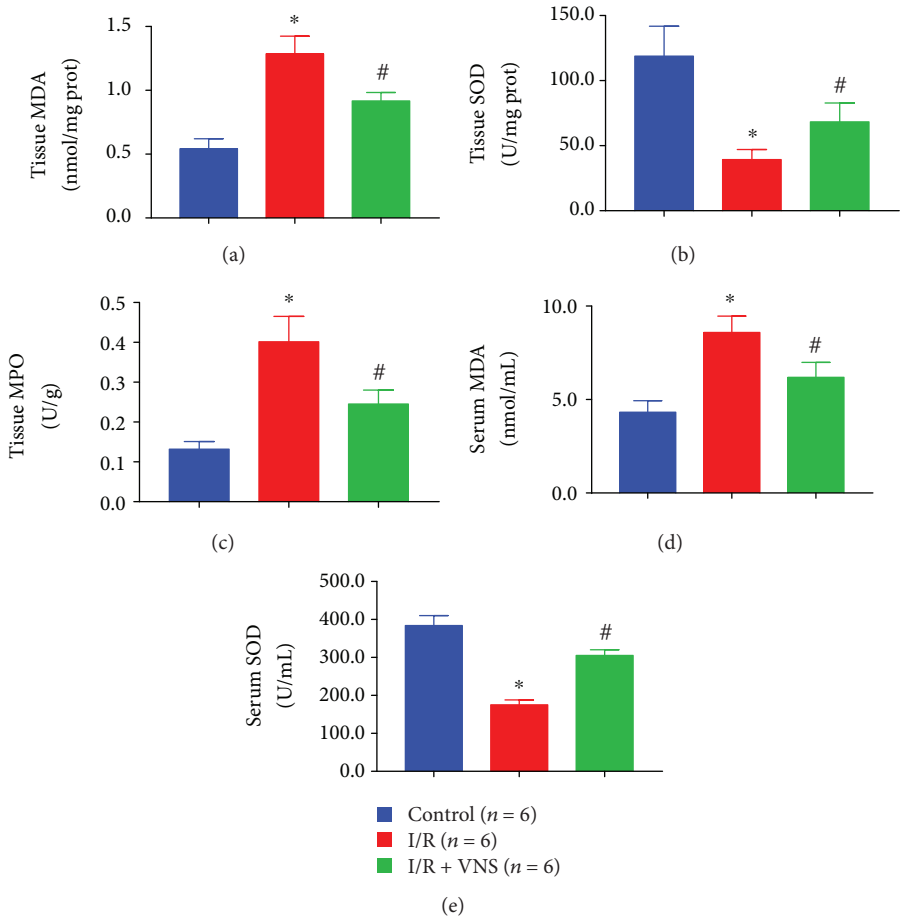

Figure 5: VNS attenuates oxidative stress in SMI/R injury. (a-c) The effect of VNS on the MDA, SOD, and MPO levels in skeletal muscle tissues. (d-e) The effect of VNS on the MDA and SOD levels in serum. $^{*}p < 0.05$ vs. control group; $^{\#}p < 0.05$ vs. I/R group. MDA: myeloperoxidase; SOD: superoxide dismutase; MPO: malondialdehyde.

vasodilating neuropeptides. Ischemia and hypoxia are common sympathoexcitatory stresses. This sympathetic vasoconstrictive effect might further exaggerate SMI/R injury [15]. Povlsen and Sirsjo have reported that treatment with guanethidine, a sympathetic nerve blocker, during reperfusion in SMI/R leads to a better prognosis [16]. Increased vagal tone might offset the sympathetic vasoconstrictive effect and protect organs from I/R injury. There are also emerging studies of this potential therapy for I/R injury. In a rat model, Jiang et al. reported that VNS treatment during cerebral I/R significantly reduced I/R injury [17]. The heart muscle is histologically similar to the skeletal muscle, and in a cardiac I/R model, VNS significantly reduced reperfusion arrhythmias and infarct size [8]. Our previous study also showed an analogous protective effect of VNS against myocardial I/R injury [18]. Such effects suggest that VNS might be a potential approach for treating SMI/R. The results of the present study are consistent with those of previous studies and demonstrate that VNS can attenuate SMI/R injury.

Currently, it is recognized that the pathophysiological mechanisms of I/R injury in the skeletal muscle include inflammation, oxidative stress, vascular endothelial damage, calcium overload, and mitochondria damage [19–22]. Corrick et al. reported that the administration of dexamethasone, a classic anti-inflammatory drug, at the onset of reperfusion ameliorated the structural and functional damage in the skeletal muscle [23], indicating the important role of inflammation in SMI/R injury. Acetylcholine (Ach) is an anti-inflammatory substance through cholinergic anti-inflammatory pathways [24]. VNS has been demonstrated to stimulate the release of Ach and might be a potential anti-inflammatory treatment in different diseases. Jonge et al. have reported that VNS could attenuate macrophage activation and suppress inflammation [25]. Similar results have been reported by Koopman et al., indicating that VNS could inhibit proinflammatory cytokine production and attenuate inflammatory disease [26]. Several researchers have applied the vagal anti-inflammatory effect in I/R injury and achieved excellent effects. Inoue et al. reported that VNS significantly reduced the expression of proinflammatory cytokines in a renal I/R rat model [7]. Similarly, our data indicate that VNS significantly reduced the inflammatory cytokine levels compared with sham VNS.

Reperfusion induced oxidative stress can promote skeletal muscle cell apoptosis [27]. It is known that inhibiting oxidative stress can effectively alleviate I/R injury. One study has shown that VNS can reduced oxidative stress in a

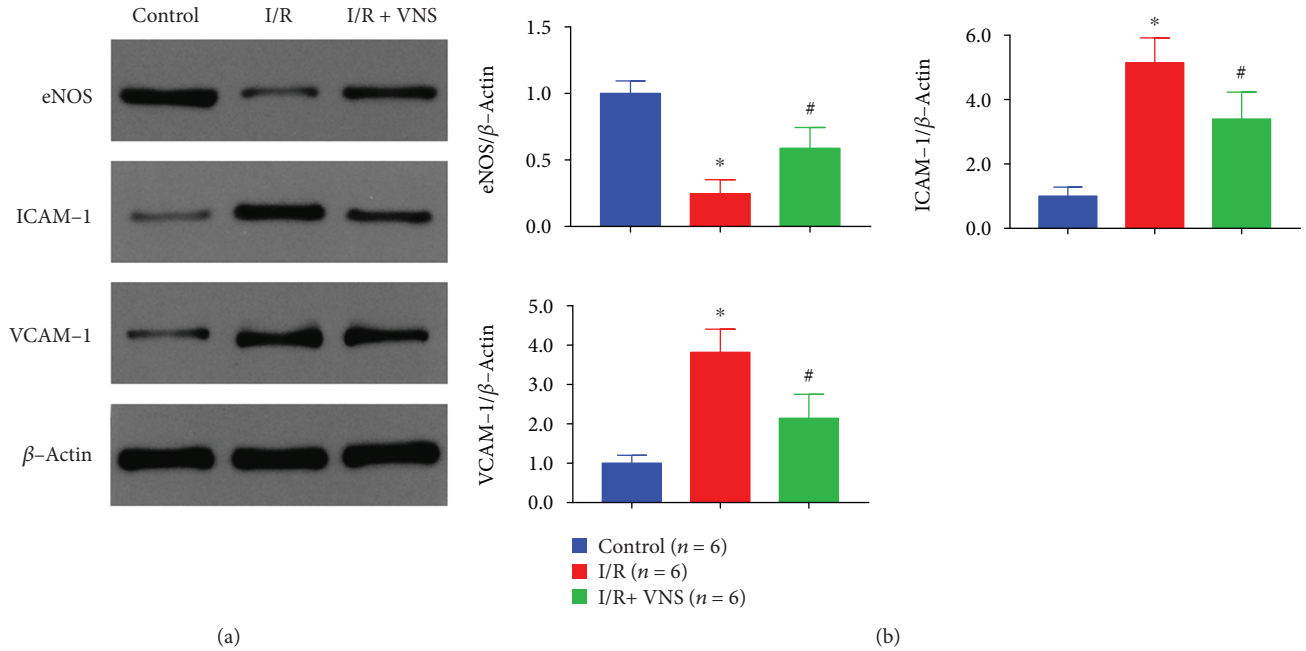

Figure 6: VNS protects vascular endothelial function. (a) Representative examples of eNOS, ICAM-1, and VCAM-1 expression in different groups. (b) Relative expression levels are shown as the ratio between the target proteins and β-actin expression levels. $^{*}p < 0.05$ vs. control group; $^{\#}p < 0.05$ vs. I/R group. eNOS: endothelial nitric oxide synthase; ICAM-1: intercellular cell adhesion molecule-1; VCAM-1: vascular cell adhesion molecule-1.

cerebral I/R rat model [17]. Our previous study indicated that VNS markedly reduced reactive oxygen species (ROS) production in a myocardial I/R canine model [18]. These data show that VNS could prevent I/R injury via an antioxidative stress effect. MPO is involved in the generation of ROS. The balance between prooxidant biomarkers (MDA) and antioxidant biomarkers (SOD) represents the activity of oxidant stress [28]. In the present study, our data suggest that VNS significantly decreased tissue MPO activity, reduced the concentration of MDA, and increased SOD activity in both tissue and serum. Therefore, we suggest that antioxidative activity may be one of potential mechanisms underlying the protective effect of VNS against SMI/R injury.

Vascular endothelial dysfunction is another mechanism involved in SMI/R injury [29]. Endothelial activation, which is defined by increased expression of cell surface adhesion molecules such as ICAM-1 and VCAM-1, was the main manifestation of vascular endothelial dysfunction [30]. The inflammatory response could activate the vascular endothelium, promote the production of proinflammatory cytokines (such as IL-6 and TNF-α), and increase the expression of ICAM-1 and VCAM-1. A previous study has shown that cholinergic agonists could suppress endothelial cell activation, as confirmed by decreased ICAM-1 expression [31]. Our results show that VNS relieved the increased expression of ICAM-1 and VCAM-1 induced by SMI/R injury. Nitric oxide (NO) is a bioactive molecule that helps dilate the blood vessels. It has been proven that NO could inhibit inflammatory cell adhesion and limit endothelial activation [32]. The expression of eNOS is essential for the production of NO and integrity of the vascular endothelium [33]. Yoshizumi et al. reported inhibiting eNOS expression could lead to endothelial dysfunction in human umbilical vein endothelial cells [34]. Previous studies have shown that increased eNOS expression leads to improvement of the endothelial function, which could improve the prognosis of SMI/R injury [11]. Li et al. reported that chronic VNS increased the expression of eNOS in ovariectomized rats [35]. In the present study, VNS significantly increased the expression of eNOS compared with sham VNS. Together with the downregulated expression of ICAM-1 and VCAM-1 and the increased eNOS expression results, our data indicated that VNS could protect the skeletal muscle from I/R injury by preserving endothelial function.

SMI/R injury is a common clinical condition. Until now, effective drug interventions to address this pathological state have been limited. The present study provides evidence that VNS could markedly reduce skeletal muscle tissue injury and cell apoptosis induced by I/R. Recently, stimulating the auricular branch of the vagus nerve has been proven to be safe and effective for achieving a similar effect as cervical VNS, which might overcome the shortcomings of conventional VNS [10, 36]. With further research to validate its safety and practicability, noninvasive VNS might become a novel technology to treat SMI/R injury in patients (see Figure 7).

4.1. Study Limitations. First, different stimulation sites and parameters have been shown to exert distinct therapeutic effects. In this study, we only verified the current stimulation parameters in left-side VNS. Further studies will aim

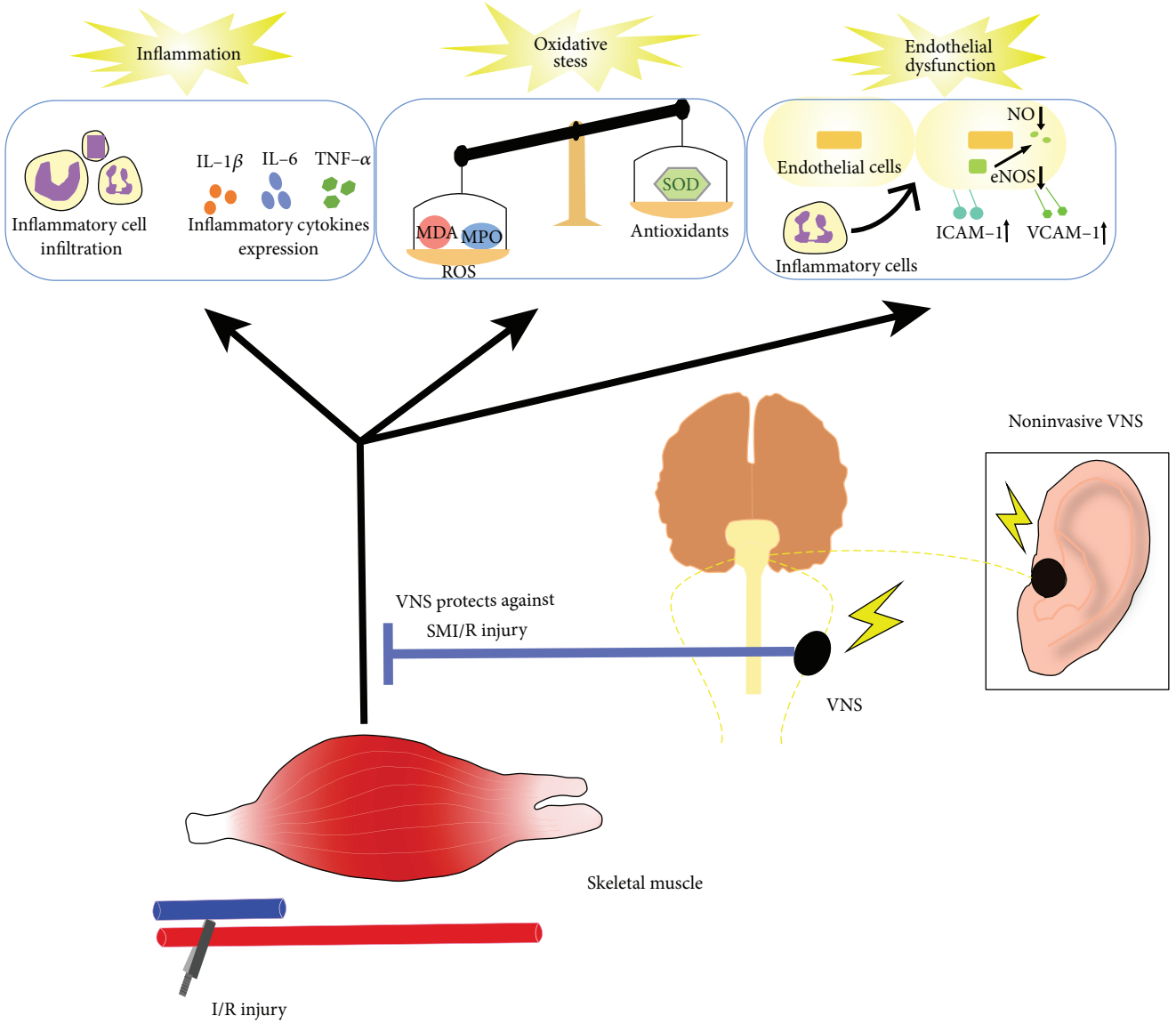

Figure 7: Schematic diagram depicting the protective effect and potential mechanisms of VNS on SMI/R injury. Noninvasive VNS may become a safe and acceptable technology for treating SMI/R patients.

to contrast bilateral VNS and explore the best stimulation parameters. Second, although we revealed several potential mechanisms by which VNS protects against SMI/R injury, the exact mechanism remains to be explored. Third, we only investigated the acute impact of VNS on SMI/R injury. Long-term effects should be verified in future studies. Fourth, we only measured the expression of eNOS as a parameter to reflect the endothelial function. The eNOS activity and NO production can be better to reflect the endothelial function. The effect of VNS on these parameters will be investigated in our further studies.

5. Conclusions

In conclusion, our data suggest that VNS could play a protective role in I/R-induced skeletal muscle injury. Its potential mechanisms may involve suppressing excessive inflammation, alleviating oxidative stress, and preserving vascular endothelial function. Although further studies are needed to validate its safety and practicability, VNS might provide a novel treatment for patients with SMI/R injury.

Data Availability

The data used to support the findings of this study are available from the corresponding author upon request.

Conflicts of Interest

The authors declare that there is no conflict of interest regarding the publication of this paper.

Authors' Contributions

Dr. Zhang and Dr. Li contributed equally to this study.

Acknowledgments

This work was supported by the National Key R&D Program of China (2017YFC1307800), National Natural Science Foundation of China (No. 81530011 and No. 81770364), and the Fundamental Research Fund for the Central Universities (2016YXMS132).

References

[1] P. M. Walker, "Ischemia/reperfusion injury in skeletal muscle," *Annals of Vascular Surgery*, vol. 5, no. 4, pp. 399–402, 1991.

[2] S. M. Gehrig and G. S. Lynch, "Emerging drugs for treating skeletal muscle injury and promoting muscle repair," *Expert Opinion on Emerging Drugs*, vol. 16, no. 1, pp. 163–182, 2011.

[3] F. W. Blaisdell, "The pathophysiology of skeletal muscle ischemia and the reperfusion syndrome: a review," *Cardiovascular Surgery*, vol. 10, no. 6, pp. 620–630, 2002.

[4] L. V. Borovikova, S. Ivanova, M. Zhang et al., "Vagus nerve stimulation attenuates the systemic inflammatory response to endotoxin," *Nature*, vol. 405, no. 6785, pp. 458–462, 2000.

[5] H. Wang, M. Yu, M. Ochani et al., "Nicotinic acetylcholine receptor alpha7 subunit is an essential regulator of inflammation," *Nature*, vol. 421, no. 6921, pp. 384–388, 2003.

[6] B. Bonaz, C. Picq, V. Sinniger, J. F. Mayol, and D. Clarencon, "Vagus nerve stimulation: from epilepsy to the cholinergic anti-inflammatory pathway," *Neurogastroenterology and Motility*, vol. 25, no. 3, pp. 208–221, 2013.

[7] T. Inoue, C. Abe, S. S. J. Sung et al., "Vagus nerve stimulation mediates protection from kidney ischemia-reperfusion injury through α7nAChR$^+$ splenocytes," *The Journal of Clinical Investigation*, vol. 126, no. 5, pp. 1939–1952, 2016.

[8] K. Shinlapawittayatorn, K. Chinda, S. Palee et al., "Low-amplitude, left vagus nerve stimulation significantly attenuates ventricular dysfunction and infarct size through prevention of mitochondrial dysfunction during acute ischemia-reperfusion injury," *Heart Rhythm*, vol. 10, no. 11, pp. 1700–1707, 2013.

[9] Y. Jiang, L. Li, B. Liu, Y. Zhang, Q. Chen, and C. Li, "PPARγ upregulation induced by vagus nerve stimulation exerts anti-inflammatory effect in cerebral ischemia/reperfusion rats," *Medical Science Monitor*, vol. 21, pp. 268–275, 2015.

[10] L. Yu, B. Huang, S. S. Po et al., "Low-level tragus stimulation for the treatment of ischemia and reperfusion injury in patients with ST-segment elevation myocardial infarction: a proof-of-concept study," *JACC: Cardiovascular Interventions*, vol. 10, no. 15, pp. 1511–1520, 2017.

[11] S. Hallström, H. Gasser, C. Neumayer et al., "S-nitroso human serum albumin treatment reduces ischemia/reperfusion injury in skeletal muscle via nitric oxide release," *Circulation*, vol. 105, no. 25, pp. 3032–3038, 2002.

[12] A. F. Liu, F. B. Zhao, J. Wang et al., "Effects of vagus nerve stimulation on cognitive functioning in rats with cerebral ischemia reperfusion," *Journal of Translational Medicine*, vol. 14, no. 1, p. 101, 2016.

[13] T. C. Yin, R. W. Wu, J. J. Sheu et al., "Combined therapy with extracorporeal shock wave and adipose-derived mesenchymal stem cells remarkably improved acute ischemia-reperfusion injury of quadriceps muscle," *Oxidative Medicine and Cellular Longevity*, vol. 2018, Article ID 6012636, 14 pages, 2018.

[14] J. K. Shoemaker, M. B. Badrov, B. K. Al-Khazraji, and D. N. Jackson, "Neural control of vascular function in skeletal muscle," *Comprehensive Physiology*, vol. 6, no. 1, pp. 303–329, 2015.

[15] E. Hagström-Toft, S. Enoksson, E. Moberg, J. Bolinder, and P. Arner, "β-Adrenergic regulation of lipolysis and blood flow in human skeletal muscle in vivo," *American Journal of Physiology-Endocrinology and Metabolism*, vol. 275, no. 6, pp. E909–E916, 1998.

[16] B. Povlsen and A. Sirsjo, "Sympathetic block significantly improves reperfusion in skeletal muscle following prolonged use of tourniquet," *Journal of Hand Surgery*, vol. 24, no. 6, pp. 738–740, 1999.

[17] Y. Jiang, L. Li, X. Tan, B. Liu, Y. Zhang, and C. Li, "miR-210 mediates vagus nerve stimulation-induced antioxidant stress and anti-apoptosis reactions following cerebral ischemia/reperfusion injury in rats," *Journal of Neurochemistry*, vol. 134, no. 1, pp. 173–181, 2015.

[18] M. Chen, X. Zhou, L. Yu et al., "Low-level vagus nerve stimulation attenuates myocardial ischemic reperfusion injury by antioxidative stress and antiapoptosis reactions in canines," *Journal of Cardiovascular Electrophysiology*, vol. 27, no. 2, pp. 224–231, 2016.

[19] S. Gillani, J. Cao, T. Suzuki, and D. J. Hak, "The effect of ischemia reperfusion injury on skeletal muscle," *Injury*, vol. 43, no. 6, pp. 670–675, 2012.

[20] D. L. Carden and D. N. Granger, "Pathophysiology of ischaemia-reperfusion injury," *The Journal of Pathology*, vol. 190, no. 3, pp. 255–266, 2000.

[21] M. Odeh, "The role of reperfusion-induced injury in the pathogenesis of the crush syndrome," *The New England Journal of Medicine*, vol. 324, no. 20, pp. 1417–1422, 1991.

[22] H. K. Eltzschig and T. Eckle, "Ischemia and reperfusion–from mechanism to translation," *Nature Medicine*, vol. 17, no. 11, pp. 1391–1401, 2011.

[23] R. M. Corrick, H. Tu, D. Zhang et al., "Dexamethasone protects against tourniquet-induced acute ischemia-reperfusion injury in mouse hindlimb," *Frontiers in Physiology*, vol. 9, p. 244, 2018.

[24] M. Rosas-Ballina, P. S. Olofsson, M. Ochani et al., "Acetylcholine-synthesizing T cells relay neural signals in a vagus nerve circuit," *Science*, vol. 334, no. 6052, pp. 98–101, 2011.

[25] W. J. de Jonge, E. P. van der Zanden, F. O. The et al., "Stimulation of the vagus nerve attenuates macrophage activation by activating the Jak2-STAT3 signaling pathway," *Nature Immunology*, vol. 6, no. 8, pp. 844–851, 2005.

[26] F. A. Koopman, S. S. Chavan, S. Miljko et al., "Vagus nerve stimulation inhibits cytokine production and attenuates disease severity in rheumatoid arthritis," *Proceedings of the National Academy of Sciences of the United States of America*, vol. 113, no. 29, pp. 8284–8289, 2016.

[27] H. Sies, "Oxidative stress: a concept in redox biology and medicine," *Redox Biology*, vol. 4, pp. 180–183, 2015.

[28] J. Frijhoff, P. G. Winyard, N. Zarkovic et al., "Clinical relevance of biomarkers of oxidative stress," *Antioxidants & Redox Signaling*, vol. 23, no. 14, pp. 1144–1170, 2015.

[29] W. C. Sternbergh III and B. Adelman, "The temporal relationship between endothelial cell dysfunction and skeletal muscle damage after ischemia and reperfusion," *Journal of Vascular Surgery*, vol. 16, no. 1, pp. 30–39, 1992.

[30] J. K. Liao, "Linking endothelial dysfunction with endothelial cell activation," *The Journal of Clinical Investigation*, vol. 123, no. 2, pp. 540-541, 2013.

[31] P. K. Chatterjee, Y. Al-Abed, B. Sherry, and C. N. Metz, "Cholinergic agonists regulate JAK2/STAT3 signaling to suppress endothelial cell activation," *American Journal of Physiology Cell Physiology*, vol. 297, no. 5, pp. C1294–C1306, 2009.

[32] R. De Caterina, P. Libby, H. B. Peng et al., "Nitric oxide decreases cytokine-induced endothelial activation. Nitric oxide selectively reduces endothelial expression of adhesion molecules and proinflammatory cytokines," *The Journal of Clinical Investigation*, vol. 96, no. 1, pp. 60–68, 1995.

[33] M. Siragusa and I. Fleming, "The eNOS signalosome and its link to endothelial dysfunction," *Pflügers Archiv*, vol. 468, no. 7, pp. 1125–1137, 2016.

[34] M. Yoshizumi, M. A. Perrella, J. C. Burnett Jr., and M. E. Lee, "Tumor necrosis factor downregulates an endothelial nitric oxide synthase mRNA by shortening its half-life," *Circulation Research*, vol. 73, no. 1, pp. 205–209, 1993.

[35] P. Li, H. Liu, P. Sun et al., "Chronic vagus nerve stimulation attenuates vascular endothelial impairments and reduces the inflammatory profile via inhibition of the NF-κB signaling pathway in ovariectomized rats," *Experimental Gerontology*, vol. 74, pp. 43–55, 2016.

[36] J. Fang, P. Rong, Y. Hong et al., "Transcutaneous vagus nerve stimulation modulates default mode network in major depressive disorder," *Biological Psychiatry*, vol. 79, no. 4, pp. 266–273, 2016.

Hindawi
Oxidative Medicine and Cellular Longevity
Volume 2019, Article ID 4617801, 12 pages
https://doi.org/10.1155/2019/4617801

Review Article

Changes in Redox Signaling in the Skeletal Muscle with Aging

Péter Szentesi,[1] László Csernoch,[1] László Dux,[2] and Anikó Keller-Pintér[2]

[1]*Department of Physiology, Medical Faculty, University of Debrecen, Debrecen H-4002, Hungary*
[2]*Department of Biochemistry, Faculty of Medicine, University of Szeged, Szeged H-6720, Hungary*

Correspondence should be addressed to Anikó Keller-Pintér; keller.aniko@med.u-szeged.hu

Received 22 June 2018; Revised 5 November 2018; Accepted 22 November 2018; Published 17 January 2019

Guest Editor: Christina Karatzaferi

Reduction in muscle strength with aging is due to both loss of muscle mass (quantity) and intrinsic force production (quality). Along with decreased functional capacity of the muscle, age-related muscle loss is associated with corresponding comorbidities and healthcare costs. Mitochondrial dysfunction and increased oxidative stress are the central driving forces for age-related skeletal muscle abnormalities. The increased oxidative stress in the aged muscle can lead to altered excitation-contraction coupling and calcium homeostasis. Furthermore, apoptosis-mediated fiber loss, atrophy of the remaining fibers, dysfunction of the satellite cells (muscle stem cells), and concomitant impaired muscle regeneration are also the consequences of increased oxidative stress, leading to a decrease in muscle mass, strength, and function of the aged muscle. Here we summarize the possible effects of oxidative stress in the aged muscle and the benefits of physical activity and antioxidant therapy.

1. Introduction

With improved life quality conditions and the availability of treatments, life expectancy and consequently the number of elderly in the population have increased [1]. This change in population composition places increasing emphasis on the treatment of chronic, noncommunicable diseases as they have become major causes of death and disability worldwide, thus driving the need to understand the mechanism of aging and find treatments for age-related diseases [2].

The skeletal muscle is the largest organ in the body comprising ~40% of its mass. It plays fundamental roles in movement, posture, and energy metabolism. The loss of skeletal muscle mass and function with age can have a major impact on quality of life and results in increased dependence and frailty. Age-related decline of skeletal muscle function (sarcopenia) results in strength loss [3]. This loss stems from two major sources, reductions in muscle mass (i.e., quantity) and decrease in its intrinsic capacity for producing force (i.e., quality). Both can be the consequence of several factors (Figure 1), including oxidative stress that is the result of the accumulation of reactive oxygen and nitrogen species (ROS/RNS). The free-radical theory of aging was established more than 60 years ago [4] and has become one of the most studied theories to have been proposed. It is now accepted that this theory and its various spin-offs cannot alone explain the aging process [5, 6]. Nevertheless, huge amounts of data indicate that ROS-mediated aging phenotypes and age-related disorders exist [7, 8].

During physiological homeostasis the overall oxidative balance is maintained by the production of ROS/RNS from several sources and their removal by antioxidant systems, including endogenous or exogenous antioxidant molecules. At physiological concentrations ROS/RNS play essential roles in a variety of signaling pathways. There is an optimal level of ROS/RNS to sustain both cellular homeostasis and adaptive responses, and both too low and too high levels of ROS/RNS are detrimental to cell functions [9]. The skeletal muscle consumes large quantities of oxygen and can generate great amounts of ROS and also reactive nitrogen species. Mitochondria are one of the most important sources of ROS in the skeletal muscle; furthermore, NADPH oxidase (NOX) [10], xanthine oxidase [11], and phospholipase A2 (PLA2) [12, 13] are also involved in ROS production.

The origin of the increased ROS production and oxidative damage is mitochondrial dysfunction with aging [14], caused by age-related mitochondrial DNA mutations, deletions, and damage [15], as well as the impaired ability

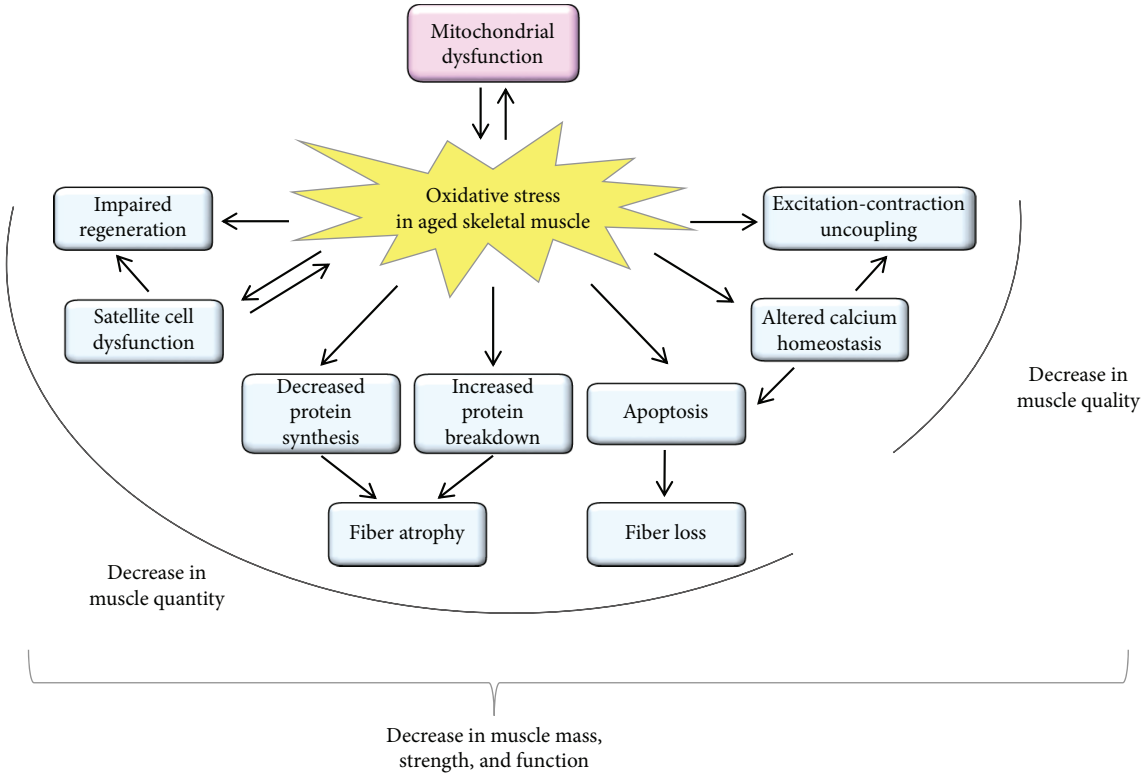

Figure 1: Schematic summary of the effects of oxidative stress in the aged skeletal muscle. The age-related increase in oxidative stress can result in mitochondrial dysfunction, and the dysfunctional mitochondria can further generate reactive oxygen species. The increased oxidative stress can lead to a decrease both in muscle quality and in muscle quantity. As a consequence of the increased oxidative stress, excitation-contraction uncoupling, altered calcium homeostasis, apoptosis-mediated fiber loss, atrophy of the remaining fibers, dysfunction of the satellite cells (muscle stem cells), and impaired muscle regeneration can be observed in the aged muscle leading to a decrease in muscle mass, strength, and function.

of muscle cells to remove dysfunctional mitochondria [16]. Oxidative phosphorylation impairment can lead to decreased ATP production and further generation of ROS [4]. Interestingly, aging is associated not only with an increase in oxidative damage but also with an upregulation of antioxidant enzymes in the skeletal muscle [9]. Furthermore, the iron content of the mitochondria in the skeletal muscle increases with aging, amplifying the oxidative damage with the generation of ROS [17]. Increased ROS production, mitochondrial DNA damage, and mitochondrial dysfunction was observed in aged muscles [18–20].

The skeletal muscle is highly plastic and shows several adaptations towards mechanical and metabolic stress [21, 22]. Oxidative stressors, like ROS, have long been taken into account as harmful species with negative effects in the skeletal muscle [23]. Proteins such as biomolecules are frequently affected by oxidation; thus, elevated ROS levels can cause reversible or irreversible posttranslational modification of cysteine, selenocysteine, histidine, and methionine. Oxidative posttranslational modifications of proteins are characteristic in the aged muscle, such as carbonylation which alters protein function [24]. The oxidative capacity of muscles is strongly associated with health and overall well-being. Enhanced oxidative capacity in the skeletal muscle protects against several pathological phenomena (insulin resistance, metabolic dysregulation, muscle loss with aging, and increased energetic deficits in myopathies) [25, 26]. These protective effects are largely associated with enhanced mitochondrial function and elevated numbers of mitochondria, which can protect against cellular stress.

Given the rapidly aging population, it is essential to better understand the development, progression, prevention, and treatment of age-related muscle diseases. The aim of this review is to discuss the possible effects of age-related oxidation on the skeletal muscle and highlight the benefits of physical activity and intake of antioxidant compounds to protect from oxidative stress.

2. Oxidative Stress and EC-Coupling Machinery in Aging

Ca^{2+}, as a second messenger, is necessary for muscle contraction. Ca^{2+} can originate from the extracellular space (the heart and smooth muscle) and from the intracellular store of the sarcoplasmic reticulum (SR) (in the skeletal muscle exclusively from SR). Excitation-contraction (EC) coupling, the steps from the trigger action potential to the development of force, starts with the activation of the voltage sensor dihydropyridine-sensitive, L-type Ca^{2+} channels (DHPRs). These can open the Ca^{2+} release channel ryanodine receptor (RyR) of SR [27]. The released Ca^{2+} freely diffuses into the intracellular space and, after binding with

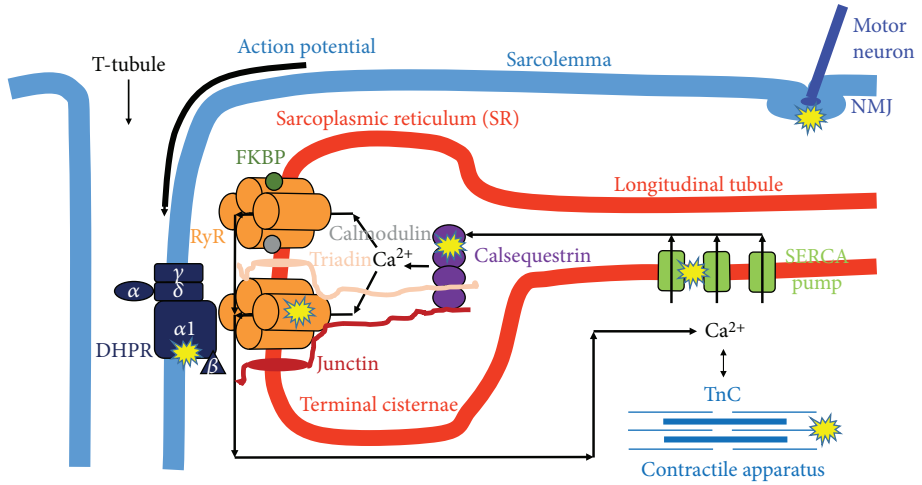

FIGURE 2: Possible actions of age-related oxidative stress reducing skeletal muscle contraction. Accumulation of reactive oxygen and nitrogen species in the aged muscle results in protein modification and/or damage that could reduce muscle quality by altering muscle fiber activation at the neuromuscular junction (NMJ), excitation-contraction (EC) coupling (DHPR, RyR, SERCA, calsequestrin), and cross-bridge cycling within the myofibrillar apparatus. DHPR: dihydropyridine receptor; FKBP: FK506 binding protein; RyR: ryanodine receptor; SERCA: sarco/endoplasmic reticulum Ca^{2+} pump; TnC: troponin-C.

troponin-C (TnC), initiates muscle contraction. During relaxation, the Ca^{2+} is taken up by the sarco/endoplasmic reticulum calcium pump (SERCA) into the SR [28]. If any step in the EC-coupling pathway is disrupted, the voltage-induced Ca^{2+} release from SR will be deficient and less cytoplasmic Ca^{2+} will be available to bind with TnC (Figure 2).

EC coupling has a unique structure in muscle fibers, called calcium release units (CRUs). They are formed by two membrane systems: the transverse- (t-) tubule, where the trigger action potential (depolarization) from the sarcolemma goes into the fiber, and the calcium store SR terminal cisternae [29]. In a fully developed skeletal muscle fiber, a central t-tubule usually forms junctions with two SR forming a triad. The voltage sensor DHPRs localized in the t-tubule membrane [30] are in direct connection with the closely apposed calcium release channel RyRs in the SR membrane.

2.1. RyR. Mammalian RyR has three isoforms, which were originally identified in the skeletal muscle (RyR1), in the heart muscle (RyR2), and in the brain (RyR3). It is now known that some tissues express all three mammalian RyR isoforms [31–33]. Several cellular compounds (e.g., ATP, HCl, Ca^{2+}, and Mg^{2+}), specific proteins (phosphatases and kinases), and endogenous oxidative species can regulate RyR functions [34]. Abramson and Salama [35] were the first to propose a redox-dependent gating model of RyR, in which the channel pore opens after the oxidation and closes after the reduction of critical sulfhydryl moieties within the RyR complex. Gating transitions of the RyR channel are extremely fast; the open state usually lasts no longer than a few milliseconds; thus, this hypothesis has been called into question because of its slow kinetic [36]. Additionally, isolated RyR1 reconstituted in an artificial lipid bilayer functioned similarly independently of the presence of cofactors to maintain the catalytic transfer of electrons [37].

Another possibility to control RyR1 gating is the transmembrane redox potential of SR. In healthy mammalian cells, the redox potential of the cytosol is approximately -230 mV [38]. The majority of redox buffers within the cytosol of a muscle cell are based on the relative concentration of oxidized (GSSG) and reduced (GSH) glutathione or NADH and NAD^+. In different nonmuscle cells, GSSG and GSH transporters have been found across the ER membrane [38, 39]. These transporters play an essential role in establishing and maintaining the membrane redox potential gradient. It was shown that glutathione transport across SR/ER membranes is very fast and correlates with the expression of RyR1 in terminal cisternae [40]. These findings imply the presence of one or more transmembrane redox sensors in the RyR1 channel.

To study the redox regulation of RyR1 channel activity, Feng et al. [41] used artificial lipid bilayer membranes and precisely controlled the redox state by adjusting the [GSSG]/[GSH] ratio to change redox potentials on both the lumenal and cytoplasmic sides of the reconstituted channel. Redox sensing may represent a widespread mechanism by which RyR1 channels respond to local changes in transmembrane redox potential. As mentioned above, disulfide bond formation (sulfhydryl oxidation) in RyR1 usually takes place in the oxidizing environment of the SR lumen, not in the reducing environment of the cytosol.

Pessah et al. [42] demonstrated that RyR1 channel gating was accompanied by changes in the microenvironment of hyperreactive Cys residues. It was assumed that the localized redox potential could influence the domain with the redox sensor, which might change the stability of the closed state. This means that the closed but not the open conformation of RyR1 senses redox changes. In this framework, the rapid gating transitions of RyR1 would not coincide with oxidation and reduction of disulfide bonds, and local changes in the

redox environment would influence the overall operation of the channel.

With advancing age, RyR becomes increasingly oxidized and nitrosylated, which leads to leaky release channels. RyR1 from aged mice was shown to be more oxidized and cysteine-nitrosylated compared to that from young animals. Furthermore, these RyR channels lacked the stabilizing subunit FKBP12. Treating aged mice with the small molecule rycal drug S107 stabilized binding of FKBP12 to RyR1 reducing intracellular Ca^{2+} leakage, enhancing Ca^{2+} release from SR, decreasing ROS, and improving muscle exercise [43]. Similarly, increased Ca^{2+} leakage from the SR, primarily through the RyRs, was found in type I fibers of aged humans, and a reducing treatment with dithiothreitol inhibited RyR Ca^{2+} leakage, thus increasing net SR Ca^{2+} accumulation [44]. Other evidence of partially defective SR in the aged muscle is the decreased frequency of spontaneous Ca^{2+} release (spark) through RyR, observed by Park et al. [45] and the authors of this review (unpublished data).

The expression of RyR also changes with age. Unpublished data of the authors of this review showed reduced RyR expression in aging mice. The whole tetramer was almost completely absent in the EDL muscle of old animals, and only a smaller amount of degraded RyR was found. Interestingly, this was not the case in mice that did voluntary exercise throughout their entire life.

2.2. RyR-Associated Proteins. A lot of studies have investigated the redox dependence of accessory proteins of RyR1, which contribute to the tight regulation of channel activity in the mammalian skeletal muscle. These proteins include the voltage sensor skeletal dihydropyridine receptor (L-type Ca^{2+} channel), calmodulin, triadin, junctin, FKBP12 (12 kDa FK506 binding protein), and calsequestrin in the SR lumen [34, 46].

To date there is no evidence that triadin and junctin have any role in the redox regulation of RyR1. On the other hand, reactive sulfhydryl groups within RyR1 channels have been shown to help the binding of calmodulin, and functional responses of calmodulin to RyR1 may be redox regulated [47]. It was proposed that probably more than one class of sulfhydryl residues within the RyR1 channel complex suffer chemical modification, each contributing to a specific function. This question is still open because of the structural complexity of RyR1 and its associated proteins.

Calsequestrin-1 is a high-capacity Ca^{2+} buffer, localized in the lumen of SR in close proximity to RyR1. It has been demonstrated that nNOS and NOX2 also colocalize with RyRs at the triad junctions, and the latter generate ROS, which stimulate Ca^{2+} release from the SR through RyR1 [48]. Recently, it was hypothesized that in muscle fibers lacking Calsequestrin-1, the close positioning of either nNOS or NOX2 to RyR1 and the Ca^{2+}-dependent activation of nNOS could be the consequence of increased production of ROS and RNS. This could finally lead to nitrosylation and glutathionylation of specific cysteine residues causing oxidative modifications that further increase the probability of leaky RyR1 channels [49].

RyR1 has four subunits to bind the small FK506 protein (FKBP12) [50]. FKBP12 associates mainly with the skeletal muscle isoform to regulate RyR1 function. Pharmacological removal of FKBPs causes uncoupling of RyR1 ion channels from their neighbors and thus activates Ca^{2+} release from SR [51]. A recent study shows that the 1,4 benzoderivative S107 binds to multiple RyR1 sites with low affinity and stabilizes the RyR1-FKBP12 complex depending on the redox state of the calcium channel [52].

2.3. DHPR. DHPR is located in the t-tubules and plays a role in EC coupling as the voltage sensor triggering Ca^{2+} release from the SR after an action potential. More than 20 years ago, Delbono et al. [53] recorded a significant reduction of maximum charge movement and L-type calcium current in muscle fibers from biopsies of 65-75-year-old patients. This was accompanied with decreased Ca^{2+} release from the SR. Just a few years later it was shown that ROS may also target DHPRs, since ROS alter the dynamics of muscle K^+ contractures [54]. A later study by the same research group using the mammalian diaphragm demonstrated an increase in tension after antioxidant application that is clearly dependent on DHPR function [55]. These results support the hypothesis that the DHPR redox state and RyR function are modulated in an interactive manner and modify contractility.

It was also shown that the expression of the $\alpha 1$ subunit of DHPR decreases with age and this is associated with the loss of skeletal muscle strength [56]. These findings were amplified by the fact that DHPR expression levels can be regulated by different mechanisms, independently from gene transcription or mRNA expression. In a very recent study, a novel finding was reported that cytoplasmic-located fast skeletal muscle troponin T3 (TnT3) regulates DHPR expression in skeletal muscle fibers and calpain-induced cleavage of TnT3 is associated with DHPR downregulation in aged mice [57]. The reduced DHPR expression with aging increases the number of uncoupled RyR1s and, thus, decreases SR Ca^{2+} release which leads to EC uncoupling and finally decreased force production.

2.4. SERCA. The sarco/endoplasmic reticulum Ca-ATPase (SERCA) is the calcium pump that uptakes Ca^{2+} from the cytosol to the SR during muscle relaxation. It has an important role in maintaining the resting intracellular Ca^{2+} concentration (around 100 nM). Evidence for NO inhibition of the Ca-ATPase was observed in the rabbit skeletal muscle, where sustained contractions led to significant (40–50%) inactivation of the pump [58]. One possible explanation could be the reactions with critical SH groups, since peroxynitrite treatment of Ca-ATPase from the rabbit skeletal muscle was correlated with oxidative and nitrosative modifications of cysteines at several positions, of which one was deemed responsible for enzyme inhibition [59]. Recently it was shown that SERCA1 is reversibly regulated via NO-dependent S-glutathiolation of specific cysteine residues which are embedded within the transmembrane domains of the pump. Some specific amino acid peroxides react selectively with a subset of cysteine residues of SERCA1, representing one of the targets for NO-dependent S-glutathiolation [60]. In a

parallel study it was also demonstrated that antioxidant treatment affects intracellular Ca^{2+} concentration, increasing the maximum rates of ATP hydrolysis and uptake of Ca^{2+} by SERCA in the diaphragm [61].

The 53 kDa isoform of sarcalumenin, the major luminal glycoprotein associated with SERCA, was found to be downregulated in the aged human muscle [62]. Interestingly this was accompanied with the upregulation of Calsequestrin-1. In a recent study on humans, it was shown that these changes were reversed after 9 weeks of training by electrical stimulation [63] of the *vastus lateralis* muscle of sedentary senior volunteers. The decreased active SERCA, and thus insufficient SR Ca^{2+} content, can also be explained by the findings of Boncompagni et al. [64]. Their electron microscopic study proved the presence of SERCA and Calsequestrin-1-rich tubular aggregates in the aging mouse skeletal muscle. They hypothesized that polymerization of SERCA induces its inactivity and this decreases the Ca^{2+} uptake capacity of SR. Similarly, the accumulated inactive Calsequestrin-1 in tubular aggregates is missing from SR and leads to reduced Ca^{2+} storage capacity.

3. The Effects of Age-Dependent Structural Changes in the Skeletal Muscle

It has been suggested by Renganathan and colleagues [56] that an uncoupling between DHPR and RyR1 in the CRUs (insufficient transmission of the sarcolemmal depolarization to the calcium release channel) with aging is one of the major determinants of the progressive decline in muscle strength. This has been supported by transmission EM studies [65], which show a progressive disarrangement of triads in the aging human skeletal muscle. This results in a drastic reduction in the overall number of CRUs available for releasing Ca^{2+} to initiate the sliding of contractile filaments and generate force. Notwithstanding that the total number of CRUs is decreased, on average by more than 50% in the aging muscle, the decrease in the total amount of both DHPR and RyR1 was less, because the decrease in the total number of SR/t-tubule junctions is accompanied by an increase in the average size of RyR clusters which compensate for the loss of triads.

Besides Ca^{2+}, ATP is also necessary to generate force, as well as for relaxation in the skeletal muscle. The main source of ATP is mitochondria. It was shown that mitochondria and CRUs are functionally linked to each other via ROS- and Ca^{2+}-mediated cross-talk [66]. Furthermore, these two organelles are structurally connected by tethers, which promote proximity and sufficient calcium signaling [67]. In the aged muscle, not only the ultrastructure, density, and disposition of mitochondria and CRUs but also their reciprocal associations are altered. The density of CRUs and mitochondria is decreased in the aged muscle, with an increased number of damaged mitochondria and mitochondria misplaced from their normal triadic position. A significant reduction in CRU-mitochondria pair density and their tethering was also observed in aged mice. These changes were accompanied with increased oxidative stress and with decreased mitochondrial Ca^{2+} uptake and SR Ca^{2+} release [68]. These wrong direction changes in the skeletal muscle can be prevented by regular exercise. The number of mitochondria is higher in athletic than in sedentary seniors, and furthermore, the number of CRU-mitochondria pairs is three times higher in senior sportsmen than in sedentary individuals. Since the correct association between CRUs and mitochondria is necessary for efficient ATP production, this can explain the significantly superior muscle performance in lifelong exercising seniors [68]. Similar results were obtained with mice that had access to running wheels for the second part of their lives (from 1 to 2 years of age) [69]. The authors of these studies concluded in their results that the huge age-dependent decrease affecting EC-coupling apparatuses and mitochondrial functions in the skeletal muscle of humans and mice can be partly associated with inactivity in old age.

4. Oxidative Stress and Satellite Cell Dysfunction with Aging

The skeletal muscle has the remarkable ability to regenerate in response to injury. This regenerative capacity is due to the muscle stem cells (MuSCs), also called satellite cells that reside between the muscle fiber and its surrounding basal lamina [70]. The satellite cells are mitotically and physiologically in a quiescent state (a G0 reversible arrest state) in the healthy muscle and express the Pax7 transcription factor. They are stimulated upon muscle injury to enter the cell cycle and proliferate extensively and form myoblasts that will subsequently differentiate and fuse to form muscle fibers. The differentiated myocytes are capable of fusing together and, with the preexisting myofibers, restore the muscle tissue. A small subset of the expanding satellite cells does not commit to terminal differentiation but self-renews to restore the quiescent satellite cell pool for further needs [71]. The regenerative function of satellite cells declines with age [72, 73] (Figure 3). At advanced geriatric age, this decline is maximal owing to transition from a normal quiescence into an irreversible senescence (a G0 irreversible arrest).

The age-related deficits in muscle regeneration have been linked to changes in the satellite cell environment (such as inflammatory status) and/or satellite cell-intrinsic mechanisms [74]. Both the number and the functionality of satellite cells decrease with age [75–79], switching from quiescence to a senescent state [76]. The satellite cells are unequally distributed among the different fiber types and differ between muscles. In the rat extensor digitorum longus (EDL) muscle, satellite cells are observed most frequently on type IIA fibers and at approximately equal frequencies on type IIB and type I fibers [80]. Interestingly, the soleus contains a considerably higher percentage of satellite cells than the EDL [80]. In the young adults, satellite cell content did not differ between type I and type II muscle fibers [81]. Aging is associated with a switch from fast to slow fiber type [82]. The abundance of resident satellite cells declines with age in myofibers from both fast- and slow-twitch muscles in mice [83], and a decrease in FGF signaling as a possible limiting factor of satellite cell function during muscle aging has been identified [83]. In contrast, satellite cell content is reported to be specifically reduced in type II skeletal muscle fibers in the elderly,

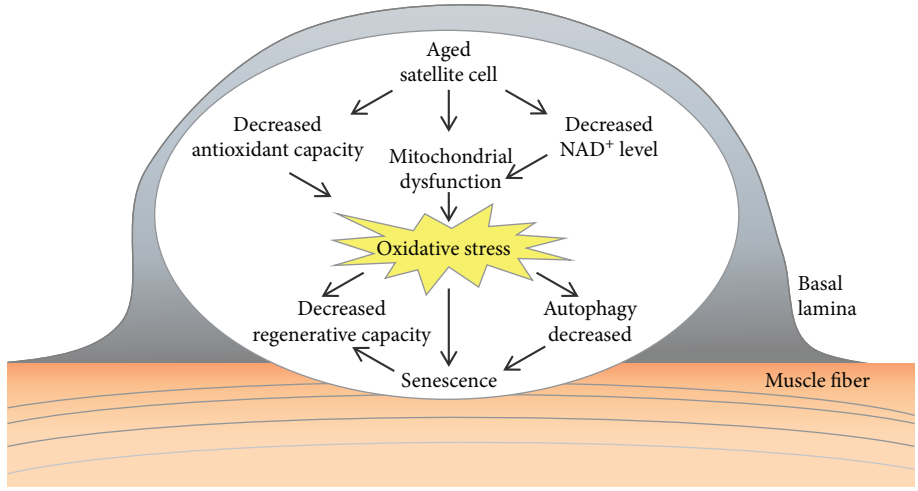

Figure 3: Age-related alterations in satellite cells. Mitochondrial dysfunction and decreased antioxidant capacity of aged satellite cells can lead to increased oxidative stress. The satellite cell dysfunction results in decreased regenerative capacity of the muscle. As a consequence of increased oxidative stress, a decrease in autophagy can lead to senescence.

but not in type I fibers [84]. This decline in satellite cell content might be an important factor in the etiology of type II muscle fiber atrophy, which accompanies the loss of skeletal muscle with age [81, 84].

The function of satellite cells is altered by oxidative stress with aging. In the aged muscle, the satellite cells exhibit a reduced capacity to proliferate and self-renew. The decrease in the self-renewing muscle stem cell pool can lead to decreased regenerative capacity of the muscle. The quiescent satellite cells have a low metabolic rate and display only a few active mitochondria and therefore are exposed to low levels of oxidative stress [85]. Gene expression studies have also indicated differences in the transcriptional profile of aged versus young satellite cells, e.g., changes in genes associated with mitochondrial function [86]. The ROS production was higher in isolated satellite cells from the aged muscle [87]. Furthermore, a decline in antioxidant capacity in satellite cells was also observed with age, diminishing satellite cell function with increased ROS levels [88]. It was reported that the antioxidant activity of catalase and glutathione transferase is reduced in aged satellite cells [89]. Several redox-dependent signaling pathways are deregulated in aged satellite cells; decreased Notch [90], increased Wnt (wingless/integrated) [91], increased p38/MAPK (mitogen-activated protein kinase) [77], and JAK-STAT3 (Janus kinase-signal transducer of activation) [92] signaling were observed.

Mitochondrial dysfunction can result from decreased NAD^+ (nicotinamide adenine dinucleotide) levels of the cells. Stem cells are thought to rely predominantly on glycolysis to yield energy, decreasing NAD^+ concentration [93]. The reduction of the cellular NAD^+ level and its effect on mitochondrial activity was shown to be a pivotal switch to modulate satellite cell senescence [78]. Treatment with the NAD^+ precursor, nicotinamide riboside, induced the mitochondrial unfolded protein response and synthesis of prohibitin proteins, rejuvenated the muscle stem cells in aged mice, and enhanced life span [78].

The activities of the ubiquitin-proteasome system, autophagy, and chaperones appear to decline with age [94]. During myogenesis and regeneration, an increase in protein synthesis and removal of misfolded proteins can be observed [73]. Oxidative stress can influence muscle satellite cells by altering their protein homeostasis. Basal autophagy is essential to maintain the stem cell quiescent state [95]. Autophagy was shown to be essential to maintain the stemness of satellite cells by preventing the senescence caused by mitochondrial dysfunction and oxidative stress associated with aging [95].

5. Age-Related Muscle Loss and Oxidative Stress

Sarcopenia, the age-associated generalized and progressive reduction in muscle mass, increases the susceptibility to muscle injury, serious falls, obesity, and diabetes [96], predicting frailty, disability, poor quality of life, and mortality in the elderly [97–101]. The prevalence of low muscle mass is estimated between 8 and 40% depending on the population studied and the methods used to identify sarcopenia; it ranges from 15% at 65 years to 50% at 80 years [100, 101]. Progressive muscle loss starts at approximately the age of 40 years; it is estimated at about 8% per decade until the age of 70 years and then it increases to 15% per decade [102]. Reduction in muscle mass is usually combined with an increase in body fat mass; the accumulation of fat can be observed within the muscle fibers. The high levels of ROS in the aging muscle can induce the transition of satellite cells into an adipogenic phenotype. This muscle-to-fat transition can explain the increased intramuscular adipose tissue associated with sarcopenia [103, 104].

Age-related muscle atrophy was shown to be associated with a decrease in the total number of muscle fibers and a simultaneous decrease in the size of the individual fibers. It was reported that age-related muscle loss in rodents [105] and humans [82] can occur due to the loss of muscle fibers

and a decrease in the cross-sectional area of the remaining fibers. Several factors were reported to contribute to muscle atrophy with aging. The role of reduced protein synthesis, declines in neural function, hormonal deficits, chronic low-grade inflammation, loss of mitochondrial function, nuclear apoptosis, reduced function of satellite cells, and oxidative stress was reported [96, 106].

A relationship was observed between oxidative stress and muscle mass [107–110]. The disruption of signaling pathways involving skeletal muscle reactive oxygen species has received increasing attention [6]. Age-associated accumulation of nitrotyrosine in muscle proteins was reported [108]. The accumulation of mitochondrial and nuclear DNA damage leads to the loss of skeletal muscle fibers [111]. Mitochondria-mediated apoptosis represents a central process driving age-related muscle loss [112]. Mitochondrial dysfunction is related not only to the loss of its capacity to generate ATP but also to the activation of apoptotic pathways leading to the irreversible cell loss that is characteristic of sarcopenia [112].

Further studies have shown that ROS accumulation can increase proteolysis leading to loss of muscle mass; increased ROS production activates the ubiquitin-proteasome pathway. Aging is associated with greater proteasome content and activity [113], increased expression of the ubiquitin ligase MuRF1 (Muscle RING-finger protein-1) and atrogin-1 [114], and increased calpain activity [115]; however, further studies are required to explore the role of oxidative stress in these age-related alterations. The potential role of age-dependent mitochondrial dysfunction and cumulative oxidative stress as the underlying cause of age-associated fiber atrophy remains controversial; the pharmacological attenuation of age-related mitochondrial redox changes failed to rescue the age-associated muscle fiber atrophy, implying that the muscle mitochondrial redox environment is not a key regulator of fiber atrophy during sarcopenia [3].

Recently it was reported that sedentary humans display an age-related decline in the mitochondrial protein optic atrophy 1 (OPA1) that is associated with muscle loss [116]. FoxOs (Forkhead box proteins) are master regulators of autophagy and the ubiquitin-proteasome system [117] and are activated by oxidative stress and Akt inhibition. Importantly, the acute inhibition of OPA1 results in an increased oxidative stress, and *in vivo* inhibition of FoxOs was sufficient to reduce muscle atrophy in $Opa1^{-/-}$ mice [117].

6. Antioxidant Therapies and Effects of Exercise on the Aged Muscle

The effects of exercise on aging in the skeletal muscle are very controversial. There is widespread agreement that oxidation could increase during exercise. Early studies have suggested that ROS play important roles in the inflammatory response to high-intensity or long-lasting exercise [118]. On the other hand, it has also long been known that moderate exercise increases the antioxidant capacity of the skeletal muscle by mitochondrial remodeling [119]. A more recent study suggested that endurance training stimulates mitochondrial remodeling which leads to an increase in mitochondrial content and function [120]. Unfortunately recent rodent models suggest that exercise-induced mitochondrial remodeling is defective in the aged muscle [121]. In contrast, as mentioned above, moderate exercise can improve the number of CRU-mitochondria pairs and thus provide more ATP and Ca^{2+} for contraction [68]. Furthermore, resistance-type exercise training represents an effective strategy to increase satellite cell content and reverse type II muscle fiber atrophy in humans [81].

Another target of exercise against oxidative stress is the increased activity of enzymatic antioxidants (i.e., glutathione peroxidase, catalase, and superoxide dismutase) accompanying the exercise-induced ROS generation. For example, skeletal muscle-specific manganese superoxide dismutase-deficient mice, which showed reduced exercise activity without atrophy, presented significantly improved exercise activity of the skeletal muscle after a single administration of an antioxidant [122].

Numerous investigations have aimed to explore the effects of antioxidant treatment on skeletal muscle performance. Some of them also studied old muscles and found positive effects of such a treatment. For example, hydroxytyrosol, which has high free-radical-scavenging capabilities, caused increased *in vivo* force in aged rats [123]. Recent studies showed positive effects of resveratrol [124], some plant extracts (*Rhus coriaria* [125] and *Rosmarinus officinalis* [126]), and vitamins (vitamin C [127]). The increasing number of similar studies nowadays shows the importance and topicality of finding good antioxidant treatment for the aged muscle.

As discussed above, several studies report an elevation in levels of oxidized protein and DNA in the older skeletal muscle. To date, RyR is the only key protein in EC coupling for which lifelong voluntary training was investigated and found to improve its expression level in aged mice (unpublished data of the authors). The data showed a beneficial antioxidant effect of selenium supplementation on skeletal muscle performance in old animals. However, as the authors could not prove the direct effects of antioxidant treatment on ROS production, there are several key proteins in EC coupling which could be positively altered and, thus, enhance force production.

The effect of antioxidant compounds on aged satellite cells has already been reported. Tocotrienol is a vitamin E analogue bearing high antioxidant activity. The tocotrienol-rich fraction (TRF) replenished the regenerative capacity of the human senescent satellite cells [128]; furthermore, TRF is able to ameliorate antioxidant defence mechanisms and improve replicative senescence-associated oxidative stress in human satellite cells [129]. The vitamin E analogue trolox treatment prevented the appearance of senescence markers, restored the expansion, and rescued the proliferative and regenerative defect of geriatric satellite cells [72]. The effect of resveratrol was studied in the mouse myoblast cell and showed protection against ROS by improving Sirt1 (Sirtuin1) levels, increasing antioxidant production, and reducing apoptotic signaling and cell death [130]. Interestingly, the effect of exercise on the oxidative stress of satellite cells has not yet been investigated in the literature. The protective effects

of exercise, resveratrol, and their combination was shown to increase muscle mass in rats, probably associated with antiapoptotic signaling pathways through activation of AMPK (AMP-activated protein kinase)/Sirt1 [131]. In contrast, administration of the long-term mitochondria-targeted antioxidant, mitoquinone mesylate, failed to attenuate age-related oxidative damage or rescue the loss of muscle mass and function in the skeletal muscle of old mice [132].

7. Concluding Remarks

Lifelong maintenance of muscle mass and strength is a global health challenge. With an aging population, the problem of sarcopenia is becoming more and more important, and effective strategies are required to improve muscle performance. An average 30-year-old will lose about 25% of his or her muscle strength by age 70 and 50% of it by age 80. The improvement of mobility and independence is key for old people, and it relieves society from healthcare and social support costs. Our knowledge about the signaling pathways mediating age-related muscle loss is still limited. Oxidative stress and subsequent alterations in signaling pathways could lead to different pathophysiological events at different stages of life, especially in old age. As was shown in this review, a lot of targets in skeletal muscle could be altered by increased oxidative stress with aging. Some of them are targets of intrinsic factors, but there are some which depend mainly on extrinsic actions. The effects of oxidative stress in muscles are so diverse that improving only one step is usually not enough to get better muscle performance. This means that only combined therapy could be effective, and continuous training will also allow muscle fibers to incorporate higher levels of exogenous antioxidants from dietary supplements.

In conclusion, the risks of oxidative stress-induced damage can be minimized with regular exercise, which has beneficial effects on physical and mental health. We have to emphasize that while it is never too late to begin exercise, an early start and regular practice throughout life would greatly improve outcomes in later years and slow down a body's aging process. A lot of people try to start a training program late in life, when muscle performance is already diminished. It follows that muscle research has to promote the development of a new generation of physically active, healthy elderly citizens. To achieve this, and to minimize oxidative stress, the key could be a carefully developed exercise protocol combined with adequate antioxidant supplementation. However, exercise can be restricted due to orthopedic or cardiopulmonary limitations, which highlights the importance of the exploration of antioxidant therapy or nontraditional exercise. Regular exercise to maintain muscle function also has beneficial effects by reducing oxidative stress, not only in the muscle, but in all tissue, a fact that intrinsically would reduce/delay aging.

Conflicts of Interest

The authors declare that there is no conflict of interest regarding the publication of this paper.

Acknowledgments

This work was supported by a grant from the Hungarian National Research, Development and Innovation Office (NKFIH NK-115461), the GINOP-2.3.2-15-2016-00040 project, the EFOP-3.6.2-16-2017-00006, and the UNKP-17-4 New National Excellence Program of the Ministry of Human Capacities (Hungary). The project is cofinanced by the European Union and the European Regional Development Fund.

References

[1] R. Suzman, J. R. Beard, T. Boerma, and S. Chatterji, "Health in an ageing world–what do we know?," *Lancet*, vol. 385, no. 9967, pp. 484–486, 2015.

[2] J. L. Shadrach and A. J. Wagers, "Stem cells for skeletal muscle repair," *Philosophical Transactions of the Royal Society of London. Series B, Biological Sciences*, vol. 366, no. 1575, pp. 2297–2306, 2011.

[3] G. K. Sakellariou, T. Pearson, A. P. Lightfoot et al., "Mitochondrial ROS regulate oxidative damage and mitophagy but not age-related muscle fiber atrophy," *Scientific Reports*, vol. 6, no. 1, p. 33944, 2016.

[4] D. Harman, "Aging: a theory based on free radical and radiation chemistry," *Journal of Gerontology*, vol. 11, no. 3, pp. 298–300, 1956.

[5] A. D. Romano, G. Serviddio, A. de Matthaeis, F. Bellanti, and G. Vendemiale, "Oxidative stress and aging," *Journal of Nephrology*, vol. 23, Supplement 15, pp. S29–S36, 2010.

[6] J. Viña, C. Borras, K. M. Abdelaziz, R. Garcia-Valles, and M. C. Gomez-Cabrera, "The free radical theory of aging revisited: the cell signaling disruption theory of aging," *Antioxidants & Redox Signaling*, vol. 19, no. 8, pp. 779–787, 2013.

[7] F. L. Muller, M. S. Lustgarten, Y. Jang, A. Richardson, and H. van Remmen, "Trends in oxidative aging theories," *Free Radical Biology & Medicine*, vol. 43, no. 4, pp. 477–503, 2007.

[8] A. B. Salmon, A. Richardson, and V. I. Perez, "Update on the oxidative stress theory of aging: does oxidative stress play a role in aging or healthy aging?," *Free Radical Biology & Medicine*, vol. 48, no. 5, pp. 642–655, 2010.

[9] E. Le Moal, V. Pialoux, G. Juban et al., "Redox control of skeletal muscle regeneration," *Antioxidants & Redox Signaling*, vol. 27, no. 5, pp. 276–310, 2017.

[10] S. K. Powers and M. J. Jackson, "Exercise-induced oxidative stress: cellular mechanisms and impact on muscle force production," *Physiological Reviews*, vol. 88, no. 4, pp. 1243–1276, 2008.

[11] F. Derbre, B. Ferrando, M. C. Gomez-Cabrera et al., "Inhibition of xanthine oxidase by allopurinol prevents skeletal muscle atrophy: role of p 38 MAPKinase and E3 ubiquitin ligases," *PLoS One*, vol. 7, no. 10, article e46668, 2012.

[12] D. Nethery, D. Stofan, L. Callahan, A. DiMarco, and G. Supinski, "Formation of reactive oxygen species by the contracting diaphragm is PLA(2) dependent," *Journal of Applied Physiology*, vol. 87, no. 2, pp. 792–800, 1999.

[13] M. C. Gong, S. Arbogast, Z. Guo, J. Mathenia, W. Su, and M. B. Reid, "Calcium-independent phospholipase A2 modulates cytosolic oxidant activity and contractile function in murine skeletal muscle cells," *Journal of Applied Physiology*, vol. 100, no. 2, pp. 399–405, 2006.

[14] J. Miquel, A. C. Economos, J. Fleming, and J. E. Johnson Jr., "Mitochondrial role in cell aging," *Experimental Gerontology*, vol. 15, no. 6, pp. 575–591, 1980.

[15] E. Bua, J. Johnson, A. Herbst et al., "Mitochondrial DNA-deletion mutations accumulate intracellularly to detrimental levels in aged human skeletal muscle fibers," *American Journal of Human Genetics*, vol. 79, no. 3, pp. 469–480, 2006.

[16] H. N. Carter, C. C. Chen, and D. A. Hood, "Mitochondria, muscle health, and exercise with advancing age," *Physiology*, vol. 30, no. 3, pp. 208–223, 2015.

[17] X. Xu, C. N. (. J.). Chen, E. A. Arriaga, and L. D. V. Thompson, "Asymmetric superoxide release inside and outside the mitochondria in skeletal muscle under conditions of aging and disuse," *Journal of Applied Physiology*, vol. 109, no. 4, pp. 1133–1139, 2010.

[18] C. M. Lee, L. E. Aspnes, S. S. Chung, R. Weindruch, and J. M. Aiken, "Influences of caloric restriction on age-associated skeletal muscle fiber characteristics and mitochondrial changes in rats and mice[a]," *Annals of the New York Academy of Sciences*, vol. 854, 1 TOWARDS PROLO, pp. 182–191, 1998.

[19] J. Wanagat, Z. Cao, P. Pathare, and J. M. Aiken, "Mitochondrial DNA deletion mutations colocalize with segmental electron transport system abnormalities, muscle fiber atrophy, fiber splitting, and oxidative damage in sarcopenia," *The FASEB Journal*, vol. 15, no. 2, pp. 322–332, 2001.

[20] R. Calvani, A. M. Joseph, P. J. Adhihetty et al., "Mitochondrial pathways in sarcopenia of aging and disuse muscle atrophy," *Biological Chemistry*, vol. 394, no. 3, pp. 393–414, 2013.

[21] M. A. Smith and M. B. Reid, "Redox modulation of contractile function in respiratory and limb skeletal muscle," *Respiratory Physiology & Neurobiology*, vol. 151, no. 2-3, pp. 229–241, 2006.

[22] J. Farup, F. de Paoli, K. Bjerg, S. Riis, S. Ringgard, and K. Vissing, "Blood flow restricted and traditional resistance training performed to fatigue produce equal muscle hypertrophy," *Scandinavian Journal of Medicine & Science in Sports*, vol. 25, no. 6, pp. 754–763, 2015.

[23] J. M. Lawler, Z. Hu, and W. S. Barnes, "Effect of reactive oxygen species on K^+ contractures in the rat diaphragm," *Journal of Applied Physiology*, vol. 84, no. 3, pp. 948–953, 1998.

[24] M. A. Baraibar, M. Gueugneau, S. Duguez, G. Butler-Browne, D. Bechet, and B. Friguet, "Expression and modification proteomics during skeletal muscle ageing," *Biogerontology*, vol. 14, no. 3, pp. 339–352, 2013.

[25] T. Wenz, F. Diaz, B. M. Spiegelman, and C. T. Moraes, "Activation of the PPAR/PGC-1alpha pathway prevents a bioenergetic deficit and effectively improves a mitochondrial myopathy phenotype," *Cell Metabolism*, vol. 8, no. 3, pp. 249–256, 2008.

[26] V. Ljubicic, P. Miura, M. Burt et al., "Chronic AMPK activation evokes the slow, oxidative myogenic program and triggers beneficial adaptations in *mdx* mouse skeletal muscle," *Human Molecular Genetics*, vol. 20, no. 17, pp. 3478–3493, 2011.

[27] G. Meissner and X. Lu, "Dihydropyridine receptor-ryanodine receptor interactions in skeletal muscle excitation-contraction coupling," *Bioscience Reports*, vol. 15, no. 5, pp. 399–408, 1995.

[28] F. Wuytack, L. Raeymaekers, H. Smedt et al., "$Ca2^+$-transport ATPases and their regulation in muscle and brain," *Annals of the New York Academy of Sciences*, vol. 671, 1 Ion-Motive AT, pp. 82–91, 1992.

[29] C. Franzini-Armstrong and A. O. Jorgensen, "Structure and development of E-C coupling units in skeletal muscle," *Annual Review of Physiology*, vol. 56, no. 1, pp. 509–534, 1994.

[30] S. H. Yuan, W. Arnold, and A. O. Jorgensen, "Biogenesis of transverse tubules and triads: immunolocalization of the 1,4-dihydropyridine receptor, TS28, and the ryanodine receptor in rabbit skeletal muscle developing in situ," *The Journal of Cell Biology*, vol. 112, no. 2, pp. 289–301, 1991.

[31] R. Coronado, J. Morrissette, M. Sukhareva, and D. M. Vaughan, "Structure and function of ryanodine receptors," *American Journal of Physiology-Cell Physiology*, vol. 266, no. 6, pp. C1485–C1504, 1994.

[32] T. Furuichi, D. Furutama, Y. Hakamata, J. Nakai, H. Takeshima, and K. Mikoshiba, "Multiple types of ryanodine receptor/$Ca2^+$ release channels are differentially expressed in rabbit brain," *The Journal of Neuroscience*, vol. 14, no. 8, pp. 4794–4805, 1994.

[33] F. Mori, M. Fukaya, H. Abe, K. Wakabayashi, and M. Watanabe, "Developmental changes in expression of the three ryanodine receptor mRNAs in the mouse brain," *Neuroscience Letters*, vol. 285, no. 1, pp. 57–60, 2000.

[34] M. Fill and J. A. Copello, "Ryanodine receptor calcium release channels," *Physiological Reviews*, vol. 82, no. 4, pp. 893–922, 2002.

[35] J. J. Abramson and G. Salama, "Critical sulfhydryls regulate calcium release from sarcoplasmic reticulum," *Journal of Bioenergetics and Biomembranes*, vol. 21, no. 2, pp. 283–294, 1989.

[36] J. H. Shin, G. H. Yoo, C. J. Lee, and C. K. Suh, "Fast and slow gating types of SR ryanodine receptor/channel purified from canine latissimus dorsi muscle," *Yonsei Medical Journal*, vol. 37, no. 1, pp. 72–80, 1996.

[37] I. N. Pessah, C. Beltzner, S. W. Burchiel, G. Sridhar, T. Penning, and W. Feng, "A bioactive metabolite of benzo[a]-pyrene, benzo[a]pyrene-7,8-dione, selectively alters microsomal Ca2+ transport and ryanodine receptor function," *Molecular Pharmacology*, vol. 59, no. 3, pp. 506–513, 2001.

[38] C. Hwang, A. Sinskey, and H. Lodish, "Oxidized redox state of glutathione in the endoplasmic reticulum," *Science*, vol. 257, no. 5076, pp. 1496–1502, 1992.

[39] G. Bánhegyi, L. Lusini, F. Puskás et al., "Preferential transport of glutathione *versus* glutathione disulfide in rat liver microsomal vesicles," *Journal of Biological Chemistry*, vol. 274, no. 18, pp. 12213–12216, 1999.

[40] M. Csala, R. Fulceri, J. Mandl, A. Benedetti, and G. Bánhegyi, "Ryanodine receptor channel-dependent glutathione transport in the sarcoplasmic reticulum of skeletal muscle," *Biochemical and Biophysical Research Communications*, vol. 287, no. 3, pp. 696–700, 2001.

[41] W. Feng, G. Liu, P. D. Allen, and I. N. Pessah, "Transmembrane redox sensor of ryanodine receptor complex," *The Journal of Biological Chemistry*, vol. 275, no. 46, pp. 35902–35907, 2000.

[42] I. N. Pessah, K. H. Kim, and W. Feng, "Redox sensing properties of the ryanodine receptor complex," *Frontiers in Bioscience*, vol. 7, no. 1, pp. a72–a79, 2002.

[43] D. C. Andersson, M. J. Betzenhauser, S. Reiken et al., "Ryanodine receptor oxidation causes intracellular calcium leak and muscle weakness in aging," *Cell Metabolism*, vol. 14, no. 2, pp. 196–207, 2011.

[44] C. R. Lamboley, V. L. Wyckelsma, M. J. McKenna, R. M. Murphy, and G. D. Lamb, "Ca(2+) leakage out of the sarcoplasmic reticulum is increased in type I skeletal muscle fibres in aged humans," *The Journal of Physiology*, vol. 594, no. 2, pp. 469–481, 2016.

[45] K. H. Park, N. Weisleder, J. Zhou et al., "Assessment of calcium sparks in intact skeletal muscle fibers," *Journal of Visualized Experiments*, no. 84, article e50898, 2014.

[46] J. J. Mackrill, S. O'Driscoll, F. A. Lai, and T. V. McCarthy, "Analysis of type 1 ryanodine receptor-12 kDa FK506-binding protein interaction," *Biochemical and Biophysical Research Communications*, vol. 285, no. 1, pp. 52–57, 2001.

[47] J. Z. Zhang, Y. Wu, B. Y. Williams et al., "Oxidation of the skeletal muscle Ca^{2+} release channel alters calmodulin binding," *American Journal of Physiology-Cell Physiology*, vol. 276, no. 1, pp. C46–C53, 1999.

[48] C. Hidalgo, G. Sánchez, G. Barrientos, and P. Aracena-Parks, "A transverse tubule NADPH oxidase activity stimulates calcium release from isolated triads via ryanodine receptor type 1 *S* -glutathionylation," *Journal of Biological Chemistry*, vol. 281, no. 36, pp. 26473–26482, 2006.

[49] A. Michelucci, S. Boncompagni, M. Canato, C. Reggiani, and F. Protasi, "Estrogens protect calsequestrin-1 knockout mice from lethal hyperthermic episodes by reducing oxidative stress in muscle," *Oxidative Medicine and Cellular Longevity*, vol. 2017, Article ID 6936897, 15 pages, 2017.

[50] C. Franzini-Armstrong and F. Protasi, "Ryanodine receptors of striated muscles: a complex channel capable of multiple interactions," *Physiological Reviews*, vol. 77, no. 3, pp. 699–729, 1997.

[51] G. P. Ahern, P. R. Junankar, and A. F. Dulhunty, "Subconductance states in single-channel activity of skeletal muscle ryanodine receptors after removal of FKBP12," *Biophysical Journal*, vol. 72, no. 1, pp. 146–162, 1997.

[52] Y. Mei, L. Xu, H. F. Kramer, G. H. Tomberlin, C. Townsend, and G. Meissner, "Stabilization of the skeletal muscle ryanodine receptor ion channel-FKBP12 complex by the 1,4-benzothiazepine derivative S107," *PLoS One*, vol. 8, no. 1, article e54208, 2013.

[53] O. Delbono, K. S. O'Rourke, and W. H. Ettinger, "Excitation-calcium release uncoupling in aged single human skeletal muscle fibers," *The Journal of Membrane Biology*, vol. 148, no. 3, pp. 211–222, 1995.

[54] J. M. Lawler and S. K. Powers, "Oxidative stress, antioxidant status, and the contracting diaphragm," *Canadian Journal of Applied Physiology*, vol. 23, no. 1, pp. 23–55, 1998.

[55] J. M. Lawler, J. H. Kim, H. B. Kwak, and W. S. Barnes, "Redox modulation of diaphragm contractility: interaction between DHPR and RyR channels," *Free Radical Biology & Medicine*, vol. 49, no. 12, pp. 1969–1977, 2010.

[56] M. Renganathan, M. L. Messi, and O. Delbono, "Dihydropyridine receptor-ryanodine receptor uncoupling in aged skeletal muscle," *The Journal of Membrane Biology*, vol. 157, no. 3, pp. 247–253, 1997.

[57] T. Zhang, A. S. Pereyra, Z. M. Wang et al., "Calpain inhibition rescues troponin T3 fragmentation, increases Cav1.1, and enhances skeletal muscle force in aging sedentary mice," *Aging Cell*, vol. 15, no. 3, pp. 488–498, 2016.

[58] B. M. Klebl, A. T. Ayoub, and D. Pette, "Protein oxidation, tyrosine nitration, and inactivation of sarcoplasmic reticulum Ca2+-ATPase in low-frequency stimulated rabbit muscle," *FEBS Letters*, vol. 422, no. 3, pp. 381–384, 1998.

[59] R. I. Viner, T. D. Williams, and C. Schoneich, "Peroxynitrite modification of protein thiols: oxidation, nitrosylation, and S-glutathiolation of functionally important cysteine residue (s) in the sarcoplasmic reticulum Ca-ATPase," *Biochemistry*, vol. 38, no. 38, pp. 12408–12415, 1999.

[60] E. S. Dremina, V. S. Sharov, M. J. Davies, and C. Schöneich, "Oxidation and inactivation of SERCA by selective reaction of cysteine residues with amino acid peroxides," *Chemical Research in Toxicology*, vol. 20, no. 10, pp. 1462–1469, 2007.

[61] A. R. Tupling, C. Vigna, R. J. Ford et al., "Effects of buthionine sulfoximine treatment on diaphragm contractility and SR Ca2+ pump function in rats," *Journal of Applied Physiology*, vol. 103, no. 6, pp. 1921–1928, 2007.

[62] M. Gueugneau, C. Coudy-Gandilhon, O. Gourbeyre et al., "Proteomics of muscle chronological ageing in post-menopausal women," *BMC Genomics*, vol. 15, no. 1, p. 1165, 2014.

[63] S. Mosole, S. Zampieri, S. Furlan et al., "Effects of electrical stimulation on skeletal muscle of old sedentary people," *Gerontology and Geriatric Medicine*, vol. 4, p. 233372141876899, 2018.

[64] S. Boncompagni, F. Protasi, and C. Franzini-Armstrong, "Sequential stages in the age-dependent gradual formation and accumulation of tubular aggregates in fast twitch muscle fibers: SERCA and calsequestrin involvement," *Age*, vol. 34, no. 1, pp. 27–41, 2012.

[65] S. Boncompagni, L. d'Amelio, S. Fulle, G. Fano, and F. Protasi, "Progressive disorganization of the excitation-contraction coupling apparatus in aging human skeletal muscle as revealed by electron microscopy: a possible role in the decline of muscle performance," *The Journals of Gerontology Series A: Biological Sciences and Medical Sciences*, vol. 61, no. 10, pp. 995–1008, 2006.

[66] V. Eisner, G. Csordas, and G. Hajnoczky, "Interactions between sarco-endoplasmic reticulum and mitochondria in cardiac and skeletal muscle – pivotal roles in Ca^{2+} and reactive oxygen species signaling," *Journal of Cell Science*, vol. 126, no. 14, pp. 2965–2978, 2013.

[67] S. Boncompagni, A. E. Rossi, M. Micaroni et al., "Mitochondria are linked to calcium stores in striated muscle by developmentally regulated tethering structures," *Molecular Biology of the Cell*, vol. 20, no. 3, pp. 1058–1067, 2009.

[68] S. Zampieri, L. Pietrangelo, S. Loefler et al., "Lifelong physical exercise delays age-associated skeletal muscle decline," *The Journals of Gerontology Series A: Biological Sciences and Medical Sciences*, vol. 70, no. 2, pp. 163–173, 2015.

[69] L. Csernoch, J. Fodor, D. al-Gaadi et al., "Modified calcium homeostasis in aged mouse skeletal muscle," *Biophysical Journal*, vol. 112, no. 3, p. 99a, 2017.

[70] A. Mauro, "Satellite cell of skeletal muscle fibers," *The Journal of Biophysical and Biochemical Cytology*, vol. 9, no. 2, pp. 493–495, 1961.

[71] N. A. Dumont, C. F. Bentzinger, M. C. Sincennes, and M. A. Rudnicki, "Satellite cells and skeletal muscle regeneration," *Comprehensive Physiology*, vol. 5, no. 3, pp. 1027–1059, 2015.

[72] L. Garcia-Prat and P. Munoz-Canoves, "Aging, metabolism and stem cells: spotlight on muscle stem cells," *Molecular and Cellular Endocrinology*, vol. 445, pp. 109–117, 2017.

[73] Y. C. Jang, M. Sinha, M. Cerletti, C. Dall'Osso, and A. J. Wagers, "Skeletal muscle stem cells: effects of aging and metabolism on muscle regenerative function," *Cold Spring Harbor Symposia on Quantitative Biology*, vol. 76, pp. 101–111, 2012.

[74] L. Garcia-Prat, P. Sousa-Victor, and P. Munoz-Canoves, "Functional dysregulation of stem cells during aging: a focus on skeletal muscle stem cells," *The FEBS Journal*, vol. 280, no. 17, pp. 4051–4062, 2013.

[75] J. V. Chakkalakal and A. S. Brack, "Extrinsic regulation of satellite cell function and muscle regeneration capacity during aging," *Journal of Stem Cell Research & Therapy*, vol. 1, no. S11, p. 001, 2012.

[76] P. Sousa-Victor, S. Gutarra, L. García-Prat et al., "Geriatric muscle stem cells switch reversible quiescence into senescence," *Nature*, vol. 506, no. 7488, pp. 316–321, 2014.

[77] J. D. Bernet, J. D. Doles, J. K. Hall, K. Kelly Tanaka, T. A. Carter, and B. B. Olwin, "p38 MAPK signaling underlies a cell-autonomous loss of stem cell self-renewal in skeletal muscle of aged mice," *Nature Medicine*, vol. 20, no. 3, pp. 265–271, 2014.

[78] H. Zhang, D. Ryu, Y. Wu et al., "NAD^+ repletion improves mitochondrial and stem cell function and enhances life span in mice," *Science*, vol. 352, no. 6292, pp. 1436–1443, 2016.

[79] A. C. Keefe, J. A. Lawson, S. D. Flygare et al., "Muscle stem cells contribute to myofibres in sedentary adult mice," *Nature Communications*, vol. 6, no. 1, p. 7087, 2015.

[80] M. C. Gibson and E. Schultz, "The distribution of satellite cells and their relationship to specific fiber types in soleus and extensor digitorum longus muscles," *The Anatomical Record*, vol. 202, no. 3, pp. 329–337, 1982.

[81] L. B. Verdijk, T. Snijders, M. Drost, T. Delhaas, F. Kadi, and L. J. C. van Loon, "Satellite cells in human skeletal muscle; from birth to old age," *Age*, vol. 36, no. 2, pp. 545–557, 2014.

[82] J. Lexell, C. C. Taylor, and M. Sjostrom, "What is the cause of the ageing atrophy? Total number, size and proportion of different fiber types studied in whole vastus lateralis muscle from 15- to 83-year-old men," *Journal of the Neurological Sciences*, vol. 84, no. 2-3, pp. 275–294, 1988.

[83] G. Shefer, D. P. van de Mark, J. B. Richardson, and Z. Yablonka-Reuveni, "Satellite-cell pool size does matter: defining the myogenic potency of aging skeletal muscle," *Developmental Biology*, vol. 294, no. 1, pp. 50–66, 2006.

[84] L. B. Verdijk, R. Koopman, G. Schaart, K. Meijer, H. H. C. M. Savelberg, and L. J. C. van Loon, "Satellite cell content is specifically reduced in type II skeletal muscle fibers in the elderly," *American Journal of Physiology. Endocrinology and Metabolism*, vol. 292, no. 1, pp. E151–E157, 2007.

[85] A. H. Tang and T. A. Rando, "Induction of autophagy supports the bioenergetic demands of quiescent muscle stem cell activation," *The EMBO Journal*, vol. 33, no. 23, pp. 2782–2797, 2014.

[86] S. Bortoli, V. Renault, E. Eveno, C. Auffray, G. Butler-Browne, and G. Piétu, "Gene expression profiling of human satellite cells during muscular aging using cDNA arrays," *Gene*, vol. 321, pp. 145–154, 2003.

[87] A. D. Minet and M. Gaster, "Cultured senescent myoblasts derived from human vastus lateralis exhibit normal mitochondrial ATP synthesis capacities with correlating concomitant ROS production while whole cell ATP production is decreased," *Biogerontology*, vol. 13, no. 3, pp. 277–285, 2012.

[88] S. Beccafico, C. Puglielli, T. Pietrangelo, R. Bellomo, G. Fano, and S. Fulle, "Age-dependent effects on functional aspects in human satellite cells," *Annals of the New York Academy of Sciences*, vol. 1100, no. 1, pp. 345–352, 2007.

[89] S. Fulle, S. Didonna, C. Puglielli et al., "Age-dependent imbalance of the antioxidative system in human satellite cells," *Experimental Gerontology*, vol. 40, no. 3, pp. 189–197, 2005.

[90] I. M. Conboy, M. J. Conboy, G. M. Smythe, and T. A. Rando, "Notch-mediated restoration of regenerative potential to aged muscle," *Science*, vol. 302, no. 5650, pp. 1575–1577, 2003.

[91] A. S. Brack, M. J. Conboy, S. Roy et al., "Increased Wnt signaling during aging alters muscle stem cell fate and increases fibrosis," *Science*, vol. 317, no. 5839, pp. 807–810, 2007.

[92] M. T. Tierney, T. Aydogdu, D. Sala et al., "STAT3 signaling controls satellite cell expansion and skeletal muscle repair," *Nature Medicine*, vol. 20, no. 10, pp. 1182–1186, 2014.

[93] K. Ito and T. Suda, "Metabolic requirements for the maintenance of self-renewing stem cells," *Nature Reviews Molecular Cell Biology*, vol. 15, no. 4, pp. 243–256, 2014.

[94] M. Narita, "Quality and quantity control of proteins in senescence," *Aging*, vol. 2, no. 5, pp. 311–314, 2010.

[95] L. García-Prat, M. Martínez-Vicente, E. Perdiguero et al., "Autophagy maintains stemness by preventing senescence," *Nature*, vol. 529, no. 7584, pp. 37–42, 2016.

[96] S. E. Alway, M. J. Myers, and J. S. Mohamed, "Regulation of satellite cell function in sarcopenia," *Frontiers in Aging Neuroscience*, vol. 6, p. 246, 2014.

[97] I. Janssen, S. B. Heymsfield, and R. Ross, "Low relative skeletal muscle mass (sarcopenia) in older persons is associated with functional impairment and physical disability," *Journal of the American Geriatrics Society*, vol. 50, no. 5, pp. 889–896, 2002.

[98] S. Ali and J. M. Garcia, "Sarcopenia, cachexia and aging: diagnosis, mechanisms and therapeutic options - a mini-review," *Gerontology*, vol. 60, no. 4, pp. 294–305, 2014.

[99] R. R. Wolfe, "Optimal nutrition, exercise, and hormonal therapy promote muscle anabolism in the elderly," *Journal of the American College of Surgeons*, vol. 202, no. 1, pp. 176–180, 2006.

[100] M. J. Gomes, P. F. Martinez, L. U. Pagan et al., "Skeletal muscle aging: influence of oxidative stress and physical exercise," *Oncotarget*, vol. 8, no. 12, pp. 20428–20440, 2017.

[101] S. C. Y. Yu, K. S. F. Khow, A. D. Jadczak, and R. Visvanathan, "Clinical screening tools for sarcopenia and its management," *Current Gerontology and Geriatrics Research*, vol. 2016, Article ID 5978523, 10 pages, 2016.

[102] T. N. Kim and K. M. Choi, "Sarcopenia: definition, epidemiology, and pathophysiology," *Journal of Bone Metabolism*, vol. 20, no. 1, pp. 1–10, 2013.

[103] C. L. Rice, D. A. Cunningham, D. H. Paterson, and M. S. Lefcoe, "Arm and leg composition determined by computed tomography in young and elderly men," *Clinical Physiology*, vol. 9, no. 3, pp. 207–220, 1989.

[104] R. Vettor, G. Milan, C. Franzin et al., "The origin of intermuscular adipose tissue and Its pathophysiological implications," *American Journal of Physiology. Endocrinology and Metabolism*, vol. 297, no. 5, pp. E987–E998, 2009.

[105] C. K. Daw, J. W. Starnes, and T. P. White, "Muscle atrophy and hypoplasia with aging: impact of training and food restriction," *Journal of Applied Physiology*, vol. 64, no. 6, pp. 2428–2432, 1988.

[106] E. Marty, Y. Liu, A. Samuel, O. Or, and J. Lane, "A review of sarcopenia: enhancing awareness of an increasingly prevalent disease," *Bone*, vol. 105, pp. 276–286, 2017.

[107] P. M. Siu, E. E. Pistilli, and S. E. Alway, "Age-dependent increase in oxidative stress in gastrocnemius muscle with unloading," *Journal of Applied Physiology*, vol. 105, no. 6, pp. 1695–1705, 2008.

[108] H. Murakami, C. Guillet, N. Tardif et al., "Cumulative 3-nitrotyrosine in specific muscle proteins is associated with muscle loss during aging," *Experimental Gerontology*, vol. 47, no. 2, pp. 129–135, 2012.

[109] H. Tohma, A. F. el-Shafey, K. Croft, T. Shavlakadze, M. D. Grounds, and P. G. Arthur, "Protein thiol oxidation does not change in skeletal muscles of aging female mice," *Biogerontology*, vol. 15, no. 1, pp. 87–98, 2014.

[110] K. Baumann, "Cellular senescence: senescence and reprogramming go hand-in-hand," *Nature Reviews Molecular Cell Biology*, vol. 18, no. 1, p. 4, 2017.

[111] P. A. Figueiredo, M. P. Mota, H. J. Appell, and J. A. Duarte, "The role of mitochondria in aging of skeletal muscle," *Biogerontology*, vol. 9, no. 2, pp. 67–84, 2008.

[112] E. Marzetti, S. E. Wohlgemuth, H. A. Lees, H.-Y. Chung, S. Giovannini, and C. Leeuwenburgh, "Age-related activation of mitochondrial caspase-independent apoptotic signaling in rat gastrocnemius muscle," *Mechanisms of Ageing and Development*, vol. 129, no. 9, pp. 542–9, 2008.

[113] M. Altun, H. C. Besche, H. S. Overkleeft et al., "Muscle wasting in aged, sarcopenic rats is associated with enhanced activity of the ubiquitin proteasome pathway," *The Journal of Biological Chemistry*, vol. 285, no. 51, pp. 39597–39608, 2010.

[114] S. Clavel, A. S. Coldefy, E. Kurkdjian, J. Salles, I. Margaritis, and B. Derijard, "Atrophy-related ubiquitin ligases, atrogin-1 and MuRF1 are up-regulated in aged rat tibialis anterior muscle," *Mechanisms of Ageing and Development*, vol. 127, no. 10, pp. 794–801, 2006.

[115] E. Dargelos, C. Brulé, L. Combaret et al., "Involvement of the calcium-dependent proteolytic system in skeletal muscle aging," *Experimental Gerontology*, vol. 42, no. 11, pp. 1088–1098, 2007.

[116] C. Tezze, V. Romanello, M. A. Desbats et al., "Age-associated loss of OPA1 in muscle impacts muscle mass, metabolic homeostasis, systemic inflammation, and epithelial senescence," *Cell Metabolism*, vol. 25, no. 6, pp. 1374–1389.e6, 2017.

[117] G. Milan, V. Romanello, F. Pescatore et al., "Regulation of autophagy and the ubiquitin–proteasome system by the FoxO transcriptional network during muscle atrophy," *Nature Communications*, vol. 6, no. 1, article 6670, 2015.

[118] Y. Hellsten, U. Frandsen, N. Orthenblad, B. Sjødin, and E. A. Richter, "Xanthine oxidase in human skeletal muscle following eccentric exercise: a role in inflammation," *The Journal of Physiology*, vol. 498, no. 1, pp. 239–248, 1997.

[119] J. O. Holloszy and E. F. Coyle, "Adaptations of skeletal muscle to endurance exercise and their metabolic consequences," *Journal of Applied Physiology: Respiratory, Environmental and Exercise Physiology*, vol. 56, no. 4, pp. 831–838, 1984.

[120] D. A. Hood, "Mechanisms of exercise-induced mitochondrial biogenesis in skeletal muscle," *Applied Physiology, Nutrition, and Metabolism*, vol. 34, no. 3, pp. 465–472, 2009.

[121] V. Ljubicic, A. M. Joseph, P. J. Adhihetty et al., "Molecular basis for an attenuated mitochondrial adaptive plasticity in aged skeletal muscle," *Aging (Albany NY)*, vol. 1, no. 9, pp. 818–830, 2009.

[122] H. Kuwahara, T. Horie, S. Ishikawa et al., "Oxidative stress in skeletal muscle causes severe disturbance of exercise activity without muscle atrophy," *Free Radical Biology & Medicine*, vol. 48, no. 9, pp. 1252–1262, 2010.

[123] S. Pierno, D. Tricarico, A. Liantonio et al., "An olive oil-derived antioxidant mixture ameliorates the age-related decline of skeletal muscle function," *Age*, vol. 36, no. 1, pp. 73–88, 2014.

[124] M. H. Muhammad and M. M. Allam, "Resveratrol and/or exercise training counteract aging-associated decline of physical endurance in aged mice; targeting mitochondrial biogenesis and function," *The Journal of Physiological Sciences*, vol. 68, no. 5, pp. 681–688, 2018.

[125] F. Najjar, F. Rizk, G. Carnac et al., "Protective effect of *Rhus coriaria* fruit extracts against hydrogen peroxide-induced oxidative stress in muscle progenitors and zebrafish embryos," *PeerJ*, vol. 5, article e4144, 2017.

[126] K. M. Wills, R. M. Mitacek, G. G. Mafi et al., "Improving the lean muscle color of dark-cutting beef by aging, antioxidant-enhancement, and modified atmospheric packaging," *Journal of Animal Science*, vol. 95, no. 12, pp. 5378–5387, 2017.

[127] J. C. Richards, A. R. Crecelius, D. G. Larson, and F. A. Dinenno, "Acute ascorbic acid ingestion increases skeletal muscle blood flow and oxygen consumption via local vasodilation during graded handgrip exercise in older adults," *American Journal of Physiology. Heart and Circulatory Physiology*, vol. 309, no. 2, pp. H360–H368, 2015.

[128] J. J. Lim, W. Z. Wan Ngah, V. Mouly, and N. Abdul Karim, "Reversal of myoblast aging by tocotrienol rich fraction post-treatment," *Oxidative Medicine and Cellular Longevity*, vol. 2013, Article ID 978101, 11 pages, 2013.

[129] S. C. Khor, W. Z. Wan Ngah, Y. A. Mohd Yusof, N. Abdul Karim, and S. Makpol, "Tocotrienol-rich fraction ameliorates antioxidant defense mechanisms and improves replicative senescence-associated oxidative stress in human myoblasts," *Oxidative Medicine and Cellular Longevity*, vol. 2017, Article ID 3868305, 17 pages, 2017.

[130] S. Haramizu, S. Asano, D. C. Butler et al., "Dietary resveratrol confers apoptotic resistance to oxidative stress in myoblasts," *The Journal of Nutritional Biochemistry*, vol. 50, pp. 103–115, 2017.

[131] Z. Y. Liao, J. L. Chen, M. H. Xiao et al., "The effect of exercise, resveratrol or their combination on sarcopenia in aged rats via regulation of AMPK/Sirt 1 pathway," *Experimental Gerontology*, vol. 98, pp. 177–183, 2017.

[132] G. K. Sakellariou, T. Pearson, A. P. Lightfoot et al., "Long-term administration of the mitochondria-targeted antioxidant mitoquinone mesylate fails to attenuate age-related oxidative damage or rescue the loss of muscle mass and function associated with aging of skeletal muscle," *The FASEB Journal*, vol. 30, no. 11, pp. 3771–3785, 2016.

Hindawi
Oxidative Medicine and Cellular Longevity
Volume 2018, Article ID 8927104, 10 pages
https://doi.org/10.1155/2018/8927104

Research Article

Upregulation of Heme Oxygenase-1 by Hemin Alleviates Sepsis-Induced Muscle Wasting in Mice

Xiongwei Yu,[1,2] Wenjun Han,[1] Changli Wang,[1] Daming Sui,[1,3] Jinjun Bian,[1] Lulong Bo,[1] and Xiaoming Deng[1]

[1]*Faculty of Anesthesiology, Changhai Hospital, Naval Medical University, Shanghai 200433, China*
[2]*Department of Anesthesiology, 285th Hospital of the CPLA, Handan 056001, China*
[3]*Department of Anesthesiology, Chengdu Military General Hospital, Chengdu 610083, China*

Correspondence should be addressed to Lulong Bo; nbastars@126.com and Xiaoming Deng; deng_x@yahoo.com

Received 5 June 2018; Revised 13 September 2018; Accepted 4 October 2018; Published 8 November 2018

Guest Editor: Marco Sandri

Hemin, an inducer of heme oxygenase-1 (HO-1), can enhance the activation of HO-1. HO-1 exhibits a variety of activities, such as anti-inflammatory, antioxidative, and antiapoptotic functions. The objective of this study was to investigate the effects of hemin on sepsis-induced skeletal muscle wasting and to explore the mechanisms by which hemin exerts its effects. Cecal ligation and perforation (CLP) was performed to create a sepsis mouse model. Mice were randomly divided into four groups: control, CLP, CLP plus group, and CLP-hemin-ZnPP (a HO-1 inhibitor). The weight of the solei from the mice was measured, and histopathology was examined. Cytokines were measured by enzyme-linked immunosorbent assay (ELISA). Real-time quantitative reverse transcription polymerase chain reaction (qRT-PCR) and Western blotting were used to assess the expression levels of HO-1 and atrogin-1. Furthermore, we investigated the antioxidative effects of HO-1 by detecting malondialdehyde (MDA) levels and superoxide dismutase (SOD) activity. CLP led to dramatic skeletal muscle weakness and atrophy, but pretreatment with hemin protected mice against CLP-mediated muscle atrophy. Hemin also induced high HO-1 expression, which resulted in suppressed proinflammatory cytokine and reactive oxygen species (ROS) production. The expression of MuRF1 and atrogin-1, two ubiquitin ligases of the ubiquitin-proteasome system- (UPS-) mediated proteolysis, was also inhibited by increased HO-1 levels. Hemin-mediated increases in HO-1 expression exert protective effects on sepsis-induced skeletal muscle atrophy at least partly by inhibiting the expression of proinflammatory cytokines, UPS-mediated proteolysis, and ROS activation. Therefore, hemin might be a new treatment target against sepsis-induced skeletal muscle atrophy.

1. Introduction

Sepsis is defined as a life-threatening organ dysfunction due to a dysregulated host response to infection [1]. In the United States, nearly 10% of all deaths result from severe sepsis or its related complications every year [2]. Skeletal muscle atrophy and muscle weakness occurring from sepsis have become recognized as important issues in sepsis survivors [3]. A large number of critically ICU patients suffer from severe muscle wasting and impaired muscle function, which can delay respirator weaning and persist long after hospital discharge, thus reducing the patients' quality of life [4, 5].

Muscle atrophy results from an imbalance between muscle proteolysis and protein synthesis. When proteolysis overwhelms protein synthesis, muscle atrophy occurs [6, 7]. Protein degradation within muscle appears to rely on three pathways: ubiquitin-proteasome system- (UPS-) mediated proteolysis, autophagy, and calcium-dependent calpains [8]. However, the pathway that has received the most attention is the UPS-mediated proteolysis, which is believed to play a dominant role in skeletal muscle atrophy [9]. Two ubiquitin ligases, MuRF1 and atrogin-1, are key positive regulators of UPS-mediated proteolysis and are upregulated in all rodent models of skeletal muscle atrophy [10–12]. Additionally, these proteins have been widely used as markers of muscle wasting. Sepsis-induced cytokine secretion can also enhance microvascular permeability, allowing circulating toxins to impair axon activity [13]. The nutrition deficiency in muscle

caused by impaired axons may lead to muscle atrophy. As some myofibrillar proteins possess sulfhydryl groups that are sensitive to oxidation, sepsis-induced reactive oxygen species (ROS) appear to contribute to muscle wasting [14]. Thus, inhibiting proinflammatory cytokines and ROS should be an effective method to reverse muscle wasting.

Heme oxygenase-1 (HO-1), also called heat shock protein 32 (Hsp32), is an inducible enzyme that can convert heme into carbon monoxide, biliverdin, and free iron [15, 16]. Recent findings reported that HO-1 and its metabolites exerted anti-inflammatory, antioxidative, and antiapoptotic activities [17, 18]. As metabolites of HO-1, CO and biliverdin were shown to contribute to stimulating the host defense response against sepsis and modulating inflammatory mediators in mice [18]. Previous studies support the beneficial effects of HO-1 and its product in an experimental model of sepsis [19]. We hypothesized that the induction of HO-1 plays a pivotal role in sepsis-induced skeletal muscle wasting.

In our study, we used hemin as an inducer of HO-1 and examined whether hemin exerts a protective effect against septic muscle atrophy in mice. We also investigated the potential mechanism of its protective effect.

2. Materials and Methods

2.1. Sepsis Model. Cecal ligation and perforation (CLP) was performed on 8-week-old male C57BL/6 mice obtained from the Experimental Animal Center of the Naval Medical University. All animals were fed a standard laboratory diet and water and were acclimatized for at least l week before use. All experimental procedures involving animals were approved by the Animal Care and Use Committee of the Second Military Medical University. After we anesthetized the mice with 2%–3% sevoflurane, a midline laparotomy was performed, and the cecum was exposed. The contents of the intestines were extruded to the tip of the cecum, and then the cecum was ligated 1 cm from the tip with a 3-0 silk suture. We performed a double puncture of the cecum wall with a 22-gauge needle. The abdominal wall was closed with a continuous 3-0 silk suture in two layers. Sham-operated mice were subjected to exposure of the peritoneum and cecum but did not undergo ligation or puncture. No antibiotics were used. The mortality of the septic mice is 25% at day 1, while it elevated to 50% at day 7, indicating that the severity is moderate to severe.

2.2. Chemical Treatment and Experimental Groups. Hemin and zinc protoporphyrin-IX (ZnPP, a HO-1 inhibitor) (Sigma-Aldrich, St. Louis, MO) were dissolved in dimethyl sulfoxide (DMSO) and then diluted with phosphate-buffered saline (PBS) to a concentration of 10 mg/ml. Mice were randomly divided into four groups: control group (A), CLP group (B), CLP plus hemin group (C), and CLP-hemin-ZnPP group (D). Mice in groups A and B were intraperitoneally (i.p.) injected with 200 μl PBS containing 2% DMSO 1 day before surgery. Mice in group C were injected with the same volume of hemin solution (50 mg/kg, i.p.) 1 day before surgery, and mice in group D were injected with the same volume of a mixture of hemin (50 mg/kg, i.p.) and ZnPP (20 mg/kg, i.p.). We provided the same quantity of food and water to all four groups.

2.3. Measurements of Muscle Mass and Protein Breakdown Rates. The skin of the hind limbs was stripped for gross comparisons of muscle mass. The solei of the mice were collected and weighed at baseline and at 1, 3, 5, and 7 days after surgery. We interpreted the weight of soleus as an evaluation of muscle mass loss. Twenty-four hours after CLP or sham surgery, the solei of the mice were dissected and incubated for 2 hours in a shaking water bath at 37°C as previously described [20, 21]. Because tyrosine cannot be synthesized or degraded in muscle, protein breakdown rates were determined by testing the net release of free tyrosine into the incubation medium containing cycloheximide, a compound that prevents the reincorporation of tyrosine into protein.

2.4. Histopathology Examination. Tibialis anterior (TA) tissues were fixed with 10% buffered formalin at room temperature, embedded in paraffin, and sliced into 5 μm sections. The sections were then stained with hematoxylin-eosin (H&E) for morphological evaluation under a light microscope (Leica, DM-IL-LED). We observed the transverse sections taken at the midpoints of the legs. The muscle fiber size was recorded by measuring the cross-sectional area (CSA) of the skeletal muscle fiber.

2.5. Real-Time Quantitative Reverse Transcription Polymerase Chain Reaction (qRT-PCR). Six mice from each group were randomly killed 1, 4, and 7 days after CLP, after which the TA muscles were harvested. Total RNA was extracted from the TA tissue using TRIzol reagent (Invitrogen) according to the manufacturer's instructions. cDNA was synthesized using a PrimeScript™ 1st strand cDNA synthesis kit (TaKaRa). Quantitative PCR was performed using a SYBR green PCR kit (Invitrogen, Carlsbad, CA). The PCR conditions were as follows: initial heating at 95°C for 30 s, 40 cycles of denaturation at 95°C for 5 s and annealing at 60°C for 30 s, one extension at 95°C for 15 s, and a final tal0extension at 60°C for 30 s. The following primers were used: 5′-TGTGGGTGTATCGGATGGAG-3′ and 5′-GGCAGAGTCTTCCACAGT-3′ for atrogin-1, 5′-TTTGACACCCTCTACGCCAT-3′ and 5′-TTGGCACTTGAGAGAGAGGAAGGT-3′ for MuRF1, and 5′-TTCAGAAGGGTCAGGTCC-3′ and 5′-CAGTGAGGCCCATACCAGAA-3′ for HO-1.

The generation of PCR products was identified by melting-curve analysis. Relative mRNA levels of atrogin-1, MuRF1, and HO-1 were normalized to those of GAPDH.

2.6. HO-1 Activity Assay. The activity of HO-1 was identified via bilirubin generation according to the method described by Gong et al. [18]. Briefly, frozen TA samples were homogenized in lysis buffer. A sample fraction was harvested and washed by multiple centrifugations. The pellet was solubilized in 0.1 M K_2HPO_3 by sonication and stored at −80°C until extraction with chloroform. The extracted bilirubin

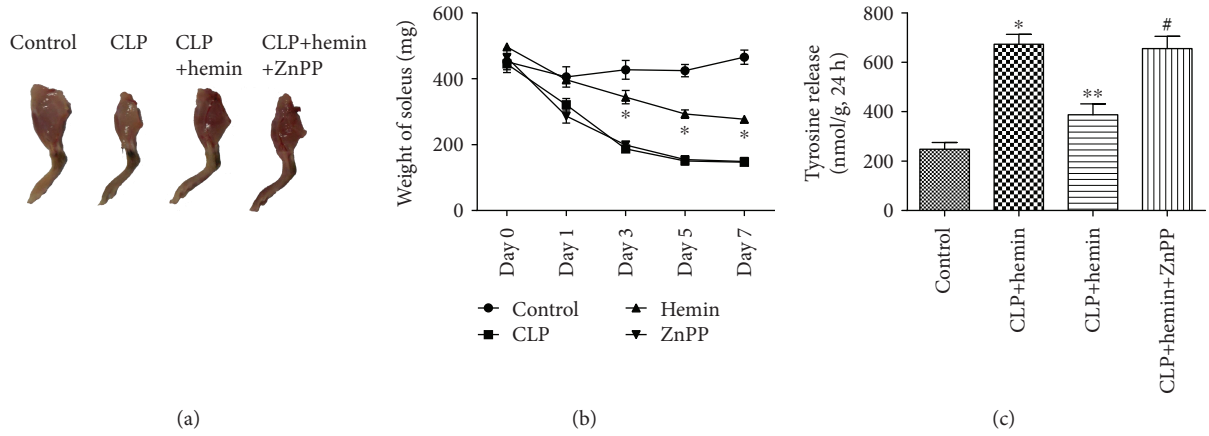

Figure 1: Hemin ameliorated muscle mass loss and mitigated the protein breakdown rates. (a) Gross comparisons of muscle mass (8-week-old mice, 3 days after CLP surgery). (b) The weight of the solei from mice in the hemin group was improved, especially on days 3, 5, and 7 after surgery. $^{*}p < 0.001$ (hemin vs. CLP), $n = 6$. (c) Protein breakdown rates as measured by the tyrosine concentration. $^{*}p < 0.001$ (control vs. CLP), $^{**}p < 0.001$ (hemin vs. CLP), $^{\#}p < 0.001$ (ZnPP vs. hemin), $n = 6$.

was measured by the difference in absorbance at 464 nm and 530 nm.

2.7. Cytokine Analysis. Blood was collected via cardiac puncture with heparin-treated syringe needles and centrifuged at 1000g for 10 min to harvest the serum. Sera were assayed for mouse TNF-α and IL-6 with a murine enzyme-linked immunosorbent assay (ELISA) kit (eBioscience, San Diego, CA) as described by the manufacturer.

2.8. Western Blotting Analysis. Briefly, the TA tissues were homogenized, and the proteins were resolved on polyacrylamide SDS gels and electrophoretically transferred to polyvinylidene difluoride membranes. The membranes were blocked with 5% (w/v) fat-free milk in Tris-buffered saline containing 0.05% Tween-20, incubated with Abs (Abcam) against mouse HO-1, atrogin-1, or MuRF1 at 4°C overnight, and finally incubated with secondary Abs. After the immunoreactive protein bands were visualized, the protein levels were normalized to the band density of β-actin (Abcam), which served as an internal control. The corresponding semiquantitative analysis was performed by measuring the optical density using the ImageJ software, and β-actin was used as an internal control.

2.9. Assay of TA Lipid Peroxidation and Antioxidant Enzyme Activities. Malondialdehyde (MDA), the end product of lipid peroxidation, is a marker of tissue peroxidation. We evaluated the degree of tissue peroxidation by measuring the MDA levels. Superoxide dismutase (SOD) activity was measured to analyze the activity of antioxidant enzymes. At 24 hours after CLP, we harvested the TA muscle and measured the MDA levels and SOD activity according the methods described by Andrianjafiniony et al. [22].

2.10. Statistical Analysis. The study results are presented as the mean ± standard deviation (SD). Differences between group means were calculated by one-way analysis of variance (ANOVA) or Student's t-test. All data were analyzed using Prism 5.0 (GraphPad Software, USA). $p < 0.05$ was considered statistically significant.

3. Results

3.1. Administration of Hemin Ameliorated the Loss of Muscle Mass. As shown in Figure 1(a), the size of the hind limbs was significantly atrophic after CLP surgery. However, administration of hemin partly reduced this effect, but treatment with ZnPP, an inhibitor of HO-1, reversed the effects of hemin. The weight of the solei among the groups was not significantly different at baseline. As the time after surgery increased, only slight soleus weight loss was observed in the control group. However, there was a significant deterioration in the weight of the solei from septic mice. Administration of hemin ameliorated this loss in muscle mass, while ZnPP abrogated this protective effect (Figure 1(b)). These results suggested that hemin exerts a protective effect against the loss of muscle mass. Protein breakdown rates in septic mice increased by nearly 2-fold. There was no significant difference in the protein breakdown rates between the control and hemin groups, and the protein breakdown rates in the ZnPP group were similar to those in the CLP group (Figure 1(c)).

3.2. Hemin Pretreatment Improved Sepsis-Induced Pathological Injury of TA Tissues of Mice. The TA tissues from the CLP group revealed smaller myofibers and CSA; however, the muscle fibers from the hemin group were in better condition than those from the CLP group (Figure 2(a)). We used the CSA of the muscle fibers to assess the degree of muscle atrophy. The CSA of the fibers from the CLP group was significantly smaller than that of the fibers from the control group. The administration of hemin positively affected the myofiber size, whereas mice in the ZnPP group showed a similar myofiber size to mice in the CLP group (Figure 2(b)).

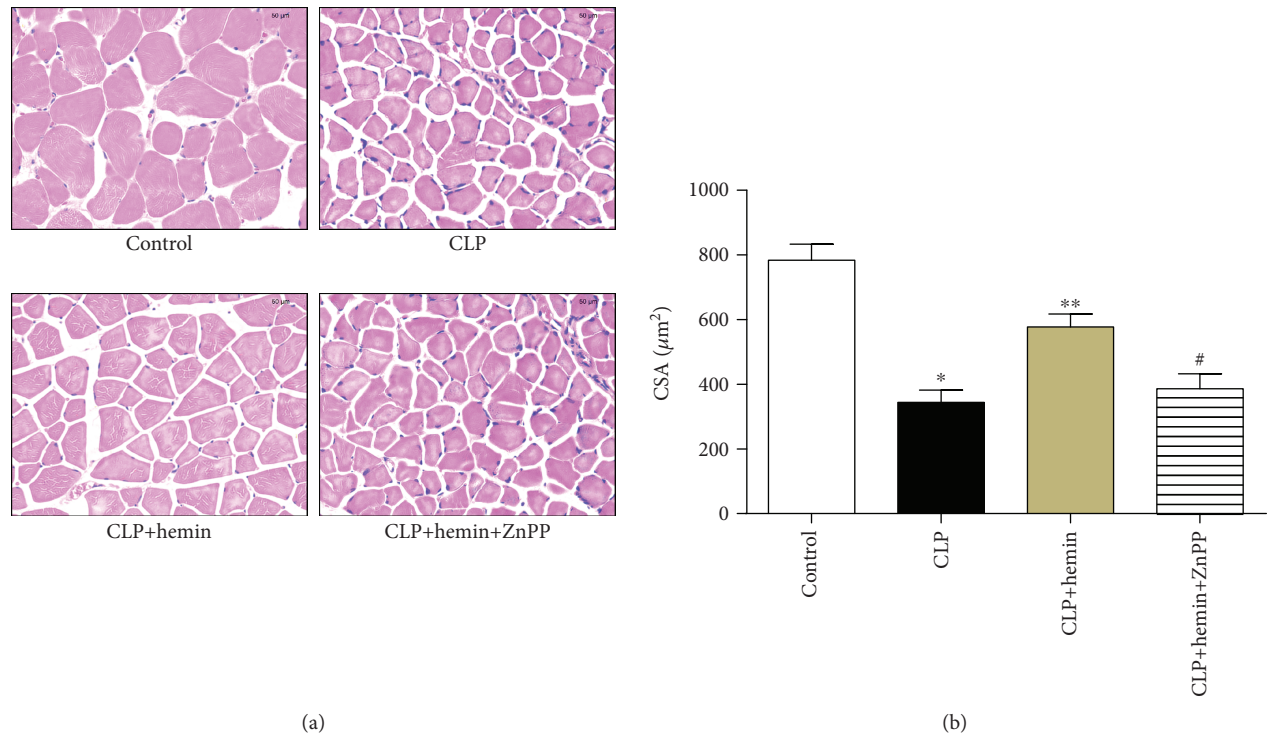

Figure 2: Histopathology examination of TA muscles at day 5 after surgery. (a) Skeletal muscle fibers from the CLP group exhibited a smaller cross-sectional area (CSA) than those from the control and hemin groups (H&E staining, 40x magnification, scale bar = 50 μm). (b) Quantification of the CSA of TA muscles from the different groups. $^{*}p < 0.001$ (CLP vs. the control group), $^{**}p < 0.01$ (hemin vs. the CLP group), $^{\#}p < 0.05$ (ZnPP vs. the hemin group), $n = 6$.

3.3. Hemin Upregulated the Expression and Activity of HO-1 in TA. The qRT-PCR results showed that HO-1 levels and activity were higher in the CLP group than in the sham group ($p < 0.05$), indicating that sepsis could induce HO-1 activation and its activity. We also found that hemin administration significantly increased the HO-1 levels and its activation and that the change in HO-1 expression in the hemin group was higher than that in the control and CLP groups (Figure 3(a)). ZnPP, an inhibitor of HO-1, suppressed HO-1 activation but did not affect hemin-induced upregulation of HO-1 expression (Figure 3(b)). We also found that the protein expression of HO-1 was slightly elevated in the CLP group compared with that in the control group. Pretreatment with hemin significantly enhanced HO-1 protein expression, but ZnPP administration did not affect the increased expression of HO-1 (Figures 3(c) and 3(d)).

3.4. Hemin Contributed to the Reduction in Proinflammatory Cytokine Levels. Because changes in proinflammatory cytokine levels play an important role in sepsis and may be involved in muscle atrophy, we examined the production of cytokines. The plasma levels of the proinflammatory cytokines TNF-α and IL-6 were significantly upregulated in mice that underwent the CLP procedure compared with those in mice from the sham group (Figure 4). High HO-1 expression induced by hemin could suppress these increases, and the serum levels of TNF-α and IL-6 did not show a significant difference between the CLP and ZnPP groups.

3.5. Hemin Enhanced the Antioxidant Defense Response. Compared with the control group, the CLP group showed a statistically significant increase in the plasma levels of MDA. MDA levels were lower in the hemin-pretreated mice than in mice in the CLP group. MDA levels in mice in the ZnPP group were slightly higher than those in mice in the CLP group, but there was no statistically significant difference (Figure 5(a)). Muscle SOD activity in mice in the hemin group was obviously higher than that in mice in the CLP group, and the protective function of hemin was abrogated by ZnPP (Figure 5(b)).

3.6. Hemin Inhibited the Expression of Muscle Atrophy Markers. Atrogin-1 and MuRF1 function as muscle-specific ubiquitin E3 ligases that tag proteins destined for ubiquitin-proteasomal proteolysis; thus, they are two of the most important genes upregulated in the process of muscle atrophy. Figures 6(a) and 6(b) show that the mRNA expression levels of atrogin-1 and MuRF1 were significantly upregulated in the TA tissues from CLP mice, especially at 1 day and 4 days after surgery. The enhanced expression of HO-1 induced by hemin reduced the expression of atrogin-1 and MuRF1 in the hemin group compared with that in the CLP group. The expression of the two ubiquitin E3 ligases was higher in the ZnPP group than in the HO-1 group. As shown in Figures 6(c) and 6(d), the protein expression of atrogin-1 and MuRF1 was elevated in the CLP group compared to the observed levels in the control group. Pretreatment with

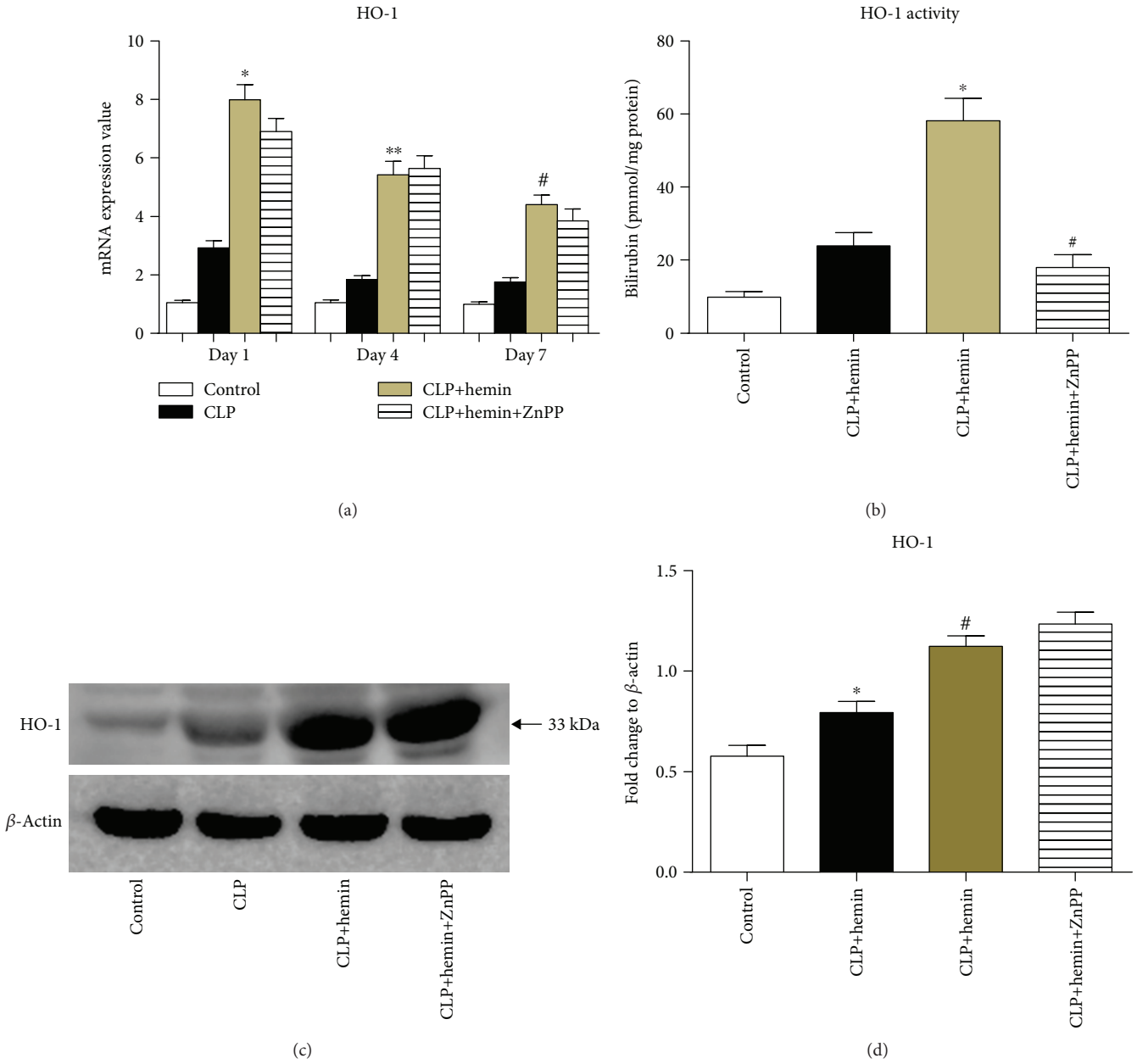

Figure 3: Hemin induces high HO-1 expression and increased HO-1 activation. (a) Hemin pretreatment can promote HO-1 mRNA expression at 1, 4, and 7 days after surgery ($^{*}p < 0.001$ vs. CLP at 1 day, $^{**}p < 0.001$ vs. CLP at 4 days, $^{\#}p < 0.05$ vs. CLP at 7 days). (b) Hemin enhanced the enzyme activity of HO-1, but ZnPP treatment reversed this effect ($^{*}p < 0.01$ vs. CLP, $^{\#}p < 0.01$ vs. CLP + hemin; $n = 6$). (c) Western blot analysis of levels of the HO-1 protein. (d) Results of the corresponding semiquantitative analysis of levels of the HO-1 protein based on the optical density measured using the ImageJ software; the data are presented as means ± SEM and are representative of three separate experiments ($^{*}p < 0.01$ vs. control, $^{\#}p < 0.01$ vs. CLP).

hemin dampened the protein expression of these two E3 ligases. However, in the ZnPP group, the protein expression of atrogin-1 and MuRF1 was upregulated.

4. Discussion

In our study, we used the CLP mouse model of sepsis to investigate the protective role of hemin in skeletal muscle wasting. Mice in the CLP group showed reduced muscle force and severe pathological atrophy of myosin fibers. Hemin succeeded in promoting the expression of HO-1 in CLP mice. Compared with mice in the CLP group, hemin-pretreated mice showed an apparent improvement in skeletal muscle force and ameliorated muscle atrophy.

Many factors, such as aging, weightlessness, immobilization, corticosteroids, hyperglycemia, and sepsis, may cause loss of muscle mass and muscle atrophy [23]. Previous studies have shown that early initiation of physical rehabilitation and minimization of deep sedation may prevent disuse atrophy and muscle weakness [24]. Muscle atrophy in critically ill

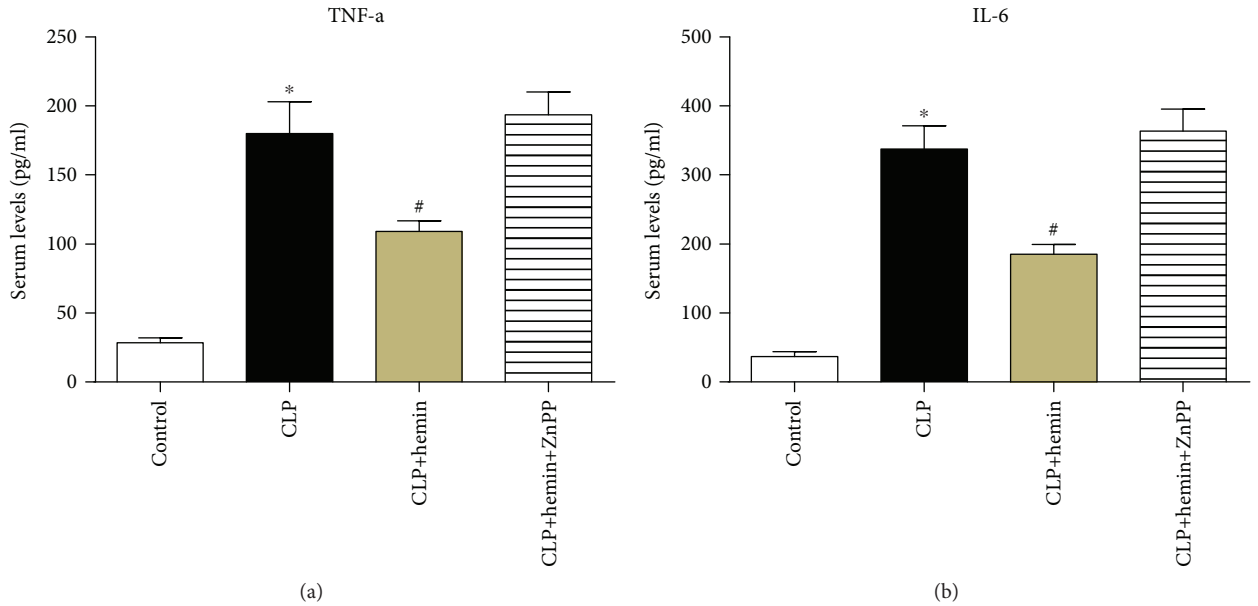

Figure 4: Sepsis induced high serum levels of TNF-α and IL-6. Hemin pretreatment reduced the levels of TNF-α and IL-6. (a) $^{*}p < 0.0001$ vs. control, $^{\#}p < 0.05$ vs. CLP; $n = 6$. (b) $^{*}p < 0.0001$ vs. control, $^{\#}p < 0.01$ vs. CLP; $n = 6$ (1 day after surgery).

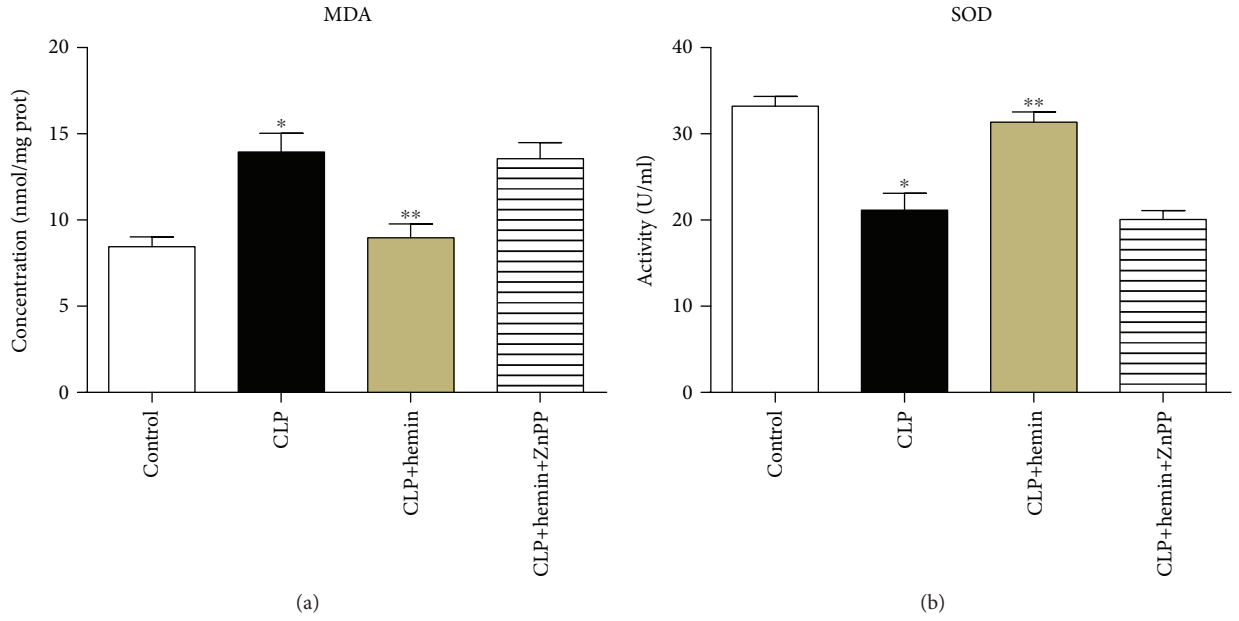

Figure 5: Oxidative stress response in TA muscle at 24 hours after CLP. (a) MDA concentration. $^{*}p < 0.05$ vs. the control group; $^{**}p < 0.05$ vs. the CLP group; $n = 6$. (b) SOD activity measurement. $^{*}p < 0.01$ vs. the control group; $^{**}p < 0.01$ vs. the CLP group; $n = 6$.

patients could also be attenuated by intensive insulin therapy [25], suggesting that glycemia control is an effective way to protect against muscle proteolysis.

The mechanisms of muscle breakdown are complicated. The ubiquitin-proteasome system plays a primary role in sepsis-induced muscle atrophy, which suggests that ubiquitin ligases may be involved in the development of muscle atrophy during sepsis [26]. There is persistent loss of myosin heavy chain (MyHC) in the skeletal muscle of severe critically ill patients that manifests shortly after ICU admission [27]. MyHC and many other myofibrillar proteins (such as myosin-binding proteins) were regarded as MuRF1 substrates [28]. The atrogin-1 substrates recognized thus far include MyoD, which is thought to control myoblast identity and differentiation [29]. As a result, atrogin-1 and MuRF1, the two muscle-specific ubiquitin ligases, have become potential therapeutic targets [30]. Sepsis, systemic inflammatory response syndrome, and multiple organ failure seem to play a crucial role in leading to muscle atrophy [31]. Proinflammatory cytokines such as TNF-α and IL-6 influence the blood-nerve barrier and promote endothelial cell leukocyte activation, which damages the axon [32]; this impaired nerve

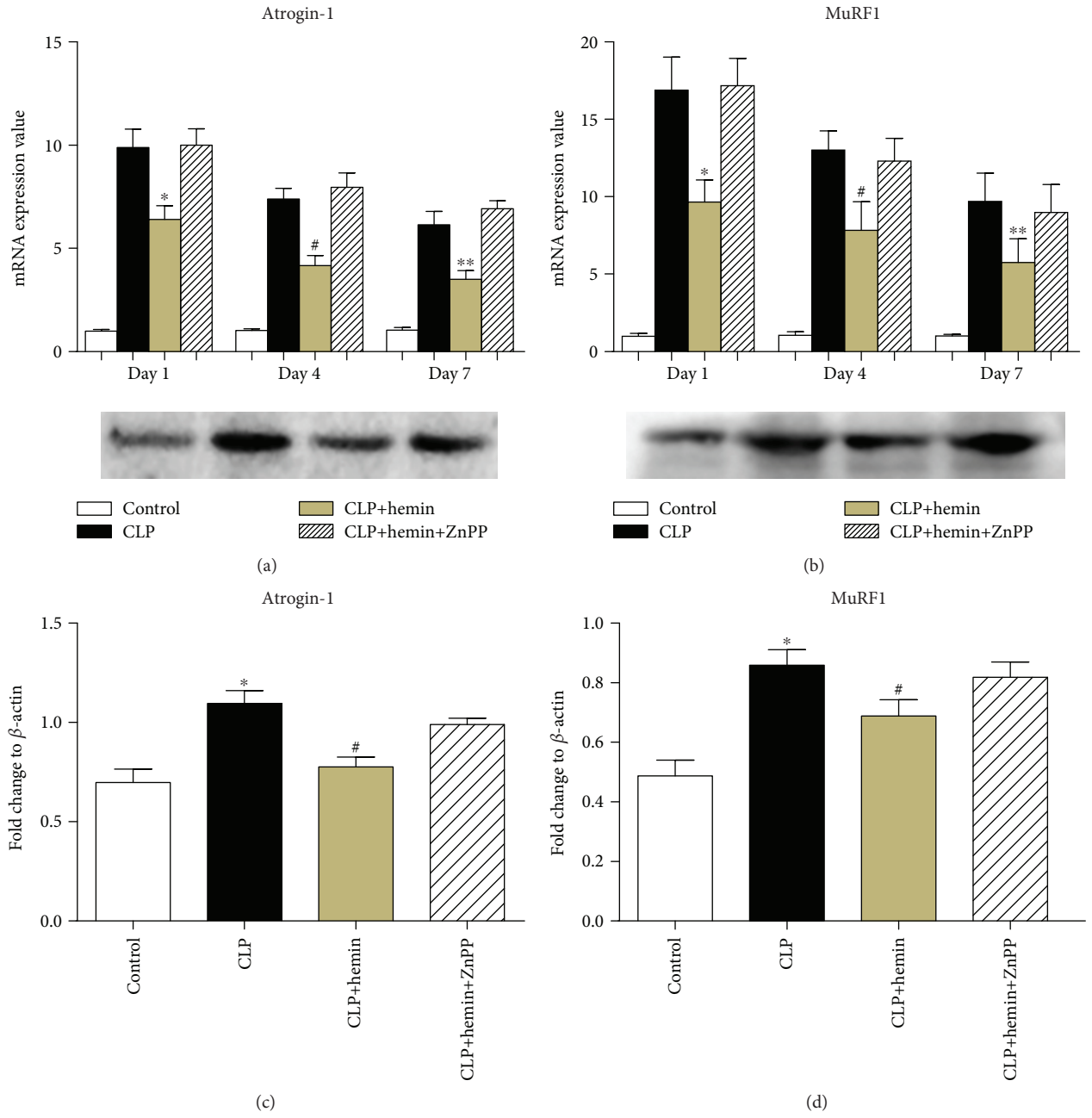

Figure 6: The levels of CLP-induced muscle atrophy markers were elevated, and HO-1 suppressed the mRNA and protein expression of atrogin-1 and MuRF1. (a) HO-1 inhibited the mRNA expression of atrogin-1 at 1, 4, and 7 days after surgery ($^{*}p < 0.01$ vs. CLP at 1 day, $^{\#}p < 0.05$ vs. CLP at 4 days, $^{**}p < 0.01$ vs. CLP; $n = 6$). (b) HO-1 suppressed the mRNA expression of MuRF1 during sepsis at 1, 4, and 7 days after surgery ($^{*}p < 0.01$ vs. CLP at 1 day, $^{\#}p < 0.01$ vs. CLP at 4 days, $^{**}p < 0.01$ vs. CLP at 7 days; $n = 6$). (c, d) Western blot analysis of levels of the atrogin-1 and MuRF1 proteins. Results of the corresponding semiquantitative analysis of levels of the HO-1 protein based on the optical density measured using the ImageJ software; the data are presented as means ± SEM and are representative of three separate experiments ($^{*}p < 0.01$ vs. control, $^{\#}p < 0.01$ vs. CLP). The protein expression of atrogin-1 and MuRF1 was upregulated in the CLP group. Hemin suppressed the protein expression of these two ligases; however, ZnPP administration abrogated the protective effects of hemin (1 day after surgery).

function may contribute to muscle atrophy. TNF-α, IL-6, and other proinflammatory cytokines can also initiate network cascades that activate the FoxO family, the members of which stimulate the expression of MuRF1 and atrogin-1 [30, 33].

HO-1, the rate-limiting enzyme in heme degradation, was reported to confer cytoprotection against oxidative stress and inflammation in several animal models [34]. The major function of HO-1 is to catabolize the oxidative degradation of heme into biliverdin, CO, and free iron. Biliverdin is an effective antioxidant that eliminates peroxyl radicals, and CO exhibits strongly antiapoptotic and anti-inflammatory activities [35]. Previous in vivo and in vitro studies have

demonstrated that HO-1 reduces the production of proinflammatory cytokines, including TNF-α and IL-6, and inhibits the activation of NF-κB and MAPK signaling during sepsis [36]. HO-1 may prevent liver fibrosis and alleviate lung pathological injury by suppressing NF-κB signaling pathways [37, 38]. Many factors, such as hyperoxia, hypoxia, endotoxins, and nitric oxide, can promote elevated HO-1 expression [39]. In our study, we found that during the early stage of sepsis (24 hours after CLP surgery), there was an obvious increase in HO-1 levels in the CLP group. Hemin, a substrate of HO-1, can enhance the activation of HO-1. In our experiments, we used hemin as an inducer of HO-1 and found that hemin can stimulate HO-1 activation. To identify whether the protective function rooted in HO-1 was mediated by hemin or by other subjects, we included a CLP mouse group treated with ZnPP, an inhibitor of HO-1 that can suppress the enzyme activity of HO-1. We found that mice in the ZnPP group showed no improvements in muscle condition; thus, the protective effects were due to HO-1 but not hemin or other related constituents. Interestingly, we found that ZnPP does not influence the expression of HO-1 but can inhibit its activity, indicating that the protective function of HO-1 may depend on its metabolites.

In our experiments, we found that high levels of HO-1 suppress the gene expression of atrogin-1 and MuRF1, suggesting that HO-1 inhibits muscle fiber atrophy partly by downregulating ubiquitin ligase activation. The CLP model mice showed high levels of TNF-α and IL-6 expression in the skeletal muscle. HO-1 suppressed the levels of these proinflammatory cytokines, indicating that HO-1 may inhibit muscle atrophy partly via its protective role against CIP. Oxidative stress is an important contributor to the etiology of skeletal muscle dysfunction. Appropriate levels of oxidants are required for normal cell adaptation and function, and high levels of ROS negatively affect the structure and function of macromolecules such as proteins, DNA, and lipids [40]. High levels of ROS may also activate proteolytic systems, thus causing enhanced protein breakdown in skeletal muscles, which results in enhanced MuRF1 levels leading to muscle atrophy [41]. Our study shows that HO-1-treated mice exhibited a high level of SOD activity and relatively low MDA levels, indicating that HO-1 exerted a protective role in muscle atrophy partly via its antioxidative function.

Regarding the experimental group design, we considered that after surgery, mice in the CLP group and control group may have different appetites, and food intake can also cause differences in muscle mass. To address this, we offered the same quantity of food to all the groups (the exact food quantity was designated based on the results of our preliminary experiments). There are still some questions our experiments did not elucidate. First, we only explored the protective mechanism of HO-1 in the proteolysis process of muscle atrophy, but we did not investigate whether HO-1 can promote muscle protein synthesis. Second, a recent finding showed that hemin exhibited cytotoxicity in colon-derived epithelial cells in a dose- and time-dependent manner. Hemin can downregulate the expression of the 18 kDa translocator protein, which contributes to cell proliferation [42]. Therefore, we must explore other functions of hemin aside from its protective role against muscle atrophy. There are also some limitations in our experiments. First, the experiments were done in both slow-twitch and fast-twitch muscles. It is then difficult to address whether the effect of hemin is specific or not. Second, although the CLP-induced muscle weakness is evident, we did not perform objective measurement to illustrate the issue.

5. Conclusion

In conclusion, our findings showed that hemin may promote the elevated expression of HO-1, which exerts a protective function against sepsis-induced skeletal muscle wasting. HO-1 can reduce muscle proteolysis partly by inhibiting the expression of proinflammatory cytokines and muscle-specific ubiquitin ligases. HO-1 can also exert a protective role by suppressing ROS activation in the skeletal muscle. Therefore, hemin might be a new treatment target against sepsis-induced skeletal muscle atrophy.

Data Availability

The data including muscle mass loss, soleus weight of mice, protein breakdown rates, H&E stating of TA muscles, expression of HO-1, HO-1 activity, Western blot, expression of TNF-alpha and IL-6, MDA, SOD, and expression of atrogin-1 and MuRF1 used to support the findings of this study are included within the article.

Conflicts of Interest

The authors declare that they have no competing interests.

Authors' Contributions

Xiongwei Yu, Wenjun Han, and Changli Wang contributed equally to the article. Xiongwei Yu and Wenjun Han performed the research and analyzed the data. Lulong Bo and Xiaoming Deng designed the research, ensured correct analysis of the data, and wrote the manuscript. Changli Wang, Daming Sui, and Jinjun Bian assisted in the design of the research, oversaw the collection of the data, and contributed to the writing of the manuscript. All authors critically revised the manuscript and gave final approval of the manuscript.

Acknowledgments

This work was supported by the National Natural Science Foundation of China (nos. 81471845, 81671887, and 81671939), the Shanghai Outstanding Youth Medical Professionals Training Program (no. 2017YQ015), and the Key Developing Discipline Program of Shanghai (no. 2015ZB0102).

References

[1] C. W. Seymour, V. X. Liu, T. J. Iwashyna et al., "Assessment of clinical criteria for sepsis: for the third international consensus definitions for sepsis and septic shock (sepsis-3)," *The Journal*

of the American Medical Association, vol. 315, no. 8, pp. 762–774, 2016.

[2] R. Namas, R. Zamora, R. Namas et al., "Sepsis: something old, something new, and a systems view," *Journal of Critical Care*, vol. 27, no. 3, pp. 314.e1–314.e11, 2012.

[3] J. B. Poulsen, "Impaired physical function, loss of muscle mass and assessment of biomechanical properties in critical ill patients," *Danish Medical Journal*, vol. 59, no. 11, article B4544, 2012.

[4] M. Wilcox and M. Herridge, "Long-term outcomes in patients surviving acute respiratory distress syndrome," *Seminars in Respiratory and Critical Care Medicine*, vol. 31, no. 1, pp. 55–65, 2010.

[5] T. Takei, "Intensive care unit-acquired weakness: development of polyneuropathy and myopathy in critically ill patients," *Brain and Nerve*, vol. 66, no. 2, pp. 161–170, 2014.

[6] P. Bonaldo and M. Sandri, "Cellular and molecular mechanisms of muscle atrophy," *Disease Models & Mechanisms*, vol. 6, no. 1, pp. 25–39, 2012.

[7] J. Batt, C. C. dos Santos, J. I. Cameron, and M. S. Herridge, "Intensive care unit-acquired weakness: clinical phenotypes and molecular mechanisms," *American Journal of Respiratory and Critical Care Medicine*, vol. 187, no. 3, pp. 238–246, 2013.

[8] C. C. Dos Santos and J. Batt, "ICU-acquired weakness: mechanisms of disability," *Current Opinion in Critical Care*, vol. 18, no. 5, pp. 509–517, 2012.

[9] D. Attaix, S. Ventadour, A. Codran, D. Béchet, D. Taillandier, and L. Combaret, "The ubiquitin-proteasome system and skeletal muscle wasting," *Essays in Biochemistry*, vol. 41, pp. 173–186, 2005.

[10] M. Sandri, "Signaling in muscle atrophy and hypertrophy," *Physiology*, vol. 23, no. 3, pp. 160–170, 2008.

[11] S. C. Bodine, E. Latres, S. Baumhueter et al., "Identification of ubiquitin ligases required for skeletal muscle atrophy," *Science*, vol. 294, no. 5547, pp. 1704–1708, 2001.

[12] M. Llano-Diez, A. M. Gustafson, C. Olsson, H. Goransson, and L. Larsson, "Muscle wasting and the temporal gene expression pattern in a novel rat intensive care unit model," *BMC Genomics*, vol. 12, no. 1, p. 602, 2011.

[13] C. F. Bolton, "Neuromuscular manifestations of critical illness," *Muscle & Nerve*, vol. 32, no. 2, pp. 140–163, 2005.

[14] C. Coirault, A. Guellich, T. Barbry, J. L. Samuel, B. Riou, and Y. Lecarpentier, "Oxidative stress of myosin contributes to skeletal muscle dysfunction in rats with chronic heart failure," *American Journal of Physiology. Heart and Circulatory Physiology*, vol. 292, no. 2, pp. H1009–H1017, 2007.

[15] K. Ohta, T. Kikuchi, S. Arai, N. Yoshida, A. Sato, and N. Yoshimura, "Protective role of heme oxygenase-1 against endotoxin-induced uveitis in rats," *Experimental Eye Research*, vol. 77, no. 6, pp. 665–673, 2003.

[16] M. D. Maines, "The heme oxygenase system: past, present, and future," *Antioxidants & Redox Signaling*, vol. 6, no. 5, pp. 797–801, 2004.

[17] D. Morse, L. Lin, A. M. K. Choi, and S. W. Ryter, "Heme oxygenase-1, a critical arbitrator of cell death pathways in lung injury and disease," *Free Radical Biology & Medicine*, vol. 47, no. 1, pp. 1–12, 2009.

[18] X. Gong, L. Zhang, R. Jiang, M. Ye, X. Yin, and J. Wan, "Anti-inflammatory effects of mangiferin on sepsis-induced lung injury in mice via up-regulation of heme oxygenase-1," *The Journal of Nutritional Biochemistry*, vol. 24, no. 6, pp. 1173–1181, 2013.

[19] X. Qian, T. Numata, K. Zhang et al., "Transient receptor potential melastatin 2 protects mice against polymicrobial sepsis by enhancing bacterial clearance," *Anesthesiology*, vol. 121, no. 2, pp. 336–351, 2014.

[20] Q. Chen, N. Li, W. Zhu et al., "Insulin alleviates degradation of skeletal muscle protein by inhibiting the ubiquitin-proteasome system in septic rats," *Journal of Inflammation*, vol. 8, no. 1, p. 13, 2011.

[21] K. Duan, W. Yu, Z. Lin et al., "Insulin ameliorating endotoxaemia-induced muscle wasting is associated with the alteration of hypothalamic neuropeptides and inflammation in rats," *Clinical Endocrinology*, vol. 82, no. 5, pp. 695–703, 2015.

[22] T. Andrianjafiniony, S. Dupré-Aucouturier, D. Letexier, H. Couchoux, and D. Desplanches, "Oxidative stress, apoptosis, and proteolysis in skeletal muscle repair after unloading," *American Journal of Physiology. Cell Physiology*, vol. 299, no. 2, pp. C307–C315, 2010.

[23] P. O. Hasselgren, "β-Hydroxy-β-methylbutyrate (HMB) and prevention of muscle wasting," *Metabolism*, vol. 63, no. 1, pp. 5–8, 2014.

[24] P. A. Mendez-Tellez and D. M. Needham, "Early physical rehabilitation in the ICU and ventilator liberation," *Respiratory Care*, vol. 57, no. 10, pp. 1663–1669, 2012.

[25] G. Biolo, M. de Cicco, S. Lorenzon et al., "Treating hyperglycemia improves skeletal muscle protein metabolism in cancer patients after major surgery," *Critical Care Medicine*, vol. 36, no. 6, pp. 1768–1775, 2008.

[26] C. J. Wray, J. M. V. Mammen, D. D. Hershko, and P. O. Hasselgren, "Sepsis upregulates the gene expression of multiple ubiquitin ligases in skeletal muscle," *The International Journal of Biochemistry & Cell Biology*, vol. 35, no. 5, pp. 698–705, 2003.

[27] T. Wollersheim, J. Woehlecke, M. Krebs et al., "Dynamics of myosin degradation in intensive care unit-acquired weakness during severe critical illness," *Intensive Care Medicine*, vol. 40, no. 4, pp. 528–538, 2014.

[28] S. Cohen, J. J. Brault, S. P. Gygi et al., "During muscle atrophy, thick, but not thin, filament components are degraded by MuRF1-dependent ubiquitylation," *The Journal of Cell Biology*, vol. 185, no. 6, pp. 1083–1095, 2009.

[29] L. A. Tintignac, J. Lagirand, S. Batonnet, V. Sirri, M. P. Leibovitch, and S. A. Leibovitch, "Degradation of MyoD mediated by the SCF (MAFbx) ubiquitin ligase," *The Journal of Biological Chemistry*, vol. 280, no. 4, pp. 2847–2856, 2005.

[30] Z. Puthucheary, S. Harridge, and N. Hart, "Skeletal muscle dysfunction in critical care: wasting, weakness, and rehabilitation strategies," *Critical Care Medicine*, vol. 38, Supplement 10, pp. S676–S682, 2010.

[31] G. Hermans, B. de Jonghe, F. Bruyninckx, and G. Berghe, "Clinical review: critical illness polyneuropathy and myopathy,," *Critical Care*, vol. 12, no. 6, p. 238, 2008.

[32] E. Apostolakis, N. A. Papakonstantinou, N. G. Baikoussis, and G. Papadopoulos, "Intensive care unit-related generalized neuromuscular weakness due to critical illness polyneuropathy/myopathy in critically ill patients," *Journal of Anesthesia*, vol. 29, no. 1, pp. 112–121, 2015.

[33] B. Pajak, S. Orzechowska, B. Pijet et al., "Crossroads of cytokine signaling–the chase to stop muscle cachexia," *Journal of*

Physiology and Pharmacology, vol. 59, Supplement 9, pp. 251–264, 2008.

[34] A. Grochot-Przeczek, J. Dulak, and A. Jozkowicz, "Haem oxygenase-1: non-canonical roles in physiology and pathology," *Clinical Science*, vol. 122, no. 3, pp. 93–103, 2012.

[35] S. W. Ryter, D. Morse, and A. M. K. Choi, "Carbon monoxide and bilirubin: potential therapies for pulmonary/vascular injury and disease," *American Journal of Respiratory Cell and Molecular Biology*, vol. 36, no. 2, pp. 175–182, 2007.

[36] T. S. Lee and L. Y. Chau, "Heme oxygenase-1 mediates the anti-inflammatory effect of interleukin-10 in mice," *Nature Medicine*, vol. 8, no. 3, pp. 240–246, 2002.

[37] H. Yang, L. F. Zhao, Z. F. Zhao, Y. Wang, J. J. Zhao, and L. Zhang, "Heme oxygenase-1 prevents liver fibrosis in rats by regulating the expression of PPARγ and NF-κB," *World Journal of Gastroenterology*, vol. 18, no. 14, pp. 1680–1688, 2012.

[38] K. Kang, C. Nan, D. Fei et al., "Heme oxygenase 1 modulates thrombomodulin and endothelial protein C receptor levels to attenuate septic kidney injury," *Shock*, vol. 40, no. 2, pp. 136–143, 2013.

[39] C. S. T. Origassa and N. O. S. Câmara, "Cytoprotective role of heme oxygenase-1 and heme degradation derived end products in liver injury," *World Journal of Hepatology*, vol. 5, no. 10, pp. 541–549, 2013.

[40] E. Barreiro, "Protein carbonylation and muscle function in COPD and other conditions," *Mass Spectrometry Reviews*, vol. 33, no. 3, pp. 219–236, 2014.

[41] S. Sriram, S. Subramanian, P. K. Juvvuna et al., "Myostatin augments muscle-specific ring finger protein-1 expression through an NF-kB independent mechanism in SMAD3 null muscle," *Molecular Endocrinology*, vol. 28, no. 3, pp. 317–330, 2014.

[42] C. Gemelli, B. M. Dongmo, F. Ferrarini, A. Grande, and L. Corsi, "Cytotoxic effect of hemin in colonic epithelial cell line: involvement of 18 kDa translocator protein (TSPO)," *Life Sciences*, vol. 107, no. 1-2, pp. 14–20, 2014.

Hindawi
Oxidative Medicine and Cellular Longevity
Volume 2018, Article ID 6364821, 8 pages
https://doi.org/10.1155/2018/6364821

Research Article

Effects of Redox Disturbances on Intestinal Contractile Reactivity in Rats Fed with a Hypercaloric Diet

Iara L. L. de Souza,[1,2] Elba dos S. Ferreira,[1] Anderson F. A. Diniz,[1] Maria Thaynan de L. Carvalho,[3] Fernando R. Queiroga,[1] Lydiane T. Toscano,[4] Alexandre S. Silva,[4] Patrícia M. da Silva,[5] Fabiana de A. Cavalcante,[1,2] and Bagnólia A. da Silva[1,6]

[1]*Programa de Pós-graduação em Produtos Naturais e Sintéticos Bioativos, Centro de Ciências da Saúde, Universidade Federal da Paraíba, João Pessoa, PB, Brazil*
[2]*Departamento de Fisiologia e Patologia, Centro de Ciências da Saúde, Universidade Federal da Paraíba, João Pessoa, PB, Brazil*
[3]*Centro de Ciências da Saúde, Universidade Federal da Paraíba, João Pessoa, PB, Brazil*
[4]*Departamento de Educação Física, Centro de Ciências da Saúde, Universidade Federal da Paraíba, João Pessoa, PB, Brazil*
[5]*Programa de Pós-graduação em Biologia Celular e Molecular, Centro de Ciências Exatas e da Natureza, Universidade Federal da Paraíba, João Pessoa, PB, Brazil*
[6]*Departamento de Ciências Farmacêuticas, Centro de Ciências da Saúde, Universidade Federal da Paraíba, João Pessoa, PB, Brazil*

Correspondence should be addressed to Bagnólia A. da Silva; bagnolia@ltf.ufpb.br

Received 23 June 2018; Accepted 27 September 2018; Published 25 October 2018

Academic Editor: Jeferson L. Franco

Few studies have associated the effects of changes in caloric intake and redox disturbances in the gastrointestinal tract. Therefore, the present study aimed at evaluating the hypercaloric diet consumption influence on the contractile reactivity of intestinal smooth muscle, morphology, and oxidative stress of rat ileum. Wistar rats were randomly divided into groups that received a standard diet and fed with a hypercaloric diet for 8 weeks. Animals were euthanized, and the ileum was isolated to isotonic contraction monitoring. Morphology was evaluated by histological staining and oxidative stress by quantification of malondialdehyde levels and total antioxidant activity. Cumulative concentration-response curves to KCl and carbachol were attenuated in rats fed with a hypercaloric diet compared to those that received a standard diet. In addition, an increase in caloric intake promotes a rise in the thickness of the longitudinal smooth muscle layer of rat ileum and tissue malondialdehyde levels, characterizing lipid peroxidation, as well as a decrease in the antioxidant activity. Thus, it was concluded that the consumption of a hypercaloric diet impairs rat intestinal contractility due to mechanisms involving modifications in the intestinal smooth muscle architecture triggered by redox disturbances.

1. Introduction

World Health Organization (WHO) defines obesity as a chronic condition characterized by an excessive accumulation of adipose tissue that causes health risk [1]. Therefore, obesity is categorized in the 10th revision of the International Classification of Diseases (ICD-10) at endocrine, nutritional, and metabolic diseases section [2].

Currently, several models develop obesity in animals through genetic mutations. However, most cases of human obesity are considered polygenic because of several gene integration. Thus, when analyzing the genesis of obesity in

humans, the induction of this disease in animals through the consumption of highly palatable and hypercaloric diets is indicated as the most appropriate [3].

Recently, our research group established a model of erectile dysfunction in Wistar rat associated to a hypercaloric diet consumption and characterized by an increase in body adiposity, endothelial dysfunction, and systemic oxidative stress [4]. The integral role of oxidative stress in the genesis of diseases affecting smooth muscle cells has been highlighted, mainly due to evidence of free radicals influence on contractility and/or relaxation of smooth muscle cells [5, 6].

The reactive oxygen species (ROS) are signaling agents under physiological conditions and control healing processes, apoptosis, and maintenance of smooth muscle tone and proliferation of this tissue, among others [7, 8]. ROS include a variety of free radicals, such as superoxide anion (O^{2-}) and hydroxyl radicals (OH^{-}), as well as nonradical oxygen derivatives such as hydrogen peroxide (H_2O_2), hypochlorous acid (HClO), peroxynitrite ($ONOO^{-}$), and ozone (O_3) [9].

An imbalance resulting from overproduction of ROS can damage proteins, lipids, DNA, and other cellular components [10, 11]. In order to contain the formation of these ROS, the organism presents enzymatic and nonenzymatic antioxidant systems, and both play a fundamental role in the prevention of oxidation resulting from ROS [12]. The enzymatic antioxidant system comprises superoxide dismutase (SOD), glutathione peroxidase (GSH-PX) and reductase (GSH-Rd), and catalase, which are the enzymes responsible for removing O^{2-}, organic hydroperoxides, and H_2O_2, respectively [13, 14]. The nonenzymatic system involves a group of antioxidants that can be complexed in compounds produced *in vivo*, such as glutathione, ubiquinone, and uric acid, and in compounds obtained directly from the diet such as α-tocopherol (vitamin E), β-carotene, ascorbic acid (vitamin C), and phenolic compounds such as flavonoids [11, 15].

In view of this information, changes in the balance between oxidative stress and body antioxidant defenses, with a predominance of ROS, observed when there is an increase in caloric intake, raise the probability of the development of organic dysfunctions. However, few studies have reported the effect of a change in dietary pattern on intestinal disorders; despite the abnormalities on intestinal contraction are related to pathophysiological processes, such as constipation, diarrhea, and intestinal colic [16]. Therefore, the aim of this study was to investigate the influence of hypercaloric diet consumption on the contractile reactivity of intestinal smooth muscle, morphology, and oxidative stress on rat ileum.

2. Materials and Methods

2.1. Animals. Wistar rats (*Rattus norvegicus*), 2 months old (approximately 150 g), were obtained from the Bioterium Professor Thomas George from Universidade Federal da Paraíba (UFPB). The animals were maintained under controlled ventilation and temperature (21 ± 1°C) with water *ad libitum* in a 12 h light-dark cycle (light on from 6 to 18 h). The experimental procedures were performed following the principles of guidelines for the ethical use of animals in applied etiology studies [17] and from the Conselho Nacional de Controle de Experimentação Animal of Brazil [18] and were previously approved by the Ethics Committee on Animal Use of UFPB (protocol no. 0201/14).

2.2. Groups and Diets. Animals were randomly divided into two groups (10 rats/group): rats that received a standard diet (Presence®) containing by weight 23% protein, 63% carbohydrate, and 4% lipids with energy density 3.8 kcal/g (SD) and rats fed with a hypercaloric diet composed by a standard diet (Presence®), milk chocolate, peanuts, and sweet biscuit in the proportion of 3 : 2 : 2 : 1 (HD) [19]. The hypercaloric diet containing by weight 23% protein, 45% carbohydrate, and 16% lipids with the energy density of 4.2 kcal/g was prepared weekly and supplied to animals as pellets [4]. The experimental groups were fed for 8 weeks.

2.3. Drugs. Potassium chloride (KCl), calcium chloride ($CaCl_2$), magnesium chloride ($MgCl_2$), sodium chloride (NaCl), and formaldehyde were purchased from Vetec Química Fina Ltda. (Brazil). Sodium bicarbonate ($NaHCO_3$) and glucose ($C_6H_{12}O_6$) were purchased from Dinâmica (Brazil). Sodium monobasic phosphate (NaH_2PO_4), sodium hydroxide (NaOH), and hydrochloric acid (HCl) were purchased from Nuclear (Brazil). These substances, except glucose, NaCl, and $NaHCO_3$, were diluted in distilled water to obtain each solution, which was maintained under refrigeration.

Carbamylcholine hydrochloride (CCh) was purchased from Merck (USA). Cremophor®, thiobarbituric acid, tetramethoxypropane, perchloric acid, Mayer's hematoxylin, and eosin were acquired from Sigma-Aldrich (Brazil). All substances were diluted in distilled water as needed for each experimental protocol. The carbogen mixture (95% O_2 and 5% CO_2) was obtained from White Martins (Brazil).

2.4. Ileum Isolation. Animals were euthanized by guillotine and the ileum was removed, cleaned of connective tissue and fat, immersed in physiological solution at room temperature, and bubbled with carbogen mixture (95% O_2 and 5% CO_2). In order to record the isotonic contractions, ileum segments (2–3 cm) were individually suspended in organ baths (5 mL) by cotton yarn and registered on the smoked drum through levers coupled to kymographs (DTF) with a thermostatic pump model Polystat 12002 Cole-Parmer (Vernon Hills) that controlled the organ bath temperature.

The physiological solution of Tyrode was used and has the composition (in mM) as follows: NaCl (150.0), KCl (2.7), $CaCl_2$ (1.8), $MgCl_2$ (2.0), $NaHCO_3$ (12.0), NaH_2PO_4 (0.4), and D-glucose (5.5). The pH was adjusted to 7.4, and the ileum was stabilized for 1 h under a resting tension of 1 g at 37°C and bubbled with a carbogen mixture [20].

2.5. Contractile Reactivity Measurement. The ileum was assembled as previously described. After a stabilization period of 30 min to verify the organ functionality, a contraction was induced with 30 mM KCl. Subsequently, cumulative

concentration-response curves were obtained to KCl (10^{-3}–3×10^{-1} M) and CCh (10^{-9}–3×10^{-5} M).

The contractile reactivity was evaluated based on the values of the maximum effect (E_{max}) and the negative logarithm of the molar concentration of a substance that produced 50% of its maximal effect (pCE_{50}) of both contractile agents, calculated from the concentration-response curves obtained. The maximum amplitude obtained from the SD group concentration-response curve was elected as 100%, and the HD was assessed referring to it.

2.6. Histological Analysis. Ileum segments were assembled as previously described fixed in 10% formaldehyde solution and subjected to a standard histological procedure. This process was composed of the following steps: (1) tissue dehydration at increasing alcohol series of 70% for 24 h and 80, 96, and 100% (third bath) during 1 h each; (2) tissue diaphanization/bleaching with immersion in 100% xylene alcohol (1 : 1) during 1 h, followed by two baths in pure xylene during 1 h each; (3) tissue embedding in paraffin, wherein the sample was immersed in two baths of liquid paraffin (heated to 50°C) during 1 h each. Then, samples were embedded in new paraffin.

The blocks obtained were cut to 5 μm thick in cross-section of the ileum and stained with Mayer's hematoxylin/eosin [21]. Digital images of histological sections were obtained and analyzed with an optical microscope with an attached camera. In this analysis, two cross-sections per animal were photographed, and the second quadrant of the ileum circumference was used to measure both circular and longitudinal muscle layers using the Leica Qwin 3.1 software [22].

2.7. Assessment of Lipidic Peroxidation Levels. Lipid peroxidation was measured by the chromogenic product of 2-thiobarbituric acid (TBA) reaction with malondialdehyde (MDA) that is a product formed as a result of membrane lipid peroxidation [23]. Therefore, ileum segments were homogenized with KCl (1 : 1), and samples of tissue homogenate (250 μL) were incubated at 37°C for 60 min. After that, the mixture was precipitated with 35% perchloric acid and centrifuged at 1207g for 20 min at 4°C. Then, the supernatant was collected and 400 μL of 0.6% TBA was added and incubated at 95–100°C for 1 h. After cooling, the samples were read in a spectrophotometer at a wavelength of 532 nm (Biospectro, SP-220 model-Brazil). The determination of the MDA concentration was made by substituting the absorbance values in the MDA standard curve obtained on the basis of a standard solution (1 μL of 1,1,3,3- tetramethoxypropane in 70 mL distilled water) diluted in series of 250, 500, 750, 1000, 1250, 1500, 1750, 2000, 2250, 2500, 2750, and 3000 μL of distilled water.

2.8. Antioxidant Activity Assay. The ileum homogenate was assembled as previously described. In addition, an aliquot of 1.25 mg of DPPH was diluted in ethanol (100 mL), kept under refrigeration, and protected from light. Then, 3.9 mL of DPPH solution was added with 100 μL of the supernatant ileum homogenate on appropriate centrifuge tubes. These tubes were vortexed and left to stand for 30 min, centrifuged at 1207g for 15 min at 20°C. Then, the samples were read in a spectrophotometer at a wavelength of 515 nm (Biospectro, SP-220 model-Brazil) [24].

Results were expressed as the percentage of the oxidation inhibition: $AOA = 100 - (((DPPH^{\cdot}\ R)\ S/(DPPH^{\cdot}\ R)\ W) \times 100)$, where $(DPPH^{\cdot}\ R)\ S$ and $(DPPH^{\cdot}\ R)\ W$ correspond to the concentration of $DPPH^{\cdot}$ remaining after 30 min, measured in the sample (S) and white (W) prepared with distilled water.

2.9. Statistical Analysis. Results were expressed as the mean and standard error of the mean (S.E.M.) and statistically analyzed using Student's *t*-test to the intergroup comparison. Cumulative concentration-response curves were fitted, and pCE_{50} values were obtained by nonlinear regression [25]. Values were significantly different when $p < 0.05$. All data were analyzed by GraphPad Prism® version 5.01 (GraphPad Software Inc., USA), and the visualization of histological sections was performed on Q-Capture® Pro version 7.0 software.

3. Results

3.1. Contractile Reactivity Measurement. In the HD group, cumulative concentration-response curves to KCl (10^{-3}–3×10^{-1} M) were attenuated with the reduction on E_{max} from 100% (SD) to 42.7 ± 3.1%. However, the pCE_{50} value of the HD group ($pCE_{50} = 1.8 \pm 0.8$) showed no statistical difference compared to the SD group ($pCE_{50} = 1.8 \pm 0.2$) (Figure 1(a), Table 1, $n = 5$).

Meanwhile, cumulative concentration-response curves to CCh (10^{-9}–3×10^{-5} M) were shifted to the right in rats fed with a hypercaloric diet ($pCE_{50} = 6.6 \pm 0.1$) compared to the SD group ($pCE_{50} = 6.3 \pm 0.05$). In addition, E_{max} value was decreased on HD related to SD ($E_{max} = 32.7 \pm 7.5$ and 100%, respectively), changing both potency and efficacy of CCh (Figure 1(b), Table 1, $n = 5$).

3.2. Histological Analysis. The circular smooth muscle layer thickness of rat ileum has no significant difference between HD (48.3 ± 4.0 μm) and SD groups (47.0 ± 1.8 μm). However, the longitudinal smooth muscle layer of rat ileum presented an increased thickness on rats fed with a hypercaloric diet compared to that in the SD group (36.53 ± 4.6 and 29.0 ± 1.9 μm, respectively) (Figure 2, $n = 5$).

3.3. Assessment of Lipidic Peroxidation Levels. The MDA levels in rat ileum were increased from 5.4 ± 0.2 μM/L (SD) to 7.0 ± 0.3 μM/L in rats fed with a hypercaloric diet (Figure 3(a), $n = 5$).

3.4. Antioxidant Activity Assay. The antioxidant activity in rat ileum was decreased from 93.0 ± 1.4% (SD) to 77.5 ± 1.5% in rats fed with a hypercaloric diet (Figure 3(b), $n = 5$).

4. Discussion

In this work, the influence of hypercaloric diet consumption on the contractile reactivity, morphology, and oxidative

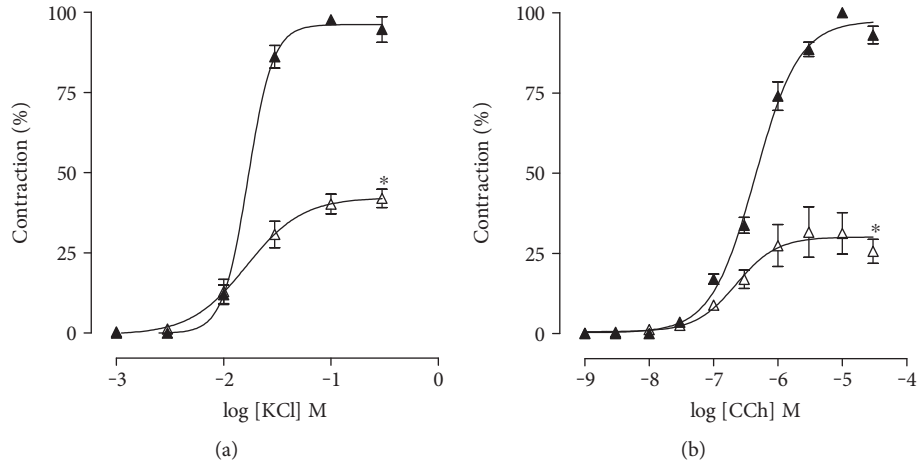

Figure 1: Cumulative concentration-response curves to KCl (a) and CCh (b) in rat ileum from both SD (▲) and HD groups (Δ). The symbols and vertical bars represent the mean and S.E.M., respectively ($n = 5$). Student's t-test, $^*p < 0.05$ (SD *vs.* HD).

Table 1: Values of E_{max} (%) and pCE_{50} of KCl and CCh in rat ileum from both SD and HD groups. Student's t-test, $^*p < 0.05$ (SD *vs.* HD) ($n = 5$).

Groups	KCl		CCh	
	E_{max} (%)	pCE_{50}	E_{max} (%)	pCE_{50}
SD	100	1.8 ± 0.2	100	6.3 ± 0.05
HD	$42.7 \pm 3.1^*$	1.8 ± 0.8	$32.7 \pm 7.5^*$	$6.6 \pm 0.1^*$

stress in rat ileum was investigated, demonstrating that an increase in caloric intake is associated with a decrease in contractile reactivity, an increase in the longitudinal smooth muscle layer thickness, lipid peroxidation, and a decrease in the antioxidant activity of this organ.

Chronic noncommunicable diseases (NCDs), such as type 2 diabetes mellitus, dyslipidemias, hypertension, and obesity, play an important and growing role in global public health due to their disabilities and early mortality. In this view, a central part of the genesis of these diseases is the excessive increase in body adiposity [26].

There are many determinants of obesity, being, therefore, a multifactorial disease characterized by the abnormal or excessive accumulation of adipose tissue [1]. Basically, obesity is caused by genetic and environmental factors, which are associated to an imbalance between energy expenditure and caloric consumption that are often determined by the consumption of diets with high energy density and high levels of fat and sugar [27, 28].

The ethical limitation in studying the mechanisms by which obesity induces physiological disorders in humans has resulted in the creation of experimental models using animals that are induced mainly by dietary and/or endocrine manipulation [29]. In these models, it is known that the consumption of hypercaloric/hyperlipidic diets is directly related to the development of various metabolic and hemodynamic disorders that result in adipose tissue hypertrophy/hyperplasia [30, 31].

Nevertheless, few studies have investigated the association of metabolic dysfunctions arising from the consumption of hypercaloric diets with possible alteration of cavernous smooth muscle reactivity on rats. Newly, Wistar rats fed with a hypercaloric diet, during eight weeks, showed increased systemic oxidative stress as well as impairment of contractile and relaxing reactivity of the corpus cavernosum in both pharmaco- and electromechanical couplings [4]. However, there is a lack of information about possible changes in intestinal contractile reactivity due to hypercaloric diet consumption, regarding the caloric content as well as the diet composition.

In view of these premises, it was decided to investigate whether the consumption of this diet, for eight weeks, would also alter the Wistar rats' intestinal contractile reactivity. Thus, the effect of the consumption of hypercaloric diet on both electro- and pharmacomechanical couplings was tested using KCl and CCh, respectively. The KCl was employed to simulate alterations on the membrane potential, which are physiologically controlled by the pacemaker of interstitial cells of Cajal located at the boundaries and in the substance of the inner circular muscle layer from which they spread to the outer longitudinal muscle layer. The CCh was used to mimic the cholinergic stimulation that happens in the intestinal smooth muscle [32, 33].

In this study, the KCl contractile efficacy was reduced in rats fed with hypercaloric diet in relation to those that received standard diet, with no change in potency (Figure 1(a), Table 1). Rembold [34] that verified an attenuation in cumulative concentration-response curves to KCl in rat ileum, decreasing its efficacy without changing the contractile potency, obtained similar results due to exercise. Thus, it is shown that an increase in caloric intake reduces the contraction elicited by the electromechanical coupling of rat ileum.

In addition, when rats consumed hypercaloric diet, a reduction was observed in both contractile efficacy and potency of CCh (Figure 1(b), Table 1). Data obtained by Araujo et al. [35] have demonstrated a similar decrease in

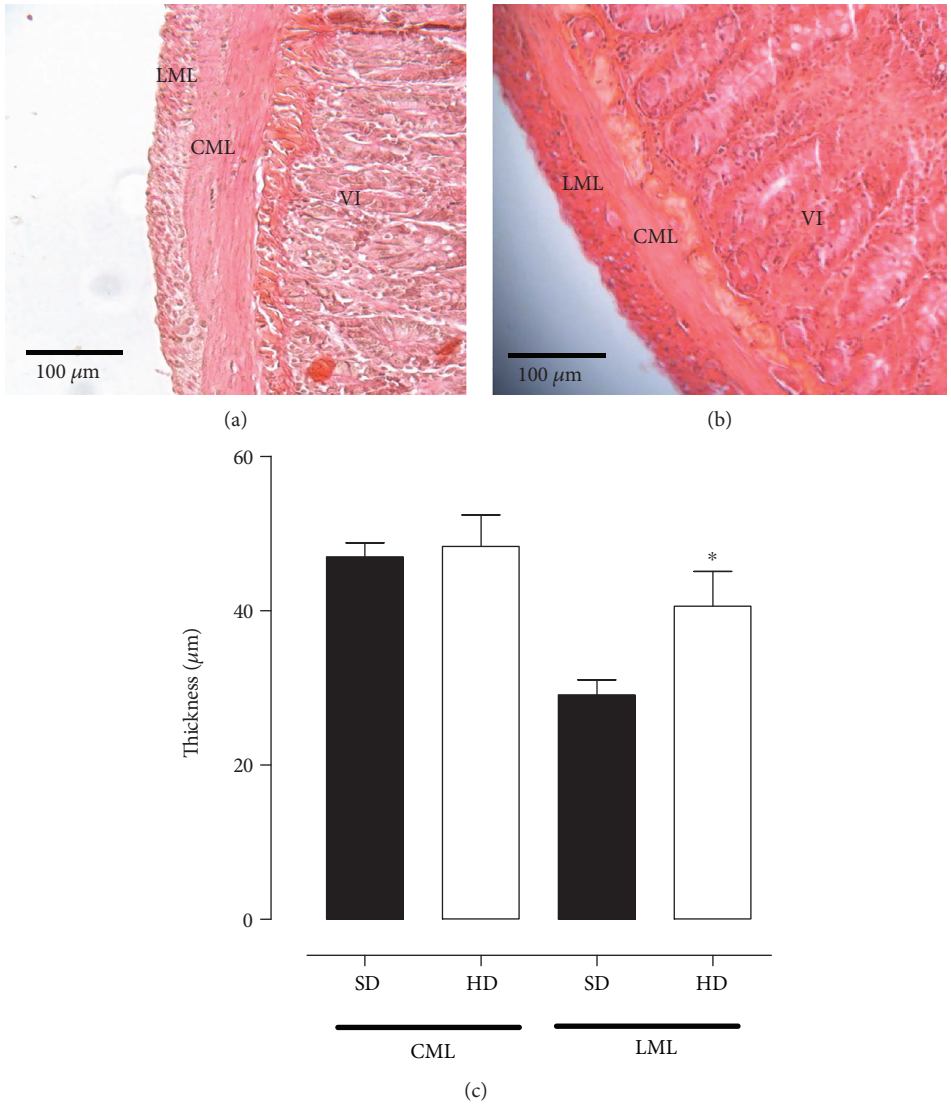

Figure 2: Microphotography of rat ileum from both SD (a) and HD groups (b) and thickness of CML and LML (c). Increased lens 20x. The symbols and vertical bars represent the mean and S.E.M., respectively ($n = 5$). Student's t-test, $^{*}p < 0.05$ (SD *vs.* HD). CML = circular muscle layer; LML = longitudinal muscle layer; VI = villus.

both efficacy and potency of CCh in the ileum of rats submitted to acute aerobic swimming exercise that were associated to a possible desensitization of intestinal muscarinic receptors. Moreover, the reperfusion process was also correlated to a reduction of ACh-induced contractile response in the ileum of rats submitted to occlusion of superior mesenteric artery plus interruption of collateral blood flow, leading to reperfusion [36]. Therefore, we demonstrate that an increase in caloric intake reduces the contraction elicited by the pharmacomechanical coupling of rat ileum, due to a less response of smooth muscle cell to cholinergic stimulation.

The synchrony between the smooth muscle layers, a circular and a longitudinal layer, modulates the intestinal contractility. In this view, Bertoni et al. [37] showed that hypertrophy of the circular smooth muscle layer is associated to an increase in contractile efficacy, whereas hypertrophy of the longitudinal smooth muscle layer exhibits a greater sensitivity to the relaxing factors, leading to a decrease in contractile efficacy. Thus, as the present study demonstrated a reduced contractility of rat ileum (Figure 1) due to hypercaloric diet consumption, it was hypothesized that changes in the architecture of the intestinal smooth muscle could be responsible for these results.

Therefore, to verify this hypothesis, histological analyses were performed on rat ileum from both experimental groups. The circular smooth muscle layer thickness was not altered by the consumption of a hypercaloric diet (Figure 2). Interestingly, an increase in the longitudinal smooth muscle layer thickness was observed (Figure 2), characterizing a hypertrophy process. Based on these results, it can be proposed that an increase in caloric intake leads to longitudinal smooth muscle layer hypertrophy and, consequently, reduced the ileum contractility (Figures 1 and 2).

A common problem related to the pathogenesis of intestinal reactivity disorders is the presence of a chronic low-grade inflammation that results in adipose tissue

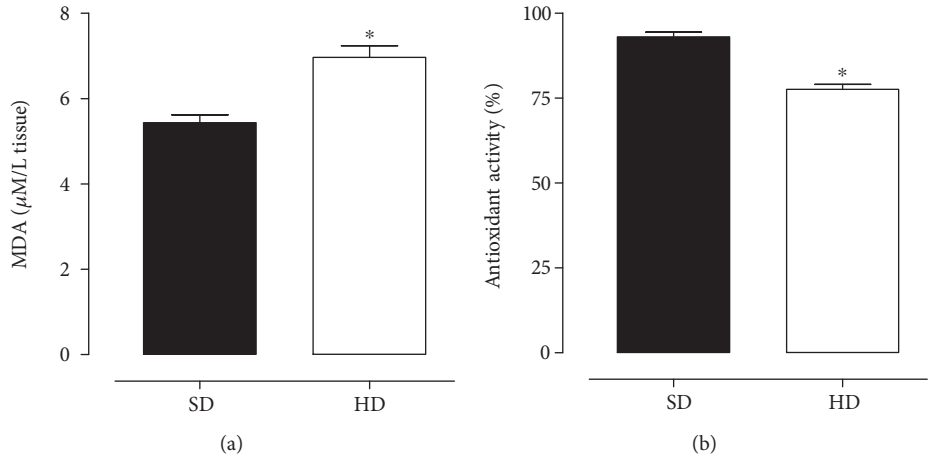

Figure 3: Concentration of MDA (a) and antioxidant activity (b) of rat ileum from both SD and HD groups. The symbols and vertical bars represent the mean and S.E.M., respectively ($n = 5$). Student's t-test, $^*p < 0.05$ (SD *vs.* HD). MDA = malondialdehyde.

hypertrophy [38]. Similar to other inflammatory processes, adipose tissue inflammation is a trigger for the oxidative stress and can be started by an increase in caloric intake. Briefly, due to the consumption of hypercaloric/hyperlipidic diets, there is an increase in glucose and circulating lipid levels resulting in the excessive supply of energetic substrates to metabolic routes. In turn, ROS production is raised, especially O^{2-}, H_2O_2, and OH^-, among others [8, 9].

It is consolidated in the literature that an imbalance in tissue peroxidation and antioxidant activity leads to oxidative damage, consequently, modulating both structure and/or function of the tissue [39–41]. Ischemia-reperfusion events in the intestinal musculature are closely related to oxidative stress [42], promoting motor and intestinal mucosa alteration, decrease in nutrient absorption, and gastrointestinal permeability [43, 44]. Other processes that also alter redox homeostasis, such as physical exercise, have already been correlated to increased lipid peroxidation. Specifically, Araujo et al. [45] showed that chronic aerobic swimming exercise increases lipid peroxidation after four weeks of exercise. Based on this information, it was decided to investigate whether the consumption of a hypercaloric diet would also alter lipid peroxidation of rat ileum. For this, the levels of MDA, a lipid peroxidation marker, were evaluated.

In studies involving oxidative stress, MDA represents a compound formed through the oxidative decomposition of polyunsaturated fatty acids from the membrane and is the most frequently quantified systemic and tissue marker [46]. MDA levels are therefore quantified through a calorimetric reaction in which two molecules of thiobarbituric acid are condensed with a molecule of MDA, and the end product is detected by spectrophotometry technique [47].

According to this methodology, it was observed that MDA concentration was increased in rat ileum from the HD group in relation to the SD group (Figure 3(a)). Souza et al. [4], using the same hypercaloric diet, showed that rats had an increase in MDA levels in plasma, characterizing a systemic oxidative stress. The remarkable increase in the level of ileum peroxidation in the HD group (Figure 3(a)) is quite suggestive that hypercaloric diet consumption also promotes tissue peroxidation. Additionally, it is an important challenge for intestinal redox homeostasis and indicates a possible compromise of the antioxidant defense system of these animals. The peroxidation increase may be a consequence of proinflammatory cytokine production (TNF-α, IL-1, and IL-6), due to excess body adiposity, since these cytokines stimulate ROS production by macrophages [48].

In biological systems, this imbalance in ROS production is counterbalanced by the body's antioxidant capacity, representing the body's ability to sequester free radicals through redox systems [49]. Knowing this, it was investigated whether the consumption of a hypercaloric diet would alter the antioxidant activity of these rats. For this, the DPPH reduction colorimetric method was used, which is based on the sample's ability to reduce the DPPH radical (purple) to 1,1-diphenyl 2-picryl hydrazine (translucent), detected by spectrophotometry technique [50].

In this study, the HD group presented a reduction in tissue antioxidant activity in relation to the SD group (Figure 3(b)). The decrease of systemic antioxidant activity was demonstrated by Souza et al. [4] using the same hypercaloric diet. Therefore, the reduction of the ileum antioxidant capacity observed in the HD group (Figure 3(b)) reinforces the idea of an imbalance between ROS production and antioxidant defense systems, correlated with an increase in MDA levels in these rats (Figure 3(a)). Since free radicals are regulators in several cellular processes, such as transcriptional factor activation, gene expression, and cell proliferation [7], it was proposed that an oxidative stress caused by the consumption of a hypercaloric diet may underlie the hypertrophy process of intestinal smooth muscle cells in rats (Figures 2 and 3).

In conclusion, the current study showed initial evidence that the consumption of a hypercaloric diet impairs rat intestinal contractility due to mechanisms involving modifications in the intestinal smooth muscle architecture triggered by redox disturbances. Thus, we provide a model to understand biochemical and metabolic processes involved in the pathophysiological changes caused by the increase in caloric intake, as well as to help to reduce the impact of the various diseases related to it.

Data Availability

The data used to support the findings of this study are available from the corresponding author upon request.

Conflicts of Interest

The authors declare that there is no conflict of interest regarding the publication of this paper.

Acknowledgments

The authors thank Coordenação de Aperfeiçoamento de Pessoal de Nível Superior (CAPES) and Conselho Nacional de Desenvolvimento Científico e Tecnológico (CNPq) for financial support. The authors thank José Crispim Duarte and Luís C. Silva for providing technical assistance and Camila Leão Luna de Souza for English review.

References

[1] WHO, *Health Topics – Obesity*, WHO, 2018.

[2] WHO, *Obesity: Preventing and Managing the Global Epidemic*, WHO, 2000.

[3] T. A. LUTZ and S. C. WOODS, "Overview of animal models of obesity," *Current Protocols in Pharmacology*, vol. 58, no. 1, pp. 5.61.1–5.61.18, 2012.

[4] I. L. L. de Souza, B. C. Barros, G. A. de Oliveira et al., "Hypercaloric diet establishes erectile dysfunction in rat: mechanisms underlying the endothelial damage," *Frontiers in Physiology*, vol. 8, 2017.

[5] A. Castela, P. Gomes, V. F. Domingues et al., "Role of oxidative stress-induced systemic and cavernosal molecular alterations in the progression of diabetic erectile dysfunction," *Journal of Diabetes*, vol. 7, no. 3, pp. 393–401, 2015.

[6] F. B. M. Priviero, H. A. F. Toque, K. P. Nunes, D. G. Priolli, C. E. Teixeira, and R. C. Webb, "Impaired corpus cavernosum relaxation is accompanied by increased oxidative stress and up-regulation of the rho-kinase pathway in diabetic (Db/Db) mice," *PLoS One*, vol. 11, no. 5, article e0156030, 2016.

[7] H. Suenaga and K. Kamata, "Lysophosphatidylcholine activates extracellular-signal-regulated protein kinase and potentiates vascular contractile responses in rat aorta," *Journal of Pharmacological Sciences*, vol. 92, no. 4, pp. 348–358, 2003.

[8] F. Mcmurray, D. A. Patten, and M. E. Harper, "Reactive oxygen species and oxidative stress in obesity-recent findings and empirical approaches," *Obesity*, vol. 24, no. 11, pp. 2301–2310, 2016.

[9] B. Halliwell, "Reactive species and antioxidants. Redox biology is a fundamental theme of aerobic life," *Plant Physiology*, vol. 141, no. 2, pp. 312–322, 2006.

[10] T. Finkel and N. J. Holbrook, "Oxidants, oxidative stress and the biology of ageing," *Nature*, vol. 408, no. 6809, pp. 239–247, 2000.

[11] B. Halliwell and J. M. C. Gutteridge, *Free Radicals in Biology and Medicine*, Oxford University Press, USA, 5 edition, 2015.

[12] P. R. B. Broinizi, E. R. S. d. Andrade-Wartha, A. M. d. O. e. Silva et al., "Propriedades antioxidantes em subproduto do pedúnculo de caju (*Anacardium occidentale* L.): efeito sobre a lipoperoxidação e o perfil de ácidos graxos poliinsaturados em ratos," *Revista Brasileira de Ciências Farmacêuticas*, vol. 44, no. 4, pp. 773–781, 2008.

[13] B. P. Yu, "Cellular defenses against damage from reactive oxygen species," *Physiological Reviews*, vol. 74, no. 1, pp. 139–162, 1994.

[14] P. G. Pietta, "Flavonoids as antioxidants," *Journal of Natural Products*, vol. 63, no. 7, pp. 1035–1042, 2000.

[15] C. De Moraes and R. C. Sampaio, "Estresse oxidativo e envelhecimento: papel do exercício físico," *Motriz. Revista de Educação Física. UNESP*, vol. 16, no. 2, pp. 506–515, 2010.

[16] Y. Sato, J. X. He, H. Nagai, T. Tani, and T. Akao, "Isoliquiritigenin, one of the antispasmodic principles of Glycyrrhiza ularensis roots, acts in the lower part of intestine," *Biological and Pharmaceutical Bulletin*, vol. 30, no. 1, pp. 145–149, 2007.

[17] C. M. Sherwin, S. B. Christiansen, I. J. Duncan et al., "Guidelines for the ethical use of animals in applied ethology studies," *Applied Animal Behaviour Science*, vol. 81, no. 3, pp. 291–305, 2003.

[18] BRASIL, Ministério da Ciência, Tecnologia e Inovação, and Conselho Nacional de Experimentação Animal, *Guia Brasileiro de Produção, Manutenção ou Utilização de Animais em Atividades de Ensino ou Pesquisa Científica: Fascículo 1: Introdução Geral*, Ministério da Ciência, Tecnologia e Inovação, Brasília–DF, 2016.

[19] D. Estadella, L. M. Oyama, A. R. Dâmaso, E. B. Ribeiro, and C. M. Oller Do Nascimento, "Effect of palatable hyperlipidic diet on lipid metabolism of sedentary and exercised rats," *Nutrition*, vol. 20, no. 2, pp. 218–224, 2004.

[20] M. Radenkovic, V. Ivetic, M. Popovic, N. Mimica-Dukic, and S. Veljkovic, "Neurophysiological effects of mistletoe (*Viscum album* L.) on isolated rat intestines," *Phytotherapy Research*, vol. 20, no. 5, pp. 374–377, 2006.

[21] D. W. Howard, E. J. Lewis, B. J. Keller, and C. Smith, *Histological Techniques for Marine Bivalve Molluscs and Crustaceans*, NOAA/National Centers for Coastal Ocean Science, Oxford, MD, USA, 2nd edition, 2004.

[22] C. A. B. de Lira, R. L. Vancini, S. S. M. Ihara, A. C. da Silva, J. Aboulafia, and V. L. A. Nouailhetas, "Aerobic exercise affects C57BL/6 murine intestinal contractile function," *European Journal of Applied Physiology*, vol. 103, no. 2, pp. 215–223, 2008.

[23] C. C. Winterbourn, J. M. C. Gutteridge, and B. Halliwell, "Doxorubicin-dependent lipid peroxidation at low partial pressures of O_2," *Journal of Free Radicals in Biology & Medicine*, vol. 1, no. 1, pp. 43–49, 1985.

[24] W. Brand-Williams, M. E. Cuvelier, and C. Berset, "Use of a free radical method to evaluate antioxidant activity," *LWT - Food Science and Technology*, vol. 28, no. 1, pp. 25–30, 1995.

[25] R. R. Neubig, M. Spedding, T. Kenakin, A. Christopoulos, and International Union of Pharmacology Committee on Receptor Nomenclature and Drug Classification., "International union of pharmacology committee on receptor nomenclature and drug classification. XXXVIII. Update on terms and symbols in quantitative pharmacology," *Pharmacological Reviews*, vol. 55, no. 4, pp. 597–606, 2003.

[26] F. Bäckhed, H. Ding, T. Wang et al., "The gut microbiota as an environmental factor that regulates fat storage," *Proceedings of the National Academy of Sciences of the United States of America*, vol. 101, no. 44, pp. 15718–15723, 2004.

[27] D. W. Haslam and W. P. T. James, "Obesity," *The Lancet*, vol. 366, no. 9492, pp. 1197–1209, 2005.

[28] J. J. Patel, M. D. Rosenthal, K. R. Miller, P. Codner, L. Kiraly, and R. G. Martindale, "The critical care obesity paradox and implications for nutrition support," *Current Gastroenterology Reports*, vol. 18, no. 9, p. 45, 2016.

[29] L. O. Pereira, R. P. d. Francischi, and A. H. Lancha Jr, "Obesidade: hábitos nutricionais, sedentarismo e resistência à insulina," *Arquivos Brasileiros de Endocrinologia e Metabologia*, vol. 47, no. 2, pp. 111–127, 2003.

[30] L. A. Velloso, "The brain is the conductor: diet-induced inflammation overlapping physiological control of body mass and metabolism," *Arquivos Brasileiros de Endocrinologia & Metabologia*, vol. 53, no. 2, pp. 151–158, 2009.

[31] A. Tchernof and J. P. Després, "Pathophysiology of human visceral obesity: an update," *Physiological Reviews*, vol. 93, no. 1, pp. 359–404, 2013.

[32] J. C. Bornstein, M. Costa, and J. R. Grider, "Enteric motor and interneuronal circuits controlling motility," *Neurogastroenterology & Motility*, vol. 16, no. s1, pp. 34–38, 2004.

[33] K. M. Sanders, S. D. Koh, T. Ordog, and S. M. Ward, "Ionic conductances involved in generation and propagation of electrical slow waves in phasic gastrointestinal muscles," *Neurogastroenterology & Motility*, vol. 16, no. s1, pp. 100–105, 2004.

[34] C. M. Rembold, "Electromechanical and pharmacomechanical coupling," in *Biochemistry of Smooth Muscle Contraction*, M. Bárány, Ed., pp. 227–239, Elsevier, San Diego, CA, USA, 1996.

[35] L. C. da Cunha Araujo, I. L. L. de Souza, L. H. C. Vasconcelos et al., "Acute aerobic swimming exercise induces distinct effects in the contractile reactivity of rat ileum to KCl and carbachol," *Frontiers in Physiology*, vol. 7, 2016.

[36] V. Ballabeni, E. Barocelli, S. Bertoni, and M. Impicciatore, "Alterations of intestinal motor responsiveness in a model of mild mesenteric ischemia/reperfusion in rats," *Life Sciences*, vol. 71, no. 17, pp. 2025–2035, 2002.

[37] S. Bertoni, V. Ballabeni, L. Flammini, T. Gobbetti, M. Impicciatore, and E. Barocelli, "Intestinal chronic obstruction affects motor responsiveness of rat hypertrophic longitudinal and circular muscles," *Neurogastroenterology & Motility*, vol. 20, no. 11, pp. 1234–1242, 2008.

[38] S. P. Weisberg, D. McCann, M. Desai, M. Rosenbaum, R. L. Leibel, and A. W. Ferrante Jr, "Obesity is associated with macrophage accumulation in adipose tissue," *The Journal of Clinical Investigation*, vol. 112, no. 12, pp. 1796–1808, 2003.

[39] K. P. Davies and A. Melman, "Markers of erectile dysfunction," *Indian Journal of Urology*, vol. 24, no. 3, pp. 320–328, 2008.

[40] K. M. Azadzoi, T. Golabek, Z. M. Radisavljevic, S. V. Yalla, and M. B. Siroky, "Oxidative stress and neurodegeneration in penile ischaemia," *BJU International*, vol. 105, no. 3, pp. 404–410, 2010.

[41] C. Vlachopoulos, N. Ioakeimidis, and C. Stefanadis, "Biomarkers, erectile dysfunction, and cardiovascular risk prediction: the latest of an evolving concept," *Asian Journal of Andrology*, vol. 17, no. 1, pp. 17–20, 2015.

[42] V. H. Ozacmak, H. Sayan, S. O. Arslan, S. Altaner, and R. G. Aktas, "Protective effect of melatonin on contractile activity and oxidative injury induced by ischemia and reperfusion of rat ileum," *Life Sciences*, vol. 76, no. 14, pp. 1575–1588, 2005.

[43] J. Liu, H. C. Yeo, E. Overvik-Douki et al., "Chronically and acutely exercised rats: biomarkers of oxidative stress and endogenous antioxidants," *Journal of Applied Physiology*, vol. 89, no. 1, pp. 21–28, 2000.

[44] M. L. Marquezi, H. A. Roschel, A. d. S. Costa, L. A. Sawada, and A. H. Lancha Jr, "Effect of aspartate and asparagine supplementation on fatigue determinants in intense exercise," *International Journal of Sport Nutrition and Exercise Metabolism*, vol. 13, no. 1, pp. 65–75, 2003.

[45] L. C. da Cunha Araujo, I. L. L. de Souza, L. H. C. Vasconcelos et al., "Chronic aerobic swimming exercise promotes functional and morphological changes in rat ileum," *Bioscience Reports*, vol. 35, no. 5, article e00259, 2015.

[46] D. del Rio, A. J. Stewart, and N. Pellegrini, "A review of recent studies on malondialdehyde as toxic molecule and biological marker of oxidative stress," *Nutrition, Metabolism and Cardiovascular Diseases*, vol. 15, no. 4, pp. 316–328, 2005.

[47] M. Giera, H. Lingeman, and W. M. A. Niessen, "Recent advancements in the LC- and GC-based analysis of malondialdehyde (MDA): a brief overview," *Chromatographia*, vol. 75, no. 9-10, pp. 433–440, 2012.

[48] J. D. Morrow, "Is oxidant stress a connection between obesity and atherosclerosis?," *Arteriosclerosis, Thrombosis and Vascular Biology*, vol. 23, no. 3, pp. 368–370, 2003.

[49] F. Brighenti, S. Valtueña, N. Pellegrini et al., "Total antioxidant capacity of the diet is inversely and independently related to plasma concentration of high-sensitivity C-reactive protein in adult Italian subjects," *British Journal of Nutrition*, vol. 93, no. 05, pp. 619–625, 2005.

[50] A. Floegel, D. O. Kim, S. J. Chung, S. I. Koo, and O. K. Chun, "Comparison of ABTS/DPPH assays to measure antioxidant capacity in popular antioxidant-rich US foods," *Journal of Food Composition and Analysis*, vol. 24, no. 7, pp. 1043–1048, 2011.

Hindawi
Oxidative Medicine and Cellular Longevity
Volume 2018, Article ID 8936251, 15 pages
https://doi.org/10.1155/2018/8936251

Research Article

Combination of Coenzyme Q_{10} Intake and Moderate Physical Activity Counteracts Mitochondrial Dysfunctions in a SAMP8 Mouse Model

C. Andreani,[1] **C. Bartolacci**,[1] **M. Guescini**,[2] **M. Battistelli**,[2] **V. Stocchi**,[2] **F. Orlando**,[3] **M. Provinciali**,[3,4] **A. Amici**,[1] **C. Marchini**,[1] **L. Tiano**,[5] **P. Orlando**,[5] **and S. Silvestri**[5,6]

[1]*University of Camerino, via Gentile III da Varano, 62032 Camerino, Italy*
[2]*University of Urbino, via Aurelio Saffi, 61029 Urbino, Italy*
[3]*Experimental Animal Models for Aging Unit Scientific Technological Area, IRCCS INRCA, via del Fossatello, 60127 Ancona, Italy*
[4]*Advanced Technological Center for Aging Research Scientific Technological Area, IRCCS INRCA, via Birarelli 8, 60121 Ancona, Italy*
[5]*Polytechnic University of Marche, Department of Life and Environmental Sciences (DISVA), via Brecce Bianche, Ancona, Italy*
[6]*Biomedfood srl, Spinoff of Polytechnic University of Marche, via Brecce Bianche, 60131 Ancona, Italy*

Correspondence should be addressed to P. Orlando; p.orlando@univpm.it

Received 12 June 2018; Accepted 29 August 2018; Published 24 October 2018

Academic Editor: Carine Smith

Aging skeletal muscles are characterized by a progressive decline in muscle mass and muscular strength. Such muscular dysfunctions are usually associated with structural and functional alterations of skeletal muscle mitochondria. The senescence-accelerated mouse-prone 8 (SAMP8) model, characterized by premature aging and high degree of oxidative stress, was used to investigate whether a combined intervention with mild physical exercise and ubiquinol supplementation was able to improve mitochondrial function and preserve skeletal muscle health during aging. 5-month-old SAMP8 mice, in a presarcopenia phase, have been randomly divided into 4 groups ($n = 10$): untreated controls and mice treated for two months with either physical exercise (0.5 km/h, on a 5% inclination, for 30 min, 5/7 days per week), ubiquinol 10 (500 mg/kg/day), or a combination of exercise and ubiquinol. Two months of physical exercise significantly increased mitochondrial damage in the muscles of exercised mice when compared to controls. On the contrary, ubiquinol and physical exercise combination significantly improved the overall status of the skeletal muscle, preserving mitochondrial ultrastructure and limiting mitochondrial depolarization induced by physical exercise alone. Accordingly, combination treatment while promoting mitochondrial biogenesis lowered autophagy and caspase 3-dependent apoptosis. In conclusion, the present study shows that ubiquinol supplementation counteracts the deleterious effects of physical exercise-derived ROS improving mitochondrial functionality in an oxidative stress model, such as SAMP8 in the presarcopenia phase.

1. Introduction

Aging is characterized by a progressive decline in skeletal muscle mass and muscular strength [1–3]. In healthy people, there is a 1% per year decline in muscle mass between 20 and 30 years of age. This decline is accelerated above 50 years of age [4, 5]. The progressive decline in muscle mass and strength with aging is known as sarcopenia [1, 6–8]. Sarcopenia is defined as a geriatric syndrome characterized by age-related muscular loss and dysfunction that cause physical disability, a poor quality of life, and death. The prevalence of this pathology in adults under the age of 70 is about 25% but increases up to 40% in 80-year-old or older people [9, 10]. This condition can lead to decreased physical activity increasing the risk of falls in aged individuals [11]. Understanding the mechanisms underneath aging-induced skeletal muscle atrophy and promoting health and mobility in the elderly are crucially important goals in order to develop therapeutic strategies [12]. Several studies pointed towards a critical role of mitochondria and their implication in age-related

degenerative processes, and many therapeutic attempts have been focused on mitochondria [13]. Indeed, these organelles play a key role in cellular bioenergetics and represent a sensitive target in muscle cells [14, 15]. Moreover, metabolism of reactive oxygen species (ROS), Ca^{2+} homeostasis, and apoptosis are controlled by mitochondria [16]. Aging of skeletal muscle determines the alteration of the structure and function of these organelles leading to mitochondrial dysfunction [17]. In this context, a growing body of evidence has highlighted a major role of oxidative stress and inflammation in promoting aging of skeletal muscle [18]. Accordingly, it has been recently reported that excessive production of mitochondrial ROS in skeletal muscle is strongly associated with sarcopenia and the impairment of energy homeostasis [19]. In fact, the physiologic equilibrium between ROS production and antioxidant defense is disrupted in aging subjects, and the accumulation of ROS during mitochondrial respiration can cause mutations in mitochondrial DNA (mtDNA) [20] which in turn lead, through a vicious cycle, to further impaired mitochondrial functionality. Moreover, many studies have reported that a decline in mitochondria content may also account for the loss of skeletal muscle mass [18], further impairing oxidative phosphorylation and ATP production [21, 22]. Mitochondrial biogenesis is regulated by the expression of nuclear and mitochondrial genes, controlled by the transcriptional coactivator peroxisome proliferator gamma coactivator-1α (PGC-1α) [23]. Vainshtein et al. [24] suggested a role of this coactivator also in the regulation of autophagy and mitophagy in skeletal muscle. These two are distinct but interconnected degradation processes aimed at eliminating damaged cellular components in response to stress stimuli. Both mitophagy and autophagy are regulated by autophagy-related genes (Atgs) including Beclin-1 and LC3 [25].

During aging, skeletal muscle fibers gradually lose the capability to remove dysfunctional mitochondria [13]. This condition could further impair mitochondrial respiration and enhance ROS production [26] contributing to the onset of sarcopenia. Previous studies suggested that an appropriate physical activity regimen can counterbalance age-associated muscular deficits by promoting mitochondrial biogenesis [27–29]. Exercise training has been reported to modulate skeletal muscle metabolism, regulating intracellular signaling pathways and thus mediating mitochondrial homeostasis [30, 31]. However, some authors raised doubts regarding the beneficial role of exercise in the elderly, claiming that physical activity-dependent ROS production could exacerbate oxidative damage inside aged skeletal muscles [32–34]. In this scenario, association of physical activity with antioxidant therapies might be an effective strategy to prevent the adverse effects of exercise in the elderly. Coenzyme Q_{10} represents a valuable candidate for oxidative stress prevention and for supporting muscle functionality [35–39]. Coenzyme Q (CoQ) consists of a quinone head which, in mammalian cells, is attached to a chain of 9 (CoQ_9) or 10 isoprene units CoQ_{10} [40]. In human tissues, the most abundant form is coenzyme Q_{10}, while in mice and rats it is coenzyme Q_9, although CoQ_{10} represents a significant proportion of total CoQ and its level is able to increase following oral supplementation [41–46]. As part of the mitochondrial electron transport chain (ETC), CoQ actively participates in oxidative phosphorylation and plays a key role in energy and redox state balance [47]. In addition, CoQ has been found in other subcellular localizations and in circulating plasma lipoproteins, where it acts as an endogenous lipophilic antioxidant in synergism with vitamin E [48]. Endogenous CoQ_{10} synthesis, the principal source of CoQ [49], has been shown to significantly decrease during aging and in certain degenerative diseases [50, 51], thus triggering cellular dysfunctionality. These evidences underlie the rationale for CoQ use in clinical practice and as a food supplement. CoQ exists in three states of oxidation: ubiquinone (CoQ), the fully oxidized form; ubisemiquinone ($CoQH^{\cdot}$), the partially reduced form; and ubiquinol ($CoQH_2$), the fully reduced form. In particular, the $CoQH_2$ form has several advantages being more bioavailable and readily usable by the organism not requiring reductive steps [52]. This is of particular relevance in conditions when reductive systems might be less efficient such as during aging or following intense physical exercise. Here, we investigated the effect of a combined approach of mild physical exercise and ubiquinol supplementation on the senescence-accelerated mouse-prone 8 (SAMP8) model in a presarcopenia phase [53, 54]. SAMP strains derived from AKR/J series [55] show senescence acceleration and age-related pathological phenotypes, similar to aging disorders seen in humans. In particular, we focused on SAMP8 mice since they exhibit the most striking features among SAMP strains in terms of life span, fast aging progression due to high oxidative stress status [56, 57], dramatic decrease in muscle mass and contractility [58, 59], and a huge reduction in type II muscle fiber size [60, 61]. The aim of this study is to develop prevention strategies able to preserve skeletal muscle health during aging by maintaining mitochondrial function through regular physical exercise and antioxidant supplementation using a senescence-accelerated mouse-prone model (SAMP8).

2. Materials and Methods

2.1. SAMP8 Housing and Treatment. Senescence-accelerated mice (SAMP8, Harlan) [58, 59, 62], aged 5 months, have been randomly divided into 4 groups ($n = 10$) as summarized hereafter: untreated controls (SED), trained (PHY), ubiquinol 10-administered (QH_2), and both trained and ubiquinol 10-supplemented (QH_2 + PHY). The PHY and QH_2 + PHY groups underwent treadmill running at 0.5 km/h, on a 5% inclination, for 30 min, 5 days per week, for 2 months up to 7 months of age [63, 64] (Figure 1). The QH_2 and QH_2 + PHY groups were supplemented with ubiquinol 10 (Kaneka) (500 mg/kg body weight/day in sunflower seed oil) via oral administration. Such QH_2 formulation was previously prepared and stored at −80°C in 500 μL aliquots to avoid repeated freezing-thawing cycles. An aliquot was thawed daily in a water bath at 60°C in the dark just prior to administration. An equal amount of sunflower seed oil was given to SED and PHY mouse groups. The animals were bred and housed under controlled temperature (20°C) and a circadian cycle (12-hour light/12-hour dark). The animals

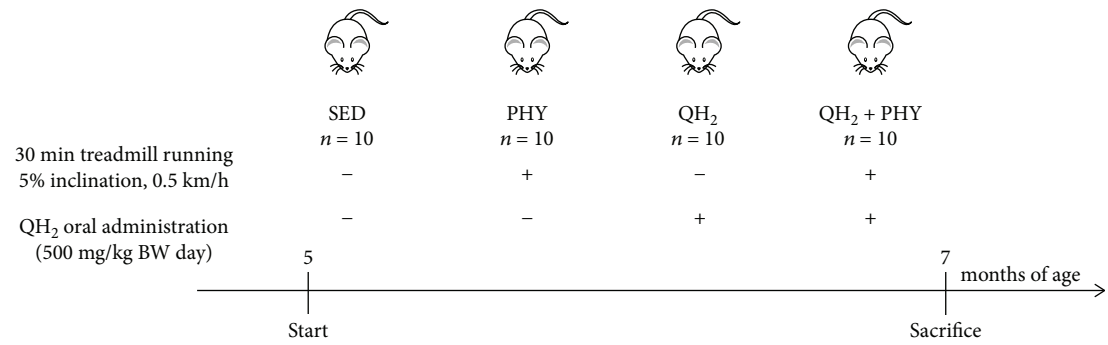

Figure 1: Scheme of SAMP8 mouse study.

were fed on chow diet and water *ad libitum*. Male mice were used for all experiments. The animal procedures followed the 2010/63/EU directive on the protection of animals used for scientific purposes and were approved by the Ethic Committee on Animal Use of the University of Camerino (protocol number 14/2012).

2.2. Tissue Collection and Analysis. Mice were rapidly sacrificed by isoflurane inhalation followed by cervical dislocation, two days after the last exercise/administration session, to avoid possible metabolic effects of the last exercise/administration bout. *Gastrocnemius* (GA), *tibialis anterior* (TA), *soleus* (SO) muscle, and cardiac muscle were carefully excised. GA samples were either immediately used for flow cytometry (FACS) analysis or preserved in liquid nitrogen for mtDNA quantification or mRNA extraction. TA and cardiac muscles were used for CoQ_9 and CoQ_{10} (total and oxidized form) quantification. TA muscles were used also for protein extraction and Western blot analysis, while SO samples were fixed in 3% glutaraldehyde for 4 hours, to be analyzed for fiber morphology, number, and ultrastructure of mitochondria by electron microscopy. Other tissues including liver, spleen, and kidneys were recovered for eventual future applications and preserved at −80°C.

2.3. Coenzyme Q_9 and Q_{10} Extraction and Quantification. TA and cardiac muscles were mechanically homogenized (two bouts at 30 Hz for 5 min) in propanol (Sigma) using 7 mm steel beads (Qiagen) and TissueLyser II (Qiagen). After centrifugation (2 min at 20,000 g, 4°C), 40 μL of the supernatant was injected into a high-performance liquid chromatography (HPLC) apparatus with an electrochemical detector (ECD), model 3016 by Shiseido Co. Ltd, to measure total coenzymes Q_9 and Q_{10} and Q_9 oxidative status. The mobile phase was 50 mM sodium perchlorate in methanol/distilled water (95/5 *v*/*v*) with a flow rate of 0.2 mL/min. Using a column-switching system, coenzymes were eluted from the concentrating column by mobile phase 2, 50 mM sodium perchlorate in methanol/isopropanol (70/30 *v*/*v*) with a flow rate of 0.08 mL/min. The column oven was set at 40°C. Pumps one and two of model 3001, autosampler model 3033, and switch valve model 3012; concentration column CQC (C8 DD; 10 mm × 4.0 mm ID); and separation column CQS (C18 AQ; 150 mm × 2.0 mm ID, particle size at 3 μm diameter) were used, all from Shiseido Co. Ltd. A peculiarity of the system was the use of a postseparation reduction column (Shiseido CQR) capable of fully reducing the peak of ubiquinone. CoQ_9 and CoQ_{10} standard solutions were previously prepared in ethanol and stored at −80°C. The oxidation potential for ECD was 650 mV. TA and cardiac muscle contents of CoQ_9 and CoQ_{10} were expressed as μg/g muscle and the oxidized form as percentage of total CoQ_9.

2.4. Electron Microscope Analysis. Control and treated SO samples were washed and immediately fixed with 2.5% glutaraldehyde in 0.1 M phosphate buffer for 1 hour, postfixed with 1% of osmium tetroxide (OsO_4) in the same buffer for 2 hours, and embedded in araldite, as previously reported [65, 66]. The sections were collected on 400-mesh nickel grids, stained with uranyl acetate, lead citrate and finally analyzed with an electron microscope at 80 kV.

2.5. Flow Cytometry Analysis

2.5.1. Skeletal Muscle Dissociation. GA muscles were dissociated into single-cell suspensions using a skeletal muscle dissociation kit (Miltenyi Biotec) according to the manufacturer's instructions. Mechanical disaggregation was performed via gentleMACS Dissociator using the m_muscle_01 program (Miltenyi Biotec).

2.5.2. Cell Viability and Cell Count. Cell viability and cell count of the obtained single-cell suspensions were evaluated using Guava ViaCount® Reagent Kit (Millipore) that discriminates among viable, apoptotic, and dead cells. Briefly, the assay exploits a mixture of cell membrane-permeable (red) and cell membrane-impermeable (yellow) DNA-binding fluorescent probes, diluted 1 : 10 in PBS, and used to stain cells immediately before reading. Cells were incubated with reagent for 5 min in the dark, and the analysis of the distribution allows the discrimination of the percentage of cell debris (R−/Y−), live cells (R+/Y−), and dead cells (R+/Y+) with Guava ViaCount software using a Guava easyCyte™ flow cytometer (Millipore).

2.5.3. Mitochondrial Membrane Depolarization. Mitochondrial membrane depolarization was measured by incubating 2.5×10^5 viable muscle cells with MitoProbe™ DiIC1(5) (Life Technologies) (40 nM final concentration) at 37°C for 20 min in the dark. During the experimental setup, a suspension of control cells, before staining, was incubated with 1 μL

Table 1: pRT-PCR primers for nDNA and mtDNA.

Target	Primer sequence_forward	Primer sequence_reverse
36B4	5′-CGACCTGGAAGTCCAACTAC-3′	5′-ATCTGCTGCATCTGCTTG-3′
COX1	5′-TCTACTATTCGGAGCCTGAGC-3′	5′-CAAAAGCATGGGCAGTTACG-3′

Table 2: Summary of used antibodies.

Primary antibodies			
Antigen	Antibody	Dilution	Brand
PGC-1α	Mouse monoclonal anti-PGC-1α	1 : 1000	Millipore
TFAM	Rabbit monoclonal anti-TFAM	1 : 2000	Abcam
VDAC1	Mouse monoclonal anti-VDAC1	1 : 1000	Abcam
H2B	Rabbit polyclonal anti-H2B	1 : 1000	Abcam
β-Actin	Mouse monoclonal anti-β-actin	1 : 1000	Cell Signaling Technology
Caspase 3	Rabbit polyclonal anti-caspase 3	1 : 1000	Cell Signaling Technology
Cleaved caspase 3	Rabbit polyclonal anti-cleaved caspase 3 (Asp175)	1 : 1000	Cell Signaling Technology
SIRT5	Rabbit monoclonal anti-SIRT5	1 : 1000	Cell Signaling Technology
Secondary antibodies			
Antibody		Dilution	Brand
HRP-conjugated goat anti-mouse IgG (H&L)		1 : 3000	Calbiochem
HRP-conjugated goat anti-rabbit IgG (H&L)		1 : 20000	Sigma-Aldrich

of carbonyl cyanide 3-chlorophenylhydrazone (CCCP) 50 mM for 5 min at 37°C in the dark. After washing with phosphate-buffered saline (PBS), cells were centrifuged at 300 g for 5 min at room temperature and finally resuspended in PBS and analyzed using the Guava easyCyte™ flow cytometer (Millipore), equipped with a red laser at 633 nm. Using the Guava InCyte software, a gate relative to cells containing depolarized mitochondria was arbitrarily set using as a reference CCCP-treated cells assuming that in this condition 90% of the cells contained depolarized mitochondria. This gate was subsequently used for all further analyses.

2.6. Mitochondrial DNA (mtDNA) Quantification. To assess mtDNA content, DNA was extracted from GA muscle using QIAamp DNA Mini kit (Qiagen) and then used for quantitative real-time PCR (qRT-PCR) on the StepOne Plus system (Applied Biosystems). The 36B4 gene was used as a nuclear DNA (nDNA) marker while the COX1 gene was used for mtDNA. The primers used are summarized in Table 1. Briefly, 10 ng of DNA was amplified using 1x SYBR Select Master Mix (Applied Biosystems), using the following protocol: 10 min denaturation at 95°C, followed by 45 cycles (95°C for 15 sec, 60°C for 15 sec, and 72°C for 30 sec) and melting curve (95°C for 15 sec, 60°C for 30 sec, and 95°C for 15 sec). Relative copy number quantification was carried out using the ΔΔCt method.

2.7. Western Blot Assay. TA muscle samples were mechanically homogenized in RIPA buffer (0.1% SDS, 1% NP40, and 0.5% CHAPS) supplemented with protease inhibitors aprotinin, sodium orthovanadate, and phenylmethylsulfonyl fluoride (Sigma-Aldrich). Lysates were incubated on ice for 30 min and then centrifuged at 16.000 g, 4°C, for 20 min. The supernatant was collected, quantified via Bradford method (Bio-Rad), and stored in aliquots at −80°C to avoid repeated freezing-thawing cycles. For Western blot analysis, an equal amount of protein lysates (20–40 μg depending on the protein assayed) were separated onto Criterion™ TGX™ precast gels (Bio-Rad) and transferred to a polyvinylidene difluoride (PVDF) membrane (Millipore) using Criterion™ Blotter (Bio-Rad). Membranes were blocked with 5% BSA-TBS-T and then overnight incubated with primary antibodies at 4°C. Secondary antibody binding was performed at RT for 1 hour. After TBS-T washing, immunoreactive bands were incubated with enhanced chemiluminescent reagent (EuroClone) and detected via ChemiDoc™ XRS+ System (Bio-Rad). Densitometry analysis was accomplished through ImageJ software using H2B (nuclear), VDAC1 (mitochondrial), and β-actin (total) as protein normalizers. The results are representative of at least three independent experiments. The antibodies used are listed in Table 2.

2.8. Gene Expression Analysis. Total RNA was extracted from GA muscles. RNA purification was performed using the E.Z.N.A.® Total RNA Kit I (Omega Bio-tek) according to the manufacturer's instructions, and contaminant DNA was digested with DNase I enzyme (Ambion). cDNA was synthesized using the Maxima Reverse Transcriptase kit (Thermo Fisher Scientific). Real-time PCR amplifications were conducted using SensiFAST SYBR Green (Bioline) according to the manufacturer's instructions, with 300 nM primers and two μL of cDNA (20 μL final reaction volume). Specific primers used are listed in Table 3.

Thermocycling was conducted using LightCycler 480 (Roche) initiated by a 2 min incubation at 95°C, followed

Table 3: Summary of used primers for Beclin, Atg12, Bnip3l, Atrogin, and GAPDH.

Target	Primer sequence_forward	Primer sequence_reverse
Beclin	5′-TGAATGAGGATGACAGTGAGCA-3′	5′-CACCTGGTTCTCCACACTCTTG-3′
Atg12	5′-TCCGTGCCATCACATACACA-3′	5′-TAAGACTGCTGTGGGGCTGA-3′
Bnip3l	5′-TTGGGGCATTTTACTAACCTTG-3′	5′-TGCAGGTGACTGGTGGTACTAA-3′
Atrogin	5′-GCAAACACTGCCACATTCTCTC-3′	5′-CTTGAGGGGAAAGTGAGACG-3′
GAPDH	5′-TCAACGGCACAGTCAAGG-3′	5′-ACTCCACGACATACTCAGC-3′

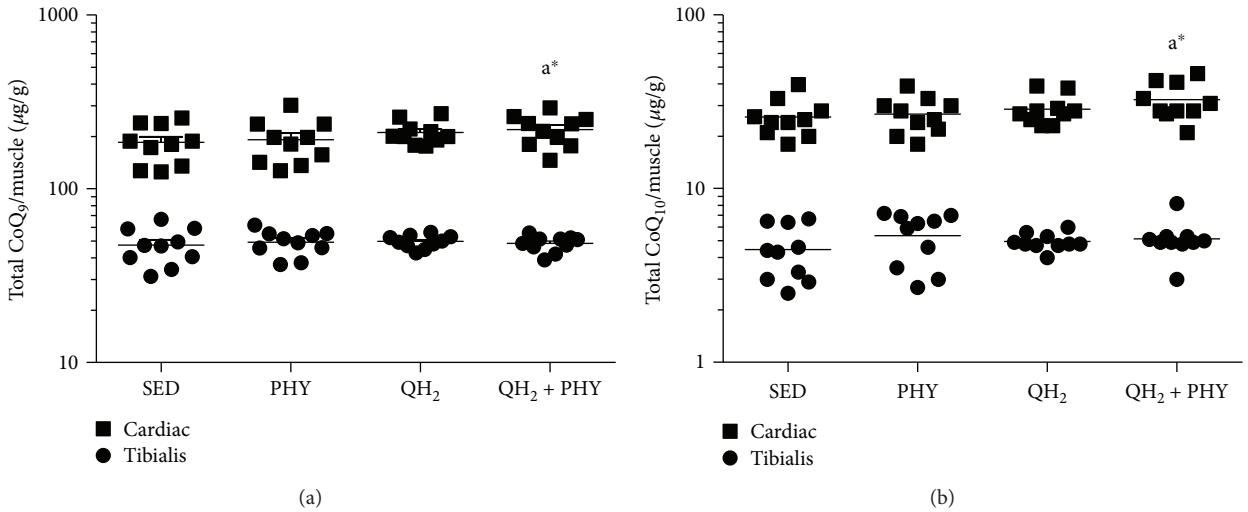

Figure 2: Total coenzyme Q_9 (a) and Q_{10} (b) levels in cardiac and *tibialis anterior* muscles, expressed as μg coenzyme/g of muscle in sedentary (SED), physical exercise (PHY), ubiquinol (QH_2), and ubiquinol associated with physical exercise (QH_2 + PHY) mouse groups ($n = 10$). $^*p < 0.05$; a = *vs.* SED.

by 40 cycles (95°C for 5 sec, 60°C for 5 sec, and 72°C for 10 sec) with a single fluorescent reading taken at the end of each cycle. Each reaction was conducted in triplicate and completed with a melting curve analysis to confirm the specificity of amplification and lack of primer dimers. Quantification was performed according to the ΔCq method, and the expression levels of GAPDH and S16 were used as a reference [67].

3. Statistical Analysis

Data are presented as mean ± SEM. All statistical analyses were performed using GraphPad Prism® 6.0 software. Unpaired two-tailed *t*-test was employed when 2 groups were compared and ANOVA for comparison between three or more groups. Two-way ANOVA with Bonferroni correction for multiple comparisons was used when 3 or more groups were compared over time. The GraphPad Prism routine for outlier identification was used to identify any out-of-range values to be excluded from the statistical analysis.

4. Results

4.1. Combination of Physical Activity and Ubiquinol Supplementation Increases Q_9 and Q_{10} Content in Cardiac Muscles and Lowers the Oxidation of Endogenous Coenzyme Q_9. Total coenzyme Q_9 and Q_{10} (CoQ_9 and CoQ_{10}) levels and oxidative status of coenzyme Q_9 were quantified by an HPLC-ECD instrument on skeletal and cardiac muscles. The results were normalized on muscle weight and expressed as μg/g of muscle. Coenzyme Q levels were very different between skeletal and cardiac muscles, the latter showing remarkably higher levels of both coenzymes (Figure 2). After ubiquinol and physical exercise (QH_2 + PHY) treatment, both coenzymes were significantly increased in the cardiac tissue, in particular +23% CoQ_9 ($p = 0.05$, Figure 2(a)) and +27% CoQ_{10} ($p = 0.03$, Figure 2(b)) with respect to the sedentary group.

To evaluate the effect of exogenous CoQ supplementation on the oxidative status of endogenous coenzyme Q_9, its oxidized form was measured as well. As shown in Figure 3, skeletal muscle is characterized by a higher extent of oxidation (on average 95% of Q_9 is oxidized) compared to cardiac muscle (35% of oxidized Q_9). Ubiquinol supplementation alone was not able to lower the oxidation of endogenous muscular CoQ. On the contrary, a significant decrease of oxidized coenzyme Q_9 was observed in skeletal muscle after regular physical exercise alone or in combination with ubiquinol supplementation (Figure 3, −4.7%, $p = 0.009$, and −3.6%, $p = 0.03$, respectively).

4.2. Physical Exercise Alone or in Combination with Ubiquinol Administration Stimulates Muscle Hypertrophy in SAMP8 Mice. To evaluate the impact of the different

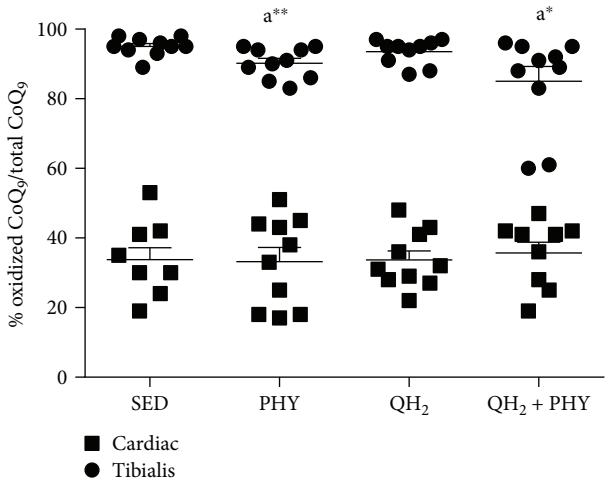

FIGURE 3: Oxidized coenzyme Q_9 level in cardiac and *tibialis anterior* muscles, expressed as percentage of oxidized of coenzyme Q_9 in sedentary (SED), physical exercise (PHY), ubiquinol (QH_2), and ubiquinol associated with physical exercise (QH_2 + PHY) mouse groups ($n = 10$). $^{*}p < 0.05$ and $^{**}p < 0.01$; (A) = *vs.* SED.

treatments on muscle fiber atrophy/hypertrophy, fiber diameter was measured for each experimental condition. Morphometrical analyses of fiber diameter revealed a gradual increase in the ubiquinol (QH_2), ubiquinol and exercise (QH_2 + PHY), and exercise (PHY) groups, with the PHY fibers having the largest average diameter (+33% compared to the SED group, $p = 0.0009$, Figures 4(a) and 4(b)). Ubiquinol treatment alone did not produce any significant variation in fiber size, nor was it able to outweigh the effect of physical exercise alone (+23%; $p = 0.02$). These data suggest that physical exercise alone or in combination with ubiquinol is able to induce muscle fiber hypertrophy.

4.3. Ubiquinol Supplementation Is Able to Improve Mitochondrial Structure and Morphology Counteracting Physical Activity-Induced Mitochondrial Depolarization. Mitochondrial ultrastructure was evaluated in skeletal muscle by transmission electron microscopy (TEM), and at functional level, mitochondrial membrane potential was evaluated in dissociated skeletal muscle cells by flow cytometry using a Nernstian fluorescent probe. As shown in Figure 5(a), in the SED experimental group, mitochondria appeared rounded or elongated, strongly damaged with rather dilated and disorganized cristae. Strikingly, muscle mitochondria of the PHY group appeared even more compromised presenting typical matrix swelling and poorly organized or absent cristae. On the contrary, mitochondria from mice supplemented with 500 mg/kg BW/day of ubiquinol alone (QH_2) or in association with physical exercise (QH_2 + PHY) appear slightly smaller but with well-preserved cristae. Mitochondrial membrane potential analysis (Figures 5(b) and 5(c)) confirmed that the altered mitochondrial ultrastructure observed in the PHY group was associated with significantly increased mitochondrial depolarization (+20% cells with depolarized mitochondria *vs.* SED group, $p = 0.03$, Figure 5(c)), suggesting that exercise might account for a bioenergetics impairment in aged muscles of 7-month-old SAMP8 mice. Notably, this increase was significantly counteracted following ubiquinol supplementation in association with regular physical exercise (QH_2 + PHY) (−12.7%, $p = 0.01$), while QH_2 alone was not able to decrease the basal level of depolarized cells which was similar to sedentary mice. These data suggest that ubiquinol supplementation in combination with regular physical exercise prevents exercise-dependent mitochondrial dysfunctions.

4.4. Combination of Physical Exercise and Ubiquinol Promotes Mitochondrial Biogenesis in the Muscles of the QH_2 + PHY Group. Mitochondrial DNA content and PGC-1α, Tfam, and SIRT5 protein levels of TA muscles were analyzed to evaluate the mitochondrial biogenesis. Notably, QH_2 + PHY treatment was not only able to preserve mitochondrial morphology and functionality (Figure 5) but also capable of modulating mitochondrial biogenesis. In particular, a significantly higher mtDNA copy number was detected in the QH_2 + PHY group compared to the two treatments alone (QH_2 + PHY *vs.* PHY, 1.35-fold change, $p = 0.03$, and QH_2 + PHY *vs.* QH_2, 1.41-fold change, $p = 0.01$, Figure 6). Moreover, the combined treatment promoted a highly significant increase in the expression of proteins involved in mitochondrial biogenesis, such as PGC-1α (+284.9%, $p < 0.0001$) and SIRT5 (+39.5%, $p = 0.02$), compared to sedentary mice (Figure 7). Regular physical exercise in association with ubiquinol supplementation was also able to increase the expression levels of TFAM although not in a significant manner. On the contrary, individual treatments, both physical exercise and ubiquinol supplementation, did not induce any changes in these markers, with the exception of a significant downregulation of SIRT5 in the trained mice.

4.5. Combination of Ubiquinol and Physical Exercise Thwarts Activation of Autophagy/Mitophagy Signals and Lowers Caspase 3-Dependent Apoptosis in the Muscles of QH_2 + PHY Mice. To assess whether the different treatments impacted muscular autophagy/mitophagy, we analyzed the mRNA expression (Figure 8) of Beclin-1 (a), Atrogin-1 (b), Atg12 (c), and Bnip3l (d) genes encoding key players involved in both these degradation processes. The association of ubiquinol supplementation and physical exercise produced a significant decrease in the mRNA expression of Beclin-1 (−1.96-fold, $p = 0.005$), Atg12 (−3.34-fold, $p = 0.003$), and Bnip3l (−4.1-fold, $p = 0.004$) if compared to the PHY group. Atrogin-1 expression decreased significantly only compared to sedentary mice ($p = 0.04$). Ubiquinol supplementation alone was able to induce a significant decrease only for Bnip3l mRNA expression to a similar extent to the combined treatment of ubiquinol and physical exercise (−3.7-fold, $p = 0.009$). To determine whether apoptosis was also modulated, cleaved caspase 3 level was also examined via Western blot assay (Figure 9). Notably, despite that all the treatments were able to significantly decrease caspase 3-dependent apoptosis with respect to SED controls, QH_2 + PHY combination triggered the most pronounced antiapoptotic effect in PHY (−76.9%), QH_2 (−82.6%), and QH_2 + PHY (−96.9%) mouse groups, respectively, compared

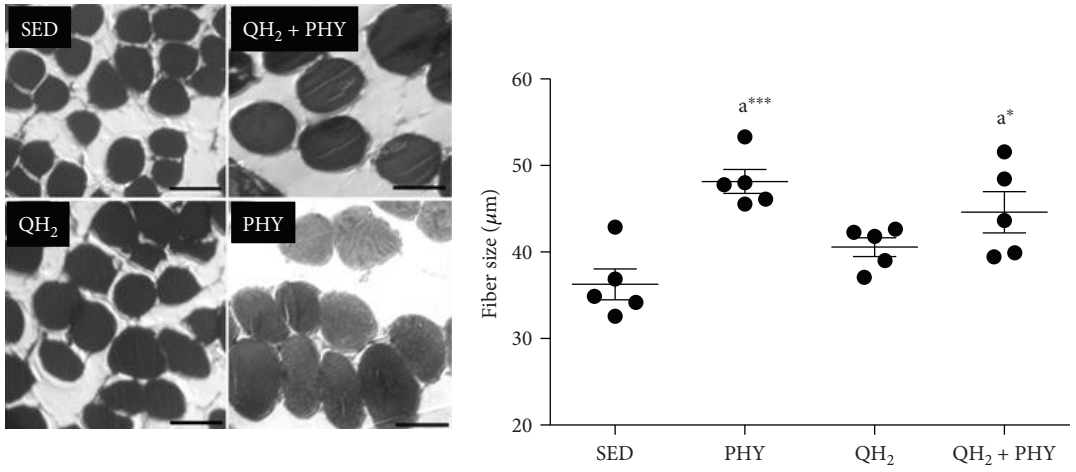

(a) (b)

Figure 4: (a) Representative microphotographs of fibers (SED, bar = 25 μm; PHY, bar = 65 μm; QH_2, bar = 35 μm; and QH_2 + PHY, ba r = 55 μm). (b) Fiber size quantification of *soleus* muscle, expressed in μm, in sedentary (SED), physical exercise (PHY), ubiquinol (QH_2), and ubiquinol associated with physical exercise (QH_2 + PHY) mouse groups ($n = 5$). $^{*}p < 0.05$ and $^{***}p < 0.001$; (A) = *vs.* SED.

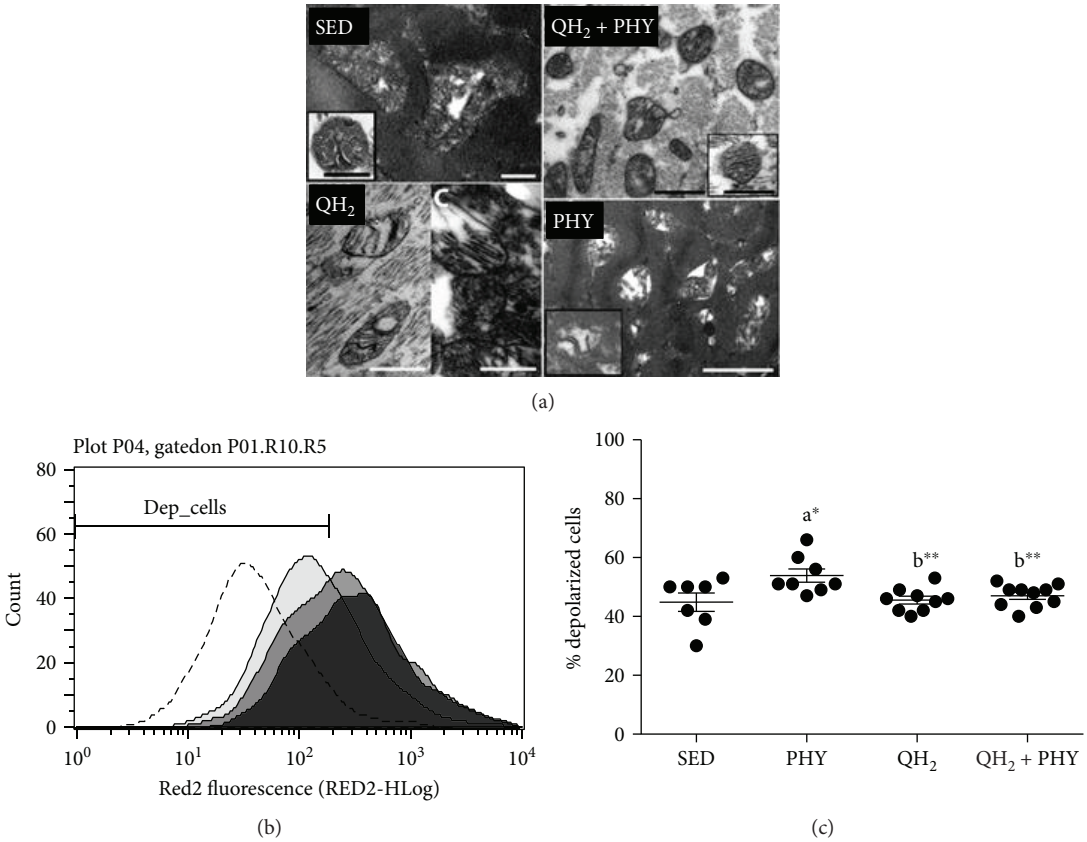

(a) (b) (c)

Figure 5: (a) TEM analysis of mitochondrial ultrastructure of *soleus* muscle (SED, bar = 200 nm; inset SED, bar = 500 nm; PHY, bar = 1 μm; QH_2, bar = 500 nm; and QH_2 + PHY, inset, and QH_2 + PHY, bar = 500 nm). (b) Mitochondrial membrane depolarization expressed as Red2 Fluorescent (RED2-HLog). (c) Percentage of depolarized cells of *gastrocnemius* muscle, respectively, in sedentary (black histogram; SED), physical exercise (light grey histogram; PHY), ubiquinol (dark grey histogram; QH_2), and ubiquinol associated with physical exercise (dark grey histogram; QH_2 + PHY) mouse groups ($n = 10$). Dashed histogram (b) represents sample control treated with CCCP.$^{*}p < 0.05$ and $^{**}p < 0.01$; (A) = *vs.* SED and (B) = *vs.* PHY.

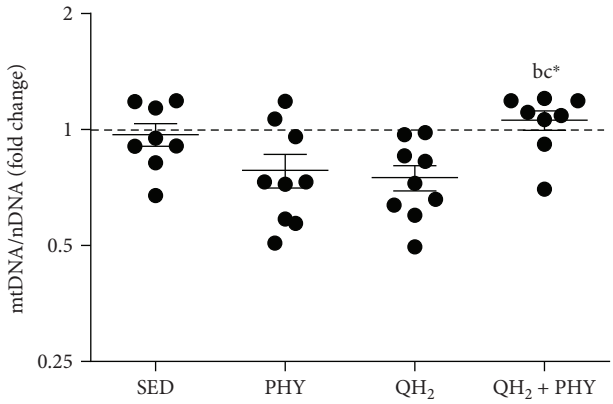

Figure 6: Fold change of copy number of mitochondrial DNA/nuclear DNA (mtDNA/nDNA) measured on *gastrocnemius* muscle in sedentary (SED), physical exercise (PHY), ubiquinol (QH_2), and ubiquinol associated with physical exercise (QH_2 + PHY) mouse groups ($n = 10$). $^*p < 0.05$; (b) = *vs.* PHY and c = *vs.* QH_2.

to SED ($p < 0.0001$, Figures 9(a) and 9(b)). Overall, these data suggest that QH_2 + PHY combination successfully lowers the expression of autophagy/mitophagy-associated genes and prevents apoptotic cell death inside the aging muscles.

5. Discussion

In the present study, senescence-accelerated prone 8 (SAMP8) mice, characterized by premature aging and high degree of oxidative stress [68], were used to investigate if a combined approach of mild physical exercise and ubiquinol ($CoQH_2$) supplementation was able to improve mitochondrial function and preserve skeletal muscle health during aging. In our experimental settings, SAMP8 mice were treated with ubiquinol, physical exercise, and a combination of both for two months starting in the presarcopenia phase (5 months) until sarcopenia onset (7 months) [53]. As expected, the skeletal muscle of 7-month-old SED mice (used as control) presented high oxidative stress, damaged mitochondria, high extent of apoptosis, and mitophagy. While ubiquinol or physical exercise alone was able only to partially rescue these impairments, the combination of ubiquinol and physical exercise significantly improved the overall structural and functional status of the skeletal muscle. Skeletal muscle senescence is associated with decreased muscle mass and mitochondrial dysfunction, and the excessive production of mitochondrial ROS seems to strongly associate with the disruption of mitochondrial energy metabolism [19]. In this context, physical exercise has been proposed as a strategy to stimulate mitochondrial respiration and biogenesis counteracting muscle decline in older subjects [27, 28]. Nonetheless, some studies have shown that ROS production could indeed exacerbate the oxidative stress in senescent muscle, which is characterized by a severely impaired antioxidant response [32–34, 69]. For these reasons, the association of mild regular physical activity and antioxidant therapies could be a powerful strategy to minimize the adverse effects of exercise during aging. In particular, coenzyme Q in its reduced and active form (ubiquinol), being a key player both in the mitochondrial electron transport chain and in the antioxidant response in biological membranes [48], may represent an ideal candidate in improving oxidative status and functionality of the senescent muscle.

CoQ_{10} level correlates to high rates of metabolism, and for this reason, it is highest in organs such as the heart, kidney, and liver (114, 66.5, and 54.9 g/g tissue, respectively) [70], probably due to the large amounts of mitochondria where it is acting as an energy transfer molecule. In fact, coenzyme Q was first isolated from beef heart mitochondria, in 1957 [71].

Accordingly, at 7 months of age, skeletal muscle content of endogenous CoQ_9 was significantly lower and more oxidized in comparison to cardiac muscle. Oral ubiquinol supplementation (500 mg/kg body weight/day) alone was unable to increase skeletal and cardiac muscle CoQ content and only the association of ubiquinol supplementation and mild treadmill running significantly increased the amount of both coenzymes in the cardiac muscle but not in the skeletal muscle. Increase of both coenzymes (endogenous CoQ_9 and dietary absorbed CoQ_{10}) in the heart suggests a higher biosynthesis rate that could be related to different mitochondrial requirements triggering both biosynthesis and incorporation. In the skeletal muscle, these changes that could be required for efficient tissue incorporation seem to occur at a much lower extent or might be less evident due to a lower mitochondrial content. Accordingly, Ernster and Dallner have previously shown that feeding rats with a comparable dosage of oxidized CoQ_{10} significantly increased its plasma content, while tissue CoQ_{10} accumulation was very moderate and variable in different tissues/organs [47]. In particular, skeletal muscle seems to have a very low ability to incorporate CoQ. However, Sohal and Forster showed that CoQ_{10} dietary supplementation in rodents was able to change the subcellular localization of CoQ, increasing the mitochondrial content of both coenzymes in various mitochondria-rich tissues, such as liver, heart, and skeletal muscle [72]. In another study, the same authors confirmed that skeletal muscle increase in CoQ_{10} following supplementation was the lowest in all analyzed tissues [73]. In the present study, we verified that the use of orally administered reduced CoQ_{10} did not provide any significant improvement in tissue uptake, showing results in line with previous reports where ubiquinone was used as active substance. This is a relevant observation since ubiquinol has been proposed as a more bioavailable form of Coenzyme Q_{10}; nonetheless, in the proposed experimental condition, the oxidative state of ubiquinol does not seem to provide any significant improvement in terms of tissue uptake.

Taken together, these data suggest that ubiquinol dietary supplementation alone might not be enough to produce its cellular accumulation, but additional stimuli, such as physical activity and mitochondrial biogenesis, could improve ubiquinol incorporation [74]. Indeed, we reported that physical exercise could therefore act as a trigger for CoQ accumulation or rearrangement at the subcellular level. This effect was particularly evident in mitochondria-rich cardiac muscle, resulting in a significant increase in the overall cellular

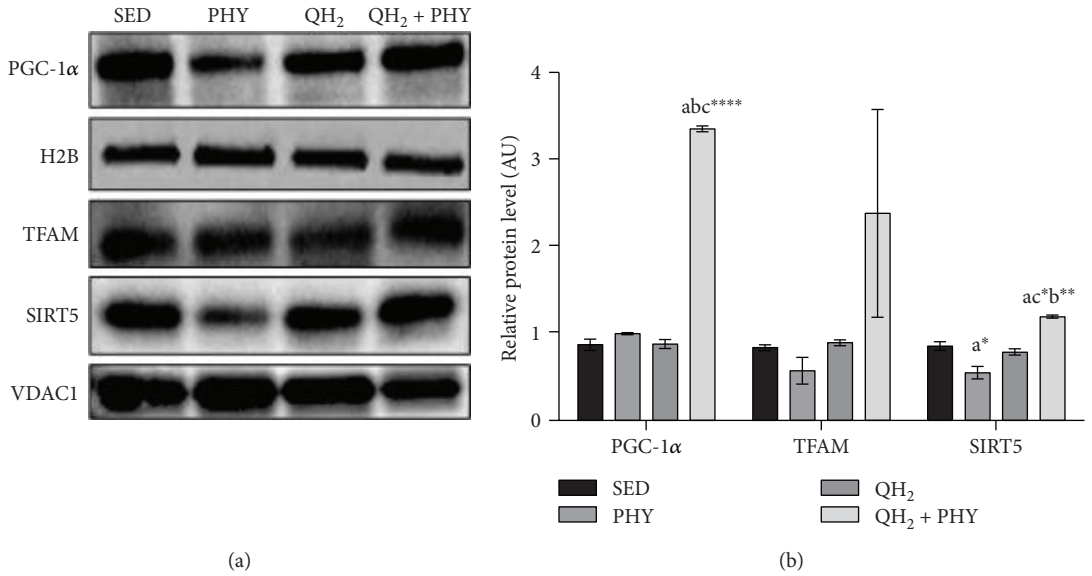

Figure 7: Western blot analysis (a) and relative protein quantification (b) of PGC-1α, TFAM, and SIRT5 expressed in tibialis anterior (TA) muscle, in sedentary (SED), physical exercise (PHY), ubiquinol (QH_2), and ubiquinol associated with physical exercise (QH_2 + PHY) mouse groups ($n = 5$). PGC-1α protein levels were normalized to H2B levels. TFAM and SIRT5 were normalized to VDAC1 levels. AU: arbitrary units. $^{*}p < 0.05$, $^{**}p < 0.01$, and $^{****}p < 0.0001$; (a) = *vs.* SED, (b) = *vs.* PHY, and (c) = *vs.* QH_2.

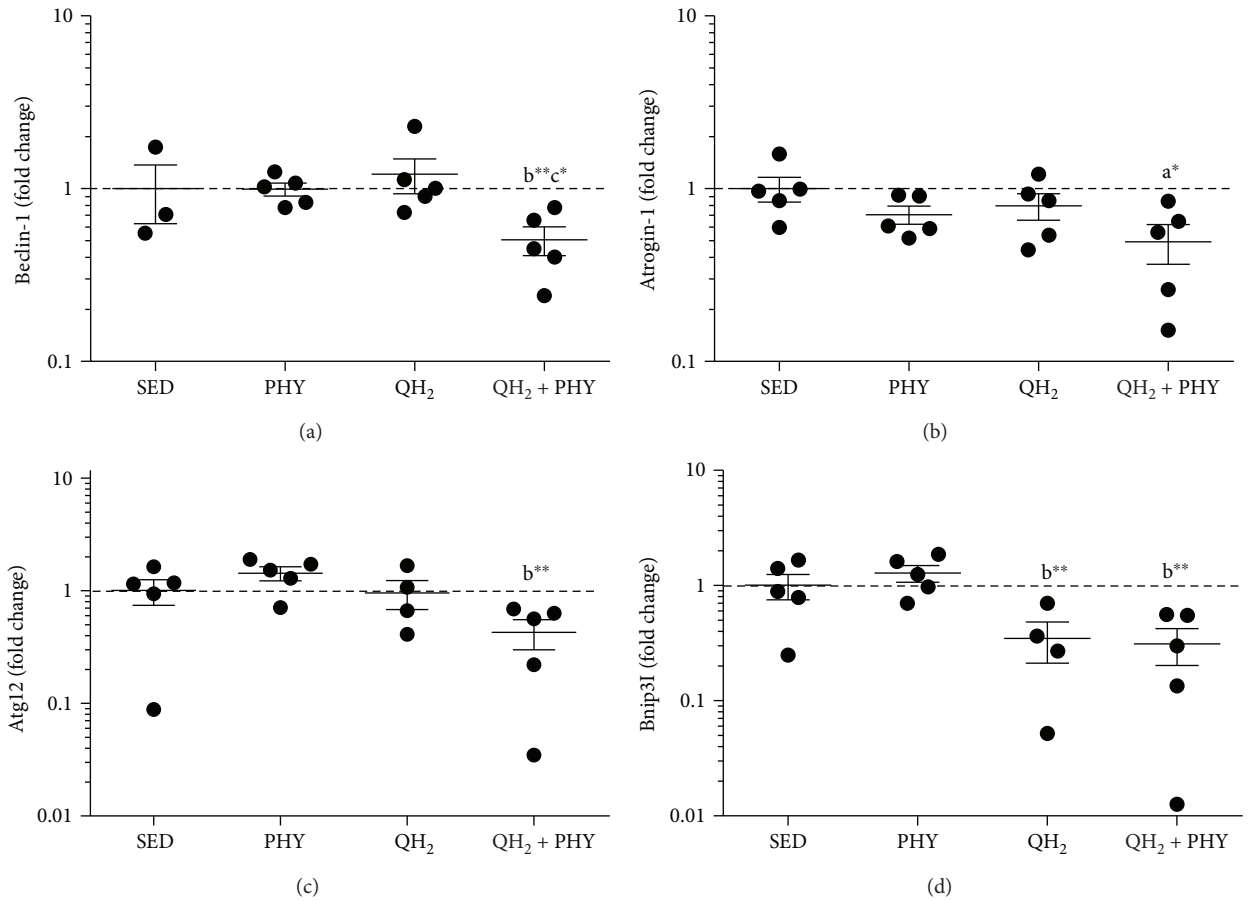

Figure 8: Gene expression (mRNA) expressed as fold change of genes Beclin (a), Atrogin (b), Atg12, (c) and Bnip3l (d) measured on *gastrocnemius* muscle in sedentary (SED), physical exercise (PHY), ubiquinol (QH_2), and ubiquinol associated with physical exercise (QH_2 + PHY) mouse groups ($n = 5$). $^{*}p < 0.05$ and $^{**}p < 0.01$; (a) = *vs.* SED, (b) = *vs.* PHY, and (c) = *vs.* QH_2.

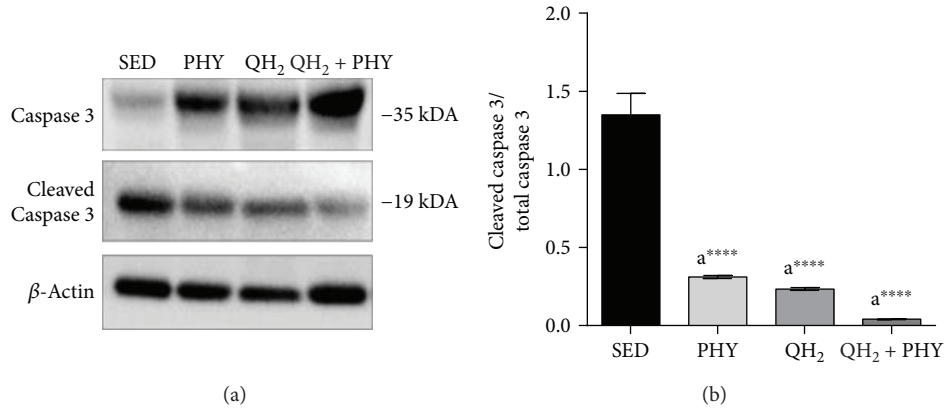

Figure 9: Immunoblot image (a) and relative protein quantification normalized to β-actin (b) of caspase 3 and cleaved caspase 3, measured on *tibialis anterior* muscle in sedentary (SED), physical exercise (PHY), ubiquinol (QH_2), and ubiquinol associated with physical exercise (QH_2 + PHY) mouse groups ($n = 5$). $^{****}p < 0.0001$; (a) = *vs.* SED.

content. Moreover, even if we did not observe a significant CoQ accumulation in the skeletal muscle, we observed functional modifications at mitochondrial and cellular levels suggesting CoQ activity without accumulation in this tissue.

We focused our investigation on skeletal muscle considering its primary involvement in physical exercise. In the SAMP8 model, physical exercise alone produces heterogeneous responses at the cellular level. On the one hand, it had a clear ergogenic effect being able to promote an increase in skeletal muscle fiber size and to improve the oxidative status of endogenous coenzyme Q_9. Accordingly, observational and intervention studies have demonstrated that physical exercise has a positive effect on muscle mass, muscle strength, and physical function in the older population [1, 2, 75, 76]. However, physical exercise also induced mitochondrial disturbances in terms of membrane depolarization. This result could be due to a reduced antioxidant activity [68] and to an intrinsic impairment of the electron transport chain [77]. Both conditions characterizing the presenescent SAMP8 mice might be further exacerbated by physical exercise in our experimental settings.

Notably, the combined treatment was able to counteract the mitochondrial impairment induced by physical exercise alone and also increased the mitochondrial number assessed as mtDNA/nDNA ratio. These data are confirmed by the analysis of PGC-1α muscle protein level, a key protein involved in the control of mitochondrial biogenesis, oxidative metabolism, and autophagy [23, 78, 79] which was significantly increased after 2 months of regular physical exercise associated with ubiquinol supplementation. Several studies reported that induction of PGC-1α, NRF-1, and Tfam expression [80–82] during physical exercise is triggered by oxidative stimuli [83]. On the contrary, aging-derived oxidative stress does not produce similar effects altering PGC-1α expression through different mechanisms [63].

Moreover, in our experimental model, increased fiber diameter in trained animals was not associated with a parallel increase in mtDNA copy number after 2 months of physical exercise, confirming that muscle hypertrophy was not linked with enhanced mitochondrial biogenesis. Shrinkage of the mitochondrial pool is a feature typical of the senescence process, and it is characterized by decreased enzymatic activity and level of mitochondrial proteins [21, 84, 85] as well as low mtDNA content [63, 86]. In this regard, it is remarkable that PGC-1α upregulation was associated with a concomitant increase in mtDNA copy number only in skeletal muscle of QH_2 + PHY mice and not in mice subjected to single interventions.

Moreover, SIRT5, which has been recently found to protect mitochondria from fragmentation and degradation, by supporting mitochondrial elongation [87], was significantly increased following 2 months of ubiquinol supplementation and regular physical exercise, further supporting a positive effect of the QH_2 + PHY combined treatment that could suggest improvement in mitochondria biogenesis.

Intriguingly, despite the improvements in the mitochondrial pool and the functionality observed in the QH_2 + PHY group, an increase in muscle fiber size was produced by physical exercise alone and to a lower extent by the combination treatment. Indeed, muscle mass depends on different factors other than mitochondrial biogenesis, such as the balance between protein synthesis and degradation. van Wessel et al. described how high oxidative fibers are small in size, despite their high capacity for protein synthesis if compared to low oxidative fibers [88]. The authors suggest that cellular energy status may be crucial in mediating either a low oxidative phenotype and a large size or a high oxidative phenotype but a small size. They also suggest that oxidative fibers have a higher rate of muscle protein degradation in the presence of low cellular energy or high oxidative stress status, a condition similar to our experimental model.

During aging, senescent cells respond to a wide range of damaging stimuli produced by the accumulation of dysfunctional proteins and organelles, among which mitochondria play a pivotal role due to their bivalent role as source, target of ROS, and master regulator of programmed cell death processes. Throughout evolution, cells developed strategies like autophagy, mitophagy, and apoptosis to manage these constraints. These tightly regulated and

interconnected processes are of pivotal importance also in the maintenance muscle homeostasis, which is dysregulated during aging and sarcopenia [89, 90]. In this context, ROS originating from mitochondria have been reported to activate both autophagy machinery [91] and caspase-dependent apoptosis [92].

In this regard, the combined treatment with ubiquinol and physical exercise not only ameliorated muscle oxidative stress and bioenergetics but also associated with a decreased expression of autophagy/mitophagy-associated genes, such as Bnip3l, Atg12, and Beclin-1 known to promote mitochondrial fragmentation and mitophagy and autophagosome formation [93, 94].

Finally, the combined treatment was also able to prevent caspase 3-dependent apoptosis. Since caspase cleavage cascade is a readout of mitochondria-associated apoptotic cell death [95–97], these data strengthen the positive impact of QH_2 + PHY combination on mitochondria. Furthermore, previous studies have shown that cytochrome c release from mitochondria activates caspase 3 that in turn cleaves respiratory complex proteins exacerbating mitochondrial dysfunction increasing ROS production [92]. The loss of muscle mass, caused by an imbalance between muscle protein synthesis (MPS) and muscle protein breakdown (MPB) [98] and consequently decline in strength, can also be due to increased activity of the ubiquitin proteasome pathway (UPP), which is also responsible for mitochondrial protein quality control. Our data, showing a decrease in Atrogin-1 expression and myogenin (MyoG) protein level (supplementary material (available here)) and highlighting a potential effect of the combined treatment, suggest also a possible downregulation of UPP proteolytic pathway, which might concur to muscle health preservation [99].

Taking into consideration the limitations of this study, associated to the fact that we did not take into account muscle fiber type composition and we did not measure the actual intramuscular ROS levels, overall in this context, our data demonstrate that ubiquinol might directly prevent cell death by acting both as mitochondrial nutrient and as ROS scavenger.

6. Conclusion

In conclusion, the present study shows that ubiquinol supplementation and physical exercise synergize at improving mitochondrial functionality, counteracting the deleterious effects of physical exercise-induced ROS in the muscles of a SAMP8 mouse model. These results suggest that ubiquinol could be a powerful dietary supplement in sports nutrition and in particular in the elderly. The use of antioxidants in sports practice is still a debated topic, because it was demonstrated that some of these molecules are able to turn off the hormetic signals generated by physical exercise. However, antioxidant compounds represent a very heterogeneous family of molecules with different targets and cellular tropism so that evidences reported for some of them should not be simply extended to all molecules with similar activities. Moreover, data available in the scientific literature referring to a quenching effect of antioxidants on adaptive response commonly refer to trained healthy subjects. Our study shows that ubiquinol, while reducing harmful effects generated by physical exercise, improves exercise-induced hormetic response in a model characterized by elevated oxidative stress and prone to premature aging such as SAMP8 mice.

Data Availability

The data used to support the findings of this study are available from the corresponding author upon request.

Conflicts of Interest

The authors declare that they have no conflicts of interest.

Authors' Contributions

Andreani C. and Bartolacci C. contributed equally to this work.

Acknowledgments

This study was supported by a grant fellowship 2017 from the Fondazione Umberto Veronesi (Silvestri S. was a recipient of grant "Post-doctoral Fellowship 2017"). The authors wish to thank Kaneka for kindly providing ubiquinol.

Supplementary Materials

Immunoblot image and relative protein quantification of myogenin (MyoG) normalized to H2B (Figure 10) were measured on *tibialis anterior* muscle of all mouse groups. The results showed how ubiquinol supplementation, in association with physical exercise (QH_2 + PHY mouse group), was significantly ($^*p < 0.05$) able to prevent the increase in MyoG protein level induced after physical exercise alone (PHY mouse group). These data highlight a protective role of ubiquinol towards the deleterious effect of mild physical exercise in an old skeletal muscle of senescence-accelerated mice, suggesting also a possible downregulation of the UPP proteolytic pathway. Figure 10: immunoblot image and relative protein quantification of myogenin (MyoG) normalized to H2B measured on *tibialis anterior* muscle in sedentary (SED), physical exercise (PHY), ubiquinol (QH_2), and ubiquinol associated with physical exercise (QH_2 + PHY) mouse groups ($n = 5$), $^*p < 0.05$. *(Supplementary Materials)*

References

[1] H. Kim, T. Suzuki, K. Saito et al., "Effects of exercise and tea catechins on muscle mass, strength and walking ability in community-dwelling elderly Japanese sarcopenic women: a randomized controlled trial," *Geriatrics & Gerontology International*, vol. 13, no. 2, pp. 458–465, 2013.

[2] M. Leenders, L. B. Verdijk, L. van der Hoeven, J. van Kranenburg, R. Nilwik, and L. J. C. van Loon, "Elderly men and women benefit equally from prolonged resistance-type exercise training," *The Journals of Gerontology Series A:*

Biological Sciences and Medical Sciences, vol. 68, no. 7, pp. 769–779, 2013.

[3] C. . K. Liu, X. Leng, F. -C. Hsu et al., "The impact of sarcopenia on a physical activity intervention: the Lifestyle Interventions and Independence for Elders Pilot Study (LIFE-P)," *The Journal of Nutrition, Health & Aging*, vol. 18, no. 1, pp. 59–64, 2014.

[4] K. Keller and M. Engelhardt, "Strength and muscle mass loss with aging process. Age and strength loss," *Muscles , Ligaments and Tendons Journal*, vol. 3, no. 4, p. 346, 2014.

[5] N. Montero-Fernández and J. A. Serra-Rexach, "Role of exercise on sarcopenia in the elderly," *European Journal of Physical and Rehabilitation Medicine*, vol. 49, no. 1, pp. 131–143, 2013.

[6] M. Brotto and E. L. Abreu, "Sarcopenia: pharmacology of today and tomorrow," *Journal of Pharmacology and Experimental Therapeutics*, vol. 343, no. 3, pp. 540–546, 2012.

[7] D. Scott, L. Blizzard, J. Fell, G. Giles, and G. Jones, "Associations between dietary nutrient intake and muscle mass and strength in community-dwelling older adults: the Tasmanian Older Adult Cohort Study," *Journal of the American Geriatrics Society*, vol. 58, no. 11, pp. 2129–2134, 2010.

[8] A. J. Cruz-Jentoft and F. Landi, "Sarcopenia," *Clinical Medicine*, vol. 14, no. 2, pp. 183–186, 2014.

[9] I. H. Rosenberg, "Sarcopenia: origins and clinical relevance," *Clinics in Geriatric Medicine*, vol. 27, no. 3, pp. 337–339, 2011.

[10] W. J. Evans, "Skeletal muscle loss: cachexia, sarcopenia, and inactivity," *The American Journal of Clinical Nutrition*, vol. 91, no. 4, pp. 1123S–1127S, 2010.

[11] G. A. Power, B. H. Dalton, and C. L. Rice, "Human neuromuscular structure and function in old age: a brief review," *Journal of Sport and Health Science*, vol. 2, no. 4, pp. 215–226, 2013.

[12] U. Granacher and T. Hortobágyi, "Exercise to improve mobility in healthy aging," *Sports Medicine*, vol. 45, no. 12, pp. 1625-1626, 2015.

[13] H. N. Carter, C. C. W. Chen, and D. A. Hood, "Mitochondria, muscle health, and exercise with advancing age," *Physiology*, vol. 30, no. 3, pp. 208–223, 2015.

[14] H. M. McBride, M. Neuspiel, and S. Wasiak, "Mitochondria: more than just a powerhouse," *Current Biology*, vol. 16, no. 14, pp. R551–R560, 2006.

[15] L. D. Tryon, A. Vainshtein, J. M. Memme, M. J. Crilly, and D. A. Hood, "Recent advances in mitochondrial turnover during chronic muscle disuse," *Integrative Medicine Research*, vol. 3, no. 4, pp. 161–171, 2014.

[16] M. P. Mattson, "Hormesis defined," *Ageing Research Reviews*, vol. 7, no. 1, pp. 1–7, 2008.

[17] A. R. Konopka and K. Sreekumaran Nair, "Mitochondrial and skeletal muscle health with advancing age," *Molecular and Cellular Endocrinology*, vol. 379, no. 1-2, pp. 19–29, 2013.

[18] D. Y. Seo, S. R. Lee, N. Kim, K. S. Ko, B. D. Rhee, and J. Han, "Age-related changes in skeletal muscle mitochondria: the role of exercise," *Integrative Medicine Research*, vol. 5, no. 3, pp. 182–186, 2016.

[19] I. Sanchez-Roman, A. Gómez, I. Pérez et al., "Effects of aging and methionine restriction applied at old age on ROS generation and oxidative damage in rat liver mitochondria," *Biogerontology*, vol. 13, no. 4, pp. 399–411, 2012.

[20] H. P. Indo, M. Davidson, H. C. Yen et al., "Evidence of ROS generation by mitochondria in cells with impaired electron transport chain and mitochondrial DNA damage," *Mitochondrion*, vol. 7, no. 1-2, pp. 106–118, 2007.

[21] K. R. Short, M. L. Bigelow, J. Kahl et al., "Decline in skeletal muscle mitochondrial function with aging in humans," *Proceedings of the National Academy of Sciences of the United States of America*, vol. 102, no. 15, pp. 5618–5623, 2005.

[22] O. E. Rooyackers, D. B. Adey, P. A. Ades, and K. S. Nair, "Effect of age on in vivo rates of mitochondrial protein synthesis in human skeletal muscle," *Proceedings of the National Academy of Sciences of the United States of America*, vol. 93, no. 26, pp. 15364–15369, 1996.

[23] Z. Wu, P. Puigserver, U. Andersson et al., "Mechanisms controlling mitochondrial biogenesis and respiration through the thermogenic coactivator PGC-1," *Cell*, vol. 98, no. 1, pp. 115–124, 1999.

[24] A. Vainshtein, E. M. A. Desjardins, A. Armani, M. Sandri, and D. A. Hood, "PGC-1α modulates denervation-induced mitophagy in skeletal muscle," *Skeletal Muscle*, vol. 5, no. 1, p. 9, 2015.

[25] N. Mizushima and B. Levine, "Autophagy in mammalian development and differentiation," *Nature Cell Biology*, vol. 12, no. 9, pp. 823–830, 2010.

[26] J. J. Wu, C. Quijano, E. Chen et al., "Mitochondrial dysfunction and oxidative stress mediate the physiological impairment induced by the disruption of autophagy," *Aging*, vol. 1, no. 4, pp. 425–437, 2009.

[27] L. DiPietro, "Physical activity in aging: changes in patterns and their relationship to health and function," *The Journals of Gerontology Series A: Biological Sciences and Medical Sciences*, vol. 56, no. 2, pp. 13–22, 2001.

[28] J. Dziura, C. Mendes de Leon, S. Kasl, and L. DiPietro, "Can physical activity attenuate aging-related weight loss in older people? The Yale Health and Aging Study, 1982–1994," *American Journal of Epidemiology*, vol. 159, no. 8, pp. 759–767, 2004.

[29] R. N. Baumgartner, S. J. Wayne, D. L. Waters, I. Janssen, D. Gallagher, and J. E. Morley, "Sarcopenic obesity predicts instrumental activities of daily living disability in the elderly," *Obesity Research*, vol. 12, no. 12, pp. 1995–2004, 2004.

[30] A. P. Russell, V. C. Foletta, R. J. Snow, and G. D. Wadley, "Skeletal muscle mitochondria: a major player in exercise, health and disease," *Biochimica et Biophysica Acta (BBA) - General Subjects*, vol. 1840, no. 4, pp. 1276–1284, 2014.

[31] S. Ketkar, A. Rathore, A. Kandhare et al., "Alleviating exercise-induced muscular stress using neat and processed bee pollen: oxidative markers, mitochondrial enzymes, and myostatin expression in rats," *Integrative Medicine Research*, vol. 4, no. 3, pp. 147–160, 2015.

[32] P. V. Komi, "Stretch-shortening cycle: a powerful model to study normal and fatigued muscle," *Journal of Biomechanics*, vol. 33, no. 10, pp. 1197–1206, 2000.

[33] G. S. Lynch, J. A. Faulkner, and S. V. Brooks, "Force deficits and breakage rates after single lengthening contractions of single fast fibers from unconditioned and conditioned muscles of young and old rats," *American Journal of Physiology-Cell Physiology*, vol. 295, no. 1, pp. C249–C256, 2008.

[34] I. M. Conboy, M. J. Conboy, G. M. Smythe, and T. A. Rando, "Notch-mediated restoration of regenerative potential to aged muscle," *Science*, vol. 302, no. 5650, pp. 1575–1577, 2003.

[35] Y. Shimomura, M. Suzuki, S. Sugiyama, Y. Hanaki, and T. Ozawa, "Protective effect of coenzyme Q10 on exercise-

induced muscular injury," *Biochemical and Biophysical Research Communications*, vol. 176, no. 1, pp. 349–355, 1991.

[36] M. Kon, F. Kimura, T. Akimoto et al., "Effect of Coenzyme Q10 supplementation on exercise-induced muscular injury of rats," *Exerc Immunol Rev*, vol. 13, pp. 76–88, 2007.

[37] M. Kon, K. Tanabe, T. Akimoto et al., "Reducing exercise-induced muscular injury in kendo athletes with supplementation of coenzyme Q10," *British Journal of Nutrition*, vol. 100, no. 4, pp. 903–909, 2008.

[38] A. Abadi, J. D. Crane, D. Ogborn et al., "Supplementation with α-lipoic acid, CoQ_{10}, and vitamin E augments running performance and mitochondrial function in female mice," *PLoS One*, vol. 8, no. 4, article e60722, 2013.

[39] G. Tian, J. Sawashita, H. Kubo et al., "Ubiquinol-10 supplementation activates mitochondria functions to decelerate senescence in senescence-accelerated mice," *Antioxidants & Redox Signaling*, vol. 20, no. 16, pp. 2606–2620, 2014.

[40] A. Lass, S. Agarwal, and R. S. Sohal, "Mitochondrial ubiquinone homologues, superoxide radical generation, and longevity in different mammalian species," *Journal of Biological Chemistry*, vol. 272, no. 31, pp. 19199–19204, 1997.

[41] S. Kamzalov, N. Sumien, M. J. Forster, and R. S. Sohal, "Coenzyme Q intake elevates the mitochondrial and tissue levels of Coenzyme Q and alpha-tocopherol in young mice," *The Journal of Nutrition*, vol. 133, no. 10, pp. 3175–3180, 2003.

[42] C. Gómez-Díaz, M. I. Burón, F. J. Alcaín et al., "Effect of dietary coenzyme Q and fatty acids on the antioxidant status of rat tissues," *Protoplasma*, vol. 221, no. 1-2, pp. 11–17, 2003.

[43] L. K. Kwong, S. Kamzalov, I. Rebrin et al., "Effects of coenzyme Q_{10} administration on its tissue concentrations, mitochondrial oxidant generation and oxidative stress in the rat," *Free Radical Biology & Medicine*, vol. 33, no. 5, pp. 627–638, 2002.

[44] H. Maruoka, K. Fujii, K. Inoue, and S. Kido, "Long-term effect of ubiquinol on exercise capacity and the oxidative stress regulation system in SAMP1 mice," *Journal of Physical Therapy Science*, vol. 26, no. 3, pp. 367–371, 2014.

[45] C. Schmelzer, J. G. Okun, D. Haas et al., "The reduced form of coenzyme Q_{10} mediates distinct effects on cholesterol metabolism at the transcriptional and metabolite level in SAMP1 mice," *IUBMB Life*, vol. 62, no. 11, pp. 812–818, 2010.

[46] M. Kitano, D. Watanabe, S. Oda et al., "Subchronic oral toxicity of ubiquinol in rats and dogs," *International Journal of Toxicology*, vol. 27, no. 2, pp. 189–215, 2008.

[47] L. Ernster and G. Dallner, "Biochemical, physiological and medical aspects of ubiquinone function," *Biochimica et Biophysica Acta (BBA) - Molecular Basis of Disease*, vol. 1271, no. 1, pp. 195–204, 1995.

[48] G. P. Littarru and L. Tiano, "Clinical aspects of coenzyme Q10: an update," *Nutrition*, vol. 26, no. 3, pp. 250–254, 2010.

[49] G. Dallner and P. J. Sindelar, "Regulation of ubiquinone metabolism," *Free Radical Biology & Medicine*, vol. 29, no. 3-4, pp. 285–294, 2000.

[50] G. P. Littarru, M. Battino, and K. Folkers, "Clinical aspects of coenzyme Q: improvement of cellular bioenergetics or antioxidant perfection?," in *Handbook of Antioxidants*, E. Cadenas and L. Packer, Eds., pp. 203–239, Marcel Decker, New York, NY, USA, 1996.

[51] A. Rötig, E. L. Appelkvist, V. Geromel et al., "Quinone-responsive multiple respiratory-chain dysfunction due to widespread coenzyme Q_{10} deficiency," *Lancet*, vol. 356, no. 9227, pp. 391–395, 2000.

[52] D. Alf, M. E. Schmidt, and S. C. Siebrecht, "Ubiquinol supplementation enhances peak power production in trained athletes: a double-blind, placebo controlled study," *Journal of the International Society of Sports Nutrition*, vol. 10, no. 1, p. 24, 2013.

[53] A. Y. Guo, K. S. Leung, P. M. Siu et al., "Muscle mass, structural and functional investigations of senescence-accelerated mouse P8 (SAMP8)," *Experimental Animals*, vol. 64, no. 4, pp. 425–433, 2015.

[54] T. Takeda, "Senescence-accelerated mouse (SAM): a biogerontological resource in aging research," *Neurobiology of Aging*, vol. 20, no. 2, pp. 105–110, 1999.

[55] J. E. Morley, H. J. Armbrecht, S. A. Farr, and V. B. Kumar, "The senescence accelerated mouse (SAMP8) as a model for oxidative stress and Alzheimer's disease," *Biochimica et Biophysica Acta (BBA) - Molecular Basis of Disease*, vol. 1822, no. 5, pp. 650–656, 2012.

[56] Y. Chiba, A. Shimada, N. Kumagai et al., "The senescence-accelerated mouse (SAM): a higher oxidative stress and age-dependent degenerative diseases model," *Neurochemical Research*, vol. 34, no. 4, pp. 679–687, 2009.

[57] F. Derbré, A. Gratas-Delamarche, M. C. Gómez-Cabrera, and J. Viña, "Inactivity-induced oxidative stress: a central role in age-related sarcopenia?," *European Journal of Sport Science*, vol. 14, Supplement 1, pp. S98–S108, 2014.

[58] W. Derave, B. O. Eijnde, M. Ramaekers, and P. Hespel, "Soleus muscles of SAMP8 mice provide an accelerated model of skeletal muscle senescence," *Experimental Gerontology*, vol. 40, no. 7, pp. 562–572, 2005.

[59] T. Nishikawa, J. A. Takahashi, T. Matsushita et al., "Tubular aggregates in the skeletal muscle of the senescence-accelerated mouse SAM," *Mechanisms of Ageing and Development*, vol. 114, no. 2, pp. 89–99, 2000.

[60] C. Moorwood, M. Liu, Z. Tian, and E. R. Barton, "Isometric and eccentric force generation assessment of skeletal muscles isolated from murine models of muscular dystrophies," *Journal of Visualized Experiments*, vol. 8, no. 71, article e50036, 2013.

[61] M. Romanick, L. D. V. Thompson, and H. M. Brown-Borg, "Murine models of atrophy, cachexia, and sarcopenia in skeletal muscle," *Biochimica et Biophysica Acta (BBA) - Molecular Basis of Disease*, vol. 1832, no. 9, pp. 1410–1420, 2013.

[62] T. Takeda, M. Hosokawa, S. Takeshita et al., "A new murine model of accelerated senescence," *Mechanisms of Ageing and Development*, vol. 17, no. 2, pp. 183–194, 1981.

[63] C. Kang, E. Chung, G. Diffee, and L. L. Ji, "Exercise training attenuates aging-associated mitochondrial dysfunction in rat skeletal muscle: role of PGC-1α," *Experimental Gerontology*, vol. 48, no. 11, pp. 1343–1350, 2013.

[64] N. Okudan, S. Revan, S. S. Balci, M. Belviranli, H. Pepe, and H. Gökbel, "Effects of CoQ_{10} supplementation and swimming training on exhaustive exercise-induced oxidative stress in rat heart," *Bratislava Medical Journal*, vol. 113, no. 07, pp. 393–399, 2012.

[65] S. Salucci, S. Burattini, F. Buontempo, A. M. Martelli, E. Falcieri, and M. Battistelli, "Protective effect of different antioxidant agents in UVB-irradiated keratinocytes," *European Journal of Histochemistry*, vol. 61, no. 3, p. 2784, 2017.

[66] M. Battistelli, S. Salucci, E. Olivotto et al., "Cell death in human articular chondrocyte: a morpho-functional study in micromass model," *Apoptosis*, vol. 19, no. 10, pp. 1471–1483, 2014.

[67] M. W. Pfaffl, "A new mathematical model for relative quantification in real-time RT–PCR," *Nucleic Acids Research*, vol. 29, no. 9, article e45, pp. 45e–445, 2001.

[68] S. Taniguchi, M. Hanafusa, H. Tsubone et al., "Age-dependency of the serum oxidative level in the senescence-accelerated mouse prone 8," *Journal of Veterinary Medical Science*, vol. 78, no. 8, pp. 1369–1371, 2016.

[69] M. J. Jackson and A. McArdle, "Age-related changes in skeletal muscle reactive oxygen species generation and adaptive responses to reactive oxygen species," *The Journal of Physiology*, vol. 589, no. 9, pp. 2139–2145, 2011.

[70] R. Saini, "Coenzyme Q10: the essential nutrient," *Journal of Pharmacy and Bioallied Sciences*, vol. 3, no. 3, pp. 466-467, 2011.

[71] F. L. Crane, Y. Hatefi, R. L. Lester, and C. Widmer, "Isolation of a quinone from beef heart mitochondria," *Biochimica et Biophysica Acta*, vol. 25, no. 1, pp. 220-221, 1957.

[72] R. S. Sohal and M. J. Forster, "Coenzyme Q, oxidative stress and aging," *Mitochondrion*, vol. 7, pp. S103–S111, 2007.

[73] R. S. Sohal, S. Kamzalov, N. Sumien et al., "Effect of coenzyme Q_{10} intake on endogenous coenzyme Q content, mitochondrial electron transport chain, antioxidative defenses, and life span of mice," *Free Radical Biology & Medicine*, vol. 40, no. 3, pp. 480–487, 2006.

[74] M. Guescini, L. Tiano, M. L. Genova et al., "The combination of physical exercise with muscle-directed antioxidants to counteract sarcopenia: a biomedical rationale for pleiotropic treatment with creatine and coenzyme Q10," *Oxidative Medicine and Cellular Longevity*, vol. 2017, Article ID 7083049, 19 pages, 2017.

[75] J. D. Crane, L. G. MacNeil, and M. A. Tarnopolsky, "Long-term aerobic exercise is associated with greater muscle strength throughout the life span," *The Journals of Gerontology Series A: Biological Sciences and Medical Sciences*, vol. 68, no. 6, pp. 631–638, 2013.

[76] S. Zampieri, L. Pietrangelo, S. Loefler et al., "Lifelong physical exercise delays age-associated skeletal muscle decline," *The Journals of Gerontology Series A: Biological Sciences and Medical Sciences*, vol. 70, no. 2, pp. 163–173, 2015.

[77] H. Nakahara, T. Kanno, Y. Inai et al., "Mitochondrial dysfunction in the senescence accelerated mouse (SAM)," *Free Radical Biology & Medicine*, vol. 24, no. 1, pp. 85–92, 1998.

[78] M. Sandri, J. Lin, C. Handschin et al., "PGC-1α protects skeletal muscle from atrophy by suppressing FoxO3 action and atrophy-specific gene transcription," *Proceedings of the National Academy of Sciences of the United States of America*, vol. 103, no. 44, pp. 16260–16265, 2006.

[79] J. Lin, C. Handschin, and B. M. Spiegelman, "Metabolic control through the PGC-1 family of transcription coactivators," *Cell Metabolism*, vol. 1, no. 6, pp. 361–370, 2005.

[80] K. Baar, A. Wende, T. Jones et al., "Adaptations of skeletal muscle to exercise: rapid increase in the transcriptional coactivator PGC-1," *The FASEB Journal*, vol. 16, no. 14, pp. 1879–1886, 2002.

[81] J. W. Gordon, A. A. Rungi, H. Inagaki, and D. A. Hood, "Selected Contribution: Effects of contractile activity on mitochondrial transcription factor A expression in skeletal muscle," *Journal of Applied Physiology*, vol. 90, no. 1, pp. 389–396, 2001.

[82] I. Irrcher, P. J. Adhihetty, T. Sheehan, A. M. Joseph, and D. A. Hood, "PPARγ coactivator-1α expression during thyroid hormone- and contractile activity-induced mitochondrial adaptations," *American Journal of Physiology-Cell Physiology*, vol. 284, no. 6, pp. C1669–C1677, 2003.

[83] C. Kang, K. M. O'Moore, J. R. Dickman, and L. L. Ji, "Exercise activation of muscle peroxisome proliferator-activated receptor-γ coactivator-1α signaling is redox sensitive," *Free Radical Biology & Medicine*, vol. 47, no. 10, pp. 1394–1400, 2009.

[84] B. Chabi, V. Ljubicic, K. J. Menzies, J. H. Huang, A. Saleem, and D. A. Hood, "Mitochondrial function and apoptotic susceptibility in aging skeletal muscle," *Aging Cell*, vol. 7, no. 1, pp. 2–12, 2008.

[85] V. Ljubicic, A. M. Joseph, P. J. Adhihetty et al., "Molecular basis for an attenuated mitochondrial adaptive plasticity in aged skeletal muscle," *Aging*, vol. 1, no. 9, pp. 818–830, 2009.

[86] S. Welle, K. Bhatt, B. Shah, N. Needler, J. M. Delehanty, and C. A. Thornton, "Reduced amount of mitochondrial DNA in aged human muscle," *Journal of Applied Physiology*, vol. 94, no. 4, pp. 1479–1484, 2003.

[87] H. Guedouari, T. Daigle, L. Scorrano, and E. Hebert-Chatelain, "Sirtuin 5 protects mitochondria from fragmentation and degradation during starvation," *Biochimica et Biophysica Acta (BBA) - Molecular Cell Research*, vol. 1864, no. 1, pp. 169–176, 2017.

[88] T. van Wessel, A. de Haan, W. J. van der Laarse, and R. T. Jaspers, "The muscle fiber type-fiber size paradox: hypertrophy or oxidative metabolism?," *European Journal of Applied Physiology*, vol. 110, no. 4, pp. 665–694, 2010.

[89] A. Dirks and C. Leeuwenburgh, "Apoptosis in skeletal muscle with aging," *American Journal of Physiology-Regulatory, Integrative and Comparative Physiology*, vol. 282, no. 2, pp. R519–R527, 2002.

[90] R. A. Gottlieb and R. S. Carreira, "Autophagy in health and disease. 5. Mitophagy as a way of life," *American Journal of Physiology-Cell Physiology*, vol. 299, no. 2, pp. C203–C210, 2010.

[91] Y. Chen, M. B. Azad, and S. B. Gibson, "Superoxide is the major reactive oxygen species regulating autophagy," *Cell Death & Differentiation*, vol. 16, no. 7, pp. 1040–1052, 2009.

[92] J. E. Ricci, R. A. Gottlieb, and D. R. Green, "Caspase-mediated loss of mitochondrial function and generation of reactive oxygen species during apoptosis," *The Journal of Cell Biology*, vol. 160, no. 1, pp. 65–75, 2003.

[93] E. Masiero, L. Agatea, C. Mammucari et al., "Autophagy is required to maintain muscle mass," *Cell Metabolism*, vol. 10, no. 6, pp. 507–515, 2009.

[94] E. Wirawan, S. Lippens, T. vanden Berghe et al., "Beclin1: a role in membrane dynamics and beyond," *Autophagy*, vol. 8, no. 1, pp. 6–17, 2012.

[95] M. Enari, H. Sakahira, H. Yokoyama, K. Okawa, A. Iwamatsu, and S. Nagata, "A caspase-activated DNase that degrades DNA during apoptosis, and its inhibitor ICAD," *Nature*, vol. 391, no. 6662, pp. 43–50, 1998.

[96] S. Sahara, M. Aoto, Y. Eguchi, N. Imamoto, Y. Yoneda, and Y. Tsujimoto, "Acinus is a caspase-3-activated protein required for apoptotic chromatin condensation," *Nature*, vol. 401, no. 6749, pp. 168–173, 1999.

[97] M. L. Coleman, E. A. Sahai, M. Yeo, M. Bosch, A. Dewar, and M. F. Olson, "Membrane blebbing during apoptosis results from caspase-mediated activation of ROCK I," *Nature Cell Biology*, vol. 3, no. 4, pp. 339–345, 2001.

[98] R. J. Stefanetti, E. Zacharewicz, P. Della Gatta, A. Garnham, A. P. Russell, and S. Lamon, "Ageing has no effect on the regulation of the ubiquitin proteasome-related genes and proteins following resistance exercise," *Frontiers in Physiology*, vol. 5, no. 30, 2014.

[99] V. Moresi, A. H. Williams, E. Meadows et al., "Myogenin and class II HDACs control neurogenic muscle atrophy by inducing E3 ubiquitin ligases," *Cell*, vol. 143, no. 1, pp. 35–45, 2010.